

Technische Universität München  
Max-Planck-Institut für Quantenoptik

# Optomechanics with Levitating Dielectrics: Theory and Protocols

Anika Carmen Pflanze

Vollständiger Abdruck der von der Fakultät für Physik  
der Technischen Universität München  
zur Erlangung des akademischen Grades eines  
Doktors der Naturwissenschaften (Dr. rer. nat.)  
genehmigten Dissertation.

Vorsitzender: Univ.-Prof. Dr. R. Gross  
Prüfer der Dissertation: 1. Hon.-Prof. J. I. Cirac, Ph.D.  
2. Univ.-Prof. Dr. W. Zwerger

Die Dissertation wurde am 12.8.2013  
bei der Technischen Universität München eingereicht  
und durch die Fakultät für Physik am 9.9.2013 angenommen.



# Abstract

This thesis focuses on cavity optomechanics with an optically levitated dielectric object. We develop the underlying theory and propose and analyze various protocols to prepare these macroscopic systems in superposition states. Optical levitation circumvents the direct thermal coupling of the mechanical oscillator to its environment and holds the promise to enable ground-state cooling even at room temperature. This thesis approaches this novel optomechanical system from two different angles reflected in the division into the main parts of **Theory** and **Protocols**.

In the first part of the thesis, we derive a theoretical description of the system from first principles. A master equation describing the interaction of light with dielectric objects of arbitrary sizes and shapes is developed. It does not rely on the point-particle approximation by taking into account scattering processes to all orders in perturbation theory and treats both the motion of the object and the light quantum-mechanically. This formalism extends the standard master-equation approach to the case where interactions among different modes of the environment are considered. We apply this general method to the specific setup of levitating dielectrics in optical cavities. Apart from photon scattering, we also take into account various other dissipation processes, *e.g.*, blackbody radiation, scattering of gas molecules, or coupling to internal vibrational modes, and compare them to the coherent coupling rates of the system. To analyze the feasibility of ground-state cooling, we derive the steady-state phonon numbers without relying on resolved-sideband or bad-cavity approximations. Within this theoretical framework, the optomechanical performance for realistic experimental parameters is analyzed. We show that cavity cooling of the center-of-mass (cm) mode to the motional ground state is possible for spheres with radius  $R \lesssim 260\text{nm}$ .

The focus of the second part of the thesis is to provide protocols for the preparation of the mechanical oscillator in nonclassical states. The realization of superposition states is essential to most of the proposed applications of nano-mechanical oscillators, *i.e.*, for sensing or to find an answer to foundational questions. We confront this problem from three different angles. First, we propose several state-preparation protocols relying on the efficient coupling to single photons, thus projecting their nonclassical

state to the mechanical oscillator. These protocols require different cavity finesses and coupling strengths and thus are suitable for implementation in various regimes. Second, preparation of the nonclassical state by coupling to a qubit, *e.g.*, a two-level atom, via the cavity mode is proposed. We show that it is possible to use such a coupling for the dissipative preparation of nonclassical states with high fidelity. This setup can be extended to a nonlinear many-partite system via stroboscopic driving of the oscillators and we illustrate the effectiveness of the state-preparation protocols even in this case. Results from both the single-photon and the dissipative-qubit protocol are not restricted to levitating spheres and may be applied to other optomechanical systems. Third, the last protocol exploits the levitation of the mechanical oscillator and is thus in particular suitable for the setup described above. We propose an optomechanical version of a double-slit experiment achieving spatial superpositions of the order on the size of the dielectric. This method provides unprecedented bounds for objective collapse models of the wave function by merging techniques and insights from cavity quantum optomechanics and matter-wave interferometry.

In summary, this thesis aims at advancing the field of optomechanics with levitating dielectrics by providing a theoretical description for this system and various protocols for the preparation of nonclassical states.

# Zusammenfassung

Thema dieser Arbeit ist Optomechanik mit schwebenden Nano-Dielektrika in optischen Resonatoren. Wir entwickeln die zugrunde liegende Theorie zur Charakterisierung dieser makroskopischen Systeme und analysieren verschiedene Protokolle, um sie in quantenmechanischen Zuständen zu präparieren. Dadurch, dass die Nano-Dielektrika optisch gefangen sind und somit nicht direkt an ihre thermische Umgebung koppeln, bergen sie die Möglichkeit sich sogar bei Raumtemperatur in ihren quantenmechanischen Grundzustand kühlen zu lassen. In dieser Arbeit untersuchen wir diese neuartigen Systeme aus zwei verschiedenen Blickwinkeln, die sich in der Gliederung in **Theorie** und **Protokolle** widerspiegeln.

Im ersten Teil leiten wir eine konsistente theoretische Beschreibung für Optomechanik mit schwebenden Dielektrika her. Wir entwickeln eine Master-Gleichung, die die Wechselwirkung zwischen Licht und dielektrischen Objekten beliebiger Größe und Form beschreibt. Sie berücksichtigt sowohl die quantisierte Bewegung des Dielektrikums, als auch die quantenmechanische Beschreibung von Licht. Die Streuung von Photonen wird in allen Ordnungen der Störungstheorie berechnet, was eine Analyse ermöglicht, die über die Punktteilchen-Näherung hinausgeht. Dieser Formalismus erweitert den Standard-Ansatz für Master-Gleichungen durch die Einbeziehung der Wechselwirkung verschiedener Moden der Umgebung. Dies führt zu einer quantenmechanischen Beschreibung, in der Renormierungskorrekturen und Dekohärenzraten vorausgesagt werden können. Wir wenden diesen allgemeinen Formalismus auf den Spezialfall schwebender Nano-Kugeln in optischen Resonatoren an. Dabei berücksichtigen wir neben der Streuung von Photonen verschiedene weitere Dekohärenz-Mechanismen wie beispielsweise die Streuung von Gasmolekülen, Schwarzkörperstrahlung, oder die Kopplung an Vibrationsmoden, und vergleichen diese mit den kohärenten Kopplungskonstanten des Systems. Um zu untersuchen ob die Nano-Kugeln in den Grundzustand gekühlt werden können, leiten wir die Phonenzahl der stationären Zustände des Systems her, ohne uns dabei der herkömmlichen Seitenband-Näherung zu bedienen. In diesem Rahmen zeigen wir, dass es möglich ist die Schwerpunktsmode (cm) von Kugeln mit Radien  $R \lesssim 260$  nm in den Grundzustand zu kühlen.

Der Fokus des zweiten Teils der Arbeit liegt darauf, Protokolle zur Präparation des nano-mechanischen Oszillators in nicht-klassischen Zuständen vorzuschlagen und zu analysieren. Die Erzeugung solcher Zustände ist ausschlaggebend für die Realisierung vieler der vorgesehenen Anwendungen optomechanischer Oszillatoren. Wir gehen dieses Problem aus drei verschiedenen Richtungen an. Erstens schlagen wir mehrere Protokolle vor, die auf der effizienten Kopplung einzelner Photonen an den mechanischen Oszillator beruhen und den nicht-klassischen photonischen Zustand auf den mechanischen übertragen. Diese Protokolle benötigen unterschiedliche Kopplungsstärken und können somit in verschiedenen Parameter-Bereichen implementiert werden. Zweitens untersuchen wir die Möglichkeit den mechanischen Oszillator durch den optischen Resonator an ein Qubit, beispielsweise ein Zwei-Niveau-Atom, zu koppeln und so in einem nicht-klassischen Zustand zu präparieren. Insbesondere präsentieren wir eine Methode mit deren Hilfe der mechanische Oszillator mit hoher Wahrscheinlichkeit dissipativ in einem stationären nicht-klassischen Zustand präpariert werden kann. Weiterhin zeigen wir, dass dieses Setup, wenn es stroboskopisch angetrieben wird, ein nichtlineares Vielteilchenteilchen-System darstellt und demonstrieren die Effektivität der Protokolle zur Präparation nicht-klassischer Zustände auch in diesem Fall. Die Methoden sowohl der Einzel-Photon-Protokolle als auch der dissipativen Präparation mit Hilfe von Qubits sind nicht auf schwebende Nano-Kugeln beschränkt, sondern können auf beliebige optomechanische Systeme angewendet werden. Drittens schlagen wir ein Protokoll vor, das auf der konkreten Implementierung mit schwebenden Nano-Dielektrika basiert. Wir diskutieren eine optomechanische Version des Doppelspaltversuches. Durch die Kombination von Techniken und Erkenntnissen aus der Optomechanik und der Materiewellen-Interferometrie ermöglicht es diese Methode, die Vorhersagen von Kollapsmodellen in einem bisher unerreichten Parameterbereich experimentell zu überprüfen.

Zusammenfassend ist es das Ziel dieser Arbeit, zur Weiterentwicklung der Optomechanik mit schwebenden Nano-Objekten in optischen Resonatoren beizutragen, indem wir sowohl ein theoretisches Fundament als auch mehrere Protokolle zur Präparation nicht-klassischer Zustände entwickeln.

# Publications

## Publications and preprints related to this thesis

1. **Master-equation approach to optomechanics with arbitrary dielectrics**  
*A. C. Pflanze, O. Romero-Isart, J. I. Cirac.*  
Phys. Rev. A **86**, 013802 (2012), See Chapter 2
2. **Optically levitating dielectrics in the quantum regime: Theory and protocols**  
*O. Romero-Isart<sup>1</sup>, A. C. Pflanze<sup>1</sup>, M. L. Juan, R. Quidant, N. Kiesel, M. Aspelmeyer, and J. I. Cirac.*  
Phys. Rev. A **83**, 013803 (2011), See Chapter 3&4
3. **Large Quantum Superpositions and Interference of Massive Nanometer-Sized Objects**  
*O. Romero-Isart, A. C. Pflanze, F. Blaser, R. Kaltenbaek, N. Kiesel, M. Aspelmeyer, and J. I. Cirac.*  
Phys. Rev. Letters **107**, 020405 (2011), See Chapter 5
4. **Optomechanics assisted with a qubit: From dissipative state preparation to many-body physics**  
*A. C. Pflanze, O. Romero-Isart, J. I. Cirac.*  
Phys. Rev. A **88**, 033804 (2013), See Chapter 6

## Other publications not included in this thesis

5. **Inter-species Tunneling in One-dimensional Bose Mixtures.**  
*A. C. Pflanze, S. Zöllner, P. Schmelcher.*  
Phys. Rev. A **81**, 023612 (2010)
6. **Material-barrier Tunneling in One-dimensional Few-boson Mixtures.**  
*A. C. Pflanze, S. Zöllner, P. Schmelcher.*  
J. Phys. B: At. Mol. Opt. Phys. **42**, 231002 (2009)

---

<sup>1</sup>These authors contributed equally



# Contents

<b>Abstract</b>	<b>i</b>
<b>Zusammenfassung</b>	<b>ii</b>
<b>Publications</b>	<b>v</b>
<b>1 Introduction</b>	<b>1</b>
1.1 Optomechanics: Quantum mechanics at unprecedented length scales . . .	1
1.2 Optomechanics with levitating dielectrics . . . . .	3
1.3 State preparation protocols for Optomechanics . . . . .	5
1.4 Outline of this thesis . . . . .	7
<b>I Theory of levitating dielectrics</b>	<b>11</b>
<b>2 Master equation for the light-matter interaction of dielectrics</b>	<b>13</b>
2.1 Introduction . . . . .	13
2.1.1 Reader's guide . . . . .	14
2.2 Physical model and Hamiltonian . . . . .	15
2.2.1 Assumptions . . . . .	15
2.2.2 Hamiltonian . . . . .	16
2.3 Master equation for arbitrary dielectrics . . . . .	19
2.3.1 Solution of the scattering equations for the free field . . . . .	20
2.3.2 General master equation for the cavity and the center-of-mass mode . . . . .	23
2.3.3 Master equation for the optomechanical setup . . . . .	25
2.4 The small-particle limit . . . . .	29
2.4.1 General master equation . . . . .	29
2.4.2 Master equation for the optomechanical setup . . . . .	30
2.A The classical approach . . . . .	31

2.B	Wigner-Weisskopf with correlations in the field . . . . .	32
2.B.1	Free photons . . . . .	33
2.B.2	Cavity field . . . . .	34
2.C	Mie scattering theory . . . . .	37
2.C.1	Expansion of the incoming electric field in terms of spherical harmonics . . . . .	37
2.C.2	Determination of the fields due to the boundary conditions . . . . .	39
2.C.3	Determination of the scattering cross section . . . . .	40
<b>3</b>	<b>Cavity-optomechanics with levitating spheres</b>	<b>41</b>
3.1	Introduction . . . . .	41
3.1.1	Reader's guide . . . . .	42
3.2	Cavity quantum-optomechanics with levitating spheres . . . . .	42
3.3	Cooling . . . . .	46
3.4	Quantum elasticity . . . . .	49
3.4.1	Vibrational eigenmodes . . . . .	49
3.4.2	Effect of the external potential . . . . .	53
3.4.3	Coupling to vibrational modes as a source of decoherence . . . . .	54
3.5	Other sources of decoherence . . . . .	55
3.5.1	Position-localization decoherence . . . . .	56
3.5.2	Scattering of air molecules . . . . .	58
3.5.3	Blackbody radiation . . . . .	59
3.5.4	Photon shot noise . . . . .	61
3.5.5	Fluctuations in the trap center . . . . .	61
3.5.6	Anisotropies in the sphere . . . . .	62
3.5.7	Coupling to two-level systems . . . . .	63
3.6	Results for given experimental parameters . . . . .	63
3.A	Justification of the adiabatic elimination of the vibrational modes . . . . .	66
<b>II</b>	<b>State preparation protocols for optomechanics</b>	<b>69</b>
<b>4</b>	<b>Single-Photon Protocols</b>	<b>71</b>
4.1	Introduction . . . . .	71
4.1.1	Reader's guide . . . . .	72
4.2	The setup . . . . .	73
4.2.1	The output field . . . . .	73
4.2.2	The displaced frame . . . . .	74
4.3	One-photon reflected . . . . .	77

4.4	Time-modulated coupling . . . . .	83
4.5	Teleportation . . . . .	87
4.6	Tomography . . . . .	90
4.A	Displacement of the output modes . . . . .	93
4.A.1	Steady-state with a driving field . . . . .	94
4.A.2	Measurement of a photon . . . . .	95
4.A.3	Switching off the driving field . . . . .	96
<b>5</b>	<b>State preparation assisted with a qubit</b>	<b>99</b>
5.1	Introduction . . . . .	99
5.1.1	Reader's guide . . . . .	100
5.2	The setup . . . . .	100
5.3	Dissipative dynamics . . . . .	102
5.3.1	Perturbation theory for degenerate Liouvillians . . . . .	103
5.3.2	Steady state with noise . . . . .	104
5.3.3	Steady state with an engineered environment . . . . .	107
5.3.4	Insights from perturbation theory . . . . .	108
5.4	Coherent dynamics . . . . .	110
5.5	Many-partite system . . . . .	111
5.5.1	State preparation of the many-partite system . . . . .	112
5.5.2	Coherent state preparation of $N$ mechanical oscillators . . . . .	114
<b>6</b>	<b>Large spatial quantum superpositions</b>	<b>117</b>
6.1	Introduction . . . . .	117
6.1.1	Reader's guide . . . . .	118
6.2	The protocol . . . . .	119
6.2.1	Step (a): Preparation of the initial state . . . . .	119
6.2.2	Step (b): Expansion of the wave function . . . . .	121
6.2.3	Step (c): The optomechanical double slit . . . . .	122
6.2.4	Step (d): The interference pattern . . . . .	125
6.3	Decoherence . . . . .	126
6.3.1	Coherence length . . . . .	126
6.3.2	Reduction of the visibility . . . . .	128
6.3.3	Standard decoherence . . . . .	128
6.3.4	Operational regime . . . . .	130
6.4	Applications: testing collapse models . . . . .	132
6.4.1	The CSL model . . . . .	132
6.4.2	Gravitationally-induced decoherence . . . . .	134

7	Conclusion and Outlook	137
8	List of parameters	141
	Bibliography	149

# Chapter 1

## Introduction

### 1.1 Optomechanics: Quantum mechanics at unprecedented length scales

This year we celebrate the 100th anniversary of the Bohr model [1], the first atomic model containing elements of quantum mechanics. In the model's derivation, Bohr gave up on several laws of classical mechanics, realizing that this theory alone was insufficient to explain the atom's stability. Today, the model embodies the paradigm shift that the evolution of quantum mechanics brought along – the theory has come a long way since then. While the beginning of the century was characterized by establishing the mathematical background of the theory and understanding its fundamental aspects [2–4], formerly purely theoretical models became accessible in the laboratory in recent years. After achieving the probably most successful technological invention of the laser in the 1950s [5,6], today novel technologies based on quantum phenomena promise to change several disparate fields. Among these, computation [7–9], telecommunication [10], cryptography [11], and metrology [12] are the most prominent examples.

Despite the rapid advances of quantum technologies, some fundamental questions have remained elusive since the early days mentioned above. Namely, the fact that while quantum mechanics gives the right description of the microscopic world, it is obviously not the right theory for macroscopic objects, has raised dispute over the years. This is illustrated most vividly in Schrödinger's famous cat paradoxon [13], and the realization of macroscopic objects in quantum states has been a long outstanding research goal in modern physics. The observation of quantum effects at a macroscopic scale would help finding the answer to such questions as: Why does the world of our every-day experience appear to behave classical, not quantum-mechanically? Is there a fundamental size limit for quantum-mechanical behavior? Can a possible quantum nature of macroscopic objects be used for technological applications?

During the past decades important advances in answering these questions experimentally have been made by seminal matter-wave interferometry experiments [14]. While interference with electrons [15], neutrons [16], and small dimers [17] has been implemented at the beginning of the last century, only recent years brought the demonstration of the wave-nature of even nanometer-sized objects [18, 19]. Besides revealing quantum-mechanical behavior at unprecedented length scales, these experiments also supported the standard quantum theory of decoherence and dissipation, developed by Leggett [20, 21], Joos and Zeh [22], and Zurek [23], among others.

Today, another promising candidate for the realization of quantum effects at a macroscopic scale are mechanical oscillators. Reduced to its essential, an optomechanical system is an optical or microwave cavity containing a mechanical element that supports oscillations (phonons) and interacts with the photons of the cavity. The earliest such systems, albeit at a very different length scale from what is used today, were the gravitational wave detectors developed in the 1970s and 1980s [24–26]. The realization that measurement and manipulation of macroscopic objects at their quantum limit was possible [27], led to the exploration of these phenomena in numerous table-top-experiments. This evolution has been advanced by technological progress in two distinct fields: on the one side, nano-science and semiconductor industries have developed processing technologies and novel materials enabling the fabrication of ultra-sensitive mechanical devices [28]. On the other side, in the field of quantum optics, and in particular cavity-quantum-electrodynamics, improvements on optical cavities as well as an improved understanding of light-matter interactions resulted in an unprecedented control over quantum-mechanical states [29]. The combination of these disciplines and the recent advances therein have led to quantum control over mechanical oscillators in optomechanical devices (see [30–33] for some reviews).

Today, there is an enormous variety of experimental implementations on different length scales. Among others, these range from implementations with atomic clouds [34–36], micromirrors [37], membranes in an optical cavity [38], to microtorroids [39], nanoscale waveguides with both an optical and a mechanical resonance [40], electromechanical systems [41, 42], and piezoelectric resonators [43]. Essential to any observation of quantum-mechanical behavior is the preparation of pure states. This is the case at low temperatures, and thus a preparation of the mechanical oscillator in the coldest state achievable, its ground state, is desirable. It has been theoretically predicted that ground-state cooling of a mechanical oscillator is indeed possible [44–48] by using the radiation pressure exerted by the photons on the mechanical structure. The technique relies on resolved sidebands, illustrating the close similarity between optomechanics and other quantum-optical systems [49]. Based on this, ground-state cooling has been realized experimentally in some of the above-mentioned systems. The first demonstra-

tion has been achieved in 2010, and did not rely on the interaction with light, but was implemented using a mechanical oscillator with such high oscillations frequencies that its ground state was reached at temperatures around 25 mK, accessible to conventional dilution refrigerators [43]. The second setup to realize ground-state cooling was an aluminum membrane tightly coupled to a superconducting microwave cavity that was prepared in its ground state by sideband cooling [50]. In the same year, the ground state was reached in a nanoscale waveguide [40], the first demonstration of optomechanical cooling. Very low phonon numbers have also been achieved in other systems, so that direct coupling between photons and phonons can be witnessed [51].

The experimental realization of the ground state has indeed demonstrated that these macroscopic oscillators reveal quantum-mechanical behavior when sufficiently isolated from the environment. The proposed applications are diverse and range from using the mechanical systems as quantum transducers [52–55], building ultra-high sensitivity detectors exploiting quantum metrology [56–59], to proposals for fundamental tests of quantum mechanics [60–63]. The two main challenges in realizing these goals are:

- An improved isolation of the mechanical oscillator from its environment to achieve longer coherence times.
- The realization of nonlinearities required for the preparation of superposition states, essential to many of the desired applications.

In the following two sections, we will further describe these challenges and outline possible solutions.

## 1.2 Optomechanics with levitating dielectrics

Achieving longer coherence times is one of the most urgent goals in the research field of optomechanics. They are required for essentially any application of the optomechanical system, such as state preparation [60, 61, 64], or metrology [56–59]. One crucial requirement for long coherence times is good isolation from the environment. In general, the interaction of a quantum system with its environment creates entanglement between the small system and its surrounding, leading to a decay of coherence and a loss of quantum-mechanical behavior in the small system [65]. Due to their increased size as compared to *e.g.*, atomic systems, nanomechanical resonators consist of many more atoms that couple to the environment resulting in decreased coherence times. In addition, in most optomechanical systems the mechanical oscillator is unavoidably attached to its suspension providing a thermal contact that prevents longer coherence times [66–71].

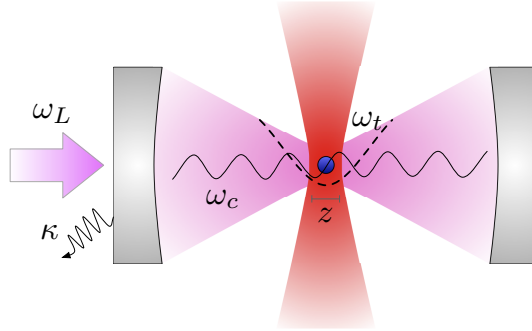


Figure 1.1: Schematic representation of the setup. A nanodielectric is confined by optical tweezers which provide a trapping frequency of  $\omega_t$ . The nanodielectric is placed inside an optical cavity with resonance frequency  $\omega_c$ , decay rate  $\kappa$ , and is driven by a laser at a frequency  $\omega_L$ .

A potential improvement to better isolate the system is to avoid its direct attachment to the thermal environment and provide the spring force for the mechanical oscillator by other means. One possibility to achieve this is to rely on optical methods *i.e.*, optical levitation with lasers. The field of optical trapping and manipulation of small neutral particles using the radiation pressure force was founded in 1970 by the seminal experiments of Ashkin [72]. Over the course of the next 40 years, the techniques of optical trapping and manipulation have stimulated revolutionary developments in the fields of atomic physics, biological sciences, and chemistry [73]. In physics, the progress in optical cooling and manipulation of single atoms opened up a plethora of novel perspectives. The precise control over the atomic degrees of freedom has created applications ranging from atom interferometry [74], quantum simulations of condensed-matter systems with ultracold gases [75], to the implementation of quantum gates for quantum-computation purposes [76].

The system proposed to implement the optical trapping are optically levitated dielectrics [77, 78] (see also [64, 79, 80]). In particular, the setup consists in optically trapping a nanodielectric by means of optical tweezers inside a high-finesse optical cavity, see Fig. 1.1 for an illustration. Due to the absence of clamping losses [66–70] the levitation allows for a very good thermal isolation and it will be shown in this thesis that this enables ground-state cooling even at room temperature. From a broader perspective using optically levitated dielectrics as a cavity-optomechanical system aims at extending the techniques developed during the last decades of optical cooling and manipulation of atoms (*e.g.*, like in cavity QED with single atoms and molecules [81–84]), back to the nanodielectrics that were first used in the early times of optical trapping [85–87].

After the original proposals [77, 78] for the setup, there has been wide experimental and theoretical progress in this direction. Part of this thesis is dedicated to providing a theoretical description of the system as a basis for further applications. More specifically, we focused on a better understanding of the theory of optomechanics with levitating dielectrics in [64], and in particular the light-matter interactions of dielectrics beyond the point-particle approximation in [88] (see Chap. 2 and Chap. 3). During the past years, several alternated setups, such as levitation of micromirrors [80], or nanodumbbells [89], and even alternative cooling techniques, such as Doppler cooling of a microsphere [79], have been proposed. Modified systems, using a loosely-clamped membrane instead of a fully-levitated object have been investigated both theoretically [90] and experimentally [91]. Moreover, diverse applications for levitated nanospheres have been studied, among these detection of single molecules [92], using them as force detectors at small length scales [93], their potential to test foundational questions such as collapse models [61, 62], or using them as detectors for gravitational waves [94]. Furthermore, there have even been proposals to use levitating nanospheres in space experiments [95].

There has also been remarkably broad experimental progress: After measuring the instantaneous velocity of the Brownian motion of a  $\mu\text{m}$ -sized particle in air [96], the same group reported feedback cooling of these glass beads in vacuum [97]. A similar direction is taken by [98], and [99, 100], where feedback cooling of nanometer-sized particles has been demonstrated. Recent experiments even reported on the implementation of a cavity in the nanomechanical system [101]. With the proposal of levitating dielectrics, also the fields of optomechanics and matter-wave-interferometry begin to overlap and stimulate each other increasingly [102]. This wide range of experiments and methods illustrates the evolution of a new generation of exciting experiments, aiming at bringing levitating dielectrics into the quantum regime. By bridging the gap between atomic physics and conventional nanomechanical resonators, they hold the promise to realize quantum mechanics in an entirely novel parameter regime.

### 1.3 State preparation protocols for Optomechanics

The achievement of ground-state cooling [40, 43, 50] constitutes a milestone for the field of optomechanics. Nevertheless, the ground state of a harmonic oscillator is a Gaussian state, which is similar to classical states. A state is called Gaussian if its characteristic function, or equivalently its Wigner function are Gaussian [103]. Some examples of Gaussian states are the vacuum state, thermal states or squeezed states. At the same time, the so-called Gaussian unitaries are operations that preserve the Gaussian character of the state. The Hamiltonians and Lindbalds forming the class of Gaussian

transformations are at most quadratic in the field operators. With its positive Wigner function, a Gaussian state is very different from the superposition states envisaged by Schrödinger in his cat paradox [13]. The preparation of non-Gaussian states is essential for most applications of nanomechanical oscillators, namely for metrology [56–58, 66, 93], quantum-information processing [104], quantum simulations [105], or fundamental tests of the foundations of quantum mechanics [60, 61, 63, 106].

This leads to the basic question of why it is so hard to realize non-Gaussian states in nanomechanical systems. In optomechanics, the initially prepared state has a Gaussian form and all Hamiltonians are linear in the couplings – precisely the setting for Gaussian states described above. Although there even exists an intrinsic nonlinearity of the optomechanical interaction at the single-photon level, the resulting couplings are usually very small [40, 51]. In most setups, the single-photon interactions are thus enhanced by strongly driving the light field [30, 31] at the price of rendering all couplings linear. Consequently, the resulting Hamiltonians are at most quadratic in the field operators and do not alter the character of an initially Gaussian state. There are several strategies to circumvent this problem. In principle, non-Gaussianities can either be achieved by

- introducing a nonlinear interaction in the Hamiltonian, or
- coupling to an auxiliary system which is in a non-Gaussian state.

Following the first strategy, in optomechanics, nonlinear interactions can be realized by increasing the single-photon coupling strength [53, 107, 108]. While this is certainly a promising path, recent experiments still require an improvement by several orders of magnitude to reach the regime where the effect of single-photon coupling can be useful [40]. Other proposals to realize nonlinearities are based on the behavior near the critical strain [109], applying inhomogeneous electrostatic fields to the oscillator [110, 111], or positioning the mechanical oscillator in the quadratic instead of the linear part of the standing wave in the cavity [61, 62].

Following the second strategy means to couple the mechanical oscillator to an auxiliary system that can be easily prepared in a non-Gaussian state. Already in the early days of this research area, several groups proposed to create non-classical states of a movable mirror [112–114] by coupling it to single photons. The idea behind these proposals is to use the optomechanical interaction to entangle a small quantum system in a non-Gaussian state with the macroscopic object. By observing the state of the small quantum system, the creation and loss of the non-classical state in the macroscopic system can be monitored. This idea was also used in the theoretical [115] and experimental [43] studies where the coupling between a micromechanical resonator

and a Cooper pair box was used to prepare entanglement between the quantum system (Cooper pair box) and the cantilever. Possible other candidates are quantum dots [116], an intrinsic two-level defect [117] or an atom's internal degrees of freedom [118]. Coupling to the atomic motion has been proposed [119] and even recently demonstrated experimentally [120] for a cloud of ultracold atoms.

In summary, progress has been made on the implementation of non-Gaussian states in optomechanics. However, their efficient experimental realization remains one of the most urgent goals in the field. Moreover, the spatial superposition size of these states is typically on the subatomic length scale. This raises the question for the right definition of macroscopic superposition states: is it more important to achieve larger superposition sizes with smaller objects or small superpositions with larger objects? There has been an extended discussion on this topic [121–126], but a general definition of macroscopicity remains elusive and the usefulness of the various definitions depends on the envisaged application. In this thesis, we propose a scheme to prepare superpositions of nanomechanical oscillators on the order of their own size in Chap. 6 (*i.e.*, large superpositions of large objects) by combining methods from matter-wave interferometry with nanomechanical oscillators.

## 1.4 Outline of this thesis

The goal of this thesis is to advance the theoretical understanding of optomechanics with levitating dielectrics by providing the theoretical background of this novel setup and proposing protocols to prepare superposition states. We approach this topic from two different angles reflected in the division of the thesis into the main blocks of **Theory** and **Protocols**. In the Theory part, we derive a master-equation description for levitating dielectrics in optical cavities from first principles. For this purpose, in Chap. 2, we combine techniques from scattering theory with quantum master equations and take into account the quantum motion of the object, the quantum nature of light, and scattering processes to all orders. This extends the standard approach of master equations to the regime where interactions between the different environmental modes are taken into account, necessary when going beyond the point-particle approximation. In Chap. 3, this master equation is applied to the particular setup of levitating dielectric spheres in optical cavities. We derive all optomechanical parameters including the most prominent decoherence mechanisms. To complete the analysis, cooling of general Gaussian systems without relying on sideband techniques is discussed. Combining these two approaches, we show that ground-state cooling is possible for small spheres fulfilling  $R \lesssim 260$  nm.

This forms the basis for the second part of the thesis which is focussed on protocols

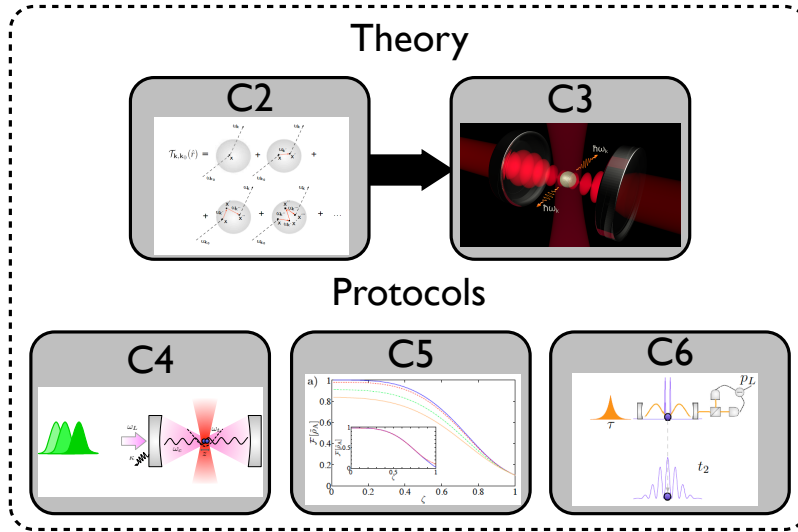


Figure 1.2: Graphical illustration of the structure of this thesis: optomechanics with levitating dielectrics is analyzed from two different perspectives. The main division is between theory and protocols. We start with a general approach to describe the light-matter interaction of dielectrics with light in Chap. 2. This is followed by Chap. 3, where the theory is applied to levitating dielectric spheres in an optical cavity. The second part on protocols contains three different approaches to the preparation of nonclassical states. Chap. 4 is based on coupling a single photon to the cavity-optomechanical system. Chap. 5 proposes to couple a mechanical oscillator to a qubit via the cavity mode and relies on dissipative state preparation. Finally, in Chap. 6, we show how to prepare the mechanical oscillator in large spatial superpositions.

for the preparation of non-Gaussian states in optomechanical systems. The urgency of this goal has been outlined in Sec. 1.3 and we propose three different angles to confront the challenge. Chap. 4 proposes to exploit single photons as a source of non-Gaussianity. In order to enhance the weak coupling between single photons and the optomechanical structure, the cavity is strongly driven. Three different approaches based on this fundamental idea are investigated: first, coupling a single-photon pulse on top of the driving field into the optomechanical cavity followed by a measurement of the reflected part of the photon. Second, in order to circumvent the measurement of the single photon, the cavity is modulated time-dependently, thus allowing for a perfect coupling of the pulse into the cavity. Third, the last protocol exploits teleportation in the bad-cavity limit to imprint the non-Gaussian state on the mechanical resonator.

While decoherence needs to be avoided during these protocols, we propose a dissipation-

based approach in Chap. 5. It promotes to couple the mechanical resonator to an intrinsically non-Gaussian two-level system. The latter enables the preparation of the mechanical-oscillator in a non-Gaussian steady state through the fast decay of the cavity. We extend this approach to many-partite systems, where we also investigate the possibility of coherent state preparation.

Both of the approaches described in Chap. 4 and Chap. 5 are applicable to any opto- or electromechanical system and do not rely on a particular implementation with levitated dielectrics. On the contrary, the last method for state preparation described in Chap. 6 relies on the flexibility of the trapping frequency and thus the levitation of the dielectric object. An optomechanical double slit is proposed that prepares the dielectric in a large spatial superposition on the order of its own size. This allows for possible tests of some of the most paradigmatic collapse models [127].

In combination, the two parts of this thesis provide both the theoretical background to utilize levitating dielectrics as optomechanical systems as well as protocols to prepare nonclassical states offering the opportunity to challenge quantum mechanics at unprecedented length scales. The thesis is concluded by an outlook and discussion of further directions in Chap. 7.



## Part I

# Theory of levitating dielectrics



## Chapter 2

# Master equation for the light-matter interaction of dielectrics

*We present a master equation describing the interaction of light with dielectric objects of arbitrary sizes and shapes. The quantum motion of the object, the quantum nature of light, as well as scattering processes to all orders in perturbation theory are taken into account. This formalism extends the standard master-equation approach to the case where interactions among different modes of the environment are considered. This is necessary when the interaction between dielectrics beyond the point-particle approximation and light is considered. We combine methods from scattering theory with quantum master equations yielding a genuine quantum description, including a renormalization of the couplings and decoherence terms. The small-particle limit within the Born-Markov approximation is recovered when neglecting interactions among the environmental modes. This chapter mainly bases on and uses parts of [88].*

### 2.1 Introduction

In quantum optomechanics, light is used to cool and control the mechanical motion of massive objects in the quantum regime [30, 31, 128, 129]. In the broad research area of cavity quantum optomechanics two classes of systems can be distinguished: the reflective case, realized in deformable Fabry-Pérot resonators [130, 131] or microtoroidal cavities [39], and the dispersive case, like in the membrane-in-the-middle configuration [38, 91, 132] or in optically levitating nano-dielectrics [64, 77, 78, 99, 133]. In the latter, the dimension of the object along the cavity axis (*i.e.*, the width of the membrane or the diameter of the nanosphere) is typically much smaller than the optical wave-

length. This implies that the dielectric can be treated as a dipole with some induced polarizability [64,78]. The problem is akin to that of single point particles, like atoms or ions, in the weak excitation regime. Thus, the theory and methods that have been developed in the context of laser cooling, trapping, and manipulation of single atoms and ions can be directly applied to optomechanical systems (see, *e.g.*, [49,134,135] for some expository articles). In particular, sideband-cooling techniques [45,47] have been successfully employed to achieve the ground state in a nano-optomechanical system [40,51] (see also [43,50]).

The control that is being achieved in dispersive quantum optomechanics opens up the challenge to explore the physics of larger objects. While this is certainly within experimental reach [97], the existing quantum theories are not applicable since the dielectric object can no longer be considered as a simple dipole. In contrast, for sizes comparable or larger than the optical wavelength, multi-scattering processes within the dielectric have to be taken into account. As it is well-known from classical nano-photonics, they give rise to a modification of the forces experienced by the system, as well as other interesting phenomena [136].

In this chapter, we present a quantum theory describing the interaction of light with the center-of-mass of non-absorbing dielectrics of arbitrary shapes and sizes. In particular, we derive a master equation for the motion of the particle and the cavity mode. This method considers the full scattering process by linking the coefficients of the master equation to the scattering matrix. It does not rely on the point-particle approximation, but takes higher orders of the scattering process into account.

This allows one to use the tools and techniques developed in the context of classical nano-photonics to determine the evolution of the quantum system. These include advanced numerical techniques, like the discrete-dipole approximation [137], the T-matrix method [138], or, for some special geometrical shapes, even analytical solutions, like the so-called Mie solution [139–141]. We compare these results to a description within an extended Wigner-Weisskopf approach. While this general theory is applicable for arbitrary dielectrics, we demonstrate that it simplifies for small objects, and correlations between different modes can be neglected.

### 2.1.1 Reader's guide

The chapter is organized as follows: In Sec. 2.2, we describe the system, list the assumptions and define the Hamiltonian. Following this, we present the main result of this chapter in Sec. 2.3: a master equation describing the interaction between light and the motion of arbitrary dielectric objects. First, the effect of the presence of a dielectric on a free electromagnetic field is discussed in Sec. 2.3.1, where the corresponding

scattering equations are solved. Based on this, we derive a general master equation describing the joint dynamics of the cavity mode and the center-of-mass motion of a dielectric in Sec. 2.3.2. An analogous derivation of the equations of motion within an extended Wigner-Weisskopf approach is given in App. 2.B. The description of the optomechanical setup is obtained by assuming the Lamb-Dicke regime and a strong driving field in Sec. 2.3.3. The chapter is rounded off in Sec. 2.4 by a discussion of the small-particle limit.

## 2.2 Physical model and Hamiltonian

In this section we describe the system consisting of a dielectric object interacting with one or several confined electromagnetic modes. We discuss the assumptions that are taken and derive the complete Hamiltonian.

### 2.2.1 Assumptions

In this description of the interaction between a dielectric with a center-of-mass position  $\hat{r}$  and a photonic field, the following assumptions are taken:

1. The object has a volume  $V$ , a density distribution  $\rho$ , and a mass  $M = \rho V$ . Note that the density distribution is assumed to be homogeneous for simplicity. In contrast to the common assumption, see *e.g.* [64], we do not restrict the size of the dielectric to the sub-wavelength scale of the light field, but allow for arbitrary sizes.
2. The relative dielectric constant  $\epsilon_r$  is assumed to be homogeneous. The permeability of the object  $\mu$  is chosen to be equal to the vacuum permeability,  $\mu = \mu_0$ , which is a good approximation for the dielectric objects we are mainly interested in.
3. As we will show in Sec. 3.4, the center-of-mass (cm) mode of dielectrics at the micron-scale is decoupled from the vibrational ones. Hence, we will only consider the motion of the cm degree of freedom  $\hat{r}$  and neglect its coupling to vibrational modes.
4. We assume the dielectric constant of the object to be real, *i.e.*, no absorption effects are taken into account. In the language of scattering theory, this signifies that only elastic scattering processes are accounted for. The effect of a nonvanishing absorption is studied in Sec. 3.5.3.

5. Throughout this chapter, we assume the electromagnetic field to be scalar and neglect polarizations for a better readability of the equations. The derivations for polarizations can be carried out in full analogy. We use the results including polarizations in the analysis of cavity optomechanics with levitating spheres in Sec. 3.2.
6. We assume that all photons are scattered into the bath modes. This is a valid assumption for geometries that do not fit the cavity's geometry like, *e.g.*, spheres, whereas for membranes the scattering into the cavity mode has to be taken into account [90].

### 2.2.2 Hamiltonian

The Hamiltonian consists of three parts,

$$\hat{H}_{\text{tot}} = \hat{H}_{\text{M}} + \hat{H}_{\text{L}} + \hat{H}_{\text{LM}} : \quad (2.1)$$

the cm motion of the dielectric is described by  $\hat{H}_{\text{M}}$ , the energy of the electromagnetic field by  $\hat{H}_{\text{L}}$ , and the interaction between the light and matter is given by  $\hat{H}_{\text{LM}}$ . For the master-equation description that we want to pursue in the proceeding, it is useful to divide the total Hamiltonian into

$$\hat{H}_{\text{tot}} = \hat{H}_{\text{S}} + \hat{H}_{\text{B}} + \hat{H}_{\text{BS}}, \quad (2.2)$$

where  $\hat{H}_{\text{S}}$  denotes the Hamiltonian describing the system,  $\hat{H}_{\text{B}}$  denotes the part describing the bath and  $\hat{H}_{\text{BS}}$  the coupling between the two. Each of these terms will be defined in the following.

#### The kinetic energy

The motion of the free untrapped dielectric is described by  $\hat{H}_{\text{M}} = \hat{p}^2/(2M)$ , where  $\hat{p}$  denotes the momentum operator of the cm coordinates in the direction we are interested in. While the dielectric object we investigate may have an arbitrary three-dimensional shape, we consider only its motion in one dimension. Due to the harmonicity of the trap, the coupling between the different directions can be neglected. Nevertheless, in many cases it might still be necessary to control the motion in the other directions, *e.g.*, via feedback cooling [92]. In particular for linear or quadratic potentials, also the coupling to internal vibrational modes of the sphere can be neglected. In the absence of an additional external potential, the Hamiltonian can be diagonalized in the basis of the vibrational eigenmodes. Adding an external potential leads to some coupling between the cm degree of freedom and the vibrational modes. The frequency of the

vibrational eigenmodes is roughly given by  $\omega_n \propto n c_{\text{sound}}/R$ , where  $c_{\text{sound}}$  denotes the sound velocity and  $R$  the extension of the dielectric. For micron-scale objects it is several orders of magnitude larger than the trapping frequencies typically achieved for the cm degree of freedom. This enables one to adiabatically eliminate the vibrational modes merely leading to a negligible renormalization of the system's energy. A detailed discussion using a theory of quantum elasticity can be found in Sec. 3.4.

### The energy of the free electromagnetic field

The energy of the free electromagnetic field is described by

$$\hat{H}_L = \frac{1}{2} \int d\mathbf{x} \left[ \epsilon_0 \hat{E}_{\text{tot}}^2(\mathbf{x}) + \frac{\hat{B}_{\text{tot}}^2(\mathbf{x})}{\mu_0} \right], \quad (2.3)$$

where  $\epsilon_0$  denotes the vacuum permittivity,  $\hat{E}_{\text{tot}}$  the electric field and  $\hat{B}_{\text{tot}}$  the magnetic one. The total electromagnetic field can be divided into a part containing the continuous modes and one or several confined modes. The continuous part is defined as

$$\hat{E}_B(\mathbf{x}) = \frac{i}{(2\pi)^{3/2}} \int d\mathbf{k} \sqrt{\frac{\omega_{\mathbf{k}}}{2\epsilon_0}} (\hat{a}_{\mathbf{k}} e^{-i\mathbf{k}\mathbf{x}} - \text{H.c.}), \quad (2.4)$$

where the label  $B$  signifies that this continuum of plane-wave modes will generally be treated as a bath. The different modes are characterized by the annihilation (creation) operators  $\hat{a}_{\mathbf{k}}$  ( $\hat{a}_{\mathbf{k}}^\dagger$ ) with a mode frequency  $\omega_{\mathbf{k}}$  and a wave vector  $\mathbf{k}$ , where we will denote  $k = |\mathbf{k}|$ . Note that we set  $\hbar = 1$  throughout this thesis. In the next step we define a confined mode of the electromagnetic field with annihilation (creation) operator  $\hat{a}_0$  ( $\hat{a}_0^\dagger$ ), mode frequency  $\omega_0$ , mode volume  $V_0$  and a mode profile given by  $f(\mathbf{x})$ . Typically it describes a mode in a cavity subject to some boundary conditions. We label this inhomogeneous part of the electromagnetic field  $S$  (for system), it is given by

$$\hat{E}_S(\mathbf{x}) = i \sqrt{\frac{\omega_0}{2\epsilon_0 V_0}} (\hat{a}_0 f(\mathbf{x}) - \text{H.c.}). \quad (2.5)$$

The extension to several inhomogeneous modes can be achieved in an analogous fashion.

### Light-matter interaction

The most interesting part of the Hamiltonian describes the interaction between the dielectric and the electromagnetic field. The response of the object's polarization is assumed to be linear to the electric field, which is fulfilled for the typical light intensities considered in this manuscript. The interaction Hamiltonian is given by

$$\hat{H}_{\text{LM}} = -\frac{1}{2} \int_{V(\hat{r})} d\mathbf{x} \hat{P}_{\text{tot}}(\mathbf{x}) \hat{E}_{\text{tot}}(\mathbf{x}), \quad (2.6)$$

where  $\hat{P}_{\text{tot}}(\mathbf{x})$  is the object's polarization and the integration is performed over the volume of the dielectric  $V$  with center-of-mass coordinate  $\hat{r}$ . Assuming  $\hat{P}_{\text{tot}}(\mathbf{x}) = \alpha_p \hat{E}_{\text{tot}}(\mathbf{x})$  and comparing the resulting relation between the polarization and the electric field for the macroscopic [142] and microscopic case (see [64] for a concise derivation), one obtains  $\alpha_p = \epsilon_0 \epsilon_r$  and

$$\hat{H}_{\text{LM}} = -\frac{\epsilon_c \epsilon_0}{2} \int_{V(\hat{r})} d\mathbf{x} \hat{E}_{\text{tot}}(\mathbf{x})^2, \quad (2.7)$$

where  $\epsilon_c = 3(\epsilon_r - 1)/(\epsilon_r + 2)$  is defined in terms of the relative dielectric constant  $\epsilon_r$ . Here, the cm is treated as an operator, such that Eq. (2.7) gives the coupling terms between the object's position and the light field.

Before describing the different contributions in detail, we reconsider the inhomogeneous mode  $\hat{E}_{\text{S}}$  that has been separated from the continuum, see Eq. (2.5). It describes one (or several) mode(s) that differs from the continuum. While in the specific setup of optomechanics with levitating spheres both the tweezer and the cavity field contribute, we describe this mode in general as the system mode. Due to the high photonic occupation numbers that might occur in the presence of a strong driving field, it can be divided into a classical part and a quantum part by displacing the operators  $\hat{a}_0 = \langle \hat{a}_0 \rangle + \hat{a}'_0$  (note that we will omit the prime hereafter). This yields an additional contribution to the electromagnetic field given by

$$\mathcal{E}_{\text{S}}(\mathbf{x}) = i\sqrt{\frac{\omega_0}{2\epsilon_0 V_0}} (\alpha f(\mathbf{x}) - \text{H.c.}), \quad (2.8)$$

where  $\mathcal{E}_{\text{S}}(\mathbf{x}, t)$  is not an operator and describes the classical part of the light field with  $\alpha = \langle \hat{a}_0 \rangle$ , the square root of the photon number. Plugging  $\hat{E}_{\text{tot}}(\mathbf{x}) = \hat{E}_{\text{S}}(\mathbf{x}) + \mathcal{E}_{\text{S}}(\mathbf{x}) + \hat{E}_{\text{B}}(\mathbf{x})$  into Eq. (2.7) leads to different contributions in the Hamiltonian  $\hat{H}_{\text{tot}}$  of Eq. (2.1). The Hamiltonian describing the system consisting of the inhomogeneous mode and the mechanical degree of freedom can be written as

$$\hat{H}_{\text{S}} = \frac{\hat{p}^2}{2M} + \omega_0 \hat{a}_0^\dagger \hat{a}_0 - \frac{\epsilon_c \epsilon_0}{2} \int_{V(\hat{r})} d\mathbf{x} \left( \mathcal{E}_{\text{S}}(\mathbf{x}) + \hat{E}_{\text{S}}(\mathbf{x}) \right)^2. \quad (2.9)$$

The energy of the bath modes is given by

$$\hat{H}_{\text{B}} = \int d\mathbf{k} \omega_{\mathbf{k}} \hat{a}_{\mathbf{k}}^\dagger \hat{a}_{\mathbf{k}} + \hat{W}(\hat{r}), \quad (2.10)$$

where  $\hat{W}(\hat{r})$  describes the interaction between different bath modes induced by the presence of the dielectric,

$$\hat{W}(\hat{r}) = -\frac{\epsilon_c \epsilon_0}{2} \int_{V(\hat{r})} d\mathbf{x} \hat{E}_{\text{B}}^2(\mathbf{x}). \quad (2.11)$$

The interaction between the system and the bath modes is denoted by

$$\hat{H}_{\text{BS}} = -\epsilon_c \epsilon_0 \int_{V(\hat{r})} d\mathbf{x} \left( \mathcal{E}_{\text{S}}(\mathbf{x}) + \hat{E}_{\text{S}}(\mathbf{x}) \right) \hat{E}_{\text{B}}(\mathbf{x}). \quad (2.12)$$

The noninteracting part of the Hamiltonian describing the energy of the system and the bath is given by

$$\hat{H}_0 = \hat{H}_{\text{S}} + \hat{H}_{\text{B}}. \quad (2.13)$$

In quantum optics, the interaction between different bath modes, Eq. (2.11), is commonly neglected. In contrast, when describing the scattering of light from larger objects, interactions among the bath modes have to be taken into account, such that it is no longer justified to neglect  $W(\hat{r})$ .  $\hat{H}_0$  thus effects a coupling between different modes of the bath, such that the bath operators are not a diagonal basis anymore. We demonstrate in the following how this problem can be addressed and connected to a description within scattering theory.

## 2.3 Master equation for arbitrary dielectrics

We give a concise description of the two modes of the system we are interested in, the mechanical mode describing the center-of-mass motion of the dielectric and the cavity mode of the light. Therefore, we trace out the other modes of the electromagnetic field, the free modes. The typical quantum-optical approach to these systems is the method of Born-Markov master equations, where the bath is eliminated to derive a description exclusively for the system's dynamics. The Hamiltonian is split into a part describing the energy of the system and the bath,  $\hat{H}_0$ , and the interaction between the two,  $\hat{H}_{\text{BS}}$ . For typical quantum-optical systems,  $\hat{H}_0$  is diagonal in the bath operators  $\hat{a}_{\mathbf{k}}$  as interactions among them are negligible, such that the transformation to the interaction picture is straightforward. The difficulty we confront when describing the interaction between light and a dielectric sphere in a cavity larger than the wavelength is that due to the large number of scattered photons, interactions within the bath, given by Eq. (2.11), have to be taken into account. This effects a Hamiltonian which is non-diagonal in the bath operators  $\hat{a}_{\mathbf{k}}$ .

The strategy to approach this problem is to first solve the equations of motion, effected by the interaction with the dielectric, for the bath operators. Connecting these expressions to the Lippmann-Schwinger equation for the scattering process of a single photon, we give the solution for the bath operators containing the full scattering interaction in Sec. 2.3.1. Subsequently, we derive the master equation in Sec. 2.3.2 describing the cavity mode and the center-of-mass mode in this new basis of bath

operators, enabling one to express all quantities in terms of scattering operators. Finally, in Sec. 2.3.3, we specify this approach to optomechanical systems, assuming a strongly-driven cavity and the Lamb-Dicke regime for the cm operator.

### 2.3.1 Solution of the scattering equations for the free field

The equations of motion of the electromagnetic field in the Heisenberg picture are determined and connected to the Lippmann-Schwinger equation. We are only interested in the homogeneous part of the electromagnetic field  $\hat{E}_B(\mathbf{x}, t)$  given by Eq. (2.4) and assume that no inhomogeneity (*i.e.*, cavity) is present, leaving us with a system fully described by  $\hat{H}_B$ , Eq. (2.10). We keep the center-of-mass operator  $\hat{r}$  in the equations of motion, but neglect its action for now assuming  $M \rightarrow \infty$ . The Heisenberg eqs. of motion can thus be determined as

$$\dot{a}_{\mathbf{k}}(t) = -i\omega_{\mathbf{k}}\hat{a}_{\mathbf{k}}(t) - i\sqrt{\frac{\epsilon_c^2\epsilon_0\omega_{\mathbf{k}}}{2(2\pi)^3}} \int_{V(\hat{r})} d\mathbf{x}\hat{E}_B(\mathbf{x}, t)e^{i\mathbf{k}\mathbf{x}}. \quad (2.14)$$

Let us first define  $\hat{E}_B = \hat{E}_B^{(+)} + \hat{E}_B^{(-)}$ , where  $\hat{E}_B^{(-)} = \hat{E}_B^{(+)\dagger}$  with

$$\hat{E}_B^{(+)}(\mathbf{x}, t) = \frac{i}{(2\pi)^{3/2}} \int d\mathbf{k}\sqrt{\frac{\omega_{\mathbf{k}}}{2\epsilon_0}} e^{-i\mathbf{k}\mathbf{x}}\hat{a}_{\mathbf{k}}(t), \quad (2.15)$$

and the incoming field is given by

$$\hat{E}_{B,\text{in}}^{(+)}(\mathbf{x}, t) = \frac{i}{(2\pi)^{3/2}} \int d\mathbf{k}\sqrt{\frac{\omega_{\mathbf{k}}}{2\epsilon_0}} e^{-i\mathbf{k}\mathbf{x}}\hat{a}_{\mathbf{k}}(0)e^{-i\omega_{\mathbf{k}}t}. \quad (2.16)$$

With these definitions at hand, we can close the set of equations given by Eq. (2.14) by carrying out the following steps: we formally integrate Eq. (2.14) over time, multiply both sides by  $i\sqrt{\omega_{\mathbf{k}}/2\epsilon_0(2\pi)^3}e^{-i\mathbf{k}\mathbf{x}}$ , and take the integration over  $\mathbf{k}$  to obtain

$$\begin{aligned} \hat{E}_B^{(+)}(\mathbf{x}, \hat{r}, t) &= \hat{E}_{B,\text{in}}^{(+)}(\mathbf{x}, t) + \int_{V(\hat{r})} d\mathbf{x}' \int d\mathbf{k} \frac{\epsilon_c\omega_{\mathbf{k}}}{2(2\pi)^3} e^{i\mathbf{k}(\mathbf{x}'-\mathbf{x})} e^{-i\omega_{\mathbf{k}}t} \\ &\times \left[ \hat{E}'_B^{(+)}(\mathbf{x}', t) \int_0^t d\tau e^{-i(\omega_0-\omega_{\mathbf{k}})\tau} + \hat{E}'_B^{(-)}(\mathbf{x}', t) \int_0^t d\tau e^{i(\omega_0+\omega_{\mathbf{k}})\tau} \right]. \end{aligned} \quad (2.17)$$

Note that we assume the spectral distribution of the electromagnetic field to be peaked at a certain frequency  $\omega_0$  and we thus have introduced the slowly-varying field  $\hat{E}'_B(\mathbf{x}, t)$  here,  $\hat{E}'_B^{\pm}(\mathbf{x}, t) = e^{\pm i\omega_0 t} \hat{E}_B^{\pm}(\mathbf{x}, t)$ . This justifies the assumption that  $\hat{E}'_B^{\pm}(\mathbf{x}, t)$  remains constant on the time scales of the system's evolution which allows one to take it out of the integration in Eq. (2.17). Integrating  $d\mathbf{k}$  in Eq. (2.17) yields a function that decays quickly in  $\tau$ . This allows for an extension of the upper integration boundary  $t$  to  $\infty$  (Markov approximation) and hence yields

$$\hat{E}_B^{(+)}(\mathbf{x}, \hat{r}, t) = \hat{E}_{B,\text{in}}^{(+)}(\mathbf{x}, t) + \frac{\epsilon_c}{2(2\pi)^3} \int_{V(\hat{r})} d\mathbf{x}' \int d\mathbf{k} e^{-i\mathbf{k}(\mathbf{x}-\mathbf{x}')} \frac{\omega_{\mathbf{k}}}{\omega_{\mathbf{k}} - \omega_0 + i\gamma} \hat{E}'_B^{(+)}(\mathbf{x}', t), \quad (2.18)$$

where the limit  $\gamma \rightarrow 0^+$  is understood. Taking the inverse transformation, the field operators can be written as

$$\hat{a}_{\mathbf{k}}(t) = \hat{a}_{\mathbf{k}}(0)e^{-i\omega_{\mathbf{k}}t} + \frac{\epsilon_c}{2} \int_{V(\hat{r})} d\mathbf{x}' \int d\mathbf{k}' e^{i(\mathbf{k}-\mathbf{k}')\mathbf{x}'} \frac{\sqrt{\omega_{\mathbf{k}'}\omega_{\mathbf{k}}}}{\omega_{\mathbf{k}'} - \omega_0 + i\gamma} \hat{a}_{\mathbf{k}'}(t). \quad (2.19)$$

This equation for the operators of the electromagnetic field resembles the Lippmann-Schwinger equation [143, 144]. In order to connect the two descriptions, enabling one to employ solutions known from scattering theory in our approach, we proceed in the same way defining

$$\mathcal{V}_{\mathbf{k},\mathbf{k}'}(\hat{r}) = \frac{\epsilon_c}{2} \int_{V(\hat{r})} d\mathbf{x}' \sqrt{\omega_{\mathbf{k}'}\omega_{\mathbf{k}}} e^{i(\mathbf{k}-\mathbf{k}')\mathbf{x}'} \quad (2.20)$$

as the matrix elements of the operator describing the scattering interaction. In analogy we define the transition matrix  $\mathcal{T}_{\mathbf{k},\mathbf{k}'}(\hat{r})$ , given by

$$\mathcal{T}_{\mathbf{k},\mathbf{k}'}(\hat{r}) = \int d\mathbf{k}'' \mathcal{V}_{\mathbf{k},\mathbf{k}''}(\hat{r}) \left( \delta(\mathbf{k}' - \mathbf{k}'') + \frac{\mathcal{T}_{\mathbf{k}''\mathbf{k}'}(\hat{r})}{\omega_{\mathbf{k}''} - \omega_{\mathbf{k}} + i\gamma} \right). \quad (2.21)$$

Note that both  $\mathcal{V}_{\mathbf{k},\mathbf{k}'}(\hat{r})$  and  $\mathcal{T}_{\mathbf{k},\mathbf{k}'}(\hat{r})$  are operators for the center-of-mass degree of freedom but not for the photonic ones. That is, if we fix  $\hat{r}$ , neglecting the object's motion,  $\mathcal{V}_{\mathbf{k},\mathbf{k}'}(\hat{r})$  and  $\mathcal{T}_{\mathbf{k},\mathbf{k}'}(\hat{r})$  are simply numbers without operator-character. By iteration, the transition matrix describes scattering processes to all orders of perturbation theory, as illustrated in Fig. 2.1 (see [144] for a more detailed derivation),

$$\begin{aligned} \mathcal{T}_{\mathbf{k},\mathbf{k}'}(\hat{r}) &= \mathcal{V}_{\mathbf{k},\mathbf{k}'}(\hat{r}) + \int d\mathbf{k}'' \mathcal{V}_{\mathbf{k},\mathbf{k}''}(\hat{r}) \frac{1}{\omega_{\mathbf{k}''} - \omega_{\mathbf{k}} + i\gamma} \mathcal{V}_{\mathbf{k}''\mathbf{k}'}(\hat{r}) \\ &+ \int d\mathbf{k}'' d\mathbf{k}''' \mathcal{V}_{\mathbf{k},\mathbf{k}''}(\hat{r}) \frac{1}{\omega_{\mathbf{k}''} - \omega_{\mathbf{k}} + i\gamma} \mathcal{V}_{\mathbf{k}''\mathbf{k}'''}(\hat{r}) \frac{1}{\omega_{\mathbf{k}'''} - \omega_{\mathbf{k}''} + i\gamma} \mathcal{V}_{\mathbf{k}'''\mathbf{k}'}(\hat{r}) + \dots \end{aligned} \quad (2.22)$$

Subsequently, Eq. (2.21) enables one to rewrite the total time evolution of the operators, Eq. (2.19) as

$$\hat{a}_{\mathbf{k}}(t) = \int d\mathbf{k}' e^{-i\omega_{\mathbf{k}'}t} \left( \delta(\mathbf{k} - \mathbf{k}') + \frac{\mathcal{T}_{\mathbf{k},\mathbf{k}'}(\hat{r})}{\omega_{\mathbf{k}'} - \omega_0 + i\gamma} \right) \hat{a}_{\mathbf{k}'}(0). \quad (2.23)$$

This expression is equivalent to the classical field equations given by Eq. (2.70). For its solution we can thus rely on the variety of methods that have been developed during the past decades described in Sec. 2.A.

A useful relation that will be used to simplify the computation of transition amplitudes for spheres in Sec. 3.2, is the optical theorem connecting the scattering amplitude in forward-direction to the scattering in all other directions [143]:

$$\text{Im}[\mathcal{T}_{\mathbf{k},\mathbf{k}'}(\hat{r})] = -\pi \int d\mathbf{k}'' |\mathcal{T}_{\mathbf{k},\mathbf{k}''}(\hat{r})|^2 \delta(\omega_{\mathbf{k}} - \omega_{\mathbf{k}'}). \quad (2.24)$$

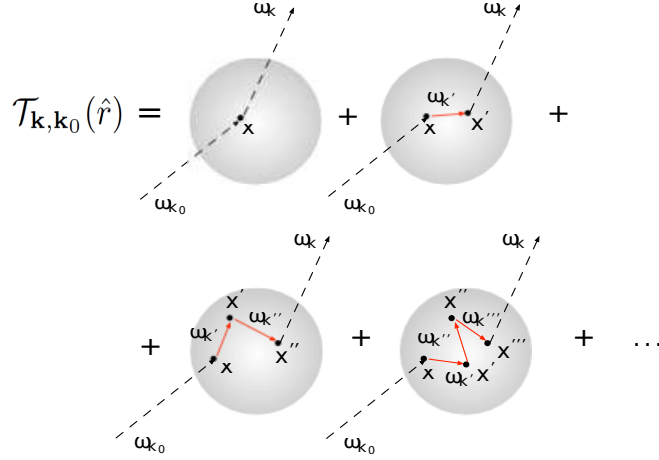


Figure 2.1: Graphical illustration of the transition matrix  $\mathcal{T}_{\mathbf{k},\mathbf{k}_0}(\hat{r})$  as an infinite series in the light-matter interaction. The first term denotes the direct interaction between the dielectric and light, the second one a process, where a photon is virtually absorbed and reemitted, the third one a process, where two intermediate photons are involved, etc.

Before we continue the analysis, to ease the notation, it is useful to define the space of mode functions in which the matrices  $\mathcal{T}_{\mathbf{k},\mathbf{k}'}(\hat{r})$  and  $\mathcal{V}_{\mathbf{k},\mathbf{k}'}(\hat{r})$  act, and consider them as operators, *i.e.*,  $\mathcal{V}_{\mathbf{k},\mathbf{k}'}(\hat{r}) = \langle \mathbf{k} | \hat{V}(\hat{r}) | \mathbf{k}' \rangle$ , where  $|\mathbf{k}\rangle$  are the basis vectors of such a space. They can be viewed as mode functions with momentum  $\mathbf{k}$ . As we describe scattering out of the cavity mode in this article, let us now define the transition amplitudes for mode shapes different from plane waves and express them in the basis  $|\mathbf{k}\rangle$ . For the Born approximation of scattering theory<sup>1</sup>, consisting in setting  $\hat{T}(\hat{r}) \approx \hat{V}(\hat{r})$ , we obtain

$$\mathcal{V}_{\mathbf{k},\mathbf{c}}(\hat{r}) = \int d\mathbf{k}' \langle \mathbf{k} | \hat{V}(\hat{r}) | \mathbf{k}' \rangle \langle \mathbf{k}' | \mathbf{c} \rangle, \quad (2.25)$$

where  $|\mathbf{c}\rangle$  describes the mode function of the cavity, which can be written as  $\langle \mathbf{x} | \mathbf{c} \rangle = f(\mathbf{x})/\sqrt{V_0}$  in position-representation, where  $f(\mathbf{x})$  is assumed to be real. Evaluating this expression yields

$$\mathcal{V}_{\mathbf{k},\mathbf{c}}(\hat{r}) = \sqrt{\frac{\epsilon_c^2 \omega_{\mathbf{k}} \omega_0}{4V_0}} \int_{V(\hat{r})} d\mathbf{x} f(\mathbf{x}) e^{i\mathbf{k}\mathbf{x}}, \quad (2.26)$$

<sup>1</sup>Note, that we refer to the Born approximation of scattering theory here, where the action of the scattering event on the electromagnetic field is neglected in the lowest-order approximation. Thus, no multi-scattering events are accounted for. This is different from the Born-Markov approximation often taken in the derivation of master equations, which assumes the separability of the density matrices of the system and the bath.

where we have used that the distribution of  $\omega_{\mathbf{k}}$  is peaked around  $\omega_0$ , allowing for the substitution  $\omega_{\mathbf{k}} \approx \omega_0$ .

### 2.3.2 General master equation for the cavity and the center-of-mass mode

Within the Born-Markov approximation, the master equation describing the system's full dynamics is given by

$$\dot{\rho}_{\text{S}}(t) \approx - \int_0^\infty \text{tr}_{\text{B}}[\hat{H}_{\text{BS}}^{\text{I}}(t), [\hat{H}_{\text{BS}}^{\text{I}}(t - \tau), \hat{\rho}_{\text{S}}(t) \otimes \hat{\rho}_{\text{B}}]] d\tau. \quad (2.27)$$

The Born-Markov approximation consists in the following assumptions: the density matrices of the system and the environment are considered to be separable,  $\hat{\rho}_{\text{tot}} = \hat{\rho}_{\text{S}} \otimes \hat{\rho}_{\text{B}}$ , and correlations between bath operators are taken to decay quickly. Furthermore, the bath is assumed to remain unchanged during the interaction with the system,  $\hat{\rho}_{\text{B}}(t) \approx \hat{\rho}_{\text{B}}(0)$ . This is valid given that the bath is very large and the effect of the interaction with the system can be neglected.

Moreover, for typical quantum-optical systems interactions between different bath operators  $\hat{a}_{\mathbf{k}}, \hat{a}_{\mathbf{k}'}^\dagger$ , Eq. (2.11), are negligible, *i.e.*,  $\hat{W}(\hat{r}) \approx 0$ , such that

$$\hat{H}_0 \approx \hat{H}_{\text{S}} + \int d\mathbf{k} \omega_{\mathbf{k}} \hat{a}_{\mathbf{k}}^\dagger \hat{a}_{\mathbf{k}}. \quad (2.28)$$

While these approximations are typically fulfilled for point-particles as demonstrated in Sec 2.4, difficulties are encountered when extending the method to larger objects. It is in particular the negligence of interactions between different bath operators that is no longer justified. More specifically, we realize that contributions, where interactions among bath operators are taken into account to different orders, scale as  $\propto (R/\lambda_c)^{2n}$ . Here,  $R$  denotes the dimensions of the object,  $\lambda_c$  the wavelength of the inhomogeneous light mode, and  $n$  the  $n$ th order of the multiple scattering process.

Consequently, an approach where these interactions are accounted for is necessary for  $R \geq \lambda_c$ . This is achieved by including the correlations between the bath operators described by  $\hat{W}(\hat{r})$  in the Hamiltonian that is used to transform to the interaction picture,

$$\hat{H}_{\text{BS}}^{\text{I}}(t) = e^{i\hat{H}_0 t} \hat{H}_{\text{BS}}(0) e^{-i\hat{H}_0 t}. \quad (2.29)$$

To find a solution, we connect this approach to the description within scattering theory given in Sec. 2.3.1. Based on this analysis, we can develop a master equation that accounts for interactions among different bath modes. As an example we now discuss the first term of the master equation, where all operators are in front of the density

matrix, in more detail:

$$\dot{\rho}_S = -\hat{a}_0^\dagger \hat{a}_0 \int_0^\infty d\tau \int d\mathbf{k} e^{i\omega_0 \tau} \langle \Omega | \mathcal{F}(t, \hat{r}) \hat{a}_{\mathbf{k}}^\dagger(0) | \Omega \rangle \langle \Omega | \hat{a}_{\mathbf{k}}(0) \mathcal{F}(t - \tau, \hat{r}) | \Omega \rangle \hat{\rho}_S + \dots \quad (2.30)$$

Here,  $|\Omega\rangle$  denotes the vacuum state and we have defined

$$\mathcal{F}(t, \hat{r}) = \sqrt{\frac{\epsilon_c^2 \omega_0 \epsilon_0}{4V_0}} \int_{V(\hat{r})} d\mathbf{x} f(\mathbf{x}) \hat{E}_B(\mathbf{x}, t), \quad (2.31)$$

where counter-rotating terms have been neglected. Let us now connect Eq. (2.30) to the description in terms of mode functions in the scattering picture. First, we shift the time dependence of  $\mathcal{F}(t, \hat{r})$  to the operators by

$$\langle \Omega | \mathcal{F}(t, \hat{r}) \hat{a}_{\mathbf{k}}^\dagger(0) | \Omega \rangle = \langle \Omega | \mathcal{F}(0, \hat{r}) \hat{a}_{\mathbf{k}}^\dagger(-t) | \Omega \rangle, \quad (2.32)$$

where the invariance of the vacuum state under time evolution has been used. In order to make the procedure more transparent, as a first step, only the 0th order Born approximation of scattering theory is identified. Subsequently, the treatment is extended to a description of all orders. The lowest order of the Born series gives  $\hat{a}_{\mathbf{k}}(t) \approx \hat{a}_{\mathbf{k}}(0) \exp(-i\omega_{\mathbf{k}} t)$ , so that we need to evaluate

$$\langle \Omega | \mathcal{F}(0, \hat{r}) \hat{a}_{\mathbf{k}}^\dagger(0) | \Omega \rangle = \sqrt{\frac{\epsilon_c^2 \omega_{\mathbf{k}} \omega_0}{4V_0}} \int_{V(\hat{r})} d\mathbf{x} f(\mathbf{x}) e^{-i\mathbf{k}\mathbf{x}}. \quad (2.33)$$

Recalling the definition of the expectation value  $\mathcal{V}_{\mathbf{k},c}(\hat{r})$  in the scattering picture, Eq. (2.26), we identify

$$\langle \Omega | \mathcal{F}(0, \hat{r}) \hat{a}_{\mathbf{k}}^\dagger(0) | \Omega \rangle = \mathcal{V}_{\mathbf{k},c}^*(\hat{r}). \quad (2.34)$$

The same procedure can now be applied without taking the Born approximation and considering the full transition matrix, by plugging Eq. (2.23) into Eq. (2.59), which yields

$$\begin{aligned} & \langle \Omega | \mathcal{F}(0, \hat{r}) \hat{a}_{\mathbf{k}}^\dagger(-t) | \Omega \rangle \\ &= \int d\mathbf{k}' \mathcal{V}_{\mathbf{k}',c}^*(\hat{r}) \left( \delta(\mathbf{k} - \mathbf{k}') + \frac{\mathcal{T}_{\mathbf{k}'\mathbf{k}}^*(\hat{r})}{\omega_{\mathbf{k}} - \omega_0 - i\gamma} \right) e^{-i\omega_{\mathbf{k}} t} \\ &= e^{-i\omega_{\mathbf{k}} t} \mathcal{T}_{\mathbf{k},c}^*(\hat{r}), \end{aligned} \quad (2.35)$$

where Eq. (2.21) has been used.

All other terms of the master equation can be determined in full analogy yielding

$$\dot{\rho}_S = i[\hat{\rho}_S, \hat{H}_S + \hat{H}_{\text{rn}}] + \int d\mathbf{k} \delta(\omega_{\mathbf{k}} - \omega_0) \left( 2\mathcal{T}_{\mathbf{k},c}(\hat{r}) \hat{a}_0 \hat{\rho}_S \hat{a}_0^\dagger \mathcal{T}_{\mathbf{k},c}^*(\hat{r}) - \left[ |\mathcal{T}_{\mathbf{k},c}(\hat{r})|^2 \hat{a}_0^\dagger \hat{a}_0, \hat{\rho}_S \right]_+ \right), \quad (2.36)$$

where  $\hat{H}_S$  is the system Hamiltonian given by Eq. (2.9) and  $\hat{H}_{\text{rn}}$  the renormalization

$$\hat{H}_{\text{rn}} = \hat{a}_0^\dagger \hat{a}_0 \int d\mathbf{k} |\mathcal{T}_{\mathbf{k},c}(\hat{r})|^2 \mathcal{P} \frac{1}{\omega_{\mathbf{k}} - \omega_0}, \quad (2.37)$$

where  $\mathcal{P}$  denotes Cauchy's principal value. Note that a similar master equation for the cm degree of freedom has been discussed in the context of scattering of air molecules [145–149].

### 2.3.3 Master equation for the optomechanical setup

In this section, we adapt the general master equation Eq. (2.36) to the specific optomechanical setup we are interested in. Therefore, we take the following approximations:

1. The inhomogeneous mode is assumed to be a strongly-driven cavity effecting large cavity occupation numbers  $n_{\text{phot}} = |\alpha|^2$ , such that  $|\alpha| \gg 1$ . This enables one to neglect certain terms in the master equation.
2. We assume the Lamb-Dicke regime: the dielectric is positioned close to the maximal slope of the standing wave in the cavity and close to the minimum of the harmonic trapping potential of the optical tweezers. The motion around its cm position is considered to be small, such that the Lamb-Dicke parameter  $\eta = k\Delta\hat{r} \ll 1$  (with  $\Delta\hat{r} = \sqrt{\langle \hat{r}^2 \rangle - \langle \hat{r} \rangle^2}$ ), facilitating an expansion of the transition operator matrix elements  $\mathcal{T}_{\mathbf{k},c}(\hat{r})$  in  $\mathbf{k}\hat{r}$ .

Displacing the cavity operator by  $\alpha$  such that  $\hat{a}_0 \rightarrow \hat{a}'_0 + \alpha$  and expanding the transition operator to second order,  $\mathcal{T}_{\mathbf{k},c}(\hat{r}) \approx \mathcal{T}_{\mathbf{k},c}(0) + \mathcal{T}'_{\mathbf{k},c}(\hat{r})|_{\hat{r}=0}\hat{r} + \mathcal{T}''_{\mathbf{k},c}(\hat{r})|_{\hat{r}=0}\hat{r}^2$  leads to a master equation, where we take into account terms that are at most of quadratic order in the cavity operators  $\hat{a}_0, \hat{a}_0^\dagger$  and the cm operators  $\hat{r} = x_0(\hat{b} + \hat{b}^\dagger)$ . Here,  $\mathcal{T}_{\mathbf{k},c}^n(\hat{r}) = \partial^n \mathcal{T}_{\mathbf{k},c}(\hat{r}) / \partial \hat{r}^n$  denotes the  $n$ th partial derivative and  $x_0 = \sqrt{1/2M\omega_t}$  the zero-point motion of the center-of mass mode where  $\omega_t$  is its trapping frequency.

In the following we give an interpretation of the different contributions to the master equation and indicate which terms yield a renormalization to the Hamiltonian, can be neglected, or describe decoherence. We describe these terms in decreasing order in  $\alpha$ .

#### Contributions $\propto |\alpha|^2$

The largest contribution to the master equation are terms  $\propto |\alpha|^2 |\mathcal{T}_{\mathbf{k},c}(0)|^2$ . As they do not contain operator-character, these terms cancel due to the master equation's bracket structure.

The next order in the Lamb-Dicke parameter  $\eta$  is given by terms  $\propto \hat{r}$ , which can be shown to vanish using Hilbert transforms and the analytic property of the function

$\mathcal{T}'_{\mathbf{k},c}(\hat{r})|_{\hat{r}=0}\mathcal{T}_{c,\mathbf{k}}^*(0)$ . The total contribution  $\propto \hat{r}$  consisting of the renormalization of the Hamiltonian and the decoherence part is hermitian and can be written as

$$\begin{aligned} \hat{H}_{\text{rn}}^{\text{shift}} = & \alpha^2 \int d\mathbf{k} \left( \delta(\omega_{\mathbf{k}} - \omega_0) \text{Im} \left[ \mathcal{T}'_{\mathbf{k},c}(\hat{r})|_{\hat{r}=0} \mathcal{T}_{c,\mathbf{k}}^*(0) \right] \right. \\ & \left. + \mathcal{P} \frac{1}{\omega_{\mathbf{k}} - \omega_0} \text{Re} \left[ \mathcal{T}'_{\mathbf{k},c}(\hat{r})|_{\hat{r}=0} \mathcal{T}_{c,\mathbf{k}}^*(0) \right] \right) \hat{r}. \end{aligned} \quad (2.38)$$

Under the assumption that  $t(\omega_{\mathbf{k}}) = \mathcal{T}'_{\mathbf{k},c}(\hat{r})|_{\hat{r}=0}\mathcal{T}_{c,\mathbf{k}}^*(0)$  is analytic in  $\omega_{\mathbf{k}}$ , the Hilbert transformation can be used to show that

$$\int d\omega_{\mathbf{k}} \mathcal{P} \frac{1}{\omega_{\mathbf{k}} - \omega_0} \text{Re} [t(\omega_{\mathbf{k}})] = -\text{Im} [t(\omega_0)] \quad (2.39)$$

and consequently  $\hat{H}_{\text{rn}}^{\text{shift}} = 0$ . Consequently, all contributions  $\propto \hat{r}$  vanish.

The only contributing terms are  $\propto \hat{r}^2$  and describe a renormalization of the trapping frequency of the dielectric provided by the optical tweezers and decoherence of the cm operator. The renormalization of the trapping frequency

$$\omega_t^0 = \omega_t + \Delta^{\text{M}} \quad (2.40)$$

can be simplified exploiting the analytic properties of the functions (in analogy to the previous analysis) and is given by

$$\Delta^{\text{M}} = |\alpha|^2 x_0^2 \int d\mathbf{k} \mathcal{P} \frac{1}{\omega_{\mathbf{k}} - \omega_0} \left[ \mathcal{T}'_{\mathbf{k},c}(\hat{r}) \mathcal{T}_{c,\mathbf{k}}'^*(\hat{r}) \right]_{\hat{r}=0}. \quad (2.41)$$

Here the unrenormalized trapping frequency is given by the contribution to Eq. (2.9)  $\propto \mathcal{E}_{\text{S}}^2$ ,

$$\omega_t^0 = \sqrt{\frac{4\epsilon_c I}{\rho c W_t^2}}. \quad (2.42)$$

The decoherence of the mechanical motion is described by

$$\mathcal{L}^{\text{M}}[\hat{\rho}_{\text{S}}] = \Gamma_{\text{phot}} \left( 2(\hat{b} + \hat{b}^\dagger)\hat{\rho}_{\text{S}}(\hat{b} + \hat{b}^\dagger) - \{(\hat{b} + \hat{b}^\dagger)^2, \hat{\rho}_{\text{S}}\}_+ \right) \quad (2.43)$$

with

$$\Gamma_{\text{phot}} = |\alpha|^2 x_0^2 \int d\mathbf{k} \delta(\omega_{\mathbf{k}} - \omega_0) \left[ \mathcal{T}'_{\mathbf{k},c}(\hat{r}) \mathcal{T}_{c,\mathbf{k}}'^*(\hat{r}) \right]_{\hat{r}=0}. \quad (2.44)$$

The decoherence of the cm thus depends on the form of the transition amplitudes with respect to the cm position. The physical process underlying this effect is recoil heating via photon scattering.

**Contributions  $\propto \alpha$** 

Also to determine the contributions  $\propto \alpha^* \hat{a}_0 |\mathcal{T}_{\mathbf{k},c}(0)|^2$ , the analyticity of the transition operator can be exploited. Applying a Hilbert transformation, we can show that these contributions cancel in full analogy to the analysis carried out above.

Terms  $\propto \alpha^* \hat{a}_0 \hat{r}$  effect both a coherent and an incoherent contribution. The incoherent part describes decoherence of the mechanical and the light degree of freedom and can be shown to be negligible. It is given by

$$\mathcal{L}^S[\hat{\rho}_S] = 2\Gamma_g(\hat{a}_0 \hat{\rho}_S(\hat{b} + \hat{b}^\dagger) - [\hat{a}_0(\hat{b} + \hat{b}^\dagger), \hat{\rho}_S]) + 2\Gamma_g^*((\hat{b} + \hat{b}^\dagger) \hat{\rho}_S \hat{a}_0^\dagger - [\hat{a}_0^\dagger(\hat{b} + \hat{b}^\dagger), \hat{\rho}_S]), \quad (2.45)$$

where

$$\Gamma_g = x_0 \alpha^* \int d\mathbf{k} \delta(\omega_{\mathbf{k}} - \omega_0) \mathcal{T}_{\mathbf{k},c}^*(0) \mathcal{T}'_{\mathbf{k},c}(\hat{r})|_{\hat{r}=0}. \quad (2.46)$$

This contribution can in general be neglected for the cm degree of freedom, as it is suppressed by  $1/\alpha$  compared to Eq. (2.43). Requiring that  $\alpha\eta \ll 1$ , we can also neglect the effect of this contribution on the cavity mode. This requirement becomes clear when comparing Eq. (2.45) to the decay of the cavity described by Eq. (3.12).

In contrast, the coherent contribution yields a non-negligible renormalization of the optomechanical coupling

$$g = g^0 + g_{rn} \quad (2.47)$$

defined by

$$g_{rn} = \alpha^* x_0 \int d\mathbf{k} \mathcal{P} \frac{1}{\omega_{\mathbf{k}} - \omega_0} \mathcal{T}_{\mathbf{k},c}(0) \mathcal{T}'_{\mathbf{k},c}(\hat{r})|_{\hat{r}=0}. \quad (2.48)$$

Here, the optomechanical coupling  $g^0$  is given by the contributions to  $H_S$  (Eq. (2.9))  $\propto \mathcal{E}_S \hat{E}_S$

$$g^0 = -x_0 \alpha \frac{\epsilon_c \omega_c^2 V}{4cV_0}. \quad (2.49)$$

Furthermore, terms  $\propto \hat{r}^2$  describe decoherence of both the mechanical mode and the light mode. Comparing to Eq. (2.44) for the cm mode, these contributions are suppressed by  $1/\alpha$  and can thus be neglected. Also for the cavity mode, these terms are negligible, given that  $\eta^2 \alpha \ll 1$ .

**Contributions  $\propto \hat{a}_0^\dagger \hat{a}_0$** 

Terms  $\propto |\mathcal{T}_{\mathbf{k},c}(0)|^2$  yield both a coherent and an incoherent contribution describing a renormalization of the resonance frequency of the cavity and a part describing the cavity's decay:

$$\mathcal{L}^L[\hat{\rho}_S] = \kappa \left( 2\hat{a}_0 \hat{\rho}_S \hat{a}_0^\dagger - [\hat{a}_0^\dagger \hat{a}_0, \hat{\rho}_S]_+ \right) \quad (2.50)$$

with

$$\kappa = \int d\mathbf{k} \delta(\omega_{\mathbf{k}} - \omega_0) |\mathcal{T}_{\mathbf{k},c}(0)|^2. \quad (2.51)$$

The renormalization of the cavity's resonance frequency

$$\tilde{\omega}_0 = \omega_0^0 + \Delta^L \quad (2.52)$$

is defined by

$$\Delta^L = \int d\mathbf{k} \mathcal{P} \frac{1}{\omega_{\mathbf{k}} - \omega_0} |\mathcal{T}_{c,\mathbf{k}}(0)|^2. \quad (2.53)$$

These are the only non-vanishing contributions as terms  $\propto \hat{r}$  are suppressed by the Lamb-Dicke parameter  $\eta$  and terms  $\propto \hat{r}^2$  even by  $\eta^2$  compared to Eqs. (3.12), (2.53).

### Final master equation

To summarize, we identify the contributions to the final master equation:

$$\dot{\rho}_S = i[\hat{\rho}_S, \hat{H}_S + \hat{H}_{rn}] + \mathcal{L}^M[\hat{\rho}_S] + \mathcal{L}^L[\hat{\rho}_S]. \quad (2.54)$$

They can be grouped as follows:

1. Contributions of Hamiltonian-type,

$$\hat{H}_S + \hat{H}_{rn} = \delta \hat{a}_0^\dagger \hat{a}_0 + \omega_t \hat{b}^\dagger \hat{b} + g(\hat{a}_0 + \hat{a}_0^\dagger)(\hat{b} + \hat{b}^\dagger), \quad (2.55)$$

where the frequencies and couplings stemming from the system's Hamiltonian  $\hat{H}_S$ , given by Eq. (2.9), are renormalized by

$$\hat{H}_{rn} = \Delta^M \hat{b}^\dagger \hat{b} + \Delta^L \hat{a}_0^\dagger \hat{a}_0 + g_{rn}(\hat{a}_0 + \hat{a}_0^\dagger)(\hat{b} + \hat{b}^\dagger). \quad (2.56)$$

The corresponding renormalizations are defined by Eqs. (2.41), (2.48), (2.53). Note that the Hamiltonian of Eq. (2.55) has been transformed to a frame rotating at the laser frequency  $\omega_L$ , where  $\delta$  now denotes its detuning from the cavity resonance frequency  $\tilde{\omega}_0$  (for details on the transformation see Sec.4.2.2).

2. The recoil heating via photon scattering of the cm mode yields  $\mathcal{L}^M[\hat{\rho}_S]$ , given by Eq. (2.43).
3. The decay of the cavity mode due to the presence of the object yielding  $\mathcal{L}^L[\hat{\rho}_S]$ , is described by Eq. (3.12).

Consequently, all frequencies, couplings, and decay rates are renormalized taking into account all terms beyond the first Born approximation of scattering theory. This enables one to use exact solutions if available, or in general to truncate the perturbation series in a controlled way.

While this master equation only contains the time evolution of the cavity and the cm operators, information about the scattered fields can be obtained by applying the quantum regression theorem. The scattered light is directly accessible in experiments and can, *e.g.*, be used to monitor the cooling of the mechanical motion [150]. To complement the analysis given here, we show how to derive the scattered fields directly in App. 2.B within an approach similar to Wigner-Weisskopf, but accounting for interaction processes between the bath modes.

## 2.4 The small-particle limit

In this section, the important limit of the general theory, where the scattering object is smaller than the wavelength,  $R \ll \lambda_c$ , is considered. In this case, it is justified to neglect the introduced couplings among the different modes of the environment described by Eq. (2.11). It is shown, that this approximation is equivalent to considering only the first order of the Born series of scattering theory and is sufficient when treating spheres smaller than the wavelength.

### 2.4.1 General master equation

Neglecting interactions among the bath modes,  $\hat{W}(\hat{r}) \approx 0$ , yields

$$\hat{H}_0 \approx \hat{H}_S + \int d\mathbf{k} \omega_{\mathbf{k}} \hat{a}_{\mathbf{k}}^\dagger \hat{a}_{\mathbf{k}}. \quad (2.57)$$

The crucial difference between this Hamiltonian and the more general one employed in the previous sections (Eq. (2.13)), is that it is already diagonal in the bath operators  $\hat{a}_{\mathbf{k}}$  significantly simplifying the further analysis. To apply the master equation given by Eq. (2.27), we transform  $\hat{H}_{\text{BS}}$  to the interaction picture

$$\hat{H}_{\text{BS}}^{\text{I}}(t) = e^{i\hat{H}_0 t} \hat{H}_{\text{BS}}(0) e^{-i\hat{H}_0 t}. \quad (2.58)$$

In analogy to Sec. 2.3.2, we consider the expectation values

$$\langle \Omega | \mathcal{F}(t, \hat{r}) \hat{a}_{\mathbf{k}}^\dagger(0) | \Omega \rangle = \langle \Omega | \mathcal{F}(0, \hat{r}) \hat{a}_{\mathbf{k}}^\dagger(-t) | \Omega \rangle, \quad (2.59)$$

and shift the time dependence to the field operators with

$$\hat{a}_{\mathbf{k}}(t) = e^{i\hat{H}_0 t} \hat{a}_{\mathbf{k}}(0) e^{-i\hat{H}_0 t} = e^{-i\omega_{\mathbf{k}} t} \hat{a}_{\mathbf{k}}(0) \quad (2.60)$$

to lowest order in the Born series. This gives

$$\langle \Omega | \mathcal{F}(0, \hat{r}) \hat{a}_{\mathbf{k}}^\dagger(-t) | \Omega \rangle = e^{-i\omega_{\mathbf{k}} t} \mathcal{V}_{c, \mathbf{k}}^*(\hat{r}), \quad (2.61)$$

with all operators and variables defined in analogy to the previous section. Inserting these expectation values into the master equation yields

$$\dot{\rho}_S = i[\hat{\rho}_S, \hat{H}_S + \hat{H}_{\text{rn}}^0] + \int d\mathbf{k} \delta(\omega_{\mathbf{k}} - \omega_0) \left( 2\mathcal{V}_{\mathbf{k},c}(\hat{r}) \hat{a}_0 \hat{\rho}_S \hat{a}_0^\dagger \mathcal{V}_{\mathbf{k},c}^*(\hat{r}) - \left[ |\mathcal{V}_{\mathbf{k},c}(\hat{r})|^2 \hat{a}_0^\dagger \hat{a}_0, \hat{\rho}_S \right]_+ \right), \quad (2.62)$$

where  $\hat{H}_S$  is the system Hamiltonian given by Eq. (2.9) and  $\hat{H}_{\text{rn}}^0$  the renormalization

$$\hat{H}_{\text{rn}}^0 = \hat{a}_0^\dagger \hat{a}_0 \int d\mathbf{k} |\mathcal{V}_{\mathbf{k},c}(\hat{r})|^2 \mathcal{P} \frac{1}{\omega_{\mathbf{k}} - \omega_0}, \quad (2.63)$$

where  $\mathcal{P}$  denotes Cauchy's principal value. This master equation relies on taking the lowest order of the Born series and can directly be obtained from Eq. (2.36) by inserting  $\mathcal{T}_{\mathbf{k},c}(\hat{r}) \approx \mathcal{V}_{\mathbf{k},c}(\hat{r})$ .

#### 2.4.2 Master equation for the optomechanical setup

We proceed to determine the optomechanical parameters for objects smaller than the wavelength obtained by considering only the lowest terms of the Born series of scattering theory. Having given the general description in the previous section, we now will discuss how the various coupling and decoherence terms are modified:

1. All terms in  $\hat{H}_S$  remain the same, the trapping frequency  $\tilde{\omega}_t$  can be determined from Eq. (2.9), which for objects much smaller than the wavelength is given by

$$\omega_t^0 = \sqrt{\frac{4\epsilon_c}{\rho c} \frac{I}{W_t^2}}, \quad (2.64)$$

where  $\rho$  is the material's density,  $I$  the laser intensity of the optical tweezer and  $W_t$  its waist. Also the optomechanical coupling  $g^0$  is given by Eq. (2.9) simplifying to

$$g^0 = -x_0 \frac{\epsilon_c \omega_c^2 V}{4cV_0}, \quad (2.65)$$

where  $V$  is the object's volume. Note that the expressions for  $\hat{H}_S$  are not affected by neglecting the coupling among the bath modes as these quantities are determined only by system operators.

2. The renormalization of the optomechanical coupling and the trapping frequency are obtained by considering only the lowest order of the Born series  $\mathcal{T}_{\mathbf{k},c}(\hat{r}) \approx \mathcal{V}_{\mathbf{k},c}(\hat{r})$  in the expressions for  $\Delta$  and  $g_{\text{rn}}$  given by Eqs. (2.41), (2.48). This gives

$$g_{\text{rn}}^0 = -\epsilon_c k_0^2 R^2 g^0 \quad (2.66)$$

with  $R$  being the sphere's radius. The renormalization of the trapping frequency is obtained by inserting the trapping mode and leads to

$$\Delta^{\text{M},0} = -\epsilon_c k_0^2 R^2 \omega_t^0. \quad (2.67)$$

3. The same procedure, namely taking the lowest order in the Born series by setting  $\mathcal{T}_{c,\mathbf{k}}(\hat{r}) \approx \mathcal{V}_{c,\mathbf{k}}(\hat{r})$  is also applied to obtain the decoherence rates. For the cavity decay rate this gives

$$\kappa^0 = \frac{\epsilon_c^2 k_0^4 V^2 c}{24\pi V_0} \quad (2.68)$$

and for the recoil heating of the cm we obtain

$$\Gamma^0 = \frac{\epsilon_c^2 k_0^6 V}{6\pi\rho\omega_t} \left( \frac{P_t}{\omega_L \pi W_t^2} + \frac{n_{\text{ph}} c}{2V_0} \right), \quad (2.69)$$

where the first term describes decoherence due to recoil heating by photons from the tweezers and the second term by photons of the cavity mode. Comparison to [64] shows that this result is in agreement with what is obtained when directly taking the Born-Markov approach, neglecting interactions between bath modes and deriving the master equation in the standard way.

## 2.A The classical approach

This Appendix sketches the solution of the equations of motion of the classical electromagnetic field, giving an overview of the possibilities and limitations of the description in classical scattering theory. The approach in the classical case is to solve Maxwell's equations [142]. Neglecting polarizations yields

$$E(\mathbf{x}, t) = E_{\text{in}}(\mathbf{x}, t) + \epsilon_c \int d\mathbf{x}' \mathcal{G}(\mathbf{x}', \mathbf{x}) E(\mathbf{x}', t), \quad (2.70)$$

where  $E_{\text{in}}(\mathbf{x}, t)$  denotes the incoming electromagnetic field and

$$\mathcal{G}(\mathbf{x}', \mathbf{x}) = |\mathbf{k}_0|^2 \frac{\exp(i|\mathbf{k}_0||\mathbf{x} - \mathbf{x}'|)}{|\mathbf{x} - \mathbf{x}'|} \quad (2.71)$$

the propagator ( $\mathbf{k}_0$  being the wave vector of the incoming field). This self-consistent equation has been intensely studied in classical scattering theory and is in general only solvable approximately. There exist only few geometries, like, *e.g.*, a cylinder, a sphere, or an ellipsoid, where analytical solutions are tractable. In the special case of a spherical object, the scattered electric field can be determined exactly by expanding the field in spherical waves and subsequently applying boundary conditions, yielding the so-called Mie solution [139–141] (see also App. 2.C). Perturbative approaches [151, 152], based on the analytical solution and an extension of the treatment via distorting the surfaces at different points, only allow for calculations of small perturbations. Numerical approaches like the discrete dipole ansatz [137] or the T-matrix method (see, *e.g.*, [138]

for an expository article) are applicable to a larger class of objects and are widely used today. Indeed, these approaches coincide with the analytical solution for perfectly spherical objects [137]. In the limit of very large dielectrics,  $R \gg \lambda_c$ , applying a ray-optics approach immensely simplifies the calculation of forces on the dielectric [153]. A further analysis of the classical solution is beyond the scope of this thesis and we refer the reader to the literature, for example, [136] for a more detailed discussion.

Once the electromagnetic field including the scattering is obtained, the classical radiation force is determined via the momentum conservation law: the force acting on the dielectric is the change in momentum of the EM field and can be determined from Maxwell's stress tensor. The total force on an object interacting with the EM field consists of the change of mechanical momentum and field momentum  $\mathbf{F}_{\text{tot}} = d\mathbf{P}_{\text{mech}}/dt + d\mathbf{P}_{\text{field}}/dt$  with

$$\begin{aligned} \frac{d}{dt}\mathbf{P}_{\text{mech}} &= \int_V d\mathbf{x}(\rho_e \mathbf{E} + \mathbf{J} \times \mathbf{B}) \\ \frac{d}{dt}\mathbf{P}_{\text{field}} &= \frac{d}{dt} \int_V d\mathbf{x}(\mathbf{E} \times \mathbf{B}), \end{aligned} \quad (2.72)$$

where  $\mathbf{B}$  denotes the magnetic field,  $\rho_e$  the charge density and  $\mathbf{J}$  the current. Rewriting and manipulating this equation (see [142] for details) yields a formulation in terms of Maxwell's stress tensor,

$$\mathbf{F}_{\text{tot}} = \int_S \mathbf{T} \mathbf{n} dA, \quad (2.73)$$

where the integration is taken over the surface  $dA$  of the object and  $\mathbf{n}$  is the outward normal vector to the closed surface  $S$ . Maxwell's stress tensor is given by the electric and magnetic fields

$$T_{\alpha\beta} = \epsilon_0 \left[ E_\alpha E_\beta + c^2 B_\alpha B_\beta - \frac{1}{2}(\mathbf{E}\mathbf{E} + c^2 \mathbf{B}\mathbf{B})\delta_{\alpha\beta} \right]. \quad (2.74)$$

Plugging in the expression for the scattered electromagnetic field in the above equation, we can determine the forces on the dielectric. This method to determine forces enables one to calculate trapping of dielectrics and also to determine radiation pressure effects. However, this approach cannot be used to determine a full dynamical description of the system and its decoherence rates.

## 2.B Wigner-Weisskopf with correlations in the field

In this Appendix, an alternative approach to the description of the interaction between a single photon and a dielectric is given within the Wigner-Weisskopf ansatz. In contrast to a direct description with master equations, where information about the light fields

can be extracted via the quantum regression theorem, the Wigner-Weisskopf approach directly yields expressions for the photonic fields. Analyzing the light emitted from the cavity yields information about the mechanical state of the system. Following [150], it is possible to determine the occupation of the mechanical mode, and thus, to monitor the cooling of the system. Complementing the master equation ansatz, in App. 2.B.1, we solve the equations of motion for the coefficients of the density matrix taking into account correlations among the free modes of the field. In full analogy to the solution of the Heisenberg equations of motion given in Sec. 2.3.1, the equations of motion for the coefficients of the density matrix can be demonstrated to be equivalent to the Lippmann-Schwinger equation enabling one to use solutions of the classical scattering equations. Subsequently, an inhomogeneity in the electromagnetic field is added in App. 2.B.2 and its effect on the scattered fields is investigated yielding a master equation describing the decay of the cavity mode.

### 2.B.1 Free photons

Here, the evolution of a single photon in a plane-wave state interacting with a dielectric is discussed. For simplicity, the motion of the object is neglected for now, assuming  $M \rightarrow \infty$ . The coefficients of the wave function in the Schrödinger picture are defined by

$$|\psi\rangle = \int d\mathbf{k} c_{\mathbf{k}}(t) \hat{a}_{\mathbf{k}}^{\dagger} |\Omega\rangle, \quad (2.75)$$

where  $|\Omega\rangle$  denotes the vacuum state. The assumption that the object's mass is infinite manifests itself in the independence of the wave function of the object's momentum state: the effect of the photon's recoil on the dielectric is neglected. Note however that the dependance of the equations of motion on  $\hat{r}$  is kept for later convenience. To obtain the equations of motion, we let the homogeneous part of the Hamiltonian given by Eq. (2.10),  $\hat{H}_B$ , act on the above wave function. This yields

$$i\dot{c}_{\mathbf{k}}(t) = \omega_{\mathbf{k}} c_{\mathbf{k}}(t) + \epsilon_c \int_{V(\hat{r})} d\mathbf{x} \int d\mathbf{k}' \sqrt{\omega_{\mathbf{k}} \omega_{\mathbf{k}'}} (c_{\mathbf{k}'}(t') e^{i(\mathbf{k}-\mathbf{k}')\mathbf{x}} + c_{\mathbf{k}'}^*(t) e^{i(\mathbf{k}+\mathbf{k}')\mathbf{x}}). \quad (2.76)$$

In order to close this system of equations, we define

$$h^{(+)}(\mathbf{x}, \hat{r}, t) = i \int d\mathbf{k} \sqrt{\omega_{\mathbf{k}}} e^{-i\mathbf{k}(\mathbf{x}+\hat{r})} c_{\mathbf{k}}(t), \quad (2.77)$$

with  $h(\mathbf{x}, \hat{r}, t) = h^{(+)}(\mathbf{x}, \hat{r}, t) + h^{(-)}(\mathbf{x}, \hat{r}, t)$ . Subsequently we multiply both sides of Eq. (2.76) by  $i \int d\mathbf{k} \sqrt{\omega_{\mathbf{k}}} \exp(-i\mathbf{k}\mathbf{x})$ . A formal integration over time and a transition to the frame rotating at a frequency  $\omega_0$ ,  $\tilde{h}(\mathbf{x}, \hat{r}, t)^{(\pm)} = \exp(\pm i\omega_0 t) h^{(\pm)}(\mathbf{x}, t)$ , yields

$$h^{(+)}(\mathbf{x}, \hat{r}, t) = h_{\text{in}}^{(+)}(\mathbf{x}, \hat{r}, t) + \epsilon_c \int d\mathbf{k} \int_{V(\hat{r})} d\mathbf{x}' e^{-i\mathbf{k}(\mathbf{x}-\mathbf{x}')} \frac{\omega_{\mathbf{k}}}{\omega_{\mathbf{k}} - \omega_0 + i\gamma} h^{(+)}(\mathbf{x}', \hat{r}, t), \quad (2.78)$$

where  $h_{\text{in}}^{(+)}(\mathbf{x}, \hat{r}, t)$  is defined in analogy to Eq. (2.16). Also here, we assume  $h^{(+)}(\mathbf{x}, \hat{r}, t)$  to be peaked at  $\omega_0$ . In order to solve this differential equation, we have taken the slowly-varying approximation, assuming that  $\tilde{h}(\mathbf{x}, \hat{r}, t)^{(\pm)}$  can be taken out of the integration that is extended to  $t \rightarrow \infty$ . A transformation back to the coefficient picture thus gives in full analogy to the operators of the electromagnetic field, Sec. 2.3.1,

$$c_{\mathbf{k}}(t) = \int d\mathbf{k}' e^{-i\omega_{\mathbf{k}'}t} \left( \delta(\mathbf{k} - \mathbf{k}') + \frac{\mathcal{T}_{\mathbf{k}, \mathbf{k}'}(\hat{r})}{\omega_{\mathbf{k}'} - \omega_0 + i\gamma} \right) c_{\mathbf{k}'}(0). \quad (2.79)$$

The coefficients contain the information about the full dynamical evolution of the system and can be used to reconstruct its density matrix.

### 2.B.2 Cavity field

In this section the analysis of the main part of this chapter is extended to the more general case, where an inhomogeneity in the electromagnetic field is present. This inhomogeneity is typically a cavity that changes the system's mode distribution. Also in this case, the cm degree of freedom is treated as a number and its motion in the cavity is neglected. We solve the Schrödinger eqs. of motion for the coefficients in Sec. 2.B.2 and subsequently derive the master equation for the time evolution of the cavity mode  $\hat{a}_0$  in Sec. 2.B.2.

#### Solution of the inhomogeneous part

The wave function including the cavity mode is written as

$$|\psi\rangle = c_0(t)\hat{a}_0^\dagger|\Omega\rangle + \int d\mathbf{k} c_{\mathbf{k}}(t)\hat{a}_{\mathbf{k}}^\dagger|\Omega\rangle + s_0|\Omega\rangle, \quad (2.80)$$

where  $s_0$  is constant and  $c_0(t)$ ,  $c_{\mathbf{k}}(t)$  are time-dependent. The Hamiltonian, Eq. (2.7) causing the scattering consists of two parts,  $\hat{W}(\hat{r})$ , Eq. (2.11) describing the coupling among the homogeneous modes and  $\hat{H}_{\text{BS}}$ , Eq. (2.12) denoting the coupling of the inhomogeneity (cavity mode) to the free ones. The following equations of motion are obtained:

$$\begin{aligned} i\dot{c}_{\mathbf{k}}(t) = & \epsilon_c \int_{V(\hat{r})} d\mathbf{x} \int d\mathbf{k}' e^{i(\mathbf{k}-\mathbf{k}')\mathbf{x}} \sqrt{\omega_{\mathbf{k}}\omega_{\mathbf{k}'}} c_{\mathbf{k}'}(t) \\ & + \epsilon_c \int_{V(\hat{r})} d\mathbf{x} \sqrt{\frac{\omega_{\mathbf{k}}\omega_0}{2V_0}} e^{-i\mathbf{k}\mathbf{x}} f(\mathbf{x}) c_0(t) + \omega_{\mathbf{k}} c_{\mathbf{k}}(t) \end{aligned} \quad (2.81)$$

and

$$i\dot{c}_0(t) = \epsilon_c \int_{V(\hat{r})} d\mathbf{x} \int d\mathbf{k} \sqrt{\frac{\omega_0\omega_{\mathbf{k}}}{2V_0}} e^{i\mathbf{k}\mathbf{x}} f^*(\mathbf{x}) c_{\mathbf{k}}(t) + \omega_0 c_0(t), \quad (2.82)$$

where the rotating-wave approximation has been taken, which is equivalent to remaining in the one-excitation manifold. Using Eq. (2.77), we can simplify Eqs. (2.81), (2.82) to obtain after an integration over time

$$h_{\text{inh}}^{(+)}(\mathbf{x}, \hat{r}, t) = h^{(+)}(\mathbf{x}, \hat{r}, t) + d(\mathbf{x}, \hat{r}, t) \quad (2.83)$$

with

$$d(\mathbf{x}, \hat{r}, t) = \int d\mathbf{k} \mathcal{A}(\mathbf{k}, \hat{r}, t) e^{i\mathbf{k}\mathbf{x}}, \quad (2.84)$$

and

$$\mathcal{A}(\mathbf{k}, \hat{r}, t) = \epsilon_c \int_0^t d\tau e^{-i(\omega_0 - \omega_{\mathbf{k}})\tau} \int_{V(\hat{r})} d\mathbf{x}' \omega_{\mathbf{k}} \sqrt{\frac{\omega_0}{2V_0}} e^{-i\mathbf{k}\mathbf{x}'} f(\mathbf{x}') c_0(\tau). \quad (2.85)$$

The first part of the integration in Eq. (2.83) has been carried out under the Markov assumption, which is justified as correlations in the electromagnetic field decay quickly. No approximation is taken for the time evolution of the inhomogeneous part and it is kept in the most general form for now. The strategy to find a solution for the inhomogeneous case described by Eq. (2.83) is to connect it to the homogeneous one, described in the previous section, Sec. 2.B.1.

The solution of the homogeneous case, Eq. (2.78), can be formally written in vector-form as

$$\begin{aligned} \mathbf{h} &= \mathbf{h}_{\text{in}} + \hat{\mathcal{B}}\mathbf{h} \\ \mathbf{h} &= \frac{1}{1 - \hat{\mathcal{B}}} \mathbf{h}_{\text{in}}, \end{aligned} \quad (2.86)$$

where  $\hat{\mathcal{B}}$  describes the scattering operator in matrix form and  $\mathbf{h}$  denotes the continuous vector-representation of  $h(\mathbf{x}, \hat{r}, t)$ . Comparing the homogeneous case to the inhomogeneous one, an additional inhomogeneous term is present leading in analogy to Eq. (2.86) to

$$\begin{aligned} \mathbf{h} &= \mathbf{h}_{\text{in}} + \hat{\mathcal{B}}\mathbf{h} + \mathbf{d} \\ \mathbf{h} &= \frac{1}{1 - \hat{\mathcal{B}}} (\mathbf{h}_{\text{in}} + \mathbf{d}), \end{aligned} \quad (2.87)$$

where  $1/(1 - \hat{\mathcal{B}})$  denotes the solution-operator for the plane-wave state. This equivalence facilitates the solution of the inhomogeneous system by connecting it to the homogeneous one. The system is initially assumed to have one photon in the cavity mode and none in the homogeneous modes,  $c_{\mathbf{k}}(0) = 0$ , such that  $\mathbf{h}_{\text{in}} = 0$  and Eq. (2.83) can be solved as

$$h_{\text{inh}}^{(+)}(\mathbf{x}, \hat{r}, t) = d_{\text{in}}(\mathbf{x}, \hat{r}, t) + \epsilon_c \int d\mathbf{k} \int_{V(\hat{r})} d\mathbf{x}' e^{-i\mathbf{k}(\mathbf{x} - \mathbf{x}')} \frac{\omega_{\mathbf{k}}}{\omega_{\mathbf{k}} - \omega_0 + i\gamma} d(\mathbf{x}, \hat{r}, t), \quad (2.88)$$

where  $d_{\text{in}}(\mathbf{x}, \hat{r}, t)$  is defined in analogy to Eq. (2.16). Taking the inverse transformation yields the solution for the coefficients  $c_{\mathbf{k}}(t)$

$$c_{\mathbf{k}}(t) = \int d\mathbf{k}' e^{-i\omega_{\mathbf{k}'}t} \left( \delta(\mathbf{k} - \mathbf{k}') + \frac{\mathcal{T}_{\mathbf{k},\mathbf{k}'(\hat{r})}}{\omega_{\mathbf{k}'} - \omega_0 + i\gamma} \right) \mathcal{A}(\mathbf{k}', \hat{r}, 0). \quad (2.89)$$

Plugging Eq. (2.88) back into Eq. (2.82), we can close the equations of motion. After taking the Markov approximation assuming that the system does not change significantly during the interaction with the environment, such that  $c_0(t - \tau) \approx c_0(t)$ , and using some standard relations for the scattering operators, the time evolution of the inhomogeneous mode in terms of transition operators is given by

$$\frac{\dot{c}_0(t)}{c_0(t)} = - \int d\mathbf{k} |\mathcal{T}_{\mathbf{k},c}(\hat{r})|^2 \left[ \pi \delta(\omega_{\mathbf{k}} - \omega_0) + i\mathcal{P} \frac{1}{\omega_{\mathbf{k}} - \omega_0} \right]. \quad (2.90)$$

The effect on the light field can be determined approximating  $\mathcal{T}_{\mathbf{k},c}(\hat{r}) \approx \mathcal{T}_{\mathbf{k},c}(0)$  thus neglecting the effect on the cm mode. Integration gives

$$c_0(t) = \exp((- \kappa + i\Delta^L)t) c_0(0) \quad (2.91)$$

with the decay rate

$$\kappa = -\text{Re} \left( \frac{\dot{c}_0(t)}{c_0(t)} \right) \quad (2.92)$$

and a Lamb shift

$$\Delta^L = -\text{Im} \left( \frac{\dot{c}_0(t)}{c_0(t)} \right). \quad (2.93)$$

These results are in accordance with Fermi's Platinum Rule, the extension of Fermi's Golden Rule to all orders in multiple-scattering processes [154].

### From the coefficients to the master equation

Starting from the wave function Eq. (2.80), the system's density matrix is obtained by tracing out the environment and can be written as [155]

$$\hat{\rho}_S(t) = \begin{pmatrix} |c_0(t)|^2 & s_0^* c_0(t) \\ s_0 c_0(t)^* & 1 - |c_0(t)|^2 \end{pmatrix}. \quad (2.94)$$

Taking the derivative gives

$$\dot{\rho}_S(t) = \begin{pmatrix} \frac{d}{dt} |c_0(t)|^2 & s_0^* \dot{c}_0(t) \\ s_0 \dot{c}_0(t)^* & -\frac{d}{dt} |c_0(t)|^2 \end{pmatrix}. \quad (2.95)$$

Using Eqs. (2.92), (2.93) finally yields

$$\dot{\rho}_S = -i \left[ \Delta^L \hat{a}_0^\dagger \hat{a}_0, \hat{\rho}_S \right] + \mathcal{L}^L[\hat{\rho}_S] \quad (2.96)$$

with

$$\mathcal{L}^L[\hat{\rho}_S] = \kappa \left( 2\hat{a}_0 \hat{\rho}_S \hat{a}_0^\dagger - [\hat{a}_0^\dagger \hat{a}_0, \hat{\rho}_S] \right), \quad (2.97)$$

where  $\Delta^L$  denotes a shift of the energy levels, and  $\kappa$  describes the decay rate of the cavity photons due to losses effected by the presence of the dielectric. This master equation and its decay rates are equivalent to the result for the light fields obtained in Sec. 2.3.

## 2.C Mie scattering theory

In this Appendix we outline the method of Mie scattering theory applicable to spherical objects, one of the few cases, where an analytic solution of light scattering beyond the point-particle approximation is possible. We only give a brief summary of the theory here, for more details we refer the reader to standard textbooks [141, 142]. The Mie solution is used in this thesis to give a description of optomechanics with levitating dielectrics in Chap. 3. The idea behind the solution is to express all fields in spherical coordinates facilitating the application of boundary conditions for spherical objects <sup>2</sup>.

### 2.C.1 Expansion of the incoming electric field in terms of spherical harmonics

In general, a plane wave can be expanded in spherical harmonics [141, 142],

$$\psi = \exp(ikz) = \exp(ikr \cos(\theta)) = \sum_{n=0}^{\infty} i^n (2n+1) j_n(kr) P_n(\cos(\theta)), \quad (2.98)$$

where  $j_n(kr)$  is a Bessel function and  $P_n(\cos(\theta))$  the Legendre polynomial. Here  $z = r \cos(\theta)$  in spherical coordinates. In combination with its conjugate this gives

$$\cos(kr \cos(\theta)) = \sum_{n=0}^{\infty} (i^n + (-i)^n) (2n+1) j_n(kr) P_n(\cos(\theta)). \quad (2.99)$$

These scalar functions are solutions to the Helmholtz equation

$$\nabla^2 \psi = -k^2 \psi. \quad (2.100)$$

---

<sup>2</sup>Note that due to the supplementary character of this section, not all of the parameters defined here are listed in Sec. 8.

As the electric fields considered throughout the thesis are not scalar, but vectorial, we are interested in the expansion of the vector field polarized in x-direction

$$\mathbf{E}(\mathbf{x}) = \mathbf{e}_x \cos(kr \cos(\theta) - \phi_0), \quad (2.101)$$

where  $\phi_0$  is an arbitrary phase shift. This solution can be constructed from the scalar solution  $\psi$  in the following way: It can be shown that when  $\psi$  fulfills the scalar Helmholtz equation, vectors constructed like

$$\mathbf{M} = \nabla \times (\mathbf{c}\psi), \quad \mathbf{N} = \frac{1}{k} \nabla \times \mathbf{M}, \quad (2.102)$$

fulfill the vector Helmholtz equation

$$\nabla^2 \mathbf{A} = k^2 \mathbf{A}, \quad (2.103)$$

where  $\mathbf{A}$  denotes any vector. Now the generating function  $\psi$  and the pilot vector  $\mathbf{c}$  have to be chosen appropriate to the problem- for the sphere, one typically chooses  $\mathbf{c} = \mathbf{r}$ , which is the radius vector and  $\psi$  is chosen such that it fulfills the scalar wave equation in spherical coordinates

$$\psi_{emn} = \cos(m\phi) P_n^m(\cos(\theta)) z_n(kr) \quad (2.104)$$

$$\psi_{omn} = \sin(m\phi) P_n^m(\cos(\theta)) z_n(kr), \quad (2.105)$$

where  $z_n(kR)$  is any Bessel function and the subscripts denote even ( $e$ ) and odd ( $o$ ). We obtain for the vectors  $\mathbf{M}, \mathbf{N}$  in component form

$$\begin{aligned} \mathbf{M}_{emn} &= -\frac{m}{\sin \theta} \sin(m\phi) P_n^m(\cos(\theta)) z_n(kr) \mathbf{e}_\theta - \cos(m\phi) \frac{dP_n^m(\cos(\theta))}{d\theta} z_n(kr) \mathbf{e}_\phi, \\ \mathbf{M}_{omn} &= -\frac{m}{\sin \theta} \cos(m\phi) P_n^m(\cos(\theta)) z_n(kr) \mathbf{e}_\theta - \sin(m\phi) \frac{dP_n^m(\cos(\theta))}{d\theta} z_n(kr) \mathbf{e}_\phi, \\ \mathbf{N}_{emn} &= \frac{z_n(kr)}{kr} \cos(m\phi) n(n+1) P_n^m(\cos(\theta)) \mathbf{e}_r + \cos(m\phi) \frac{dP_n^m(\cos(\theta))}{d\theta} \frac{1}{kr} \frac{d}{dkr} (kr z_n(kr)) \mathbf{e}_\theta \\ &\quad - m \sin(m\phi) \frac{P_n^m(\cos(\theta))}{\sin(\theta)} \frac{1}{kr} \frac{d}{dkr} (kr z_n(kr)) \mathbf{e}_\phi, \\ \mathbf{N}_{omn} &= \frac{z_n(kr)}{kr} \sin(m\phi) n(n+1) P_n^m(\cos(\theta)) \mathbf{e}_r + \sin(m\phi) \frac{dP_n^m(\cos(\theta))}{d\theta} \frac{1}{kr} \frac{d}{dkr} (kr z_n(kr)) \mathbf{e}_\theta \\ &\quad + m \cos(m\phi) \frac{P_n^m(\cos(\theta))}{\sin(\theta)} \frac{1}{kr} \frac{d}{dkr} (kr z_n(kr)) \mathbf{e}_\phi. \end{aligned} \quad (2.106)$$

From the consideration of odd and even properties of the above vectors, we see that in order to represent the unitary vector

$$\mathbf{e}_x = \sin \theta \cos \phi \mathbf{e}_r + \cos \theta \cos \phi \mathbf{e}_\theta - \sin \phi \mathbf{e}_\phi, \quad (2.107)$$

the expansion of the electric field has to be of the form

$$\mathbf{E}_i(\mathbf{x}) = E_0 \mathbf{e}_x \cos(kr \cos(\theta) - \phi_0) = E_0 \sum_{n=1}^{\infty} (\beta_n \mathbf{M}_{o1n} + \delta_n \mathbf{N}_{e1n}). \quad (2.108)$$

The coefficients  $\beta_n, \delta_n$  can be determined by the overlap with the expanded wave function under consideration of the orthogonality relations of the Legendre polynomials.  $\beta_0$  and  $\delta_0$  are always zero, such that the summation begins at  $n = 1$ . Finally

$$\mathbf{E}_i(\mathbf{x}) = E_0 \sum_{n=1}^{\infty} \left( i^n e^{-i\phi_0} + (-i)^n e^{i\phi_0} \right) \frac{2n+1}{n(n+1)} (\mathbf{M}_{o1n}^{(1)} - i \mathbf{N}_{e1n}^{(1)}), \quad (2.109)$$

where the superscript (1) denotes the use of the spherical Bessel functions of the first kind for the radial dependence.

### 2.C.2 Determination of the fields due to the boundary conditions

We can now determine the scattered field and the field inside the sphere by means of the boundary conditions at the surface of the sphere. In component form, these read

$$E_{i,\theta} + E_{s,\theta} = E_{in,\theta}, \quad E_{i,\phi} + E_{s,\phi} = E_{in,\phi} \quad (2.110)$$

$$H_{i,\theta} + H_{s,\theta} = H_{in,\theta}, \quad H_{i,\phi} + E_{s,\phi} = H_{in,\phi} \quad (2.111)$$

at  $r = R$  (radius of the sphere). Here  $E_{in}$  is the field inside the sphere,  $E_s$  is the scattered field,  $E_i$  the incoming one, and  $\mathbf{H}$  denotes the magnetic part of the electromagnetic field. From this, the field inside the sphere can be written as

$$\mathbf{E}_{in}(\mathbf{x}) = E_0 \sum_{n=1}^{\infty} \left( i^n e^{-i\phi_0} + (-i)^n e^{i\phi_0} \right) \frac{2n+1}{n(n+1)} (c_n \mathbf{M}_{o1n}^{(1)} - i d_n \mathbf{N}_{e1n}^{(1)}), \quad (2.112)$$

and the scattered field as

$$\mathbf{E}_s(\mathbf{x}) = E_0 \sum_{n=1}^{\infty} \left( i^n e^{-i\phi_0} + (-i)^n e^{i\phi_0} \right) \frac{2n+1}{n(n+1)} (-b_n \mathbf{M}_{o1n}^{(3)} + i a_n \mathbf{N}_{e1n}^{(3)}), \quad (2.113)$$

where the superscript (3), denotes the use of spherical Hankel functions for the radial dependence. The expansion coefficients can thus be obtained by the above boundary condition and can be written as

$$a_n = \frac{\sqrt{\epsilon_r} \psi_n(\sqrt{\epsilon_r} x) \psi_n'(x) - \psi_n'(\sqrt{\epsilon_r} x) \psi_n(x)}{\sqrt{\epsilon_r} \psi_n(\sqrt{\epsilon_r} x) \zeta_n'(x) - \psi_n'(\sqrt{\epsilon_r} x) \zeta_n(x)} \quad (2.114)$$

$$b_n = \frac{\psi_n(\sqrt{\epsilon_r} x) \psi_n'(x) - \sqrt{\epsilon_r} \psi_n'(\sqrt{\epsilon_r} x) \psi_n(x)}{\psi_n(\sqrt{\epsilon_r} x) \zeta_n'(x) - \sqrt{\epsilon_r} \psi_n'(\sqrt{\epsilon_r} x) \zeta_n(x)} \quad (2.115)$$

$$c_n = \frac{i}{\sqrt{\epsilon_r} \psi_n(\sqrt{\epsilon_r} x) \zeta_n'(x) - \psi_n'(\sqrt{\epsilon_r} x) \zeta_n(x)} \quad (2.116)$$

$$d_n = \frac{i}{\psi_n(\sqrt{\epsilon_r} x) \zeta_n'(x) - \sqrt{\epsilon_r} \psi_n'(\sqrt{\epsilon_r} x) \zeta_n(x)}, \quad (2.117)$$

where  $x = k_c R = 2\pi R/\lambda_c$  and  $\psi_n(x) = x j_n(x)$ ,  $\zeta_n(x) = x h^{(1)}(x)$  are the so-called *Riccati-Bessel functions*.

### 2.C.3 Determination of the scattering cross section

The scattering cross section is defined as

$$\sigma_{\text{scatt}} = \frac{W_s}{I_i}, \quad (2.118)$$

where  $I_i$  is the incident intensity

$$I_i = \frac{E_0^2 \cos^2(\phi_0) k}{2} \quad (2.119)$$

and

$$W_s = \frac{1}{2} \text{Re} \int_0^{2\pi} \int_0^\pi r^2 \sin(\theta) d\theta d\phi (\mathbf{E}_s \times \mathbf{H}_s) \mathbf{e}_r. \quad (2.120)$$

Exploiting the properties of the Legendre polynomials, we are left with

$$W_s = \frac{\pi}{k_c} \sum_{n=1}^{\infty} E_0^2 (2n+1) \cos^2\left(\frac{n\pi}{2} - \phi_0\right) (|a_n|^2 + |b_n|^2). \quad (2.121)$$

And consequently

$$\sigma_{\text{scatt}} = \frac{2\pi}{k_c^2} \sum_{n=1}^{\infty} (2n+1) \frac{\cos^2\left(\frac{n\pi}{2} - \phi_0\right)}{\cos^2(\phi_0)} (|a_n|^2 + |b_n|^2) \quad (2.122)$$

For a position of the center of mass of the sphere at  $r = \frac{\pi}{4}$ , the scattering cross section finally reads

$$\sigma_{\text{scatt}} = \frac{2\pi}{k_c^2} \sum_{n=1}^{\infty} (2n+1) (|a_n|^2 + |b_n|^2), \quad (2.123)$$

with the coefficients as defined above.

## Chapter 3

# Cavity-optomechanics with levitating spheres

*We apply the master-equation approach developed in Chapter 2 to the specific setup of levitating dielectric spheres in optical cavities. The optomechanical parameters are derived and the suitability of the system for cavity-optomechanical applications is analyzed. Different sources of decoherence e.g., photon scattering, scattering of air molecules, blackbody radiation and others are taken into account. In addition, a quantum theory of elasticity is used to study the coupling of the center-of-mass motion with internal vibrational excitations of the dielectric. To analyze the possibility of ground-state cooling, we derive an expression for the steady-state phonon numbers without relying on resolved-sideband or bad-cavity approximations. Within this theoretical framework, we analyze the optomechanical properties for realistic experimental parameters and show that cavity-cooling to the motional ground state of the cm mode is possible for spheres with  $R \lesssim 260\text{nm}$ . This chapter mainly bases on and uses parts of [64, 88].*

### 3.1 Introduction

After the original proposal [77, 78] to use levitating dielectrics as an optomechanical system, broad interest in the community with several experimental groups working on their realization has been generated [91, 97–99, 101] (also see Sec. 1.2 for a more complete introduction). We aim at providing a complete theoretical description of this novel system. This is particularly challenging when objects on the order of the optical wavelength are considered– the regime, where the point-particle approximation loses its validity. Therefore, we apply the general theory for the interaction between light and dielectrics, developed in Chap. 2, to this optomechanical setup. This promotes a theoretical derivation from first principles and all optomechanical parameters are derived

within this framework. We also take into account various decoherence mechanisms relevant for this system. We investigate the coupling of the center-of-mass motion to other (vibrational) modes of the dielectric and show that it is negligible. Also cooling is analyzed in a general framework, without relying on the common approximations. More specifically, we obtain the steady-state phonon numbers of the system without relying on the common resolved-sideband or bad-cavity approximations. We analyze the problem of laser-cooling with spheres of diameters ranging from the nm-scale to dielectrics comparable or even larger than the cavity mode wavelength. While ground-state cooling can be achieved for spheres much smaller than the wavelength, the minimal phonon numbers attainable for larger spheres oscillate around values of  $n_{\min} \approx 500$ . Note that this approach assumes that all photons are scattered into the bath modes, which is justified for objects that are not adapted to the cavity geometry, such as spheres or cylinders, but not for membranes [90].

### 3.1.1 Reader's guide

The chapter is organized as follows: in Sec. 3.2 we specify the master-equation to the experimental setup of levitating dielectric spheres in an optomechanical cavity including optomechanical couplings, decay and decoherence rates. To describe couplings between the cm motion and the vibrational modes, we derive a theory of quantum elasticity in Sec. 3.4. This is followed by an analysis of various sources of noise and decoherence in Sec. 3.5. We begin with a study of the general form of the master equation in Sec. 3.5.1 to analyze scattering of air molecules (Sec. 3.5.2), the effect of blackbody radiation (Sec 3.5.3), parametric heating due to shot noise (Sec. 3.5.4), fluctuations in the trap center (Sec. 3.5.5), anisotropies (Sec. 3.5.6), and the effect of coupling to internal two-level systems of the material (Sec. 3.5.7). In Sec. 3.3 we derive and solve the cooling equations and finally analyze the possibility of ground state cooling for realistic experimental parameters in Sec.3.6.

## 3.2 Cavity quantum-optomechanics with levitating spheres

We thus proceed to determine the optomechanical parameters related to interactions with light for levitating dielectric spheres. The setup is sketched in Fig. 3.1: a classical light field, effected by a retro-reflected optical tweezers,  $\mathcal{E}_{\text{tw}}(\mathbf{x}, t)$ , creates a harmonic trap for the cm of the dielectric, (note that trapping via a strongly-populated cavity mode can be described in full analogy). Besides, a second cavity mode  $\hat{E}_{\text{cav}}(\mathbf{x}, t)$  is

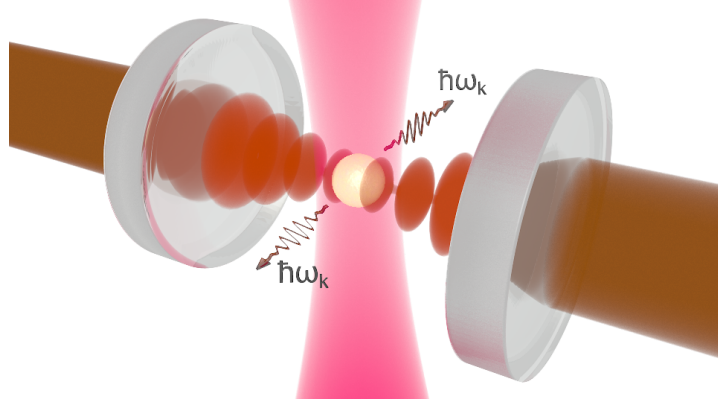


Figure 3.1: Schematic representation of the setup: A dielectric sphere of a radius similar or larger than the cavity wave length is trapped by optical tweezers providing a trapping frequency  $\omega_t$ . It is placed inside an optical cavity, where a second laser is used to optically manipulate the dielectric's center-of-mass degree of freedom.

used to manipulate it, such that

$$\begin{aligned}\hat{E}_S(\mathbf{x}, t) &= \hat{E}_{\text{cav}}(\mathbf{x}, t) \\ \mathcal{E}_S(\mathbf{x}, t) &= \mathcal{E}_{\text{tw}}(\mathbf{x}, t) + \mathcal{E}_{\text{cav}}(\mathbf{x}, t).\end{aligned}\quad (3.1)$$

The optical tweezers used for the trapping is given by

$$\mathcal{E}_{\text{tw}}(\mathbf{x}, t) = E_0 \frac{W_t}{W(y)} \exp\left(-\frac{x^2 + z^2}{W(y)^2}\right), \quad (3.2)$$

where

$$E_0 = \sqrt{\frac{P_t}{\epsilon_0 c \pi W_t^2}}, \quad (3.3)$$

$P_t$  is the laser power,  $W_t$  is the laser beam waist,

$$W(y) = W_t \sqrt{1 + \left(y \frac{\lambda_c}{\pi W_t^2}\right)^2} \quad (3.4)$$

and we assume the beam to be aligned as sketched in Fig. 3.1. While we are only interested in the classical part of this field (as it is used solely for the trapping), we include both the quantum and the classical part of the cavity field consisting of a standing wave in  $z$ -direction and a Gaussian profile in  $x$ - and  $y$ -direction,

$$\begin{aligned}\hat{E}_{\text{cav}}(\mathbf{x}, t) &= i \sqrt{\frac{\omega_0}{\epsilon_0 V_0}} (f_{\text{cav}}(\mathbf{x}) \hat{a}_0 - \text{H.c.}) \\ \mathcal{E}_{\text{cav}}(\mathbf{x}, t) &= i \sqrt{\frac{\omega_0}{\epsilon_0 V_0}} (f_{\text{cav}}(\mathbf{x}) \alpha - \text{H.c.}).\end{aligned}\quad (3.5)$$

This equation denotes the cavity field in the displaced form, where  $|\alpha|^2 = n_{\text{phot}}$  is the mean number of photons in the steady state,

$$n_{\text{phot}} = \frac{\sqrt{2P_c\kappa/\omega_0}}{i\delta + \kappa}, \quad (3.6)$$

with  $P_c$  being the power of the driving laser,  $\kappa$  the cavity decay rate and  $\delta$  the detuning. The mode function is given by

$$f_{\text{cav}}(\mathbf{x}) = \exp\left(-\frac{x^2 + y^2}{W_0^2}\right) \cos(k_{0,z}z - \varphi), \quad (3.7)$$

where  $\varphi$  denotes the equilibrium position of the dielectric,  $\mathbf{k}_0$  the wave vector of the cavity light, and the mode volume is given by  $V_0 = L\pi W_0^2/4$  with  $L$  being the cavity length and  $W_0$  its waist. While the classical term merely yields a shift of the trapping frequency and the equilibrium position, the quantum part of the mode function is used to manipulate the cm degree of freedom of the dielectric including the part describing the opto-mechanical coupling. Note that we only consider one mode of the cavity here, higher harmonics are not included, they are contained in the continuum of homogeneous modes and coupling to them is treated as losses. In case of using a second cavity mode for the trapping instead of the tweezers, Eq. (3.5) simply has to be summed over several modes with different profiles.

The full dynamics of the system is obtained taking into account the coupling of the tweezers and the cavity mode to the vacuum modes, given by Eq. (2.4). The full master equation is described by Eq. (2.54) with the corresponding decay rates given by Eq. (2.44) and Eq. (2.51), where  $\Gamma$  contains contributions of the cavity mode and the tweezers.

The specific description of spheres is eased by the availability of an analytical solution, the Mie solution, for the scattered fields and cross sections [140, 141]. Recall that the Mie solution is based on expanding the incoming electromagnetic field in spherical waves, an expansion that suits the sphere's geometry and it is thus possible to apply boundary conditions to determine the scattered fields. Note that while the polarization of the electromagnetic field has been neglected to ease the notation in the previous sections, we take it into account here. The Mie solution is defined for plane-wave states, and we use the relation

$$\mathcal{T}_{\mathbf{k},\mathbf{k}'} = \frac{ic^2}{2\pi\omega_{\mathbf{k}}} f(\mathbf{k}, \mathbf{k}') \quad (3.8)$$

between the matrix elements of the scattering operator and the classical amplitudes to simplify the solution.

For spherical objects, assuming a vanishing absorption,  $\text{Im}[\epsilon_r] \approx 0$ , it is possible to connect all quantities to the classical scattering amplitude in the forward direction

using the optical theorem, Eq. (2.24), which yields

$$f(\mathbf{k}, \mathbf{k}) = \frac{\sqrt{2\pi}}{|\mathbf{k}|} \sum_{n=1}^{\infty} (2n+1)(a_n + b_n). \quad (3.9)$$

The coefficients  $a_n, b_n$  depend on the dielectric constant and the radius of the sphere, they are defined in terms of spherical Bessel functions, see Chapter 2.C for their specific form. Hence, the optomechanical parameters can be determined:

1. The optomechanical coupling is defined by

$$g = \alpha \frac{x_0 \pi c}{2k_0 V_c} \sin(2\varphi) \text{Im} \left[ \sum_{n=1}^{\infty} (2n+1)(-1)^{n+1}(a_n + b_n) \right], \quad (3.10)$$

where  $c$  denotes the velocity of light and  $\varphi$  the position of the sphere in the cavity.

2. The total cavity decay rate is defined by

$$\kappa = \kappa_0 + \frac{c\pi}{2k_0^2 V_c} \text{Re} \left[ \sum_{n=1}^{\infty} (2n+1)(1 + (-1)^n \cos(2\varphi))(a_n + b_n) \right], \quad (3.11)$$

where  $\kappa_0$  denotes the intrinsic cavity decay rate resulting from imperfections in the mirrors and the second term describes the additional contribution effected by the presence of the dielectric.

3. The recoil heating of the dielectric due to scattering of cavity photons can be computed as

$$\Gamma_{\text{cav}} = \frac{x_0^2 c \alpha^2 \pi}{V_c} \text{Re} \left[ \sum_{n=1}^{\infty} (2n+1)(1 + (-1)^n \cos(2\varphi))(a_n + b_n) \right]. \quad (3.12)$$

Note that the recoil heating from the trapping lasers can be obtained in full analogy by inserting the tweezers mode.

Besides the minimal phonon number  $n_{\text{min}}$  describing the possibility to cool the system (close) to its quantum-mechanical ground state, another figure of merit to describe the cavity-optomechanical properties is the cooperativity  $\mathcal{C}$ . This measure for the coherent coupling between the motion and light is defined by

$$\mathcal{C} = \frac{g^2}{\Gamma \kappa} \quad (3.13)$$

and depends on the size of the particle and its position in the cavity, where  $\Gamma$  denotes the sum of all relevant decoherence mechanisms. It is in particular essential to have a sufficiently high cooperativity to perform protocols coupling the cm to the light [64].

Assuming that the object is positioned at the maximal slope of the standing wave and is much smaller than the laser's waist, the asymptotic form in the two limits of the cooperativity is given by

$$\mathcal{C} \propto \begin{cases} 1/\epsilon_c^2 k_0^6 R^6 & \text{if } R \ll \lambda_c; \\ 1/k_0^2 R^2 & \text{if } R \gg \lambda_c \end{cases} \quad (3.14)$$

under the assumption that the laser's waist is larger than the object. In case the dielectric is not fully covered by the laser's waist, the beam's Gaussian shape has to be taken into account [156] leading to an even lower cooperativity. Note that this definition applies for  $\kappa \ll \kappa_0$ , where the main contribution to the cavity decay results from the presence of the dielectric.

### 3.3 Cooling

Before applying the master equation discussed in the previous section to the particular case of cavity optomechanics with optically levitating spheres, we provide a general description of optomechanical cooling and the minimal phonon number attainable with master equations of at most quadratic order in the operators of the mechanical and the cavity mode. Cooling is in general a vital ingredient in any attempt to demonstrate quantum-mechanical behavior. Ground-state cooling in an optomechanical setup has first been studied in [45, 47, 157]. Most descriptions make certain approximations to ease calculations *e.g.*, the sideband regime is commonly employed in optomechanical setups. Here, the system will be treated in the most general way not relying on any approximations (as some of them might not be fulfilled for larger objects). The master equations we are interested in are typically of the form (given by Eq. (2.54)),

$$\dot{\rho}_S = i[\hat{\rho}_S, \hat{H}_S + \hat{H}_{\text{rn}}] + \mathcal{L}^M[\hat{\rho}_S] + \mathcal{L}^L[\hat{\rho}_S]. \quad (3.15)$$

The mean phonon number  $\langle \hat{b}^\dagger \hat{b} \rangle$  is coupled to all other expectation values of combinations of the operators  $\hat{a}_0, \hat{a}_0^\dagger, \hat{b}$ , and  $\hat{b}^\dagger$ , yielding the Eqs. of motion in matrix form

$$\dot{\mathbf{v}} = \hat{M}\mathbf{v} + \mathbf{c}, \quad (3.16)$$

where

$$\mathbf{v} = (\langle \hat{b}^\dagger \hat{b} \rangle, \langle \hat{a}_0 \hat{b}^\dagger \rangle, \langle \hat{a}_0^\dagger \hat{a}_0 \rangle, \langle \hat{a}_0^\dagger \hat{b} \rangle, \dots)^T, \quad (3.17)$$

$\hat{M}$  denotes the interaction matrix, and  $\mathbf{c}$  a constant vector. The master equation Eq. (3.15) keeps the Gaussian character for an initially Gaussian state. Subsequently, also the system of equations Eq. (3.16) is Gaussian in the operators  $\hat{a}_0, \hat{a}_0^\dagger, \dots$  and linear

in the expectation values  $\langle \hat{b}^\dagger \hat{b} \rangle$ . Since Eq. (3.16) represents a closed system of equations, they can be solved as

$$\mathbf{v} = e^{\hat{M}t} \mathbf{v}(0) + (e^{\hat{M}t} - 1) \hat{M}^{-1} \mathbf{c}, \quad (3.18)$$

yielding

$$\mathbf{v} = -\hat{M}^{-1} \mathbf{c} \quad (3.19)$$

for the steady state. The steady-state phonon number can be extracted from this quantity as

$$\bar{n}_{\text{phon}} = \lim_{t \rightarrow \infty} \langle \hat{b}^\dagger \hat{b} \rangle = \frac{A_1 - A_2 + A_3}{A_4}. \quad (3.20)$$

with

$$\begin{aligned} A_1 &= -32g^4 \delta [4\delta^2 \kappa + \kappa^3 + 16\delta(\kappa - \Gamma)\omega_t + 8\kappa\omega_t^2], \\ A_2 &= -\Gamma[4\delta^2 + \kappa^2]\omega_t [16\delta^4 + 8\delta^2(\kappa^2 - 4\omega_t^2) + (\kappa^2 + 4\omega_t^2)^2], \\ A_3 &= 4g^2 \{-\kappa(4\delta^2 + \kappa^2)[\kappa^2 + 4(\delta + \omega_t)^2]\omega_t - 2\Gamma\delta[32\omega_t^4 + (4\delta^2 + \kappa^2)^2 + 4(-20\delta^2 + 3\kappa^2)\omega_t^2]\}, \\ A_4 &= 64g^2 \delta \kappa \omega_t [16g^2 \delta + (4\delta^2 + \kappa^2)\omega_t]. \end{aligned} \quad (3.21)$$

This solution might contain unphysical results. To verify that  $\bar{n}_{\text{phon}}$  is indeed a steady state of the system, the eigenvalues of  $\hat{M}$  additionally have to fulfill  $\text{Re}[\text{eig}[\hat{M}]] \leq 0$ . In general, all parameters are determined by the properties of the system, solely the detuning  $\delta$  can be chosen. According to the definition of Eq. (2.55),  $\delta < 0$  denotes red detuning and  $\delta > 0$  blue detuning. To obtain the optimal point for cooling, one consequently has to optimize  $\bar{n}_{\text{phon}}$  with respect to  $\delta$ . Let us now compare this exact solution to the one obtained after an adiabatic elimination of the cavity mode. Starting from Eq. (3.15), we eliminate the cavity mode assuming that its decay rate is much larger than the coupling between the mechanical degree of freedom and the light,  $\kappa \gg g$ . In this case it is justified to assume that the cavity is either empty or contains only one photon, therefore reducing the master equation to the one-excitation manifold, described by  $\rho_{00}, \rho_{10}, \rho_{01}, \rho_{11}$ . Due to the fast decay of the cavity mode described by  $\kappa$ , the change of all contributions involving an excitation is approximately zero, finally yielding an equation of motion for the empty cavity  $\rho_{00}$ . After carrying out a rotating wave approximation assuming  $\omega_t \gg |g^2/(\kappa + i(\delta \pm \omega_t))|$ , the final steady state phonon occupation is given by:

$$\bar{n}_{\text{adiab}} = -\frac{[4g^2\kappa + \Gamma(\kappa^2 + 4(\omega_t - \delta)^2)][\kappa^2 + 4(\delta + \omega_t)^2]}{64g^2\delta\kappa\omega_t}. \quad (3.22)$$

To obtain the minimal occupation number, this equation needs to be optimized with respect to  $\delta$ . Comparing the adiabatically-eliminated solution to the exact one, it becomes clear that the approximation breaks down in the strong-coupling regime  $g \approx \omega_t$ ,

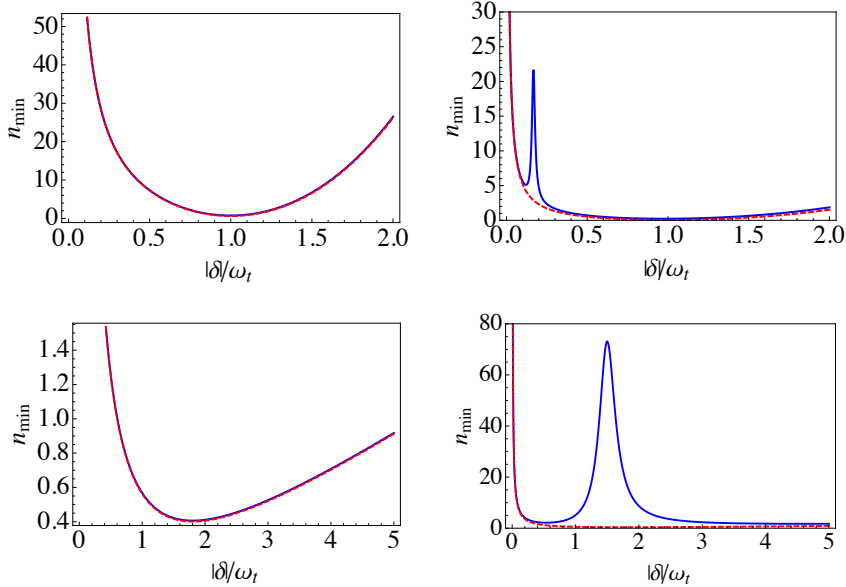


Figure 3.2: Minimal phonon numbers for different detunings comparing the exact result (blue straight line) to the one with the cavity mode eliminated (red dashed line). Differences between the two solutions evolve as  $g$  is increased. Only the regions, where a steady state is attainable have been plotted, they all lie within the red-sideband regime. For blue detuning or an optomechanical coupling which is too strong, the system is heated and no steady state can be obtained. *Upper left pannel:* Sideband-resolved regime with weak coupling,  $\kappa = 0.3 \omega_t, \Gamma = 0.03 \omega_t, g = 0.07 \omega_t$ , *Upper right pannel:*  $\kappa = 0.3 \omega_t, \Gamma = 0.03 \omega_t, g = 0.3 \omega_t$ , *Lower left pannel:* Bad-cavity limit for weak coupling  $\kappa = 3 \omega_t, \Gamma = 0, g = 0.1 \omega_t$ , *Lower right pannel:* Bad-cavity limit for strong coupling,  $\kappa = 3 \omega_t, \Gamma = 0, g = 0.864 \omega_t$

where the rotating-wave approximation is no longer valid, see Fig. 3.2 for an illustration. Note that Eq. (3.22) can be derived from Eq. (3.20) taking the approximation  $\kappa \gg g$ . In case we choose the detuning  $\delta = -\omega_t$  and  $\omega_t \gg \kappa$ , we obtain the minimal occupation number in the sideband regime

$$\bar{n}_{\text{sb}} = \left( \frac{\kappa}{4\omega_t} \right)^2 + \frac{1}{4\mathcal{C}}, \quad (3.23)$$

where  $\mathcal{C}$  denotes the cooperativity, given by Eq. (3.13).

### 3.4 Quantum elasticity

Besides the dissipation caused by the scattering of light, various sources of decoherence generally set limits on ground-state cooling of optomechanical systems and the application of state-preparation protocols. In the following chapters, we will give a detailed overview of diverse sources of decoherence and discuss the dominant ones for different sizes of the levitating dielectrics. Let us begin with the coupling of the center-of-mass motion to other internal vibrational modes. One can model the dielectric as an object containing  $N$  constituents, in this case atoms, that are coupled to each other by mutual interactions, here modeled by springs. The entire nanodielectric inherits  $N$  different modes, one of them is the center of mass mode; a collective movement of all the system's constituents into the same direction. The other modes can be described as movements of the different constituents relative to each other, mediated by the springs. All of these different modes are also coupled to each other, which, in turn, influences their form and lifetime. In principle, one can couple any of these modes to light, especially if the object is sufficiently large. The direct coupling of the cavity mode to the vibrational modes is typically very small, as will be shown below, and we focus on coupling to the cm mode throughout this thesis. We will focus on investigating the influence of the relative modes, also denoted as vibrational modes, on the center of mass mode treating them as a source of decoherence: the vibrational modes can in principle take the role of a thermal bath and prevent ground state cooling of the cm degree of freedom. In order to investigate this source of noise, we use an elasticity theory for quantum systems in this section. After introducing a field characterizing the object's deformation, we determine the vibrational eigenmodes in Sec. 3.4.1. Thereafter, we analyze the effect of an additional external potential and the induced interactions between cm and vibrational modes in Sec. 3.4.2. Finally, in Sec. 3.4.3 we discuss the effect for small objects and obtain an effective Hamiltonian by adiabatically eliminating the internal modes.

#### 3.4.1 Vibrational eigenmodes

Let us start by defining the coordinate  $\mathbf{x}'$ , which describes a point in the dielectric object. As illustrated in Fig. 3.3, this can be written in the most general form as

$$\mathbf{x}' = \mathbf{r} + \hat{R}(\phi_1, \phi_2, \phi_3) (\mathbf{u}(\mathbf{x}) + \mathbf{x}), \quad (3.24)$$

where  $\mathbf{r}$  denotes the center of mass position. We are not treating  $\mathbf{r}$  as an operator for now, but as a three-dimensional vector, and will state it explicitly when we quantize and introduce operators later in the section. In the coordinate system centered at the center of mass position,  $\mathbf{x}$  is the coordinate describing an equilibrium point and  $\mathbf{u}(\mathbf{x})$  its deformation field. The term  $\hat{R}(\phi_1, \phi_2, \phi_3)$  is the Euler rotation matrix with the

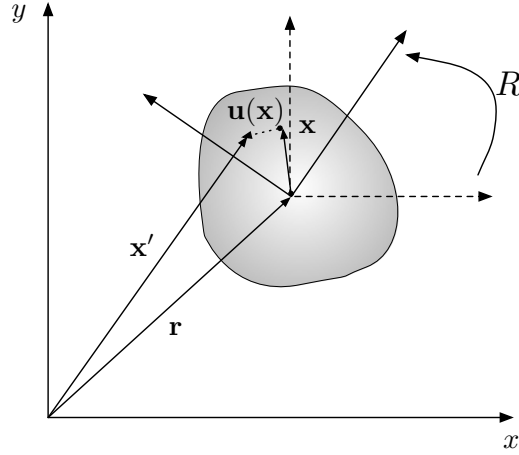


Figure 3.3: Coordinates used to describe a position  $\mathbf{x}'$  within an arbitrary dielectric object given by  $\mathbf{x}' = \mathbf{r} + \hat{R}(\phi_1, \phi_2, \phi_3) (\mathbf{u}(\mathbf{x}) + \mathbf{x})$ , where  $\mathbf{r}$  denotes the center of mass,  $\mathbf{u}(\mathbf{x})$  a small displacement from the equilibrium position  $\mathbf{x}$  and  $R(\phi_1, \phi_2, \phi_3)$  the Euler rotation matrix acting on the entire object.

Euler angles  $\phi_1, \phi_2, \phi_3$  that is used to rotate the coordinates  $\mathbf{x}$  and  $\mathbf{u}(\mathbf{x})$ . Note that the center-of-mass-position can be defined as

$$\mathbf{r} = \frac{\int d\mathbf{x} \rho(\mathbf{x}) \mathbf{x}'}{\int d\mathbf{x} \rho(\mathbf{x})}, \quad (3.25)$$

with  $\rho(\mathbf{x})$  denoting the system's density distribution. Therefore,

$$\int d\mathbf{x} \rho(\mathbf{x}) [\mathbf{x} + \mathbf{u}(\mathbf{x})] = 0. \quad (3.26)$$

In order to guarantee that  $\mathbf{r}$  remains the cm coordinate in case of a vanishing deformation field *i.e.*,  $\mathbf{u}(\mathbf{x}) = 0$ , one requires

$$\int d\mathbf{x} \rho(\mathbf{x}) \mathbf{x} = 0, \quad (3.27)$$

and consequently, the deformation field always has to fulfill

$$\int d\mathbf{x} \rho(\mathbf{x}) \mathbf{u}(\mathbf{x}) = 0. \quad (3.28)$$

The system's Lagrangian in the presence of a general three-dimensional potential  $V_{\text{ext}}(\mathbf{x}')$  reads [158, 159]

$$\mathcal{L} = \int_V d\mathbf{x} \left[ \frac{1}{2} \rho(\mathbf{x}) \dot{\mathbf{x}}'^2 - V_{\text{ext}}(\mathbf{x}') - V_E(\mathbf{x}) \right]. \quad (3.29)$$

The elasticity potential is given by

$$V_E(\mathbf{x}) = \frac{1}{2} \sum_{i,j} \sigma_{ij}(\mathbf{x}) \epsilon_{ij}(\mathbf{x}), \quad (3.30)$$

where

$$\begin{aligned} \epsilon_{ij}(\mathbf{x}) &= \frac{1}{2} \left( \frac{\partial u_i(\mathbf{x})}{\partial x_j} + \frac{\partial u_j(\mathbf{x})}{\partial x_i} \right) \\ \sigma_{ij}(\mathbf{x}) &= 2\mu_E \epsilon_{ij}(\mathbf{x}) + \lambda_E \delta_{ij} \sum_k \epsilon_{kk}(\mathbf{x}) \end{aligned} \quad (3.31)$$

are the elasticity and the stress tensor. The Lamé constants are defined as

$$\lambda_E = \frac{\sigma_E Y}{(1 + \sigma_E)(1 - 2\sigma_E)} \quad (3.32)$$

and  $\mu_E = Y[2(1 + \sigma_E)]^{-1}$ , with  $\sigma_E$  being the Poisson ratio and  $Y$  the Young modulus characterizing the elastic properties of the material. One can now replace the expression of  $\mathbf{x}'$  in the kinetic part of Lagrangian and obtains

$$\mathcal{L} = \frac{1}{2} M \dot{r}^2 + \frac{1}{2} \sum_i I_i \dot{\phi}_i^2 + \frac{1}{2} \int_V d\mathbf{x} \rho(\mathbf{x}) \dot{\mathbf{u}}(\mathbf{x})^2 - \int_V d\mathbf{x} [V_{\text{ext}}(\mathbf{x}') + V_E(\mathbf{x})], \quad (3.33)$$

where the dots denote time derivatives and  $I_i$  is the object's moment of inertia. We have used that in the kinetic part of the Lagrangian, the rotational, vibrational, and center of mass degrees of freedom decouple [159].

Let us now determine the unperturbed vibrational eigenmodes of the system, that is, the modes obtained without considering the potential density  $V_{\text{ext}}(\mathbf{x}')$ . In the following, we will assume for simplicity the homogenous case  $\rho(\mathbf{x}) = \rho$ , the non-homogeneous case can be incorporated easily. Also, we will omit the rotational modes since they decouple without the presence of the external potential. Let us first derive the Hamiltonian by defining the cm momentum as

$$p_i = \frac{\partial \mathcal{L}}{\partial \dot{r}_i} \quad (3.34)$$

and the momentum density as

$$v_i(\mathbf{x}) = \frac{\partial \mathcal{L}}{\partial \dot{u}_i(\mathbf{x})}, \quad (3.35)$$

leading to

$$H_0^{\text{el}} = \frac{\mathbf{P}^2}{2M} + \int_V d\mathbf{x} \left( \frac{\mathbf{v}(\mathbf{x})^2}{2\rho} + V_E(\mathbf{x}) \right). \quad (3.36)$$

One can determine the vibrational eigenmodes by separating variables in the corresponding equation of motion for  $\mathbf{u}(\mathbf{x}, t)$ , which reads [158]

$$\rho \ddot{\mathbf{u}}(\mathbf{x}, t) = \mu_E \nabla^2 \mathbf{u}(\mathbf{x}, t) + \frac{1}{2} \lambda_E \nabla [\nabla \cdot \mathbf{u}(\mathbf{x}, t)]. \quad (3.37)$$

Here,  $\mathbf{u}(\mathbf{x}, t)$  can be separated into transversal and longitudinal oscillation modes

$$\mathbf{u}(\mathbf{x}, t) = \mathbf{u}_\perp(\mathbf{x}, t) + \mathbf{u}_\parallel(\mathbf{x}, t), \quad (3.38)$$

where  $\nabla \cdot \mathbf{u}_\perp(\mathbf{x}, t) = 0$  and  $\nabla \times \mathbf{u}_\parallel(\mathbf{x}, t) = 0$ , and either open or periodic boundary conditions can be used. The longitudinal modes describe compression waves propagating at velocity

$$c_\parallel = \sqrt{\frac{\lambda_E + 2\mu_E}{\rho}} \quad (3.39)$$

and the transversal modes torsion wave propagating at  $c_\perp = [\mu_E/\rho]^{1/2}$ . In the following we will only consider the longitudinal modes along the cavity axis. We expand the elasticity field along the cavity axis for the eigenmodes  $u_n^0(z)$  normalized by

$$\int_V dx u_n^0(z) u_m^0(z) = \delta_{nm} V. \quad (3.40)$$

This yields

$$\begin{aligned} u(z, t) &= \sum_n u_n^0(z) Q_n(t) \\ v(z, t) &= \sum_n u_n^0(z) P_n(t), \end{aligned} \quad (3.41)$$

where  $P_n(t) = \rho \dot{Q}_n(t)$ . At this point, it is straightforward to perform a canonical quantization of the eigenmodes  $Q_n$ , by considering them as operators fulfilling the canonical commutation rules  $[\hat{Q}_n, \hat{P}_m] = i$  (the quantized eigenmodes have operator-character, they will be denoted by  $\hat{Q}_n, \hat{P}_n$  in the following). As already done in the previous sections, the momentum operator of the cm will also be quantized with the external harmonic trap. By plugging this decomposition into the Hamiltonian Eq. (3.36), one obtains after some algebra

$$\hat{H}_0^{\text{el}} = \frac{\hat{p}^2}{2M} + \sum_n \left[ \frac{\hat{P}_n^2}{2M} + \frac{1}{2} M \omega_n^2 \hat{Q}_n^2 \right], \quad (3.42)$$

where the frequency of the internal modes is given by

$$\omega_n^2 = \frac{\lambda_E(1 - \sigma_E)}{M\sigma_E} \int_V d\mathbf{x} \left[ \frac{d}{dz} u_n(z) \right]^2. \quad (3.43)$$

The eigenmodes  $u_n^0(z)$  have to be chosen accordingly to the geometry of the object. We will discuss the specific form of the mode and the value of the parameters in Sec. 3.4.3.

### 3.4.2 Effect of the external potential

The external potential  $\hat{V}_{\text{ext}}(\mathbf{x}')$  can in principle effect a coupling between the rotational, the center-of-mass, and the vibrational degrees of freedom. In case of a purely isotropic harmonic potential, it can be easily verified that the coupling vanishes. On the other hand, for arbitrarily-shaped objects, the external anharmonic part of the potential effects some coupling between all degrees of freedom. In the following analysis we assume spherical objects, for which the direct coupling between the cm and the rotational degrees of freedom vanishes. Even in the case of a prolate spheroid, the coupling is negligible, see Chapter 3.5.6. For spherical objects, there is only an indirect coupling between the cm and the rotations, mediated by the vibrational modes, which is negligible and will be omitted hereafter. Therefore, with these assumptions one can consider the center-of-mass mode to be decoupled from the rotational motion, and we consequently omit the rotational modes in the rest of the section. One can then focus on the one-dimensional case derived in the previous section by only considering the longitudinal modes.

The total Hamiltonian, including the external potential, is hence given by

$$\hat{H}^{\text{el}} = \hat{H}_0^{\text{el}} + \int_V d\mathbf{x} \hat{V}_{\text{ext}}(z') \quad (3.44)$$

Assuming that the deformations  $\hat{u}(z)$  are small and that the object is trapped at  $\hat{r} \approx 0$ , one can expand  $V_{\text{ext}}(z' = z + u(z) + \hat{r})$  to second order in  $\hat{r}$  and  $\hat{u}(z)$ , which leads to

$$\begin{aligned} \hat{H}^{\text{el}} = & \hat{H}_0^{\text{el}} + \hat{r} \int_V d\mathbf{x} V'_{\text{ext}}(z) + \frac{\hat{r}^2}{2} \int_V d\mathbf{x} V''_{\text{ext}}(z) + \frac{1}{2} \sum_{n,m} \hat{Q}_n \hat{Q}_m \int_V d\mathbf{x} u_n^0(z) u_m^0(z) V''_{\text{ext}}(z) \\ & + \sum_n \hat{Q}_n \int_V d\mathbf{x} u_n^0(z) V'_{\text{ext}}(z) + \hat{r} \sum_n \hat{Q}_n \int_V d\mathbf{x} u_n^0(z) V''_{\text{ext}}(z). \end{aligned} \quad (3.45)$$

Here, the primes denote spatial derivatives. By recalling that the external potential is, in our case, given by the light-matter interaction term Eq. (2.6), that is

$$\hat{V}_{\text{ext}}(\mathbf{x}') = -\frac{\epsilon_c \epsilon_0}{2} \hat{E}_{\text{tot}}(\mathbf{x}')^2, \quad (3.46)$$

one can understand the terms appearing in Eq. (3.45) as follows:

1. The term  $\hat{r} \int_V d\mathbf{x} V'_{\text{ext}}(z)$  yields the optomechanical coupling of the center of mass mode as described in Chapter 3.2.
2. The second term  $\hat{r}^2 \int_V d\mathbf{x} V''_{\text{ext}}(z)/2$  describes the harmonic trap for the cm mode given by the optical tweezers, as described in Chapter 3.2.

3. The term  $\hat{Q}_n \hat{Q}_m \int_V d\mathbf{x} u_n^0(z) u_m^0(z) V_{\text{ext}}''(z)/2$  gives a correction to the harmonic trap for the internal modes as well as a coupling between internal modes.
4. The first new interesting term is  $\hat{Q}_n \int_V d\mathbf{x} u_n^0(z) V_{\text{ext}}'(z)$ , which describes an optomechanical coupling between the internal modes and the cavity field.
5. Finally, the most relevant term for our purposes is  $\hat{r} \hat{Q}_n \int_V d\mathbf{x} u_n^0(z) V_{\text{ext}}''(z)$ , which describes the coupling between the vibrational degrees of freedom  $\hat{Q}_n$  and the center of mass mode  $\hat{r}$ .

Taking into consideration these terms, one can now write the center-of-mass mode as  $\hat{r} = x_0(\hat{b}^\dagger + \hat{b})$ , where  $x_0 = (2M\omega_t)^{-1/2}$  is the ground state size as defined in Sec. 2.4.2. The internal modes are defined in full analogy,  $\hat{Q}_n = q_{0,n}(\hat{c}_n + \hat{c}_n^\dagger)$ , with  $q_{0,n} = (2M\omega_n')^{-1/2}$ . Note that, due to the additional external trapping with frequency  $\omega_t$ , the effective vibrational frequencies are changed to  $\omega_n' = (\omega_t^2 + \omega_n^2)^{1/2}$  (we will omit the prime hereafter). The new part that has to be added to the total Hamiltonian  $\hat{H}_{\text{tot}}$ , see Eq. (2.1), which takes into account the presence of internal modes, is given by

$$\begin{aligned} \hat{H}_{\text{E}} = & \sum_n \omega_n \hat{c}_n^\dagger \hat{c}_n + \sum_n g_n(\hat{a}, \hat{a}^\dagger)(\hat{c}_n + \hat{c}_n^\dagger) \\ & + \sum_{n,m} \xi_{nm}(\hat{c}_n + \hat{c}_n^\dagger)(\hat{c}_m + \hat{c}_m^\dagger) + \sum_n \gamma_n(\hat{c}_n + \hat{c}_n^\dagger)(\hat{b} + \hat{b}^\dagger). \end{aligned} \quad (3.47)$$

The coupling between the cavity field (which depends on the cavity mode  $\hat{a}$ ) and the vibrational modes is given by  $g_n(\hat{a}, \hat{a}^\dagger) = q_{0,n} \int_V d\mathbf{x} V_{\text{ext}}'(z) u_n^0(z)$ . The coupling between the internal modes is  $\xi_{nm} = q_{0,n} q_{0,m} \int_V d\mathbf{x} u_n^0(z) u_m^0(z) V_{\text{ext}}''(z)/2$ . Finally, the coupling between the cm mode and the vibrational modes is given by

$$\gamma_n = x_0 q_{0,n} \int_V d\mathbf{x} V_{\text{ext}}''(z) u_n^0(z). \quad (3.48)$$

Summing up this subsection, we have derived the quantized Hamiltonian describing the coupling between the cm and the vibrational modes in the presence of an external potential density. It can be shown that for a harmonic external potential, the cm mode is decoupled from the internal ones since  $V_{\text{ext}}''(z)$  is constant and by recalling that  $\int_V d\mathbf{x} u_n^0(z) = 0$ , one obtains  $\gamma_n = 0$ . In the next section, we estimate the order of magnitude of the parameters for objects smaller or on the order of the optical wavelength in the presence of the anharmonic potential given by the standing wave.

### 3.4.3 Coupling to vibrational modes as a source of decoherence

First of all, let us estimate the order of magnitude of the internal vibrational frequencies, see Eq. (3.43), for the case of a sphere of radius  $R$ . To get an estimation of the order

of magnitude, for simplicity one can simply use the eigenmode  $u_n^0(z) = \cos(k_n z)$  with  $k_n = n\pi/(2R)$ , obtained for a cube of length  $2R$  and with open free periodic boundary conditions. Then, using typical values of Young's elasticity module  $Y$  and the Poisson constant  $\sigma_E$  (see Sec. 3.6), the vibrational frequencies for  $R = 10 \text{ nm} - 2 \mu\text{m}$  are of the order  $\omega_n \approx 10^9 - 10^{12} \text{ Hz}$  ( $\omega_n \sim nc_{\parallel}/R$ ). Note that comparing this to the typical values of the cm frequency  $\omega_t \sim 10^6 \text{ Hz}$ , the internal frequencies are five orders of magnitude larger for objects of the order of 100 nm and still three orders of magnitude apart for spheres of 10  $\mu\text{m}$ .

This large difference in frequencies between the cm modes and the internal modes enables us to adiabatically eliminate the vibrational energy levels. It is shown in App. 3.A that this approximation is justified by solving the equations of motion for the cm and vibrational operators by applying a Laplace transformation [160]. The solution obtained in this way contains parts oscillating at frequencies  $\omega_t$  and  $\omega_n$ , where all terms oscillating at  $\omega_n$  are suppressed by a factor  $\omega_t/\omega_n \ll 1$ . Thus, it is well-justified to neglect these terms and to perform an adiabatic elimination. One can perform this by eliminating the vibrational levels on top of the steady state. Within this approximation, the only effect is a shift of the trapping frequency of the cm mode given by

$$\left(\frac{\omega'_t}{\omega_t}\right)^2 = 1 - \sum_n \frac{4\gamma_n^2}{\omega_t(\omega_n - \omega_t)} \left(2\langle \hat{c}_n^\dagger \hat{c}_n \rangle + 1\right). \quad (3.49)$$

Here,  $\langle \hat{c}_n^\dagger \hat{c}_n \rangle$  is the occupation number of phonons in the vibrational mode  $n$ . By plugging in typical numbers, one gets a correction to the trapping frequency of, *e.g.*,  $(\omega'_t - \omega_t)/\omega_t \approx 10^{-12}$  for spheres of  $R = 100 \text{ nm}$ , which shows that the cm mode is decoupled from the internal modes for objects in the range  $R \lesssim 10 \mu\text{m}$  and their coupling can be neglected.

### 3.5 Other sources of decoherence

In this section, we give an overview of the various sources of heating and decoherence for levitating spheres. For spheres on the order of the optical wavelength, recoil heating by photons from the laser modes (Sec. 3.2) dominates all decoherence processes as it has been shown in Sec. 3.6. The most common decoherence mechanisms are of position-localization type and the corresponding master equation is derived in Sec 3.5.1. Besides photon scattering, the dominating processes are the scattering of air molecules (Sec. 3.5.2) and absorption and emission of blackbody radiation (Sec. 3.5.3). It is thus essential to isolate the optomechanical system from its environment to keep these rates low. For completeness, we also discuss the effect of photon shot noise (Sec. 3.5.4), anisotropies of the sphere's shape (Sec. 3.5.6), and the coupling to two-level fluctuators

present in any amorphous material (Sec. 3.5.7). We compare the various sources of dissipation and analyze the experimental parameters required for ground-state cooling in Sec. 3.6. A detailed overview of decoherence processes is given in [62, 77, 78] and we refer the reader to these articles for more information.

### 3.5.1 Position-localization decoherence

The master equation for decoherence of the center-of-mass mode for photon scattering has been derived in Sec. 3.2, Eq. (2.43) and has the form

$$\mathcal{L}^{\text{M}}[\hat{\rho}_{\text{S}}] = \Gamma_{\text{phot}} \left( 2(\hat{b} + \hat{b}^\dagger)\hat{\rho}_{\text{S}}(\hat{b} + \hat{b}^\dagger) - \{(\hat{b} + \hat{b}^\dagger)^2, \hat{\rho}_{\text{S}}\}_+ \right), \quad (3.50)$$

where  $\Gamma_{\text{phot}}$  depends on the ground-state size as described by Eq. (2.44). Essentially all decoherence mechanisms relevant for dielectric spheres are described by a master equation of this form. It is valid for decoherence due to position localization, where in this case the ground-state size  $x_0$  is the length scale of correlations as the oscillator is prepared close to its ground state. The strength of decoherence is generally described by  $\Gamma$  and depends quadratically on  $x_0$ . A generalized form of this position-localization decoherence for an arbitrary coherence length  $\Delta\mathbf{r} = |\mathbf{r} - \mathbf{r}'|$  is derived in [65, 161]. These references show that the interaction with the environment causes an exponential decay of position correlations *i.e.*,

$$\langle \mathbf{r} | \hat{\rho}_{\text{S}}(t) | \mathbf{r}' \rangle \propto e^{-\Gamma t} \langle \mathbf{r} | \hat{\rho}_{\text{S}}(0) | \mathbf{r}' \rangle. \quad (3.51)$$

In the position basis, the decoherence is qualitatively described by

$$\langle \mathbf{r} | \dot{\hat{\rho}}_{\text{S}}(t) | \mathbf{r}' \rangle = i \langle \mathbf{r} | [\hat{\rho}_{\text{S}}(t), \hat{H}_{\text{S}}] | \mathbf{r}' \rangle - \Gamma \Delta\mathbf{r} \langle \mathbf{r} | \hat{\rho}_{\text{S}}(t) | \mathbf{r}' \rangle \quad (3.52)$$

with a decoherence rate given by

$$\Gamma = \gamma \left( 1 - \exp \left[ -\frac{\Delta\mathbf{r}^2}{4a^2} \right] \right). \quad (3.53)$$

This function depends on two parameters: the localization strength  $\gamma > 0$  with dimensions of frequency, and the localization distance  $a > 0$  with dimensions of length. The values of these parameters depend on the particular source of decoherence. There are two different regimes depending on the superposition size

$$\Gamma \approx \begin{cases} \Lambda \Delta\mathbf{r}^2, & \Delta\mathbf{r} \ll 2a, \\ \gamma, & \Delta\mathbf{r} \gg 2a, \end{cases} \quad (3.54)$$

where

$$\Lambda = \frac{\gamma}{4a^2} \quad (3.55)$$

is the localization parameter. In the short-distance limit, where superpositions are smaller than the localization distance,  $\Delta \mathbf{r} \ll 2a$ , the decoherence rate depends quadratically on  $\Delta \mathbf{r}$  and the dynamics is described by Eq. (3.50). In the opposite case  $\Delta \mathbf{r} \gg 2a$ , where the superposition is much larger than the localization distance, the decoherence rate saturates and the position correlations decay as

$$\langle \mathbf{r} | \hat{\rho}_S(t) | \mathbf{r}' \rangle \propto e^{-\gamma t} \langle \mathbf{r} | \hat{\rho}_S(0) | \mathbf{r}' \rangle. \quad (3.56)$$

Let us proceed to determine the decoherence rate  $\Gamma$  more specifically for the case, where decoherence is caused by scattering of environmental particles. Research on the topic was first triggered by the work of Joos and Zeh [22] and we refer the reader to [65, 161] for extensive reviews, while we merely describe the results required for our analysis here. The decoherence rate as a function of the superposition size  $\Delta \mathbf{r} = |\mathbf{r} - \mathbf{r}'|$  is given by [65]

$$\Gamma = \int_0^\infty dq \rho(q) v(q) \int \frac{d\mathbf{n}d\mathbf{n}'}{4\pi} \left( 1 - e^{iq(\mathbf{n}-\mathbf{n}')\Delta \mathbf{r}} \right) |f(q\mathbf{n}, q\mathbf{n}')|^2. \quad (3.57)$$

Here,  $\rho(q)$  describes the number density of incoming particles with momentum  $q$  in the direction  $\mathbf{n}, \mathbf{n}'$  with  $|\mathbf{n}| = |\mathbf{n}'| = 1$ , and  $v(q) = q/m$  ( $v(q) = c$ ) the velocity distribution of massive (massless) particles of mass  $m$ . The elastic scattering amplitude is given by  $f(q\mathbf{n}, q\mathbf{n}')$ . The derivation assumes an object that is infinitely massive interacting with incoming particles that are isotropically distributed in space, for further details see [65]. As indicated in Eq. (3.54), the decoherence depends on the superposition size and the localization length. As shown in [162, 163], the thermal wavelength of the incoming scattering particles is related to the localization length and the localization strength by

$$a = \frac{\lambda_{\text{th}}}{2}, \quad (3.58)$$

and

$$\gamma = \lambda_{\text{th}}^2 \Lambda, \quad (3.59)$$

respectively. Consequently, the decoherence rate in the long-wavelength limit,  $\lambda_{\text{th}} \gg |\mathbf{r} - \mathbf{r}'|$ , is  $\Gamma \propto \Lambda \Delta \mathbf{r}^2$ . An intuitive way to understand this is the explanation that the scattering event of a single particle cannot resolve the separation  $\Delta \mathbf{r}$  and only carries an insufficient amount of which-path information. It will thus take a large number of scattering events to spatially localize the object. In contrast, in the short-wavelength-limit,  $\lambda_{\text{th}} \ll \Delta \mathbf{r}$ , the decoherence is  $\Gamma \propto \gamma$ . In this case, each interacting particle can resolve the separation  $\Delta \mathbf{r}$  carrying away the maximum of which-path information, consequently inducing the system to decohere after only one interaction. The different scaling of the decoherence rate for the two cases is illustrated in Fig. 3.4.

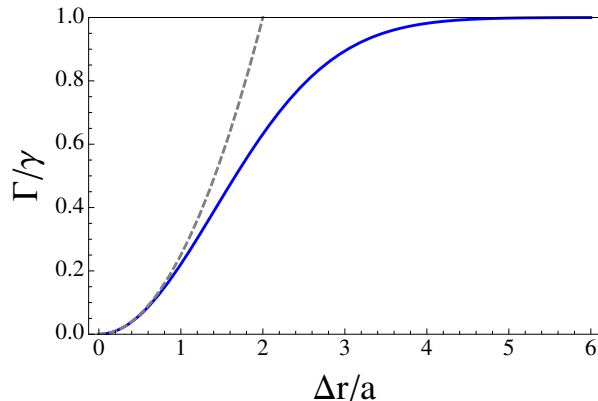


Figure 3.4: *Blue solid line:* Plot of the decoherence  $\Gamma$  (Eq. (3.54)) saturating for an increasing superposition size  $\Delta\mathbf{r}$ . For comparison, the dashed grey line describes the small-superposition limit.

### Formal solution of the master equation

To complete the analysis, let us formally solve the master equation in the position basis, Eq. (3.52), which reads

$$\langle r|\hat{\rho}_S(t)|r'\rangle = \int_{-\infty}^{\infty} \frac{dpdy}{2\pi} e^{-ipy} \mathcal{B}(p, r - r', t) \langle r + y|\hat{\rho}_0(t)|r' + y\rangle. \quad (3.60)$$

Here,  $\hat{\rho}_0(t)$  denotes the system's density matrix without taking into account decoherence. The influence of the decoherence processes are accounted for by

$$\mathcal{B}(p, r - r', t) = e^{-\gamma t} \exp \left[ \gamma \int_0^t d\tau e^{[(r-r'-p\tau/m)/(2a)]^2} \right]. \quad (3.61)$$

This term, describing the modification of the Hamiltonian evolution of the density matrix by the presence of decoherence, will be particularly useful in Sec. 6.3.

### 3.5.2 Scattering of air molecules

Here, we analyze the effect caused by the impact of air molecules in the vacuum chamber on the levitating sphere. The random scattering with the surrounding gas molecules causes heating and decoherence of the sphere and we determine the decoherence rate  $\Gamma_{\text{air}}$  for the mechanical oscillator. We consider air molecules of mass  $m$  in a vacuum chamber of room temperature  $T$  at pressure  $P$  which have a mean velocity  $\bar{v} = \sqrt{3k_B T/m}$ , where  $k_B$  is the Boltzmann constant. The decoherence caused by scattered air molecules is of localization-type described by a master equation in analogy to Eq. (2.43),

$$\mathcal{L}^{\text{air}} = \Gamma_{\text{air}} \left( 2(\hat{b} + \hat{b}^\dagger)\hat{\rho}_S(\hat{b} + \hat{b}^\dagger) - \{(\hat{b} + \hat{b}^\dagger)^2, \hat{\rho}_S\}_+ \right). \quad (3.62)$$

The thermal wavelength of air molecules is given by

$$\lambda_{\text{th}}^{\text{air}} = \frac{2\pi}{\sqrt{2\pi m k_{\text{B}} T}}. \quad (3.63)$$

For typical parameters,  $m \approx 28.97$  amu one obtains  $2a_{\text{air}} \approx 2 \cdot 10^{-11}$  m. The typical ground state size of the dielectrics we consider here is on the order of  $x_0 \approx 10^{-14}$  m and for states close to the ground state, the long-wavelength limit applies. Following [65], the decoherence rate can be derived from Eq. (3.57) and is given by

$$\Gamma_{\text{air}} \approx \frac{6\pi P}{\rho R \omega_t} \sqrt{3k_{\text{B}} T m}, \quad (3.64)$$

where  $\rho$  denotes the density of the sphere. The decoherence induced by interactions with gas molecules is thus inversely proportional to the object's size.

In contrast, in Sec. 6.3, the case of large spatial superpositions will be investigated, where the superposition size  $\Delta \mathbf{r}$  is of the order of nanometers. In this case, the thermal wavelength of the air molecules is shorter than the superposition size and scattering of air molecules goes into saturation as described in Sec. 3.5.1 and is given by

$$\gamma_{\text{air}} = \frac{16\pi P R^2}{3} \sqrt{\frac{2\pi m}{k_{\text{B}} T}}. \quad (3.65)$$

### 3.5.3 Blackbody radiation

In analogy to the scattering of laser light, absorption and emission of blackbody photons also lead to decoherence of the cm motion of the sphere. Albeit we assume the dielectrics to be non-absorbing throughout this thesis, a small imaginary part of  $\epsilon_r$   $\epsilon_r = \epsilon_1 + i\epsilon_2$  is taken into account here for completeness. We first determine the equilibrium temperature to then determine the decoherence rate caused by blackbody-radiation.

The power dissipated by blackbody radiation is usually given by

$$P_e^{\text{bb}} = A e \sigma_{\text{SB}} [T_{\text{S}}^4 - T_{\text{E}}^4], \quad (3.66)$$

where  $A$  is the area of the object,  $e$  the emissivity ( $\approx 1$ ),  $\sigma_{\text{SB}}$  the Stefan-Boltzmann constant,  $T_{\text{S}}$  the temperature of the object and  $T_{\text{E}}$  the temperature of the environment. If the sphere is of the same order or smaller than the wavelength of the blackbody radiation, the radiated power has to be modified as the object is not an efficient absorber (emitter) of radiation at this wavelength anymore. As we concentrate on dielectrics of this size, the power emitted (absorbed) through blackbody radiation for small spheres is given by [78, 164]

$$P_{e(a)}^{\text{bb}} = \frac{72\zeta(5)}{\pi^2} \frac{V}{c^3} \text{Im} \frac{\epsilon_{\text{bb}} - 1}{\epsilon_{\text{bb}} + 2} (k_{\text{B}} T_{\text{S(E)}})^5, \quad (3.67)$$

where  $\zeta(x)$  is the Riemann zeta function with  $\zeta(5) \approx 1.04$ .  $\epsilon_{\text{bb}}$  is the blackbody permittivity, which we assume to be constant throughout the blackbody radiation spectrum, and  $V$  is the volume of the sphere. The internal temperature  $T_{\text{S}}$  is determined as the equilibrium between absorption of laser photons and emission via blackbody radiation (we assume that, due to the low pressure, thermalization via scattering of air molecules is negligible). Laser photons cause an energy absorption described by [142]

$$P_{\text{abs}} = \frac{12\pi I 3\epsilon_2 V}{\lambda_c [(\epsilon_1 + 2)^2 + \epsilon_2^2]}, \quad (3.68)$$

where  $\lambda_c$  is the wavelength and  $I$  the laser intensity. Setting  $P_{\text{abs}} = P_{\text{e}}^{\text{bb}}$  yields the sphere's equilibrium temperature

$$T_{\text{S}} = \sqrt[5]{\frac{I c^3 \pi^3}{\zeta(5) 6 \lambda_c k_{\text{B}}^5} \frac{\text{Im} \frac{\epsilon_{\text{r}} - 1}{\epsilon_{\text{r}} + 2}}{\text{Im} \frac{\epsilon_{\text{bb}} - 1}{\epsilon_{\text{bb}} + 2}}} + T_{\text{E}}. \quad (3.69)$$

The decoherence by blackbody radiation consists of three contributions: emission, absorption and scattering of thermal photons :

$$\Lambda_{\text{bb}} = \Lambda_{\text{bb,e}} + \Lambda_{\text{bb,a}} + \Lambda_{\text{bb,sc}}. \quad (3.70)$$

The thermal wavelength for photons is given by

$$\lambda_{\text{th}}^{\text{bb}} = \frac{\pi^2 c}{k_{\text{B}} T_{\text{E}}}, \quad (3.71)$$

which takes values  $\lambda_{\text{th}}^{\text{bb}} \approx 10^{-4}$  m at room temperature. Thus, for this source of decoherence, the long-wavelength-limit can be employed for all superposition sizes considered in this thesis. The emission (absorption) rate of blackbody radiation is given by [65]

$$\Lambda_{\text{e(a)}}^{\text{bb}} = \frac{16\pi^5 R^3}{189} \left[ \frac{k_{\text{B}} T_{\text{E}}}{c} \right]^6 \text{Im} \left[ \frac{\epsilon_{\text{bb}} - 1}{\epsilon_{\text{bb}} + 2} \right]. \quad (3.72)$$

Scattering of blackbody radiation is described by [65]

$$\Lambda_{\text{sc}}^{\text{bb}} = \frac{8! 8 \zeta(9) c R^6}{9\pi} \left[ \frac{k_{\text{B}} T_{\text{E}}}{c} \right]^9 \text{Re} \left[ \frac{\epsilon_{\text{bb}} - 1}{\epsilon_{\text{bb}} + 2} \right], \quad (3.73)$$

where  $\zeta(x)$  again denotes the Riemann zeta function. While we merely give the resulting rates here, we refer the reader to [65, 78] for further details. For the set of experimental parameters that are specified in Sec. 3.6, the equilibrium temperature of the sphere is  $\Delta T_{\text{S}} = 270\text{K}$  above the temperature of the environment. The effect of the decoherence via blackbody radiation will be discussed in Sec. 3.6 and compared to other sources of decoherence for different sizes of the sphere.

### 3.5.4 Photon shot noise

It is well-known from atomic physics that fluctuations in the trap parameters cause atom heating and storage times are limited by trap losses [165]. While in Bose-Einstein condensate experiments this is typically circumvented by also applying magnetic traps [166], the dielectric spheres considered here are not susceptible to magnetic trapping, and fluctuations need to be considered. Photon shot noise leads to heating via fluctuations in the mechanical trapping frequency  $\omega_t$ ,

$$\omega_t(t) = \langle \omega_t(t) \rangle \left[ 1 + \frac{\delta\alpha(t)^2}{|\alpha^2|} \right], \quad (3.74)$$

where  $\langle \omega_t(t) \rangle$  is the mean trapping frequency.  $|\alpha^2|$  denotes the mean number of photons in the cavity and  $\delta\alpha^2(t)$  describes the number fluctuation of the cavity mode. These stochastic fluctuations in the spring constant lead to parametric heating depending on the form of the one-sided power spectrum of the fractional fluctuations in the spring constant [78, 165]

$$S_{\text{cav}}(\omega_t) = \frac{2}{\pi|\alpha|^4} \int_0^\infty dt \cos(\omega_t t) \langle \delta\alpha^2(t) \delta\alpha^2(0) \rangle. \quad (3.75)$$

The power spectrum for a cavity of linewidth  $\kappa$  driven on resonance can be determined as

$$S_{\text{cav}}(\omega_t) = \frac{1}{\pi|\alpha|^2} \frac{4\kappa}{\kappa^2 + 4\omega_t^2}. \quad (3.76)$$

The rate at which parametric transitions to higher phonon numbers ( $n \rightarrow n \pm 2$ ) happen, can be determined within perturbation theory and is given by [165]

$$R_{n \rightarrow n \pm 2} = \frac{\pi\omega_t^2}{16} S(2\omega_t) (n+1 \pm 1)(n \pm 1). \quad (3.77)$$

The rate at which transitions from the ground state of the mechanical oscillator happen is thus given by

$$\Gamma_{\text{shot}} = \frac{\kappa\omega_t^2}{4|\alpha|^2(\kappa^2 + 16\omega_t^2)}. \quad (3.78)$$

The contribution of this decoherence source will be quantified for specific experimental parameters in Sec. 3.6.

### 3.5.5 Fluctuations in the trap center

Another source of noise that can be treated in full analogy to the photon shot noise of the previous chapter are fluctuations in the trap center. These fluctuations are caused by vibrations of the experimental apparatus due to thermal and seismic noise and effect

fluctuations of the location of the center of the harmonic trap. A calculation within perturbation theory yields transition rates describing the heating by one phonon as

$$R_{n \rightarrow n \pm 1} = \frac{\pi}{2} M \omega_t^3 S_{\text{vib}}(\omega_t) \left( n + \frac{1}{2} \pm \frac{1}{2} \right), \quad (3.79)$$

and thus for the heating of the ground state

$$\Gamma_{\text{trap}} = \frac{\pi}{2} M \omega_t^3 S_{\text{vib}}(\omega_t). \quad (3.80)$$

Here,  $S_{\text{vib}}(\omega_t)$  describes the power spectrum of the fluctuations of the trap frequency.

### 3.5.6 Anisotropies in the sphere

In this section, we consider the effect of small deviations from the spherical shape of the dielectric. We only give a schematic overview, for more details see [78]. In case the sphere is not completely isotropic, it becomes necessary to take its rotational motion into account. We only want to give an estimation of the effect and therefore consider a simplified version of the problem: the rotation is limited to one axis and the sphere's deformation is spheroid-like. We therefore assume a prolate spheroid with semi-major axis  $a$  and semi-minor axis  $b$  with only little deviation from a sphere,  $a/b \approx 1$ . The effect of this anisotropy is twofold: on the one side, there is an indirect optical coupling between the rotational motion and the cm-motion of the sphere caused by the change in the cavity resonance frequency due to the rotational motion. Similar to the coupling to internal modes as described in Sec. 3.4, this interaction is very weak and it is shown in [78] that it can be neglected to first order for the small anisotropies considered here. On the other side, the dielectric properties of the object *i.e.*, its polarization, are changed, which leads to a modification of the trapping frequency  $\omega_t$ . Its dependance on the sphere's orientation is given by

$$\delta\omega_t(t) = \epsilon(\theta)\omega_t \cos(2\theta), \quad (3.81)$$

where  $\theta$  is defined as the angle of rotation of the spheroid. The dielectric constant depends on the deformation of the dielectric

$$\epsilon_\theta = \frac{9}{40} \frac{\epsilon_r - 1}{\epsilon_r + 2} \left[ \left( \frac{a}{b} \right)^{4/3} - 1 \right]. \quad (3.82)$$

In full analogy to the shot noise considered in 3.5.4, this leads to parametric heating with a jump rate out of the ground state given by

$$R_{0 \rightarrow 2} = \frac{1}{2} \int_0^\infty dt \cos(2\omega_t t) \langle \delta\omega_t(0) \delta\omega_t(t) \rangle. \quad (3.83)$$

Making a Gaussian approximation for the correlations leads to

$$\Gamma_{\text{anis}} = \epsilon_{\theta}^2 \frac{\sqrt{2\pi}\omega_t^2}{16\sqrt{\langle\omega_r^2\rangle}} \exp\left[-\frac{\omega_t^2}{2\langle\omega_r^2\rangle}\right], \quad (3.84)$$

with the rotational frequency  $\omega_r = d\theta/dt$ . This rate reaches its maximum for  $\omega_r = \omega_t$ . We will give an estimation of the strength of this contribution to the heating in Sec. 3.6.

### 3.5.7 Coupling to two-level systems

The dielectric spheres analyzed in this thesis typically consist of fused silica, an amorphous medium containing a large number of tunnel systems. Tunnel systems occur due to frustration in amorphous materials and have been intensively studied in the context of low-temperature physics [167]. These two-level systems couple to strain fields constituting a possible source of heating [168,169] in particular at low temperatures. This has been one of the main obstacles for ground state cooling in experiments with microtorroids and has been extensively studied [170–172]. More recently, even proposals to use these intrinsic material defects to realize nonlinearities of the optomechanical resonator [117], have been studied. However, in the setup analyzed in this thesis, this source of decoherence is not a relevant factor. The two-level systems only couple to the vibrational modes of the sphere, not to the cm mode. Subsequently, the cm mode can only indirectly couple to the tunnel systems through the vibrational modes. As it has been shown in Sec. 3.4, this coupling can be neglected for the spheres we are considering.

## 3.6 Results for given experimental parameters

In the following, both the minimal phonon number and the cooperativity are used to quantify the system's performance as an optomechanical setup. The optomechanical parameters are determined for varying sphere sizes. The experimental parameters are chosen as follows:

- **Dielectric object:** We assume spheres of fused silica with density  $\rho = 2201 \text{ kg/m}^3$ , a dielectric constant  $\text{Re}[\epsilon_r] = 2.1$  and  $\text{Im}[\epsilon_r] \sim 2.5 \times 10^{-10}$ . For the blackbody radiation of the sphere, we choose  $\epsilon_{\text{bb}} = 2.1 + 0.57i$ . We vary their radii between  $R = 10\text{nm} - 2\mu\text{m}$  and position them at the maximal slope of the cavity field,  $\varphi = \pi/4$ . Their Young modulus is  $Y = 73 \text{ GPa}$  and their Poisson constant  $\sigma = 0.17$ , giving internal vibrational modes with frequencies of the order of  $\omega_n \sim 10^9 - 10^{12} \text{ Hz}$ .

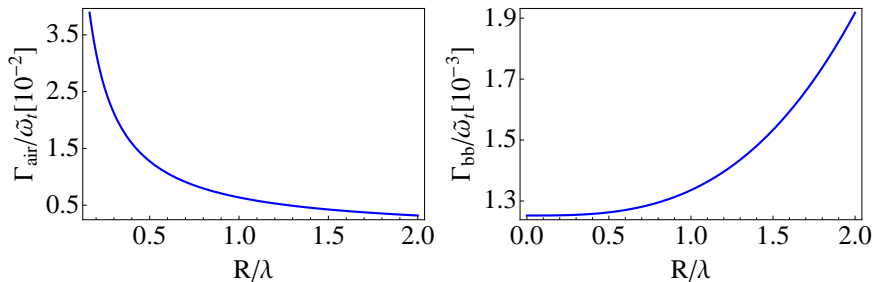


Figure 3.5: decoherence rates for levitating dielectrics for experimental parameters as given in the main text and varying sphere sizes. *Left* : Decoherence due to scattering of air molecules (Sec. 3.5.2), *Right*: Decoherence due to emission, absorption and scattering of blackbody radiation (Sec. 3.5.3)

- **Cavity:** We assume a confocal high-finesse cavity of length  $L = 4$  mm and finesse  $\mathcal{F} = 5 \times 10^5$  leading to a cavity decay rate  $\kappa_0 = c\pi/2\mathcal{F}L = 2\pi \times 44$  kHz. This cavity is impinged by a laser of power  $P_c = 0.1$  mW, wavelength  $\lambda_c = 1064$  nm, which gives a waist of  $W_0 = \sqrt{\lambda_c d/2\pi} \approx 26$   $\mu$ m. The external pressure is chosen as  $P = 10^{-6}$  mbar.
- **Optomechanical parameters:** The tweezers are constructed with a laser of wavelength  $\lambda_c = 1064$  nm and a lense of high numerical aperture. They supply a harmonic trap for the object of frequency  $\omega_t = 2\pi \times 136$  kHz in the transversal direction and a slightly smaller one in the direction of light propagation. The cavity photons have a frequency  $\omega_0 = 2\pi \times 2.8 \times 10^{14}$  Hz and the steady state photon occupation is  $|\alpha|^2 \approx 3.7 \times 10^8$ .

The dominating source of decoherence, in particular for large spheres, is the recoil heating by scattering of cavity photons,  $\Gamma_{\text{cav}}$ , described by Eq. (3.12). Other dominating sources of decoherence are the scattering of air molecules,  $\Gamma_{\text{air}}$  (Eq. (3.64)), and the scattering of blackbody radiation,  $\Gamma_{\text{bb}} = x_0^2 \Lambda_{\text{bb}}$  (Eqs. (3.70)). These decoherence mechanisms are illustrated in Fig. 3.5 for the experimental parameters given in the main text and spheres ranging from  $R = 10$  nm  $- 2$   $\mu$ m. Other sources of decoherence are given by parametric heating via photon shot noise,  $\Gamma_{\text{shot}}/\omega_t \approx 10^{-11}$  (Eq. (3.78)), which is typically negligible. Fluctuations in the trap center due to seismic and thermal noise depend on the power spectrum of the fluctuations with a typical maximum of the power spectrum at  $\omega_{\text{max}} \approx$  Hz and only a vanishing tail at the typical trapping frequencies  $\omega_t \approx 10^6$  Hz. For the experimental parameters considered here and the maximal sphere size  $R = 2$   $\mu$ m,  $\Gamma_{\text{trap}}/\omega_t \lesssim 10^{15} \text{ m}^2/\text{Hz S}_{\text{vib}}(\omega_t)$ . For the power spectral

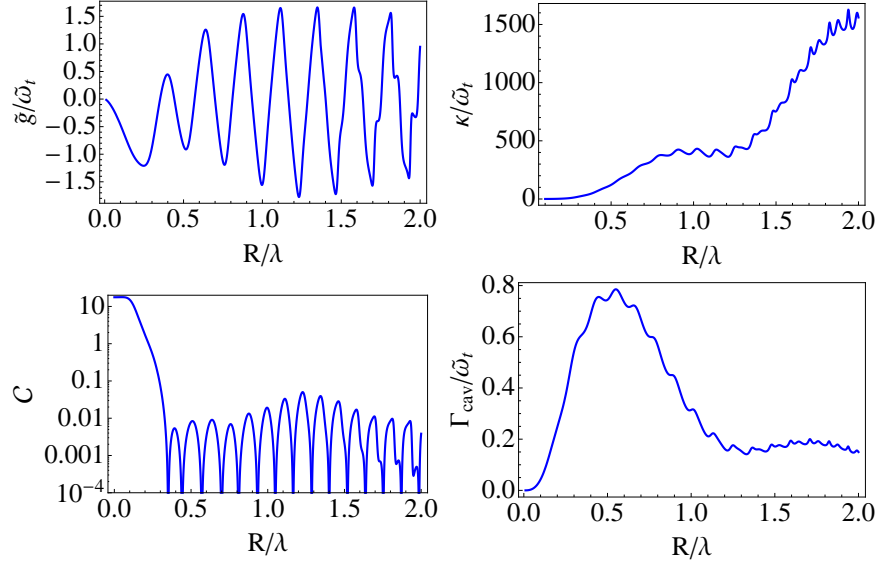


Figure 3.6: Cavity-Optomechanical parameters for different sizes of the object. *Upper left panel:* Optomechanical coupling  $g$ , *Upper right panel:* Cavity decay rate  $\kappa$ , *Lower left panel:* Cooperativity  $\mathcal{C}$ , *Lower right panel:* Decoherence due to elastic scattering of photons

distributions obtained in current experiments these fluctuations are typically negligible *e.g.*, in LIGO [173],  $S_{\text{vib}}(\omega_t) < 10^{-23} \text{ Hz/m}^2$  for  $\omega_t \approx \text{MHz}$ . However, when lower trapping frequencies and higher masses are considered, care has to be taken to control these effects. Another minor source of decoherence is given by anisotropies in the sphere's shape,  $\Gamma_{\text{anis}}$  (Eq. (3.84)). The parametric heating takes its maximum when the vibrational frequency is similar to the cm trapping,  $\langle \omega_r \rangle = \omega_t$ . In this case,  $\Gamma_{\text{anis}}/\omega_t \approx 10^{-5}$ , which is negligible compared to other sources of dissipation. Also decoherence via coupling to vibrational modes as well as coupling to two-level fluctuators can be neglected (see Secs. 3.4, 3.5.7).

Let us now take a closer look at the optomechanical parameters as illustrated in Fig. 3.6: the absolute value of the optomechanical coupling  $g$  first increases with the radius  $R$  reaching a local maximum at  $R \approx 260 \text{ nm}$ , then decreases and even vanishes at  $R \approx 370 \text{ nm}$ . In the following it continues these oscillations. The decoherence rate of the cm motion due to light scattering (see Fig. 3.5) first increases  $\propto R^3$ , then begins to fall off for  $R \gtrsim 600 \text{ nm}$ . This is due to its dependence on the ground-state size and the cross section, where the scattering is described by the Rayleigh cross section  $\propto R^6$  for small objects, to give way to a scaling  $\propto R^2$  in the limit of geometrical scattering and the squared ground state size, which is  $\propto R^{-3}$ . Also the cavity decay rate

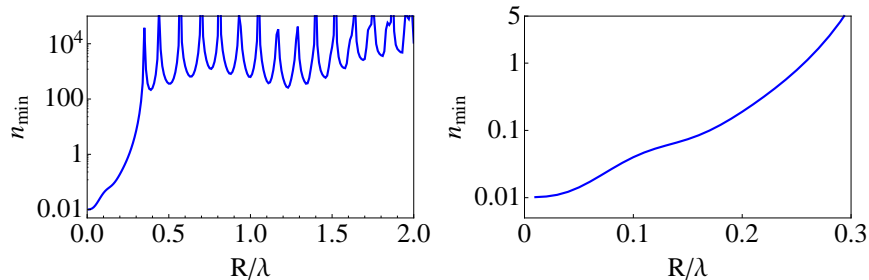


Figure 3.7: Minimal phonon numbers attainable with experimental parameters given in the main text: *Left*: Sphere sizes ranging between  $R = 10\text{nm} - 2\mu\text{m}$ , *Right*: For smaller spheres between  $R \leq 300\text{nm}$

increases  $\propto R^6$  at first, then shows some plateaus to finally converge to a scaling  $\propto R^2$ . Consequently, the cooperativity first decreases immensely to exhibit oscillations later on. These oscillations can only be predicted taking multiple-scattering processes into account. Nevertheless, the maximal values of the cooperativity are merely  $\mathcal{C} \approx 0.05$ . The minimal phonon number is obtained by minimizing the function  $\bar{n}_{\text{phon}}$  described in Eq. (3.20) with respect to  $\delta$ . While ground-state cooling is feasible for spheres  $R \lesssim 250\text{ nm}$ , only relatively large final phonon numbers can be achieved for larger spheres, *e.g.*,  $n_{\text{min}} \approx 350$  for  $R \approx 1.3\mu\text{m}$ .

### 3.A Justification of the adiabatic elimination of the vibrational modes

In this Appendix, we show that an adiabatic elimination of the vibrational modes in Sec. 3.4.3 is justified due to the separate time scales of the problem. For this purpose, the equations of motion of  $\hat{b}, \hat{b}^\dagger$  are solved via a Laplace transformation [160]. For simplicity, we neglect the coupling to the light field and among the vibrational modes for this analysis leading to a simplified Hamiltonian

$$\hat{H}_{\text{lap}} = \omega_t \hat{b}^\dagger \hat{b} + \sum_n \omega_n \hat{c}_n^\dagger \hat{c}_n + \sum_n \gamma_n (\hat{c}_n + \hat{c}_n^\dagger) (\hat{b} + \hat{b}^\dagger). \quad (3.85)$$

This gives the following equations of motion

$$\dot{b} = -i\omega_t \hat{b} - i \sum_n \gamma_n (\hat{c}_n + \hat{c}_n^\dagger) \quad (3.86)$$

$$\dot{c}_n = -i\omega_n \hat{c}_n - i\gamma_n (\hat{b} + \hat{b}^\dagger) \quad (3.87)$$

$$\dot{b}^\dagger = i\omega_t \hat{b}^\dagger + i \sum_n \gamma_n (\hat{c}_n + \hat{c}_n^\dagger) \quad (3.88)$$

$$\dot{c}_n^\dagger = i\omega_n \hat{c}_n^\dagger + i\gamma_n (\hat{b} + \hat{b}^\dagger). \quad (3.89)$$

Integrating  $\hat{c}_n$  over time and inserting it back into Eq. (3.86) gives

$$\begin{aligned} \dot{b}(t) = & -i\omega_t \hat{b} - i \sum_n \gamma_n [\hat{c}_n(0)e^{-i\omega_n t} + \hat{c}_n^\dagger(0)e^{i\omega_n t}] \\ & + \sum_n \gamma_n^2 \left[ \int_0^t e^{i\omega_n(t-\tau)} [\hat{b}^\dagger(\tau) + \hat{b}(\tau)] d\tau - \int_0^t e^{-i\omega_n(t-\tau)} [\hat{b}^\dagger(\tau) + \hat{b}(\tau)] d\tau \right]. \end{aligned} \quad (3.90)$$

Applying a Laplace transformation

$$L[f] = \int_0^\infty e^{-st} f(t) dt = \tilde{f}(s) \quad (3.91)$$

to this differential equation gives

$$s\tilde{b}(s) - \hat{b}(0) + i\omega_t \tilde{b}(s) = - \sum_n \left( \frac{i\gamma_n \hat{c}_n(0)}{s + i\omega_n} + \frac{i\gamma_n \hat{c}_n^\dagger(0)}{s - i\omega_n} \right) - [\tilde{b}(s) + \tilde{b}^\dagger(s)] F(s) \quad (3.92)$$

with

$$F(s) = \sum_n \frac{2i\omega_n \gamma_n^2}{s^2 + \omega_n^2}. \quad (3.93)$$

To obtain the equation of motion for  $\tilde{b}(t)$ , we need to write the equations in matrix form

$$\tilde{\mathbf{b}}(s) = M^{-1} \mathbf{b}(0) \quad (3.94)$$

with

$$M^{-1} = \frac{1}{s^2 + \omega_t^2 - 2iF(s)\omega_t} \begin{pmatrix} s - F(s) - i\omega_t & F(s) \\ F(s) & s + i\omega_t + F(s) \end{pmatrix}$$

and

$$\tilde{\mathbf{b}}(s) = \begin{pmatrix} \tilde{b}(s) \\ \tilde{b}^\dagger(s) \end{pmatrix}.$$

The transformed operator  $\tilde{b}(s)$  is thus given by

$$\begin{aligned} \tilde{b}(s) = & \frac{s - F(s) - i\omega_t}{s^2 + \omega_t^2 - 2iF(s)\omega_t} \tilde{b}(0) - \frac{F(s)}{s^2 + \omega_t^2 - 2iF(s)\omega_t} \tilde{b}^\dagger(0) \\ & + \frac{s + i\omega_t}{2i\omega_t F(s) - \omega_t^2 - s^2} \sum_n \left( \frac{i\gamma_n \hat{c}_n(0)}{s + i\omega_n} + \frac{i\gamma_n \hat{c}_n^\dagger(0)}{s - i\omega_n} \right). \end{aligned} \quad (3.95)$$

$F(s)$  contains several poles into which it can be decomposed. We want to show that after a back-transformation,  $\hat{b}(t)$  can be described by contributions of the system's slow time scale given by  $\omega_t$ . A back-transformation of the part describing the poles in the eqs. of motion gives

$$\begin{aligned}
& L^{-1}\left[\frac{1}{s^2 + \omega_t^2 - 2iF(s)\omega_t}\right] \\
&= \frac{\exp[i\omega_t t]}{2i\omega_t \prod_{i=1}^n (i\omega_t - i\omega_i)} + \frac{\exp[-i\omega_t t]}{2i\omega_t \prod_{i=1}^n (i\omega_t + i\omega_i)} \\
&+ \sum_{m=1}^n \left( \frac{\exp[i\omega_m t]}{2i\omega_m (i\omega_m - i\omega_t) \prod_{i \neq m} (i\omega_m - i\omega_i)} + \frac{\exp[-i\omega_m t]}{-2i\omega_m (-i\omega_m - i\omega_t) \prod_{i \neq m} (-i\omega_m - i\omega_i)} \right) \\
&\approx \frac{\exp[i\omega_t t]}{2i\omega_t \prod_{i=1}^n (i\omega_t - i\omega_i)} + \frac{\exp[-i\omega_t t]}{2i\omega_t \prod_{i=1}^n (i\omega_t + i\omega_i)}.
\end{aligned} \tag{3.96}$$

In the last line we exploit the scaling  $\omega_t/\omega_n \ll 1$  due to the separation of the cm mode from the higher vibrational modes. It is thus justified to neglect all terms except the ones given by the first two poles, as described in the last line of Eq. (3.96). The same scaling holds for the terms in the back transformation of  $\tilde{b}(s)$  as they contain at most the same number of poles as Eq. (3.96). It can thus be demonstrated that all terms in the evolution of  $\hat{b}(t)$  due to higher-order poles are suppressed by  $\omega_t/\omega_n$  and can thus be neglected. The lowest poles in the expansion that are kept correspond to the terms obtained when treating the higher-lying vibrational modes as a first-order perturbation to the cm mode [174]. This approximation is equivalent to carrying out an adiabatic elimination and we have thus shown that adiabatically eliminating the vibrational modes yields a good description of the system's dynamics, given  $\omega_t \ll \omega_n$ .

## Part II

# State preparation protocols



## Chapter 4

# Single-Photon Protocols

*We propose three protocols to prepare non-Gaussian states of a mechanical oscillator. All protocols use single photon as a resource to prepare quantum superpositions of a mechanical oscillator. The first protocol consists in sending a resonant photon on top of the driving field used to enhance its interaction with the mechanical mode, and measuring its reflected part. The motivation of the second protocol is to circumvent the single-photon measurement on top of a strong driving field by time-dependently modulating the optomechanical coupling strength allowing for a perfect mapping of the non-classical photon state. The third protocol poses less demanding requirements on the cavity and is based on a teleportation scheme. To perform full tomography of the prepared states, we propose a time-of-flight measurement of the levitating object. While the focus of this thesis is on levitating dielectrics, the state-preparation protocols presented in this chapter are general and apply to any optomechanical setup with sufficiently low decoherence rates. This chapter mainly bases on and uses parts of [64].*

### 4.1 Introduction

The idea to use single photons to prepare nonclassical states of a mechanical oscillator has been present since the early days of optomechanics. Already in Marshall *et al.* [60] (see also [175]) a scheme to prepare a superposition state of two distinct locations of a mirror through the optomechanical interaction with a single photon has been proposed. These ideas pose a major challenge to an experimental realization mainly due to the following reasons: (i) the coupling between the small quantum system and the macroscopic mechanical system is very weak and (ii) the mechanical system suffers from its fast decoherence due to the thermal contact. In this chapter, we show possible ways to circumvent these two restrictions. We propose two protocols to strongly couple a non-Gaussian light state to a mechanical object. This is achieved by using a driving field

which enhances the interaction into the strong-coupling regime (the interaction time has to be faster than the decoherence times). This enhancement of the optomechanical coupling by the driving field was suggested in [47, 176] and experimentally observed in [51]. Then, on top of the driving field, which is red-detuned, a quantum light state is sent into the cavity which is transferred to the mechanical system by the strong coupling. This idea has been introduced in [77] (see also [177, 178]). Additionally, we propose an alternative protocol that uses the weak-coupling regime to prepare non-Gaussian states. These protocols, which can be applied to general optomechanical systems, are ideally suitable for optically levitating nanodielectrics, since they do not suffer from clamping losses [77, 78], and thus possess long coherence times. The light-mechanics interfaces described in this chapter allow us to prepare non-Gaussian states by using a Gaussian Hamiltonian. Their key ingredient is to use non-Gaussian input states (similar ideas have been proposed in the context of quantum computation [179, 180]). Hence, these protocols represent an effective and simple way to produce non-linearities in optomechanical systems, a goal that is intensively pursued (see the introduction Sec. 1.3). Finally, we remark that in case of a levitating object in particular light scattering yields decoherence of the mechanical state with a rate given by  $\Gamma_{\text{phot}}$ . For sufficiently small objects, this effect is much smaller than  $\kappa$  (see Fig. 3.7). In the following, where we are interested in designing the protocols, we will neglect the effects of decoherence by assuming that the protocols can be realized on a time scale much shorter than  $1/\Gamma$ . This can be achieved by choosing small spheres,  $R \leq 100\text{nm}$ , for more details see Sec. 3.6. For other optomechanical setups, decoherence in the mechanical system can be incorporated easily into the protocols.

#### 4.1.1 Reader's guide

This chapter is organized as follows: first, in Sec. 4.2 we provide the necessary theoretical background and introduce the notation used throughout the chapter. In particular, we introduce the output field in Sec. 4.2.1 and transform the total Hamiltonian of the system in order to account for the driving field of the laser in Sec. 4.2.2. Based on this, three single-photon protocols to prepare non-Gaussian states are proposed. In Sec. 4.3, it is discussed how coupling a single photon on top of the driving field and taking a subsequent measurement of the output field prepares the mechanical oscillator in a non-Gaussian state. In Sec. 4.4, an alternative approach that circumvents the single-photon measurement by introducing a time-dependent coupling is described. In Sec. 4.5, a teleportation scheme also applicable in the bad-cavity limit is introduced. To enable a measurement of the prepared states, a tomography scheme based on a time-of-flight-measurement is proposed in Sec. 4.6. One particular theoretical diffi-

culty encountered in this analysis is the correct treatment of the displaced output field, addressed in App. 4.A.

## 4.2 The setup

### 4.2.1 The output field

So far, we have described the optomechanical system by  $\hat{H}_{\text{tot}}$  (Eq. (2.2)),

$$\hat{H}_{\text{tot}} = \hat{H}_{\text{S}} + \hat{H}_{\text{B}} + \hat{H}_{\text{BS}}, \quad (4.1)$$

containing contributions from the system, the bath, and the interaction between them. We now want to consider how photonic states can be transferred from the outside through the cavity to the mechanical mode. For this purpose, the modes that are coupled in and out of the cavity will be treated separately from  $\hat{H}_{\text{B}}$  [181,182]. In this picture, the total Hamiltonian reads

$$\hat{H}'_{\text{tot}} = \hat{H}_{\text{S}} + \hat{H}_{\text{B}} + \hat{H}_{\text{BS}} + \hat{H}_{\text{out}} + \hat{H}_{\text{cav-out}}, \quad (4.2)$$

where

$$\hat{H}_{\text{out}} = \int_0^\infty d\omega \omega \hat{a}_{\text{out}}^\dagger(\omega) \hat{a}_{\text{out}}(\omega), \quad (4.3)$$

describes the energy of the output modes and

$$\hat{H}_{\text{cav-out}} = i \int_0^\infty d\omega \gamma(\omega) \left[ \hat{a}_0^\dagger \hat{a}_{\text{out}}(\omega) - \text{H.c.} \right], \quad (4.4)$$

their interaction with the cavity mode.  $\omega$  denotes the different frequencies of the output modes,  $\hat{a}_{\text{out}}(\omega)$  ( $\hat{a}_{\text{out}}^\dagger(\omega)$ ) the annihilation (creation) of a photon in the output field, and the coupling strength between the cavity modes and the output field is approximated by  $\gamma(\omega) \approx \sqrt{\kappa/\pi}$  [181]. We are thus double-counting the output modes by writing them separately from the remaining bath. This is usually done in QED and does not pose a problem, as they have zero measure. For simplicity, we will neglect decoherence mechanisms in the description of the state preparation protocols here and also neglect the interaction between the cavity mode and all other external modes except the output mode. Consequently, we approximate

$$\hat{H}'_{\text{tot}} \approx \hat{H}_{\text{S}} + \hat{H}_{\text{out}} + \hat{H}_{\text{cav-out}} \quad (4.5)$$

for the remainder of this section and will leave the prime out for simplicity.

### 4.2.2 The displaced frame

As mentioned in the introduction, we want to enhance the interaction between photonic states and the dielectric by strongly driving the cavity mode. For this analysis, it is useful to transform the operators to the rotating frame [46, 47, 176] as outlined in Sec. 2.2.2, shifting the coherent part of the states obtained when driving the cavity with a laser. However, in contrast to what is usually done, it is also necessary to displace the output modes since they are used in the light-mechanics interface.

First, one moves the cavity and the output field to the frame rotating with the laser frequency  $\omega_L$ . This is described by the unitary operator

$$\hat{U}_r(t) = \exp \left[ -i\omega_L t \left( \hat{a}_0^\dagger \hat{a}_0 + \int_0^\infty \hat{a}_{\text{out}}^\dagger(\omega) \hat{a}_{\text{out}}(\omega) d\omega \right) \right]. \quad (4.6)$$

To ease the notation, after this transformation we redefine  $\hat{a}_{\text{out}}(\omega)$  and  $\gamma(\omega)$  such that  $\hat{a}_{\text{out}}(\omega) \equiv \hat{a}_{\text{out}}(\omega + \omega_L)$ , and  $\gamma(\omega) \equiv \gamma(\omega + \omega_L)$ . The total Hamiltonian before the displacement reads

$$\begin{aligned} \hat{H}_{\text{tot}} = & \delta \hat{a}_0^\dagger \hat{a}_0 + \omega_t \hat{b}^\dagger \hat{b} + g_0 \hat{a}_0^\dagger \hat{a}_0 (\hat{b}^\dagger + \hat{b}) + \int_{-\omega_L}^\infty d\omega \omega \hat{a}_{\text{out}}^\dagger(\omega) \hat{a}_{\text{out}}(\omega) \\ & + i \int_{-\omega_L}^\infty d\omega \gamma(\omega) (\hat{a}_0^\dagger \hat{a}_{\text{out}}(\omega) - \text{H.c.}), \end{aligned} \quad (4.7)$$

where  $\delta = \omega_c - \omega_L$ . Then, one displaces the cavity field with the displacement operator  $\hat{D}_{a0}(\alpha)$ , the mechanical mode with  $\hat{D}_b(\beta)$ , and the output modes with  $\hat{D}_{\text{out}}(\alpha_\omega)$ , that is,

$$\begin{aligned} \hat{D}_{a0}^\dagger(\alpha) \hat{a}_0 \hat{D}_{a0}(\alpha) &= \hat{a}_0 + \alpha, \\ \hat{D}_b^\dagger(\beta) \hat{b} \hat{D}_b(\beta) &= \hat{b} + \beta, \\ \hat{D}_{\text{out}}^\dagger(\alpha_\omega) \hat{a}_{\text{out}}(\omega) \hat{D}_{\text{out}}(\alpha_\omega) &= \hat{a}_{\text{out}}(\omega) + \alpha_\omega. \end{aligned} \quad (4.8)$$

After applying this transformation to the Hamiltonian, one fixes  $\alpha$ ,  $\beta$ , and  $\alpha_\omega$ , such that the terms in the Hamiltonian that contain only one or none creation or annihilation operator vanish. This corresponds to solving the following set of equations:

$$\begin{aligned} \delta \alpha + 2g_0 \alpha \beta + i \int_{-\omega_L}^\infty \gamma(\omega) \alpha_\omega d\omega &= 0, \\ \omega_t \beta + g_0 |\alpha|^2 &= 0, \\ \int_{-\omega_L}^\infty d\omega \omega \hat{a}_{\text{out}}^\dagger(\omega) \alpha_\omega - i \int_{-\omega_L}^\infty d\omega \gamma(\omega) \hat{a}_{\text{out}}^\dagger(\omega) \alpha &= 0, \end{aligned} \quad (4.9)$$

which have the solutions

$$\begin{aligned}\alpha &= \frac{\Omega_L}{i\tilde{\delta} + \kappa}, \\ \beta &= -\frac{g_0|\alpha|^2}{\omega_t}, \\ \alpha_\omega &= \left( \frac{\Omega_L}{\gamma(0)} - \pi\alpha\gamma(0) \right) \delta(\omega) + i\alpha\gamma(\omega)\mathcal{P}(\omega^{-1}).\end{aligned}\tag{4.10}$$

Here,  $\tilde{\delta} = \delta + 2g_0\beta$ , and

$$\Omega_L = \sqrt{\frac{2P_c\kappa}{\omega_L}},\tag{4.11}$$

with  $P_c$  being the laser power and  $\delta(\omega)$  the Dirac-Delta function. The symbol  $\mathcal{P}$  denotes the principal part, and we have used that  $\gamma^2(\omega) \approx \kappa/\pi$  in a finite region around  $\omega = 0$  [181] in order to perform the integral

$$\int_{-\infty}^{\infty} \mathcal{P}(\omega^{-1}) d\omega = 0.\tag{4.12}$$

In App. 4.A.1, we show how to obtain the expression of  $\alpha_\omega$  from a more physical perspective.

To sum up, the transformation applied to the Hamiltonian can be defined as  $\hat{\mathcal{D}} \equiv \hat{D}_{\text{out}}(\alpha_\omega)\hat{D}_b(\beta)\hat{D}_{a0}(\alpha)$ , and the transformed Hamiltonian is given by

$$\hat{H}'_{\text{tot}} = \hat{\mathcal{D}}^\dagger \hat{H}_{\text{tot}} \hat{\mathcal{D}} = \hat{H}'_{\text{S}} + \hat{H}'_{\text{out}} + \hat{H}'_{\text{cav-out}},\tag{4.13}$$

where

$$\hat{H}'_{\text{S}} = \omega_t \hat{b}^\dagger \hat{b} + \tilde{\delta} \hat{a}_0^\dagger \hat{a}_0 + g(\hat{a}_0^\dagger + \hat{a}_0)(\hat{b}^\dagger + \hat{b})\tag{4.14}$$

is the enhanced optomechanical Hamiltonian, and  $\hat{H}'_{\text{out}} + \hat{H}'_{\text{cav-out}}$  is transformed into

$$\hat{H}'_{\text{out}} + \hat{H}'_{\text{cav-out}} = \int_{-\omega_L}^{\infty} \omega \hat{a}'_{\text{out}}(\omega) \hat{a}_{\text{out}}(\omega) d\omega + i \int_{-\omega_L}^{\infty} \gamma(\omega) (\hat{a}'_{\text{out}}(\omega) \hat{a}_{\text{out}}(\omega) - \text{H.c.}) d\omega.\tag{4.15}$$

Note that Eq. (4.13) has the same structure as Eq. (4.7) with the only replacement  $\delta \rightarrow \tilde{\delta}$  (we will approximate  $\tilde{\delta} \approx \delta$  in the following as  $\beta g_0 \ll \delta$ ), and  $g_0 \hat{a}_0^\dagger \hat{a}_0 (\hat{b}^\dagger + \hat{b}) \rightarrow g(\hat{a}_0^\dagger + \hat{a}_0)(\hat{b}^\dagger + \hat{b})$ . As previously defined,  $g = g_0|\alpha|$ , and  $\xi = \arg(\alpha)$ , and we have redefined the  $\hat{a}_0$  ( $\hat{a}_{\text{out}}(\omega)$ ) operators as  $\hat{a}'_0 = \hat{a}_0 e^{-i\xi}$  ( $\hat{a}'_{\text{out}}(\omega) = \hat{a}_{\text{out}}(\omega) e^{-i\xi}$ ) (we omit the prime hereafter). A crucial remark is that the optomechanical coupling  $g$  is enhanced by  $\alpha$ , which is the square root of the mean number of photons inside the cavity in the steady state (see Sec. 2.2.2 for comparison). This will allow us to reach the strong coupling  $g \sim \kappa$  in the light-mechanics interface.

We remark that in case of using levitating objects, the shift to the trapping frequency as well as the shift in the equilibrium position should be taken into account in the  $\hat{H}'_S$  Hamiltonian. This would imply to change the trapping frequency to  $\omega_t \rightarrow \omega_t + \omega_{\text{sh}}$ , and the displacement of the cavity mode to  $\beta \rightarrow \beta + \xi_{\text{sh}}/\omega$ , where  $\omega_{\text{sh}}$  and  $\xi_{\text{sh}}$  describe these shift parameters. However, to keep the section in a general form, so that it can also be applied to other optomechanical systems, we will omit this effect hereafter.

The transformed Hamiltonian can now be written in the interaction picture, assuming that the free part is given by

$$\hat{H}_0 = \omega_t \hat{b}^\dagger \hat{b} + \delta \hat{a}_0^\dagger \hat{a}_0 + \int_{-\omega_L}^{\infty} \omega \hat{a}_{\text{out}}^\dagger(\omega) \hat{a}_{\text{out}}(\omega) d\omega \quad (4.16)$$

as

$$\hat{H}_{\text{tot}}^I = g(\hat{a}_0^\dagger e^{i\delta t} + \hat{a}_0 e^{-i\delta t})(\hat{b}^\dagger e^{i\omega_t t} + \hat{b} e^{-i\omega_t t}) + i \int_{-\omega_L}^{\infty} \gamma(\omega)(\hat{a}_0^\dagger \hat{a}_{\text{out}}(\omega) e^{i(\delta t - \omega t)} - \text{H.c.}) d\omega. \quad (4.17)$$

Now, by choosing a red-detuned driving  $\delta = -\omega_t$ , one can perform the rotating-wave approximation (RWA) (valid at  $\omega_t \gg g$ ), and obtain the beam-splitter interaction form of the total transformed Hamiltonian in the Schrödinger picture

$$\hat{H}_{\text{tot}}^r = \omega_t(\hat{a}_0^\dagger \hat{a}_0 + \hat{b}^\dagger \hat{b}) + g(\hat{a}_0^\dagger \hat{b} + \hat{a}_0 \hat{b}^\dagger) + \hat{H}'_{\text{out}} + \hat{H}'_{\text{cav-out}}. \quad (4.18)$$

Analogously, one can consider a blue-detuned driving  $\delta = \omega_t$  in order to get the two mode squeezing interaction Hamiltonian:

$$\hat{H}_{\text{tot}}^b = -\omega_t(\hat{a}_0^\dagger \hat{a}_0 - \hat{b}^\dagger \hat{b}) + g(\hat{a}_0^\dagger \hat{b}^\dagger + \hat{a}_0 \hat{b}) + \hat{H}'_{\text{out}} + \hat{H}'_{\text{cav-out}}. \quad (4.19)$$

These two types of interaction are used throughout the chapter to design different protocols in the light-mechanics interface.

### Initial state

All the protocols that we shall discuss in the next section assume that the initial state is the ground state cooled by the red-detuned field ( $\delta = -\omega_t$ ). As discussed in the previous section, this state is given by

$$|\text{in}\rangle = |\beta\rangle_b \otimes |\alpha\rangle_{a0} \otimes \int_{-\omega_L}^{\infty} \hat{D}_{\text{out}}(\alpha_\omega) d\omega |\Omega\rangle_{\text{out}} = \hat{\mathcal{D}} |00\Omega\rangle, \quad (4.20)$$

where “ $b(a0)$ ” labels the subspace of the mechanical mode (cavity mode), “out” the subspace of the output modes, and  $\Omega$  denotes the vacuum state for the output modes. The displacements  $\alpha$ ,  $\beta$ , and  $\alpha_\omega$  are defined in Eqs. (4.10).

Note that  $|\text{in}\rangle$  is an eigenstate of the total Hamiltonian  $\hat{H}_{\text{tot}}$ , see Eq. (4.7). This can be demonstrated by using that  $\hat{D}^\dagger \hat{H}_{\text{tot}} \hat{D} = \hat{H}_{\text{tot}}^r$  (for the red-detuned case Eq. (4.18)), and that  $\hat{H}_{\text{tot}}^r |00\Omega\rangle = 0$ , which gives

$$\hat{H}_{\text{tot}} |\text{in}\rangle = \hat{D} \hat{D}^\dagger \hat{H}_{\text{tot}} \hat{D} |00\Omega\rangle = \hat{D} \hat{H}_{\text{tot}}^r |00\Omega\rangle = 0. \quad (4.21)$$

The state  $|\text{in}\rangle$  (namely  $|00\Omega\rangle$  in the displaced frame) will be considered as the initial state upon which the protocols are designed using either the beam splitter interaction (Eq. (4.18)) or the two mode squeezing interaction (Eq. (4.19)).

### 4.3 One-photon reflected

The first protocol consists in sending one resonant photon on top of the driving field and measuring the reflected part. More specifically, the cavity is driven with a red-detuned field in order to induce the beam-splitter interaction. The mechanical object is assumed to be in its ground state. Then, on top of the driving field, a one-photon pulse centered at the resonance frequency is sent into the cavity. Impinging the cavity, part of it enters and part is reflected. At the time  $t_h$ , where the part of the beam that has entered the cavity is transferred to the mechanical oscillator through the beam-splitter interaction, the light field is switched off. Consequently, the light mode corresponding to the reflected photon is entangled with the mechanical system inside the cavity. We can obtain the exact form of the state by solving the input-output problem in the Schrödinger picture. The final state in the displaced frame is given by

$$|\psi(t_h)\rangle = c_b(t_h) |10\Omega\rangle + \int_{-\omega_L}^{\infty} d\omega c(\omega, t_h) \hat{a}_{\text{out}}^\dagger(\omega) |00\Omega\rangle, \quad (4.22)$$

where  $|n_b n_{a0}\Omega\rangle$  describes a state with  $n_b$  phonons,  $n_{a0}$  photons, and all the output modes in the vacuum state. Here, the coefficients  $c_b(t)$  and  $c(\omega, t)$  are obtained analytically. Considering Eq. (4.22) makes it clear that by measuring the quadrature of the output mode of the photon, one prepares a superposition state of zero and one phonons with coefficients given by the outcome of the measurement. Some technical issues are addressed in detail for this protocol in this thesis, such as the fact that in the original frame, the state  $|\psi(t_h)\rangle$  is displaced by a considerable amount. This makes it challenging to obtain a significant signal-to-noise ratio in the measurement of the output mode.

Let us now proceed and describe the preparation of the superposition state in more detail. The outlined protocol is general and can be applied to various optomechanical systems. Let us remark that it has already been introduced in [64, 77] and that related ideas have been reported in [177, 178]. In this section we will provide a thorough

analysis. In particular, we develop a formalism to solve the input-output formalism in the Schrödinger picture in order to be able to describe the final state of the protocol.

Let us start by sketching the different steps of the protocol:

1. Cool the mechanical motion to the ground state by the red-detuned driving field.
2. Keep the strong driving field switched on such that the beam-splitter interaction is induced inside the cavity.
3. Impinge the cavity with a resonant single-photon state, sent on top of the driving field as a result of parametric down conversion followed by a detection of a single photon [183].
4. When impinging the cavity, part of the field is reflected and part transmitted [184].
5. The beam-splitter interaction Eq. (4.18) caused by the red-detuned laser, swaps the state of light inside the cavity to the state of the mechanical motion.
6. By tuning the width of the light pulse appropriately, one finds that at time  $t_h$ , the maximum mean number of phonons of  $1/2$  in the mechanical system is obtained. At that time, the driving field is switched off. Then, the entangled state  $|E\rangle_{\text{out,b}} \sim |\tilde{0}\rangle_{\text{out}} |1\rangle_{\text{b}} + e^{i\phi} |\tilde{1}\rangle_{\text{out}} |0\rangle_{\text{b}}$  is prepared. Here out(b) stands for the reflected cavity field (mechanical motion) of the system, and  $|\tilde{0}(\tilde{1})\rangle_{\text{out}}$  is a displaced vacuum (one-photon) light state in the output mode of the cavity  $\hat{A}_{\text{out}}$ . The phase  $\phi$ , given by the light-mechanics interaction, is always fixed.
7. At a later time, once the reflected photon is far away from the cavity, a balanced homodyne measurement of the output mode is performed. The motional state collapses into the superposition state  $|\Psi\rangle_{\text{b}} = c_0 |0\rangle_{\text{b}} + c_1 e^{i\phi} |1\rangle_{\text{b}}$ , where the coefficients  $c_{0(1)}$  depend on the measurement result.

In the following we will analyze the important steps of the protocol. In the shifted frame, the initial state (according to Sec. 4.2.2) consists of a photon on top of the ground state of the mechanical oscillator. It is given by

$$|\Psi(0)\rangle = \int_{-\omega_L}^{\infty} d\omega \phi_{\text{in}}^*(\omega) \hat{a}_{\text{out}}^\dagger(\omega) |00\Omega\rangle, \quad (4.23)$$

where  $\phi_{\text{in}}^*(\omega)$  is the shape of the photon pulse which is assumed to be Gaussian

$$\phi_{\text{in}}(\omega) = \left( \frac{2}{\pi\sigma^2} \right)^{1/4} e^{-\frac{(\omega-\delta)^2}{\sigma^2}} e^{-i\omega x_{\text{in}}}. \quad (4.24)$$

Here,  $x_{\text{in}}$  is the position from which the pulse has been sent (it is considered to be large,  $x_{\text{in}} \gg 0$ , with the cavity denoting the zero-point).  $\delta = \omega_c - \omega_L = \omega_t$  is the detuning,

which shows that in the non-rotating frame the pulse is centered at the resonance frequency of the cavity. Note also that one can express the mode function in position space by the Fourier transform

$$\tilde{\phi}_{\text{in}}(x) = \frac{1}{\sqrt{2\pi}} \int d\omega \phi_{\text{in}}(\omega) e^{i\omega x}. \quad (4.25)$$

The time-evolved state with the beam-splitter interaction Eq. (4.18),

$$|\psi(t)\rangle = \exp[-i\hat{H}_{\text{tot}}^{\text{r}} t] |\psi(0)\rangle \quad (4.26)$$

can be expanded in the following basis,

$$|\psi(t)\rangle = c_b(t) |10\Omega\rangle + c_{a0}(t) |01\Omega\rangle + \int_{-\omega_L}^{\infty} c(\omega, t) \hat{a}_{\text{out}}^{\dagger}(\omega) d\omega |00\Omega\rangle. \quad (4.27)$$

The time-dependence of the coefficients can be obtained using the Wigner-Weisskopf formalism. The Schrödinger equation gives

$$\begin{aligned} \dot{c}_b(t) &= -i\omega_t c_b(t) - igc_{a0}(t), \\ \dot{c}_{a0}(t) &= -i\omega_t c_{a0}(t) - igc_b(t) + \int_{-\omega_L}^{\infty} \gamma(\omega) c(\omega, t) d\omega, \\ \dot{c}(\omega, t) &= -i\omega c(\omega, t) - \gamma(\omega) c_{a0}(t). \end{aligned} \quad (4.28)$$

This system can be further simplified by formally solving the differential equation for  $c(\omega, t)$ , plugging it into the equation for  $\dot{c}_{a0}(t)$ , and using the approximation  $\gamma(\omega) \approx \gamma(0) = \sqrt{\kappa/\pi}$ . This gives

$$\begin{aligned} \dot{c}_b(t) &= -i\omega_t c_b(t) - igc_{a0}(t), \\ \dot{c}_{a0}(t) &= -(i\omega_t + \kappa) c_{a0}(t) - igc_b(t) + \int_{-\omega_L}^{\infty} \gamma(\omega) e^{-i\omega t} c(\omega, 0) d\omega, \\ \dot{c}(\omega, t) &= -i\omega c(\omega, t) - \gamma(\omega) c_{a0}(t). \end{aligned} \quad (4.29)$$

This system of differential equations can be solved by using that  $c_{a0}(0) = c_b(0) = 0$  and  $c(\omega, 0) = \phi_{\text{in}}^*(\omega)$ . This leads to

$$\begin{aligned} c_{a0}(t) &= \sqrt{2\kappa} \int_0^t p_-(t-\tau) \tilde{\phi}_{\text{in}}^*(\tau) e^{-i\omega_t(t-\tau)} d\tau, \\ c_b(t) &= \sqrt{2\kappa} \int_0^t q(t-\tau) \tilde{\phi}_{\text{in}}^*(\tau) e^{-i\omega_t(t-\tau)} d\tau. \end{aligned} \quad (4.30)$$

The functions  $q(t)$  and  $p_{\pm}(t)$  are defined by

$$\begin{aligned} p_{\pm}(t) &= e^{-\kappa t/2} \left[ \cosh(\chi t) \pm \frac{\kappa}{2\chi} \sinh(\chi t) \right], \\ q(t) &= -i \frac{g}{\chi} e^{-\kappa t/2} \sinh(\chi t), \end{aligned} \quad (4.31)$$

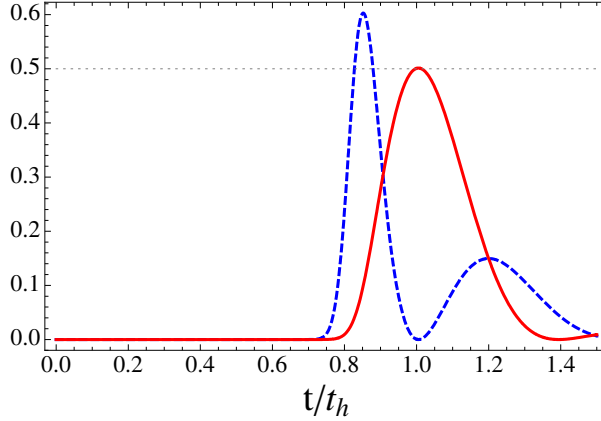


Fig. 4.1: Input-output dynamics after sending a one-photon pulse centered at  $x_{\text{in}} = 5/\kappa$  (where the cavity defines the zero point) at  $t = 0$ . A Gaussian pulse of width  $\sigma = 5.6\kappa$  is used. We plot the mean number of phonons in the mechanical system  $\bar{n}_b(t) = |c_b(t)|^2$  (red solid line) and the mean number of cavity photons  $\bar{n}_{a0}(t) = |c_{a0}(t)|^2$  (blue dashed line). We consider the strong coupling regime  $g = \kappa$ , and tune the width of the pulse so that the maximum mean number of phonons is  $\sim 1/2$  (dotted grey line) at  $t = t_h$ .

where  $\chi = \sqrt{\kappa^2/4 - g^2}$ . This result is illustrated by plotting the mean number of phonons  $\bar{n}_b(t) = |c_b(t)|^2$  and photons  $\bar{n}_{a0}(t) = |c_{a0}(t)|^2$ , see Fig. 4.1 for some parameters given in its caption. Note that at  $t = t_h$ , where

$$t_h = x_{\text{in}} + \frac{\arccos(\kappa/2g)}{\sqrt{g^2 - \kappa^2/4}}, \quad (4.32)$$

the mean number of phonons  $\bar{n}_b$  is maximized. By tuning the width of the initial pulse, one obtains that  $c_{a0}(t_h) \approx 0$  and  $|c_b(t_h)| \approx 1/\sqrt{2}$ . In this case, the total state at  $t_h$  is given by

$$|\psi(t_h)\rangle = c_b(t_h) |10\Omega\rangle + \int_{-\omega_L}^{\infty} c(\omega, t_h) \hat{a}_{\text{out}}^\dagger(\omega) d\omega |00\Omega\rangle. \quad (4.33)$$

This is an entangled state between the output photon mode, described by the pulse shape  $c(\omega, t_h)$ , and the mechanical phonon mode. In the non-displaced frame, the state at  $t_h$  is described by  $|\psi'(t_h)\rangle = \hat{\mathcal{D}} |\psi(t_h)\rangle$ .

At  $t = t_h$  the driving field is switched off. However, at this time, there is still a large number of photons  $|\alpha|^2$  present inside the cavity. They will leak out reducing the classical force that they were exerting on the mechanical system, which is described by the displacement of the mechanical system,  $\beta$ . In order to compensate this effect, one could move the center of the trap  $m\omega_t^2(x - x_t(t))^2/2$  accordingly, which yields a force term  $-m\omega_t^2 x_t(t) x_0(\hat{b} + \hat{b}^\dagger)$ , in order to keep the ground state of the harmonic oscillator.

Another effect of this leakage of photons is that the coefficient  $c_b(t_h)$  will decrease with time. Note however, that one could send a pulse that generates  $|c_b(t_h)| > 1/\sqrt{2}$  such that, after the decrease due to the leakage of coherent photons, one obtains  $|c_b(t > t_h)| = 1/\sqrt{2}$ . The discussion on how to compute and estimate this effect is given in App. 4.A.3.

Here, we simply approximate the state at  $t \gg t_h$  by

$$|\psi(t)\rangle = c_b(t_h)e^{-i\omega t(t-t_h)}\hat{D}_{\text{out}}|10\Omega\rangle + \hat{D}_{\text{out}}\hat{A}_{\text{out},t}^\dagger|00\Omega\rangle. \quad (4.34)$$

where the output mode of the cavity is defined as

$$\hat{A}_{\text{out},t}^\dagger = \int_{-\omega_L}^{\infty} \phi_{\text{out}}(\omega, t)\hat{a}_{\text{out}}^\dagger(\omega)d\omega, \quad (4.35)$$

with

$$\phi_{\text{out}}(\omega, t) = c(\omega, t_h)e^{-i\omega(t-t_h)}. \quad (4.36)$$

Note that the displacement is only in the output modes since the photons inside the cavity, and the consequent radiation force into the mechanical object, are not present at times  $t \gg t_h$  since the driving field is switched off.

### Measurement of the output mode

The final step of the protocol is the measurement of the quadrature of the output mode  $\hat{A}_{\text{out},t}$ , that is

$$\hat{X}_{\text{out},t} = \hat{A}_{\text{out},t}^\dagger + \hat{A}_{\text{out},t}. \quad (4.37)$$

This measurement consists in integrating the signal of a continuous measurement with the mode shape given by  $\phi_{\text{out}}(\omega, t)$ .

More generally, the output operator  $\hat{A}_{\text{out}}^\dagger = \int_{-\omega_L}^{\infty} \phi_{\text{out}}(\omega)\hat{a}_{\text{out}}^\dagger(\omega)d\omega$  can be written as a combination of mode operators at position  $x$  by using

$$\hat{a}_{\text{out}}(\omega) = \frac{1}{\sqrt{2\pi}} \int_0^{\infty} e^{-i\omega x}\hat{a}_{\text{out}}(x)dx, \quad (4.38)$$

leading to

$$\hat{A}_{\text{out}} = \int_0^{\infty} \tilde{\phi}_{\text{out}}(x)\hat{a}_{\text{out}}(x)dx. \quad (4.39)$$

Note that now the mode  $\hat{a}_{\text{out}}(x)$  can be determined at the position  $x = x_d$  of the detector at time  $t$  by the relation  $\hat{a}_{\text{out}}(x_d, t) = \hat{a}_{\text{out}}(x = x_d - t, 0)$ . Then, by a continuous measurement of  $\hat{a}_{\text{out}}(x_d, t)$ , one gains access to the measurement of all  $\hat{a}_{\text{out}}(x)$  and consequently, also to  $\hat{A}_{\text{out}}$  by integrating the signal over  $\tilde{\phi}_{\text{out}}(x)$  (note that  $\hat{A}_{\text{out}}$  is a linear combination of the independent modes  $\hat{a}_{\text{out}}(x)$ ).

After the continuous measurement, let us assume one obtains the value  $x_{\text{out}}$ . Then, the superposition state of the mechanical object,

$$|\Psi\rangle = \frac{1}{\sqrt{2}} (c_0 |0\rangle_b + c_1 |1\rangle_b), \quad (4.40)$$

is prepared, where  $c_{0(1)} = \langle x_{\text{out}} | 1(0) \rangle$ .

The proposed measurement of the quadrature poses an experimental challenge. If we define the two orthogonal states  $|\pm\rangle_0 = |\Omega\rangle \pm \hat{A}_{\text{out},t}^\dagger |\Omega\rangle$  and their displaced states  $|\pm\rangle = \hat{D}_{\text{out}} |\pm\rangle_0$ , one obtains that the mean value and fluctuations of  $\hat{X}_{\text{out}}$  are given by

$$\begin{aligned} \langle \hat{X}_{\text{out},t} \rangle_{\pm} &= \alpha_x + \langle \hat{X}_{\text{out},t} \rangle_{\pm,0}, \\ \langle \hat{X}_{\text{out},t}^2 \rangle_{\pm} &= \alpha_x^2 + 2\alpha_x \langle \hat{X}_{\text{out},t} \rangle_{\pm,0} + \langle \hat{X}_{\text{out},t}^2 \rangle_{\pm,0}, \end{aligned} \quad (4.41)$$

where we have defined  $\alpha_x = \hat{D}_{\text{out},t}^\dagger \hat{X}_{\text{out},t} \hat{D}_{\text{out},t} - \hat{X}_{\text{out},t}$ . Thus,  $\langle \Delta \hat{X}_{\text{out},t} \rangle_{\pm} = \langle \Delta \hat{X}_{\text{out},t} \rangle_{\pm,0}$ . This shows, that from the theoretical point of view, the two displaced states  $|\pm\rangle$  are as distinguishable as the non displaced ones  $|\pm\rangle_0$ . From the experimental point of view, the problem is that the signal-to-noise ratio in a balanced homodyne measurement is too low. Although the displacement  $\alpha_x$  can be computed by using  $\phi_{\text{out}}(\omega, t)$  and  $\alpha_\omega$  (see Eq. (4.10)), the final expression is not conclusive. In App. 4.A.2, we analyze the problem of the measurement of the output field when a photon on top of the coherent field was prepared inside the cavity. This general problem shows that the displacement of the output field is of the order of  $\alpha \sim 10^4$ : detection of a single-photon on top of such a strong driving field is challenging.

In order to circumvent this experimental challenge we propose the following solutions:

- Subtract the coherent part by destructively interfering a coherent beam with the same phase.
- Use an optomechanical system where the detuning between the resonant photon and the red-detuned driving is much larger (since  $\delta = -\omega_t$ , this would correspond to a mechanical oscillator with a high frequency). This must be done without loosening the strong coupling requirement which is based on the enhanced coupling  $g = |\Omega_L|g_0/\sqrt{\delta^2 + \kappa^2}$ .
- Use a scheme similar to the one proposed in [178], where the photon is sent in the dark port of an interferometer.
- Design a scheme where the light pulse is perfectly absorbed in the cavity and therefore no measurement is needed.

In the following section we present a protocol which follows the ideas of the last point.

## 4.4 Time-modulated coupling

Here we present a protocol that circumvents measuring the displaced output mode in the reflected one-photon protocol [64, 77]. The goal is to perfectly absorb the light pulse, which is in a non-Gaussian state, into the cavity, and transfer it to the mechanical system. This is achieved by using a time modulation of the optomechanical coupling  $g(t)$ , which can be implemented by varying the intensity of the driving field. Then, by imposing the condition that the output field, with the transformed Hamiltonian, is zero, we can obtain the equation of motion for the optomechanical coupling  $g(t)$ . In this section we also discuss some technical details on the transformation of the Hamiltonian containing time-dependent displacements. Similar ideas have been proposed in the context of quantum communication [185], and in quantum-optomechanical transducers [186].

### Time-dependent displacement

In this section, the beam-splitter interaction (4.18) cannot be employed, since the laser intensity is time-dependent. Care has to be taken when performing the time-dependent displacement. Let us start with the basic Hamiltonian in the non-displaced frame Eq. (4.7) and derive the evolution equations for  $\hat{a}_0$ ,  $\hat{b}$ , and  $\hat{a}_{\text{out}}(\omega)$

$$\begin{aligned}\frac{d}{dt}\hat{a}_0 &= -i\delta\hat{a}_0 - ig_0\hat{a}_0(\hat{b}^\dagger + \hat{b}) + \int_{-\omega_L}^{\infty} d\omega\gamma(\omega)\hat{a}_{\text{out}}(\omega, t), \\ \frac{d}{dt}\hat{b} &= -i\omega_t\hat{b} - ig_0\hat{a}_0^\dagger\hat{a}_0, \\ \frac{d}{dt}\hat{a}_{\text{out}}(\omega, t) &= -i\omega\hat{a}_{\text{out}}(\omega, t) - \gamma(\omega)\hat{a}_0.\end{aligned}\tag{4.42}$$

The tool that will be used in this section is a time-dependent driving field at the laser frequency  $\omega_L = 0$  (in the rotating frame). This can be incorporated by applying the following displacement to the output modes

$$\hat{a}_{\text{out}}(\omega, t) \rightarrow \hat{a}_{\text{out}}(\omega, t) - \sqrt{\frac{\pi}{\kappa}}\Omega_L(t)\delta(\omega),\tag{4.43}$$

where  $\delta(\omega)$  denotes the Dirac-delta function. By formally integrating the equation for  $d/dt \hat{a}_{\text{out}}(\omega, t)$ , and using the Markov approximation  $\gamma(\omega) \approx \sqrt{\kappa/\pi}$ , the system (4.42)

reads

$$\begin{aligned}
\frac{d}{dt}\hat{a}_0 &= -(i\delta + \kappa)\hat{a}_0 - ig_0\hat{a}_0(\hat{b}^\dagger + \hat{b}) + \Omega_L(t) + \sqrt{2\kappa}\hat{a}_{\text{in}}(t), \\
\frac{d}{dt}\hat{b} &= -i\omega_t\hat{b} - ig_0\hat{a}_0^\dagger\hat{a}_0, \\
\frac{d}{dt}\hat{a}_{\text{out}}(\omega, t) &= -i\omega\hat{a}_{\text{out}}(\omega, t) - \gamma(\omega)\hat{a}_0 + \sqrt{\frac{\pi}{\kappa}}\dot{\Omega}_L(t)\delta(\omega),
\end{aligned} \tag{4.44}$$

where we have defined the so-called input operator as

$$\hat{a}_{\text{in}}(t) \equiv \frac{1}{\sqrt{2\pi}} \int d\omega \hat{a}_{\text{out}}(\omega, 0) e^{-i\omega t}. \tag{4.45}$$

Next, we perform the following time-dependent displacement

$$\begin{aligned}
\hat{a}_0(t) &\rightarrow \hat{a}_0(t) + \alpha(t), \\
\hat{b}(t) &\rightarrow \hat{b}(t) + \beta(t),
\end{aligned} \tag{4.46}$$

and choose  $\alpha(t)$  and  $\beta(t)$ , such that non-operator terms in the equations for  $d/dt \hat{a}_0(t)$  and  $d/dt \hat{b}(t)$  vanish, that is

$$\begin{aligned}
\frac{d}{dt}\alpha &= -(i\delta + \kappa)\alpha - ig_0\alpha(\beta + \beta^*) + \Omega_L, \\
\frac{d}{dt}\beta &= -i\omega_t\beta - ig_0|\alpha|^2.
\end{aligned} \tag{4.47}$$

Then, we perform the following changes of variables

$$\begin{aligned}
\hat{a}_0(t) &\rightarrow \hat{a}_0(t) e^{-i\delta t}, \\
\hat{b}(t) &\rightarrow \hat{b}(t) e^{-i\omega_t t}, \\
\alpha(t) &= \frac{g(t)}{g_0} e^{i\xi},
\end{aligned} \tag{4.48}$$

( $g(t)$  is real) and perform the RWA considering the red-detuned case  $\delta = -\omega_t$ . Putting all of this together, Eqs. (4.44) read

$$\begin{aligned}
\frac{d}{dt}\hat{a}_0 &= -\kappa\hat{a}_0 - ig(t)e^{i\xi}\hat{b} + \sqrt{2\kappa}\hat{a}_{\text{in}}(t)e^{i\delta t}, \\
\frac{d}{dt}\hat{b} &= -ig(t)e^{-i\xi}\hat{a}_0, \\
\frac{d}{dt}\hat{a}_{\text{out}}(\omega, t) &= -i\omega\hat{a}_{\text{out}}(\omega, t) - \gamma(\omega) \left[ \hat{a}_0 e^{-i\delta t} + \alpha(t) \right] + \sqrt{\frac{\pi}{\kappa}}\dot{\Omega}_L(t)\delta(\omega).
\end{aligned} \tag{4.49}$$

We have neglected the small terms (not proportional to  $\alpha$ )  $-ig_0\hat{a}_0(\hat{b} + \hat{b}^\dagger)$ ,  $-ig_0\hat{a}_0^\dagger\hat{a}_0$ , and  $-ig_0\hat{a}_0(\beta + \beta^*)$  in the equation of motion. In particular  $-ig_0\hat{a}_0(\beta + \beta^*)$ , which is smaller than  $-ig_0\hat{a}_0\delta$ , complicates the equation describing the shape of  $g(t)$  (to be derived below) and is neglected since it does not change the physics of the problem.

Finally, note that Eqs. (4.47) give the solution for the time-dependent laser amplitude  $\Omega_L(t)$  such that the time-dependent coupling  $g(t)$  is implemented. In the next sections, we derive the pulse  $g(t)$  for which any light state is absorbed into the cavity and therefore perfectly mapped onto the mechanical system.

### Condition for perfect absorption

The formal condition for perfect absorption can be derived as follows. After the transformations are made, the evolution equation for  $\hat{a}_{\text{out}}(\omega, t)$  reads

$$\frac{d}{dt}\hat{a}_{\text{out}}(\omega, t) = -i\omega\hat{a}_{\text{out}}(\omega, t) - \gamma(\omega)\hat{a}_0e^{-i\delta t} - \gamma(\omega)\alpha(t) + \sqrt{\frac{\pi}{\kappa}}\dot{\Omega}_L(t)\delta(\omega). \quad (4.50)$$

By formally integrating this equation for the initial condition  $t = 0$ , as well as for the final condition  $t = t_1$ , and subtracting these two solutions after integrating over  $\omega$ , one obtains (using the approximation  $\gamma(\omega) \approx \sqrt{\kappa/\pi}$  and that  $\Omega_L(0) = \Omega_L(t_1) = 0$ )

$$0 = \hat{a}_{\text{in}}(t) - \frac{1}{\sqrt{2\pi}} \int_{-\omega_L}^{\infty} e^{-i\omega(t-t_1)} \hat{a}_{\text{out}}(\omega, t_1) - \sqrt{2\kappa} \left( \hat{a}_0(t) e^{-i\delta t} + \alpha(t) \right). \quad (4.51)$$

This is the so called input-output relation [181], which relates the output field (the second term containing the  $\hat{a}_{\text{out}}(\omega, t_1)$  modes) with the input field  $\hat{a}_{\text{in}}(t)$ , the quantum field from the cavity  $\hat{a}_0(t)$ , and its coherent part  $\alpha(t)$ . The condition for perfect absorption is that the mean value of the output field only contains the coherent part from the cavity, that is

$$\frac{1}{\sqrt{2\pi}} \int_{-\omega_L}^{\infty} d\omega e^{-i\omega(t-t_1)} \langle \hat{a}_{\text{out}}(\omega, t_1) \rangle = -\sqrt{2\kappa}\alpha(t). \quad (4.52)$$

With this condition, Eq. (4.51) reads

$$\langle \hat{a}_{\text{in}}(t) \rangle = \sqrt{2\kappa} \langle \hat{a}_0(t) \rangle e^{-i\delta t}. \quad (4.53)$$

One can now plug this condition into the Eqs. (4.49) and obtains

$$\begin{aligned} \left\langle \frac{d}{dt} \hat{a}_0(t) \right\rangle &= \kappa \langle \hat{a}_0(t) \rangle - ig(t) \langle \hat{b}(t) \rangle e^{i\xi}, \\ \left\langle \frac{d}{dt} \hat{b}(t) \right\rangle &= -ig(t) \langle \hat{a}_0(t) \rangle e^{-i\xi}, \end{aligned} \quad (4.54)$$

which can be further simplified to

$$\eta(t)\dot{g}(t) - \dot{\eta}(t)g(t) + g^3(t) \langle \hat{a}_0(t) \rangle = 0, \quad (4.55)$$

where

$$\eta(t) = \kappa \langle \hat{a}_0(t) \rangle - \left\langle \frac{d}{dt} \hat{a}_0(t) \right\rangle. \quad (4.56)$$

### State-independent pulse

The solution of Eq. (4.55) yields the optomechanical pulse  $g(t)$  necessary to perfectly transmit a light state into the mechanical system. In order to obtain a state-independent solution, we will assume that a coherent state with phase  $\alpha_s$  is sent to the cavity and we will show that the solution does not depend on  $\alpha_s$ . Therefore any linear combination of coherent states (and therefore any state since they form a complete basis) will be perfectly transmitted to the cavity with the pulse  $g(t)$ .

The initial state is assumed to be

$$|\psi(0)\rangle = \exp \left[ \alpha_s \int_{-\omega_L}^{\infty} \phi_{\text{in}}(\omega) \hat{a}_{\text{out}}^\dagger(\omega) d\omega - \text{H.c.} \right] |00\Omega\rangle, \quad (4.57)$$

where  $\phi_{\text{in}}^*(\omega)$  is the shape of the pulse. One can then obtain that

$$\langle \hat{a}_{\text{in}}(t) \rangle = \alpha_s \tilde{\phi}_{\text{in}}^*(t), \quad (4.58)$$

where  $\tilde{\phi}_{\text{in}}^*(t)$  is the Fourier transform of  $\phi_{\text{in}}(\omega)$ , and using Eq. (4.53),

$$\langle \hat{a}_0(t) \rangle = \frac{\alpha_s \tilde{\phi}_{\text{in}}^*(t) e^{i\delta t}}{\sqrt{2\kappa}}. \quad (4.59)$$

Then, Eq. (4.55) reads

$$[\kappa\mu(t) - \dot{\mu}(t)]\dot{g}(t) - [\kappa\dot{\mu}(t) - \ddot{\mu}(t)]g(t) + \mu(t)g^3(t) = 0, \quad (4.60)$$

where

$$\mu(t) \equiv \tilde{\phi}_{\text{in}}^*(t) e^{i\delta t}. \quad (4.61)$$

This is the main result of the section since its solution yields the time-dependent coupling  $g(t)$  for perfect mapping of any light state into the mechanical system: it does not depend on the coherent phase  $\alpha_s$ . In Fig. 4.2, the solution  $g(t)$  is plotted considering  $\phi_{\text{in}}(\omega)$  to be the same Gaussian pulse as used in the reflected one-photon protocol, see Eq. (4.24).

As an example, let us assume that one wants to transfer a photon in a superposition state described by

$$|\psi\rangle = \frac{1}{\sqrt{2}} |00\Omega\rangle + \frac{1}{\sqrt{2}} \int_{-\infty}^{\infty} d\omega \phi_{\text{in}}(\omega) \hat{a}_{\text{out}}^\dagger(\omega) |00\Omega\rangle. \quad (4.62)$$

In Fig. 4.2 the mean value of  $\hat{b}(t)$  is plotted using the  $g(t)$  solution obtained for the Gaussian case. As expected,  $\langle \hat{b}(t) \rangle$  attains the value  $1/2$ , showing that the superposition state  $(|0\rangle + |1\rangle)/\sqrt{2}$  has been prepared.

To sum up, this protocol facilitates a perfect mapping of any state of light into the mechanical system without performing any measurement, merely by using a smooth modulation of the optomechanical coupling.

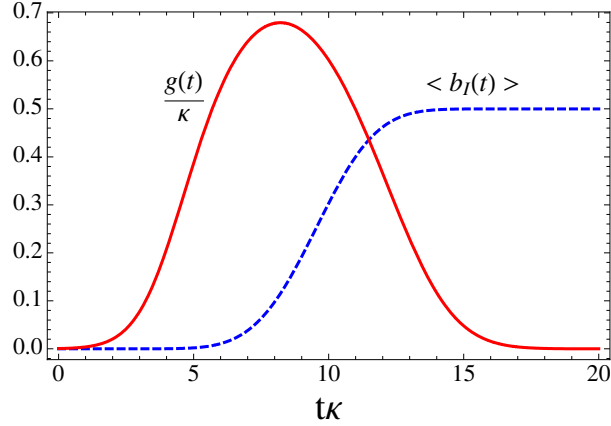


Fig. 4.2: Perfect state transfer of a  $|0\rangle + |1\rangle$  photonic state by sending a Gaussian light pulse of width  $\sigma = 2\kappa/3$  from a distance  $x_{\text{in}} = 10\kappa$ . We plot the time modulation of  $g(t)/\kappa$  (solid red line) and  $\langle \hat{b}(t) \rangle$  (dashed blue line). After the modulation, when  $g(t) = 0$ , one obtains that  $\langle \hat{b}(t) \rangle = 1/2$ . This shows that the superposition state has been mapped to the mechanical system without requiring a measurement.

## 4.5 Teleportation

Both protocols described in Sec. 4.3 and Sec. 4.4 require a moderately strong coupling  $g \sim \kappa$ . Despite the vast experimental progress [51], this regime still poses a challenge to most optomechanical setups. As an alternative, in this section we derive a protocol, called teleportation in the bad-cavity limit ( $\kappa > g$ ), which does not require the strong-coupling regime [64, 77]. Once the mechanical oscillator is in the ground state, it consists in driving the cavity with a blue-detuned field, such that the two-mode-squeezing interaction is induced inside the cavity. The two-mode squeezed state is then prepared by the optomechanical coupling between the mechanical mode and the cavity mode, which rapidly leaks out of the cavity. The output mode of the cavity, which is in a two-mode squeezed state with the mechanical system, can then be used as an entanglement channel to teleport [187, 188] a non-Gaussian state of light from outside the cavity onto the mechanical system (see Fig. 4.3 for an illustration of the protocol). This protocol has first been introduced as an interface between quantum dots in optical cavities [189]. In this reference, a detailed discussion of the protocol is provided, which applies to our optomechanical setup in complete analogy. Thus, we will only summarize and remark the important aspects of the protocol here.

Using the Hamiltonian Eq. (4.19), one can obtain the equations of evolution for

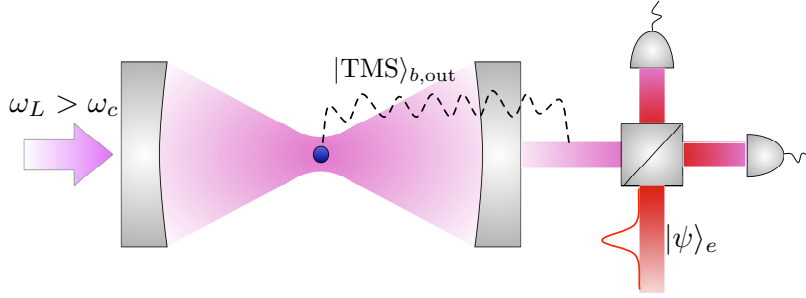


Figure 4.3: Schematic representation of a light-mechanics interface of teleportation in the bad-cavity limit. The cavity is driven by a blue-detuned laser which induces a two-mode squeezing interaction between the cavity mode and the mechanical mode. Being in the bad cavity limit  $\kappa > g$ , the cavity photons, which are in a two-mode squeezed state  $|\text{TMS}\rangle$  with the mechanical phonons, rapidly leak out. The output field is combined in a beam splitter together with the non-Gaussian state to be teleported  $|\psi\rangle_e$ . A measurement of the output quadratures realizes the Bell measurement required for teleportation [188].

$\hat{a}_0(t)$  and  $\hat{b}(t)$ ,

$$\begin{aligned} \frac{d}{dt}\hat{a}_0(t) &= -(i\delta + \kappa)\hat{a}_0(t) - ig\hat{b}^\dagger(t) + \sqrt{2\kappa}\hat{a}_{\text{in}}(t) \\ \frac{d}{dt}\hat{b}(t) &= -i\omega_t\hat{b}(t) - ig\hat{a}_0^\dagger(t). \end{aligned} \quad (4.63)$$

Transforming to the interaction picture ( $\hat{a}_0(t) \rightarrow \hat{a}_0(t)e^{-i\delta t}$  and  $\hat{b}(t) \rightarrow \hat{b}(t)e^{-i\omega_t t}$ ), and considering the bad cavity limit ( $\kappa \gg g$ ) one can adiabatically eliminate  $\hat{a}_0(t)$ , by setting  $d/dt \hat{a}_0(t) = 0$ . This gives

$$\frac{d}{dt}\hat{b}(t) = \frac{g^2}{\kappa}\hat{b}(t) - ig\sqrt{\frac{2}{\kappa}}\hat{a}_{\text{in}}^\dagger(t)e^{-i\delta t}. \quad (4.64)$$

Formally integrating this equation and using the initial conditions  $\langle \hat{a}_{\text{in}}^\dagger(t)\hat{a}_{\text{in}}(t) \rangle = \langle \hat{b}^\dagger(0)\hat{b}(0) \rangle = 0$  (the mechanical initial state is assumed to be in the ground state) yields

$$\langle \hat{b}^\dagger(t)\hat{b}(t) \rangle = e^{2\frac{g^2}{\kappa}t} - 1. \quad (4.65)$$

This can be used to obtain the squeezing parameter  $r$  of the entangled state, which will provide the fidelity of the teleportation scheme. As proved in [189], the output mode of the cavity and the mechanical system are in the two-mode-squeezed state  $|\text{TMS}\rangle_{b,\text{out}}$ ,

defined by (in the displaced frame)

$$\begin{aligned}
|\text{TMS}\rangle_{b,\text{out}} &= \hat{S}(r_{\text{sq}} e^{i\phi}) |00\rangle \\
&= \frac{1}{\cosh r_{\text{sq}}} \sum_{n=0}^{\infty} \left[ -e^{i\phi} \tanh r_{\text{sq}} \right]^n |nn\rangle_{b,\text{out}} \\
&\equiv \sum_{n=0}^{\infty} \hat{\Theta}^n |nn\rangle_{b,\text{out}}.
\end{aligned} \tag{4.66}$$

Here,  $\phi = \pi/2$  with the squeezing operator defined as

$$\hat{S}(r_{\text{sq}} e^{i\phi}) = \exp[-r_{\text{sq}}(e^{i\phi} \hat{a}_{\text{out}}^\dagger \hat{b}^\dagger - e^{-i\phi} \hat{a}_{\text{out}} \hat{b})]. \tag{4.67}$$

The squeezing parameter  $r$  can be obtained using the relation

$$\langle \hat{b}^\dagger \hat{b} \rangle = \frac{\cosh r - 1}{2} \tag{4.68}$$

as

$$r_{\text{sq}} = \text{arcosh} \left( 2e^{2g^2 t/\kappa} - 1 \right). \tag{4.69}$$

The teleportation fidelity is given by [190]

$$\mathcal{F}_{\text{tel}} = \frac{1}{1 + e^{-2r_{\text{sq}}}}. \tag{4.70}$$

Let us now discuss the fact that the entangled state in the original frame is given by

$$\hat{D}_b(\beta) \hat{D}_{\text{out}}(\alpha_{\text{out}}) |\text{TMS}\rangle_{b,\text{out}}. \tag{4.71}$$

Here,  $\hat{D}_{\text{out}}(\alpha_{\text{out}})$  is the displacement operator of the output mode, which is displaced by  $\alpha_{\text{out}}$  as a consequence of the displacement of the output operators  $\hat{a}_{\text{out}}(\omega)$  by  $\alpha_\omega$  (analogously to the discussion in App. 4.A.2). First, let us generally define the teleportation scheme as the map  $\mathcal{K}$  that teleports a light state  $|\psi\rangle_e$  as follows:

$$\mathcal{K} \left[ |\text{TMS}\rangle_{b,\text{out}} \otimes |\psi\rangle_e \right] = |\psi'\rangle_b. \tag{4.72}$$

Here, the subindex  $e$  labels the external system containing the state that will be teleported. Let us remark that perfect teleportation  $|\langle \psi | \psi' \rangle| = 1$  can only be achieved for the maximally entangled state  $r_{\text{sq}} \rightarrow \infty$ . In order to determine the output state in the original frame, let us first transform the initial state

$$\begin{aligned}
\hat{D}_b \hat{D}_{\text{out}} |\text{TMS}\rangle_{b,\text{out}} &= \hat{D}_b \hat{\mathcal{O}}_b \otimes \hat{D}_{\text{out}} \sum_{n=0}^{\infty} |nn\rangle_{b,\text{out}} \\
&= [\hat{D}_b \hat{\mathcal{O}}_b \hat{D}_{\text{out}}^\dagger]_b \otimes \mathbb{1} \sum_{n=0}^{\infty} |nn\rangle_{b,\text{out}},
\end{aligned} \tag{4.73}$$

where  $\hat{\mathcal{O}}_b = \sum_{n=0}^{\infty} \Theta^n |n\rangle\langle n|$ . The relation  $\hat{A} \otimes \hat{B} \sum_n |nn\rangle = \hat{A}\hat{B}^\top \otimes \mathbb{1} \sum_n |nn\rangle$  has been used, where  $\hat{B}^\top$  denotes the transpose of  $\hat{B}$ . Using this relation, the output state of the teleportation scheme with the original state is given by

$$\mathcal{K} \left[ \hat{D}_b \hat{D}_{\text{out}} |\text{TMS}\rangle_{b,\text{out}} \otimes |\psi\rangle_e \right] = \hat{D}_b \hat{\mathcal{O}}_b \hat{D}_{\text{out}}^\top |\psi\rangle_b. \quad (4.74)$$

This gives the final state of the teleportation protocol in the original frame. Note that  $\hat{D}_{\text{out}}^\top(\alpha_{\text{out}}) = \hat{D}_{\text{out}}^\dagger(\alpha_{\text{out}}^*)$ . Therefore, one can get rid of this displacement by teleporting the state  $\hat{D}(\alpha_{\text{out}}^*) |\psi\rangle_e$ , such that the state teleported in the mechanical system is given by  $\hat{D}_b(\beta) \mathcal{O} |\psi\rangle_b$  (the displacement  $\hat{D}_b(\beta)$  can also be reduced by varying the center of the trap when switching off the cavity lasers). Besides, note that one can in principle also choose the appropriate initial state  $|\psi\rangle$  in order to prepare a desired mechanical system  $|\phi\rangle$ , such that  $\hat{D}_b |\phi\rangle_b = \hat{D}_b \mathcal{O} |\psi\rangle_b$ .

## 4.6 Tomography

This chapter is concluded by providing a direct method to perform full tomography of the state of the mechanical oscillator. In general optomechanical systems, tomography can be carried out by coupling the mechanical resonator to a well-controlled quantum system (*e.g.*, a qubit), subsequently measuring the quantum system. This could be analogously achieved in our setup by mapping the mechanical state to the cavity mode using the enhanced beam-splitter interaction and performing full tomography of the output field. However, this technique suffers from the drawback that the output field contains a quantum state displaced by the large driving field and therefore, the signal-to-noise ratio would be challenging for experimental detection with present-day technology.

The method we propose here performs direct tomography of the mechanical oscillator [64]. It is well-known that measuring the rotated phase-quadrature operator

$$\hat{\mathcal{X}}(\theta) = e^{i\theta} \hat{b}^\dagger + e^{-i\theta} \hat{b}, \quad (4.75)$$

for all  $\theta$ , facilitates the reconstruction of the Wigner function and therefore contains all the information about the state of the harmonic oscillator [183]. In this section we propose an alternative method to *directly* perform full tomography of the mechanical system. In particular, we exploit the analogy of levitated nanodielectric objects to atomic physics, more specifically to cold gases, where time-of-flight measurements are used to experimentally probe different many-body states [75]. In particular, the protocol to perform direct full tomography of the mechanical state consists of the following steps (see Fig. 4.4):

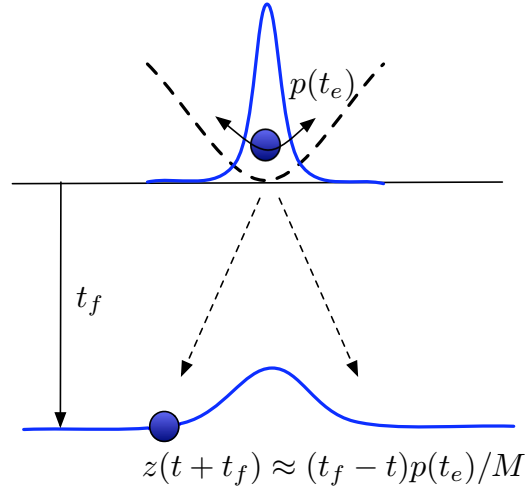


Figure 4.4: Schematic illustration of the time-of-flight protocol to perform full tomography of the mechanical state. The momentum operator at times  $t_e$ , which corresponds to the rotated phase-quadrature  $\hat{\chi}(\omega_t t_e + \pi/2)$ , is determined by measuring the position of the dielectric after some time of flight. By repeating the experiment at different times  $t_e$ , one can perform full tomography of the mechanical state.

1. We consider that at  $t = 0$  a particular state  $|\psi\rangle$  in the mechanical system is prepared (for instance, a non-Gaussian state using the light-mechanics interface introduced in Secs. 4.3, 4.4, 4.5). Immediately after the preparation of the state, the cavity field is switched off and only the optical trapping remains switched on. During these transient times the center of the trap has to be changed in order to account for the variation in the classical force created by the driving field, as discussed in the light-mechanics interface.
2. Then, during some given time  $t_e$ , the system is evolving within the harmonic potential, such that the mechanical momentum operator in the Heisenberg picture is given by

$$\hat{p}(t) = ip_m(\hat{b}^\dagger e^{i\omega_t t} - \hat{b} e^{-i\omega_t t}), \quad t \in [0, t_e], \quad (4.76)$$

where  $p_m = \sqrt{M\omega_t/2}$ .

3. At  $t = t_e$ , the trap is switched off and the nanodielectric falls freely for the time of flight  $t_f$ , such that the distance from the center of the cavity along the cavity

axis is given by

$$\begin{aligned}\hat{z}(t_e + t_f) &= \hat{z}(t_e) + (t_f - t_e) \frac{\hat{p}(t_e)}{M} \\ &\sim (t_f - t_e) \frac{\hat{p}(t_e)}{M},\end{aligned}\tag{4.77}$$

where we assume that  $t_f$  is sufficiently large such that

$$(t_f - t_e) \frac{\hat{p}(t_e)}{M} \gg \hat{z}(t_e).\tag{4.78}$$

4. At  $t = t_e + t_f$ , the position-operator  $\hat{z}(t_e + t_f)$  is measured (*e.g.*, by imaging the object and measuring the center of the light spot at the screen), which means that the in-trap momentum  $\hat{p}(t_e)$  is effectively measured.
5. The experiment is repeated in order to obtain statistics for any time  $t_e \in [0, 2\pi/\omega_t]$ .

The data gained in this protocol provides the statistical distribution of the rotated phase-quadrature operator,  $\hat{\mathcal{X}}(\theta)$ . There exists the following one-to-one relation between the momentum operator and the rotated quadrature phase operator,

$$\hat{p}(t_e) = \hat{\mathcal{X}}(\omega_t t_e + \pi/2).\tag{4.79}$$

Let us now discuss some experimental considerations. First, we will estimate the order of magnitude of  $t_f$  (and therefore the time-of-flight distance  $d_f = Gt_f^2/2$ , where  $G$  is the gravitational acceleration). In particular, let us assume that after the time of flight the position can be measured with a resolution given by  $\delta z$ . This implies that the object has to spread over a distance much larger than  $\delta z$ , which means that  $t_f \gg M\delta z/p_m$  is required. Using the parameters given in Sec. 3.6 and sphere sizes  $R \approx 50\text{nm}$ , one obtains that  $t_f$  is of the order of tens of ms, which would require a time-of-flight distance of the order of one centimeter. Although this position resolution is feasible, the requirement could even be relaxed with the same duration of time of flight. The idea is to amplify the oscillation via driving the field with a blue-detuned laser prior to the time of flight. More specifically, let us assume that just after the preparation of the mechanical state, the cavity is impinged with a laser detuned to the blue sideband of the cavity. This corresponds to including an additional step (point 1.b) between steps 1 and 2 in the previous protocol. The blue-detuned driving is performed during a certain time  $\tau < 1/\Gamma$  (where  $\Gamma$  is the decoherence rate when the cavity field is switched on). After this amplification, the momentum operator is transformed to

$$\hat{p}(\tau) = ip_m p_+(\tau) (\hat{b}^\dagger e^{i\omega_t \tau} - \hat{b} e^{-i\omega_t \tau}) + \hat{p}_{\text{cav}}(\tau),\tag{4.80}$$

where  $p_+(\tau)$  is the amplifying parameter given by

$$p_+(\tau) = e^{-\kappa t/2} \left[ \cosh(\chi\tau) + \frac{\kappa}{2\chi} \sinh(\chi\tau) \right] \quad (4.81)$$

with  $\chi = \sqrt{g^2 + \kappa^2/4}$ . The term  $p_{\text{cav}}(\tau)$  results from the entanglement of the mechanical system to the cavity field due to the two-mode-squeezing interaction. It reads

$$\hat{p}_{\text{cav}}(\tau) = [q^*(\tau)e^{i\omega\tau}\hat{a}_0(0) + \text{H.c.}], \quad (4.82)$$

where

$$q(t) = -ige^{-\frac{\kappa t}{2}} \frac{\sinh(\chi t)}{\chi}, \quad (4.83)$$

and fulfills  $\langle \hat{p}_{\text{cav}}(\tau) \rangle = 0$  (the cavity field is empty at  $t = 0$ ) and  $\langle \hat{p}_{\text{cav}}^2(\tau) \rangle = |q(\tau)|^2$ . After this amplification, step 2 of the protocol follows. If one assumes  $g = \kappa = 2\pi \times 100$  kHz, and  $\tau = 0.02$  ms, one obtains that  $p_+(\tau) \sim 10^3$  and hence with the same time of flight  $t_f$  the required resolution is only

$$\delta z \ll t_f p_m p_+(\tau) / M \sim 100 \mu\text{m}; \quad (4.84)$$

three orders of magnitude lower. Note that the amplification is restricted by keeping the nanodielectric object in the region, where it still sees the slope of the standing wave, i.e., the condition  $x_0 p_+(\tau) < 1$  nm has to be fulfilled, where  $x_0 \sim 10^{-12}$  m is the ground state size. In addition, one has to make sure that a sufficiently good signal-to-noise ratio is achieved.

Let us remark that the rotated quadrature  $\chi(\theta)$  could, in principle, also be measured by a quantum non-demolition measurement. This could be done by using the back-action evasion scheme proposed by Braginsky in the 80's [24], and recently revised from a quantum noise perspective [191]. This protocol would also benefit from the absence of clamping losses in the setup. The key idea of this method is to impinge the cavity at the two motional sidebands, a scheme that has already been realized with trapped ions [150, 192].

The time of flight protocol presented in this section exploits the unique property of using levitating objects in quantum optomechanical systems; the mechanical resonator is unattached to other objects and therefore can fall freely.

## 4.A Displacement of the output modes

In this section we show how the expression of the displacement of the output modes,  $\alpha_\omega$ , results from the steady state in the presence of a driving field. Then we discuss how to measure a photon created on top of the coherent cavity driving in the output

field. To simplify the problem, we assume a cavity of resonance frequency  $\omega_c$ , driven by a laser at  $\omega_L$ . For this purpose, we exclusively analyze the cavity mode and the output modes and take into account the mechanical mode only in the last subsection 4.A.3. In the rotating frame with  $\delta = \omega_c - \omega_L$ , the Hamiltonian reads

$$\hat{H}_{L-out} = \delta \hat{a}_0^\dagger \hat{a}_0 + \int_{-\omega_L}^{\infty} \omega \hat{a}_{out}^\dagger(\omega) \hat{a}_{out}(\omega) d\omega + i \int_{-\omega_L}^{\infty} \gamma(\omega) (\hat{a}_0^\dagger \hat{a}_{out}(\omega) - \text{H.c.}) d\omega. \quad (4.85)$$

#### 4.A.1 Steady-state with a driving field

The initial state of the cavity and the output modes is given by.

$$|\text{in}\rangle = |\alpha\rangle \otimes \int_{-\omega_L}^{\infty} d\omega \delta(\omega) \hat{D}_{out}(\alpha_0) |\Omega\rangle. \quad (4.86)$$

Here, the cavity is in a coherent state with phase  $\alpha$ , and all the output modes are empty, only the laser mode is in a coherent state with phase  $\alpha_0 = \Omega_L/\gamma(0)$ . In the following, we will compute the final state

$$|\text{st}\rangle = \lim_{t \rightarrow \infty} \exp[-i\hat{H}_{L-out}t] |\text{in}\rangle. \quad (4.87)$$

First, let us write the Heisenberg equations of motion:

$$\begin{aligned} \frac{d}{dt} \hat{a}_0(t) &= -i\delta \hat{a}_0(t) + \int_{-\omega_L}^{\infty} d\omega \gamma(\omega) \hat{a}_{out}(\omega, t), \\ \frac{d}{dt} \hat{a}_{out}(\omega, t) &= -i\omega \hat{a}_{out}(\omega, t) - \gamma(\omega) \hat{a}_0(t). \end{aligned} \quad (4.88)$$

Then, one can formally integrate the differential equation for  $\hat{a}_{out}(\omega, t)$ ,

$$\hat{a}_{out}(\omega, t) = e^{-i\omega t} \hat{a}_{out}(\omega, 0) - \gamma(\omega) \int_0^t d\tau \hat{a}_0(\tau) e^{-i\omega(t-\tau)}. \quad (4.89)$$

This solution can be inserted into the differential equation for  $\hat{a}_0(t)$ . By using the approximation  $\gamma(\omega) \approx \gamma(0) = \sqrt{\kappa/\pi}$ , one gets

$$\frac{d}{dt} \hat{a}_0(t) = -(i\delta + \kappa) \hat{a}_0(t) + \int_{-\omega_L}^{\infty} \gamma(\omega) e^{-i\omega t} \hat{a}_{out}(\omega, 0), \quad (4.90)$$

which can be integrated to

$$\hat{a}_0(t) = e^{-(i\delta + \kappa)t} \hat{a}_0(0) + \int_0^t d\tau \int_{-\omega_L}^{\infty} d\omega \gamma(\omega) e^{-i\omega\tau} \hat{a}_{out}(\omega, 0) e^{-(i\delta + \kappa)(t-\tau)}. \quad (4.91)$$

Taking the mean value of this expression, using that  $\langle \hat{a}_0(0) \rangle = \alpha$  and  $\langle \hat{a}_{out}(\omega, 0) \rangle = \alpha_0$ , gives

$$\langle \hat{a}_0(t) \rangle = e^{-(i\delta + \kappa)t} \alpha + \gamma(0) \alpha_0 \frac{1 - e^{-(i\delta + \kappa)t}}{i\delta + \kappa}. \quad (4.92)$$

In the steady state, this is

$$\alpha \equiv \lim_{t \rightarrow \infty} \langle \hat{a}_0(t) \rangle = \frac{\gamma(0)\alpha_0}{i\delta + \kappa} = \frac{\Omega_L}{i\delta + \kappa}. \quad (4.93)$$

Note that we have assumed that the initial coherent state of the cavity is equal to the steady state obtained when driving the cavity with the laser. Let us now compute the mean value of the output modes, which after some algebra is given by

$$\begin{aligned} \langle \hat{a}_{\text{out}}(\omega, t) \rangle &= \alpha_0 \delta(\omega) - \gamma(\omega) \int_0^t d\tau \langle \hat{a}_0(\tau) \rangle e^{-i\omega(t-\tau)} \\ &= \alpha_0 \delta(\omega) - \alpha \gamma(\omega) \int_0^t d\tau e^{-i\omega\tau}. \end{aligned} \quad (4.94)$$

Then, the steady-state phase of the output modes can be expressed by

$$\begin{aligned} \alpha_\omega &= \lim_{t \rightarrow \infty} \langle \hat{a}_{\text{out}}(\omega, t) \rangle \\ &= [\alpha_0 - \pi\alpha\gamma(0)] \delta(\omega) + i\alpha\gamma(\omega) \mathcal{P}(\omega^{-1}), \end{aligned} \quad (4.95)$$

which is identical to the expression used in Eq. (4.10).

It can be easily shown that the Hamiltonian is invariant under the displacement operation  $\hat{\mathcal{D}} = \hat{D}_a \hat{D}_{\text{out}}$ , with  $\hat{D}_a^\dagger \hat{a}_0 \hat{D}_a = \hat{a}_0 + \alpha$ , and  $\hat{D}_{\text{out}}^\dagger \hat{a}_{\text{out}}(\omega) \hat{D}_{\text{out}} = \hat{a}_{\text{out}}(\omega) + \alpha_\omega$ . By using that  $\mathcal{P} \int_{-\infty}^{\infty} \omega^{-1} d\omega = 0$ , one can check that

$$\hat{\mathcal{D}}^\dagger \hat{H}_{\text{L-out}} \hat{\mathcal{D}} = \hat{H}_{\text{L-out}}. \quad (4.96)$$

This implies that the steady state

$$|\text{in}\rangle = \hat{\mathcal{D}} |0\Omega\rangle = |\alpha\rangle \otimes \int_{-\omega_L}^{\infty} d\omega \hat{D}(\alpha_\omega) |0\Omega\rangle \quad (4.97)$$

is indeed an eigenstate of the Hamiltonian:

$$\hat{H}_{\text{L-out}} |\text{in}\rangle = \hat{\mathcal{D}} \hat{\mathcal{D}}^\dagger \hat{H}_{\text{L-out}} \hat{\mathcal{D}} |0\Omega\rangle = \hat{\mathcal{D}} \hat{H}_{\text{L-out}} |0\Omega\rangle = 0. \quad (4.98)$$

#### 4.A.2 Measurement of a photon

In this section we compute the displacement of the output mode of the cavity. We assume that at  $t = 0$  a photon is present inside the cavity in the displaced frame, such that

$$|\psi(0)\rangle = |1\Omega\rangle. \quad (4.99)$$

The Wigner-Weisskopf formalism gives for the state at some later time

$$|\psi(t)\rangle = c_{a0}(t) |1\Omega\rangle + \int_{-\omega_L}^{\infty} d\omega c(\omega, t) \hat{a}_{\text{out}}^\dagger(\omega) |0\Omega\rangle, \quad (4.100)$$

where the coefficients are given by

$$\begin{aligned} c_{a0}(t) &= e^{-(i\delta+\kappa)t}, \\ c(\omega, t) &= \frac{\gamma(\omega) (e^{-i\omega t} - e^{-(i\delta+\kappa)t})}{i(\omega - \delta) + \kappa}. \end{aligned} \quad (4.101)$$

For large  $t$ , the final state is given by  $|\psi(t)\rangle = \hat{A}_{\text{out},t}^\dagger |0\Omega\rangle$ , where the collective output mode is defined as

$$\hat{A}_{\text{out},t} = \int \phi_{\text{out}}^*(\omega) e^{i\omega t} \hat{a}_{\text{out}}(\omega) d\omega, \quad (4.102)$$

with the mode function

$$\phi_{\text{out}}(\omega) = \frac{\gamma(\omega)}{\kappa - i(\omega - \delta)}. \quad (4.103)$$

Let us now compute the number of photons in this collective mode after transforming back to the non-displaced frame. By using the expression of the displacement of the output modes  $\alpha_\omega$ , one obtains for the displacement of the output mode  $\hat{A}_{\text{out},t}$ ,

$$\alpha_{\text{out}} = \int_{-\omega_L}^{\infty} \phi_{\text{out}}(\omega) e^{i\omega t} \alpha_\omega d\omega = \alpha. \quad (4.104)$$

### 4.A.3 Switching off the driving field

In this Appendix, the final state of the one-photon protocol after switching off the driving field is discussed. The Hamiltonian in the frame rotating with the laser frequency  $\omega_L$ , is given by

$$\begin{aligned} \hat{H}'_{\text{tot}} &= \omega_t \hat{b}^\dagger \hat{b} + \delta \hat{a}_0^\dagger \hat{a}_0 + \int_{-\omega_L}^{\infty} \omega \hat{a}_{\text{out}}^\dagger(\omega) \hat{a}_{\text{out}}(\omega) d\omega + g_0 \hat{a}_0^\dagger \hat{a}_0 (\hat{b}^\dagger + \hat{b}) \\ &+ i \int_{-\omega_L}^{\infty} \gamma(\omega) (\hat{a}_0^\dagger \hat{a}_{\text{out}}(\omega) - \text{H.c.}) d\omega + \lambda(t) (\hat{b}^\dagger + \hat{b}), \end{aligned} \quad (4.105)$$

where the term with  $\lambda(t)$  accounts for the variation of the center of the harmonic trap. By writing the Langevin equations, and considering that there are no input fields since they have already been switched off, one obtains

$$\begin{aligned} \frac{d}{dt} \hat{a}_0 &= -i\delta \hat{a}_0 - \kappa \hat{a}_0 - ig_0 \hat{a}_0 (\hat{b}^\dagger + \hat{b}), \\ \frac{d}{dt} \hat{b} &= -i\omega_t \hat{b} - ig_0 \hat{a}_0^\dagger \hat{a}_0 - i\lambda(t). \end{aligned} \quad (4.106)$$

By displacing the operators by  $\hat{a}_0 \rightarrow \hat{a}_0 + \alpha$ , and restricting

$$\begin{aligned} \dot{\alpha} &= -i\delta \alpha - \kappa \alpha, \\ 0 &= -ig_0 |\alpha|^2 - i\lambda(t), \end{aligned} \quad (4.107)$$

the following equations are obtained:

$$\begin{aligned}\frac{d}{dt}\hat{a}_0 &= -i\delta\hat{a}_0 - \kappa\hat{a}_0 - ig_0|\alpha|(\hat{b}^\dagger + \hat{b}), \\ \frac{d}{dt}\hat{b} &= -i\omega_t\hat{b} - ig_0|\alpha|(\hat{a}_0^\dagger + \hat{a}_0).\end{aligned}\tag{4.108}$$

In the interaction picture one can perform the RWA in order to get

$$\begin{aligned}\frac{d}{dt}\hat{a}_0 &= -\kappa\hat{a}_0 - ig(t)\hat{b}, \\ \frac{d}{dt}\hat{b} &= -ig(t)\hat{a}_0,\end{aligned}\tag{4.109}$$

where

$$g(t) = g_0|\alpha(0)|e^{-\kappa t}.\tag{4.110}$$

The equation for  $\hat{b}$  is then given by

$$\frac{d^2}{dt^2}\hat{b} - \frac{d}{dt}\hat{b}\left(\frac{\dot{g}(t)}{g(t)} - \kappa\right) + \hat{b}g^2(t) = 0.\tag{4.111}$$

The solution of this equation gives an estimation for the variation of the mechanical state by switching off the driving field.



## Chapter 5

# State preparation assisted with a qubit

*We propose and analyze nonlinear optomechanical protocols that can be implemented by adding a single atom to an optomechanical cavity. In particular, we show how to engineer the environment in order to dissipatively prepare the mechanical oscillator in a superposition of Fock states with fidelity close to one. Furthermore, we demonstrate that a single atom in a cavity with several mechanical oscillators can be exploited to realize nonlinear many-partite systems by stroboscopically driving the mechanical oscillators. This can be used to prepare nonlinear many-partite states by either applying coherent protocols or engineering dissipation. The analysis of the protocols is carried out using a perturbation theory for degenerate Liouvillians and numerical tools. Our results apply to other systems where a qubit is coupled to a mechanical oscillator via a bosonic mode, e.g., in cavity quantum electromechanics. This chapter mainly bases on and uses parts of [118].*

### 5.1 Introduction

As outlined in the introduction, Sec. 1.3, the preparation of non-Gaussian states is one of the most urgent challenges in optomechanics. Having investigated the coupling of a single photon to the mechanical oscillator in Chap. 4, here we propose to couple the mechanical oscillator to an auxiliary system that can easily be prepared in a nonclassical state. In particular, we propose to add a single atom to the optomechanical cavity and to couple the mechanical oscillator to its internal structure. This is motivated by the improved finesse of optomechanical cavities approaching the strong-coupling regime for single atoms [51, 193].

We show that not only may coherent methods be applied to realize non-Gaussian

physics, but that the strong decoherence through the cavity can prepare the nanomechanical oscillator in a non-Gaussian steady state with fidelity close to one. The main idea is to exploit the dissipation rather than treating it as an obstacle [194]. While this approach has been proposed to prepare squeezed and entangled states of mechanical oscillators [48, 195–202], here we show how to use it to prepare non-Gaussian states. We extend the analysis to many-partite systems, where we show that adding  $N$  mechanical oscillators into a cavity containing the single atom, realizes a system with  $N$  nonlinear modes. This is achieved via stroboscopically driving the oscillators' frequencies. Based on this, we show how both dissipative and coherent state-preparation methods may be applied. The results presented here are applicable to the general case where a single qubit is coupled to a mechanical oscillator via a bosonic mode. This can be achieved in a variety of physical systems, *e.g.*, in cavity quantum electromechanics [43, 50].

### 5.1.1 Reader's guide

The Chapter is organized as follows: in Sec. 5.2 we describe the system, list the assumptions and define the Hamiltonian. Following this, in Sec. 5.3, we present the main result of this chapter, the dissipative preparation of the system in a non-Gaussian state. First, a general perturbation theory for degenerate Liouvillians is described in Sec. 5.3.1 that will be used throughout the chapter to explain the numerical result. Based on this, we describe how the interplay between the jump operators and the noise terms of the mechanical oscillator and the qubit prepares the system in a steady state in Sec. 5.3.2. To increase the fidelity for the preparation of the non-Gaussian state, additional noise operators are included in Sec. 5.3.3. This is followed by an analysis of their perturbative effect in Sec. 5.3.4. For comparison, in Sec. 5.4 the coherent approach for state preparation is described. The analysis is rounded off by the extension of the protocol to many-partite systems in Sec. 5.5, where both dissipative (Sec. 5.5.1) and coherent protocols (Sec. 5.5.2) are described.

## 5.2 The setup

We consider a two-level system and a mechanical oscillator both coupled to a cavity. The system's Hamiltonian is given by

$$\begin{aligned} \hat{H}_{\text{mq}} = & \delta \hat{a}_1^\dagger \hat{a}_1 + \frac{\Delta}{2} \hat{\sigma}_z + \omega_t \hat{b}^\dagger \hat{b} + g(\hat{a}_1^\dagger \hat{b} + \hat{a}_1 \hat{b}^\dagger) - g_q(\hat{a}_1 \hat{\sigma}^+ + \hat{a}_1^\dagger \hat{\sigma}^-) + \Omega(\hat{\sigma}^+ + \hat{\sigma}^-) \\ & + \hat{H}_{\text{aux}}, \end{aligned} \quad (5.1)$$

with

$$\hat{H}_{\text{aux}} = \delta^{\text{aux}} \hat{a}_2^\dagger \hat{a}_2 - g^{\text{aux}}(\hat{a}_2^\dagger \hat{b}^\dagger + \hat{a}_2 \hat{b}) + g_q^{\text{aux}}(\hat{a}_2^\dagger \hat{\sigma}^+ + \hat{a}_2 \hat{\sigma}^-). \quad (5.2)$$

$\hat{b}(\hat{b}^\dagger)$  describe the annihilation (creation) operators of the mechanical mode at frequency  $\omega_t$ . We assume that the cavity supports two modes with annihilation (creation) operators  $\hat{a}_i(\hat{a}_i^\dagger)$  ( $i = 1, 2$ ) detuned by  $\delta$  and  $\delta^{\text{aux}}$  respectively. Both modes are strongly driven,  $\hat{a}_1$  ( $\hat{a}_2$ ) with a red (blue)-detuned field, such that their single-photon coupling strength is enhanced by the square root of the number of steady-state photons to  $g$  ( $g^{\text{aux}}$ ) (see Sec. 4.2.2 for more details on the displacement of the driving field). The qubit is described by the lowering (raising) operators  $\hat{\sigma}^-$  ( $\hat{\sigma}^+$ ) detuned from the laser frequency by  $\Delta$ , strongly driven at  $\Omega$ , and coupled to the two cavity modes by  $g_q$  and  $g_q^{\text{aux}}$  respectively.

The dissipative processes are described by master equations of Lindblad form. The loss of cavity photons with a decay rate  $\kappa$  is given by

$$\mathcal{L}^L[\hat{\rho}] = 2\kappa \left[ \hat{a}_1 \hat{\rho} \hat{a}_1^\dagger - \frac{1}{2} \{ \hat{a}_1^\dagger \hat{a}_1, \hat{\rho} \}_+ \right]. \quad (5.3)$$

The decay of the auxiliary mode  $\hat{a}_2$  is defined in full analogy with decay rate  $\kappa_{\text{aux}}$ . The dissipation caused by the qubit is given by

$$\mathcal{L}^Q[\hat{\rho}] = \Gamma_q \left[ \hat{\sigma}^- \hat{\rho} \hat{\sigma}^+ - \frac{1}{2} \{ \hat{\sigma}^+ \hat{\sigma}^-, \hat{\rho} \}_+ \right], \quad (5.4)$$

where  $\Gamma_q$  is the spontaneous emission rate. For the mechanical oscillator the decoherence at a rate  $\Gamma_m$  is described by

$$\mathcal{L}^M[\hat{\rho}] = \Gamma_m \left[ (\hat{b} + \hat{b}^\dagger) \hat{\rho} (\hat{b}^\dagger + \hat{b}) - \frac{1}{2} \{ (\hat{b} + \hat{b}^\dagger)^2, \hat{\rho} \}_+ \right]. \quad (5.5)$$

We choose decoherence of the localization type [64, 88] *e.g.*, dominant in levitating dielectrics (see also Sec. 3.6 for more details). For a different decoherence mechanism, the analysis is in full analogy.

Throughout the chapter we consider the regime where the cavity merely mediates the interaction between the oscillator and the two-level system, and can be adiabatically eliminated. Therefore, the following conditions have to be fulfilled: first, the coupling between the cavity and both the oscillator and the qubit has to be small, fulfilling either  $g_{q(m)}/\kappa \ll 1$  (dissipative dynamics, see Sec. 5.3), or  $g_q/|\delta - \Delta| \ll 1, g/|\delta - \omega_t| \ll 1$  (coherent dynamics, see Sec. 5.4), or both conditions. Second, the interaction mediated by the cavity has to be stronger than the dissipative processes leading to the good-cooperativity requirement for both the qubit  $\mathcal{C}_q = g_q^2/(\kappa\Gamma_q) > 1$ , and the mechanical oscillator  $\mathcal{C}_m = g^2/(\kappa\Gamma_m) > 1$ . Note that the more demanding strong-coupling limit,  $g > \Gamma_m, \kappa$  and  $g_q > \Gamma_q, \kappa$  is not necessary (the same conditions apply to the cavity mode  $\hat{a}_2$ ).

Possible realizations of the Hamiltonian of Eq. (5.1) range from electromechanical setups [41, 50], where a microresonator couples a mechanical oscillator to a superconducting qubit, to cavity-optomechanical systems with a cavity mediating the interaction between a two-level atom and a mechanical membrane [119, 120, 193] or a levitating sphere [64, 77, 78]. Remarkably, in the specific case of levitating spheres, the regime where ground-state cooling is possible makes the same cavity suitable for coupling to single atoms [64]. This is due to the fact that in this case, the cooperativity of the mechanical oscillator reduces to the single-atom case  $\mathcal{C}_m = \mathcal{C}_q$  and only depends on cavity parameters <sup>1</sup>.

### 5.3 Dissipative dynamics

The goal of preparing non-Gaussian states of nano-mechanical oscillators is often hindered by the unavoidable occurrence of dissipation. In contrast, the proposed protocol exploits the interaction with the environment to prepare a mechanical oscillator in a non-Gaussian dark state with fidelity close to one. This goes along the line of ideas developed and analyzed recently for a variety of different systems [194, 200, 201, 203]. We assume the limit where dissipation dominates, namely  $g_{q(m)}/\kappa \ll 1$ , and choose  $g = g_q$ ,  $\Omega = 0$ ,  $\Delta = \delta = \omega_t$ , and  $\hat{H}_{\text{aux}} = 0$ . An adiabatic elimination of the cavity mode in the Hamiltonian, Eq. (5.1), yields an effective dissipative dynamics governed by the Liouvillian

$$\mathcal{L}_0[\hat{\rho}] = \Gamma_{\text{eff}} \left[ \hat{J}_0 \hat{\rho} \hat{J}_0^\dagger - \frac{1}{2} \{ \hat{J}_0^\dagger \hat{J}_0, \hat{\rho} \}_+ \right]. \quad (5.6)$$

Here, the jump operator is given by  $\hat{J}_0 = \hat{b} - \hat{\sigma}^-$  and the effective decay rate by  $\Gamma_{\text{eff}} = 2g^2/\kappa$ .  $\mathcal{L}_0[\hat{\rho}]$  possesses two degenerate steady states,

$$\hat{\rho}_A = \frac{1}{2} (|g, 1\rangle + |e, 0\rangle) (\langle g, 1| + \langle e, 0|), \quad (5.7)$$

and  $\hat{\rho}_B = |g, 0\rangle\langle g, 0|$ . Here,  $g$  ( $e$ ) describes the qubit's ground (excited) state in the basis of  $\hat{\sigma}_z$ , and 0 (1) the ground (excited) state of the phononic mode. While  $\hat{\rho}_A$  is a non-Gaussian entangled state for the phonon,  $\hat{\rho}_B$  describes the Gaussian ground state. This degeneracy can be lifted by additional dissipative terms and is very sensitive to any perturbation, as shown below. The goal is to lift the degeneracy such that the

<sup>1</sup>Light-induced dissipation processes dominate  $\Gamma_m$  reducing the cooperativity of the nanomechanical resonator to the one of the single-atom case entirely determined by the cavity,  $\mathcal{C}_m = \mathcal{C}_q = c^3/(2\omega_c^2 V_c \kappa)$ , where  $V_c$  is the cavity volume and  $c$  the speed of light. The minimal phonon number attainable when cooling a mechanical oscillator in the resolved sideband regime is given by  $n_{\text{min}} = (\kappa/(4\omega_t))^2 + 1/(4\mathcal{C}_m)$ , thus the two conditions are equivalent.

probability to prepare  $\hat{\rho}_A$  is maximized. To achieve this, we introduce a perturbation theory for degenerate Liouvillians in Sec. 5.3.1. Following this, we investigate the steady states including the noise operators  $\mathcal{L}^Q$  (Eq. (5.4)) and  $\mathcal{L}^M$  (Eq. (5.5)) in Sec. 5.3.2. In Sec. 5.3.3, an additional general linear jump operator is introduced and specified such that the probability to prepare the non-Gaussian state is maximized. In Sec. 5.3.4, the analysis is completed by a consideration of the perturbative regime that explains the results.

### 5.3.1 Perturbation theory for degenerate Liouvillians

In the following, we give a description of the perturbation theory for degenerate Liouvillians [194] used throughout the paper. In order to determine the steady state of a Liouvillian described by

$$\mathcal{L} = \mathcal{L}_0 + \epsilon \mathcal{L}_{\text{pert}}, \quad (5.8)$$

with  $\epsilon \ll 1$ , we can treat  $\mathcal{L}_{\text{pert}}$  as a perturbation to  $\mathcal{L}_0$ . The underlying concept is to provide an effective description of the dynamics of the fast subspace (given by  $\mathcal{L}_{\text{pert}}$ ) by applying a transformation that dresses the eigenstates of the slow subspace (given by  $\mathcal{L}_0$ ). An expansion of the effective Liouvillian in terms of the perturbation parameter  $\epsilon$  yields

$$\mathcal{L}_{\text{eff}} = \mathcal{L}_0 + \epsilon \mathbb{P} \mathcal{L}_{\text{pert}} \mathbb{P} - \epsilon^2 \mathbb{P} \mathcal{L}_{\text{pert}} \mathbb{Q} \mathcal{L}_0^{-1} \mathbb{Q} \mathcal{L}_{\text{pert}} \mathbb{P} + \dots, \quad (5.9)$$

where  $\mathbb{P}$  ( $\mathbb{Q} = \mathbb{1} - \mathbb{P}$ ) projects into the subspace that is kept (eliminated). In the following, we show how to determine  $\mathbb{P}$ . We define

$$\mathbb{P} = \hat{\rho}_A \otimes \chi_A + \hat{\rho}_B \otimes \chi_B. \quad (5.10)$$

Its action on an arbitrary density matrix  $\hat{\mu}$  is given by

$$\mathbb{P} \hat{\mu} = \hat{\rho}_A \text{tr}(\chi_A \hat{\mu}) + \hat{\rho}_B \text{tr}(\chi_B \hat{\mu}). \quad (5.11)$$

Here,  $\hat{\rho}_i$  ( $\chi_i$ ) (with  $i = A, B$ ) denote right (left) eigenvectors of the Liouvillian  $\mathcal{L}_0$  ( $\mathcal{L}_0^\diamond$ ) with eigenvalue zero, where  $\mathcal{L}_0^\diamond$  denotes the Liouville operator acting on left states. That is,

$$\mathcal{L}_0[\hat{\rho}_{A(B)}] = 0, \quad (5.12)$$

and

$$\chi_{A(B)} \mathcal{L}_0^\diamond = 0. \quad (5.13)$$

Besides, for  $\mathbb{P}$  to be a projector,

$$\mathbb{P}(\mathbb{P} \hat{\rho}) = \mathbb{P}(\hat{\rho}) \quad (5.14)$$

and the completeness relation

$$\sum_{i,j=A,B} \hat{\rho}_i \otimes \chi_j = 1 \quad (5.15)$$

have to be fulfilled. This imposes biorthonormality,  $\text{tr}(\chi_A \hat{\rho}_B) = \text{tr}(\chi_B \hat{\rho}_A) = 0$  and  $\text{tr}(\chi_A \hat{\rho}_A) = \text{tr}(\chi_B \hat{\rho}_B) = 1$ . Since the definition of  $\mathbb{P}$  is not unique due to the degeneracy of the Liouvillian  $\mathcal{L}_0$ , we impose the additional condition on

$$\mathbb{P} \mathcal{L}_{\text{pert}} \mathbb{P} = \sum_{i,j=A,B} \text{tr}(\chi_i \mathcal{L}_{\text{pert}}[\hat{\rho}_j]) \hat{\rho}_i \otimes \chi_j \quad (5.16)$$

to be diagonal, *i.e.*,  $\text{tr}(\chi_i \mathcal{L}_{\text{pert}}[\hat{\rho}_j]) = 0$  for  $i \neq j$ . This is analogous to degenerate perturbation theory in the Hamiltonian case.

The steady state of the Liouvillian in perturbation theory to first order is thus given by the eigenstate of  $\mathcal{L}_0 + \epsilon \mathbb{P} \mathcal{L}_{\text{pert}} \mathbb{P}$  with eigenvalue zero. It can be shown that  $\mathcal{L}_0 + \epsilon \mathbb{P} \mathcal{L}_{\text{pert}} \mathbb{P}$  with Liouvillians of Lindblad form always possess a zero eigenvalue. To prove this, it is sufficient to demonstrate <sup>2</sup>

$$\text{tr}[(\mathcal{L}_0 + \epsilon \mathbb{P} \mathcal{L}_{\text{pert}} \mathbb{P})[\hat{\mu}]] = 0. \quad (5.17)$$

The Lindblad form of  $\mathcal{L}_0$  and the trace's invariance under cyclic permutations yields  $\text{tr}(\mathcal{L}_0[\hat{\mu}]) = 0$ . Furthermore,

$$\begin{aligned} \text{tr}(\mathbb{P} \mathcal{L}_{\text{pert}} \mathbb{P}[\hat{\mu}]) &= \sum_{i,j=A,B} \text{tr}(\chi_i \mathcal{L}_{\text{pert}}[\hat{\rho}_j]) \text{tr}(\chi_j \hat{\mu}) \\ &= \sum_{j=A,B} \text{tr}(\chi_j \hat{\mu}) \text{tr}\left(\mathcal{L}_{\text{pert}}[\hat{\rho}_j] \underbrace{\sum_{i=A,B} \chi_i}_{=1}\right) \\ &= 0, \end{aligned} \quad (5.18)$$

where the completeness of the left eigenvectors  $\sum_i \chi_i = 1$  and the Lindblad form of  $\mathcal{L}_{\text{pert}}$  have been used.

Higher orders of the perturbation theory can be determined analogously, but we will restrict the analysis to the lowest order in  $\epsilon$  throughout this chapter.

### 5.3.2 Steady state with noise

We analyze the effect of the additional noise caused by the spontaneous decay of the atom  $\mathcal{L}_q$  (Eq. (5.4)) and the decoherence of the mechanical oscillator  $\mathcal{L}_m$  (Eq. (5.5)).

---

<sup>2</sup>Given the spectrum of  $\mathcal{L}_{\text{eff}}$  with the real part of all eigenvalues smaller or equal to zero, and the preservation of the trace, its direct consequence is the existence of a steady state.

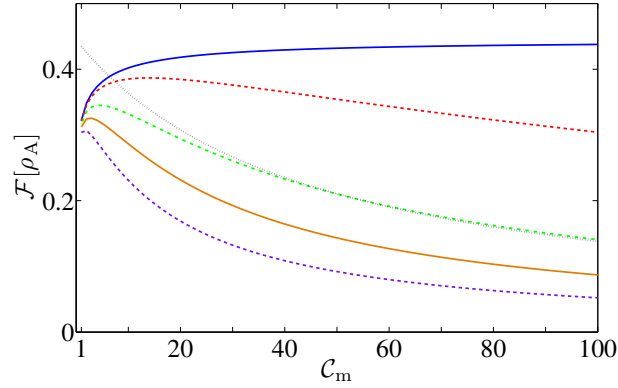


Figure 5.1: (Color online) Fidelity for the preparation of the non-Gaussian state  $\hat{\rho}_A$  as a function of  $\mathcal{C}_m$  for different qubit cooperativities  $\mathcal{C}_q$ . *Solid blue*:  $\mathcal{C}_q = \infty$ , *Dashed red*:  $\mathcal{C}_q = 100$ , *Dash-dotted green*:  $\mathcal{C}_q = 20$  (*Dotted black*: comparison to the analytic result for  $\mathcal{C}_q = 20$ ), *Solid orange*:  $\mathcal{C}_q = 10$ , *Dashed purple*:  $\mathcal{C}_q = 5$ .

These additional Liouvillians lift the original degeneracy of the steady state of  $\mathcal{L}_0$ . Perturbation theory to first order yields the unique dark state

$$\hat{\rho}_{\text{SS}} = \alpha_n \hat{\rho}_A + \beta_n \hat{\rho}_B \quad (5.19)$$

for  $\mathcal{L}_0 + \mathbb{P}(\mathcal{L}_m + \mathcal{L}_q)\mathbb{P}$ . The coefficients depend on the noise parameters and are given by

$$\alpha_n = \frac{4\Gamma_m}{4\Gamma_q + 9\Gamma_m} \quad (5.20)$$

and

$$\beta_n = \frac{4\Gamma_q + 5\Gamma_m}{4\Gamma_q + 9\Gamma_m}. \quad (5.21)$$

To complement the analytical study, we carry out a numerical evaluation of the steady state, which is shown to be in good agreement with the perturbation theory for  $\mathcal{C}_q, \mathcal{C}_m \gg 1$ , as illustrated in Fig. 5.1. As expected from the analytical result, the fidelity to prepare the entangled non-Gaussian state  $\hat{\rho}_A$  is maximized for  $\Gamma_q = 0$  and can reach

$$\mathcal{F}[\hat{\rho}_A] = \text{tr}[\hat{\rho}_{\text{SS}}\hat{\rho}_A] = \alpha_n = 4/9. \quad (5.22)$$

The optimal value of  $\mathcal{C}_m$  to maximize  $\mathcal{F}[\hat{\rho}_A]$  for a given  $\mathcal{C}_q$  can be read from Fig. 5.1. Thus, the system's inherent noise leads to the preparation of a mechanical oscillator in a non-Gaussian state with a fidelity  $\mathcal{F}[\hat{\rho}_A] \leq 4/9$ .

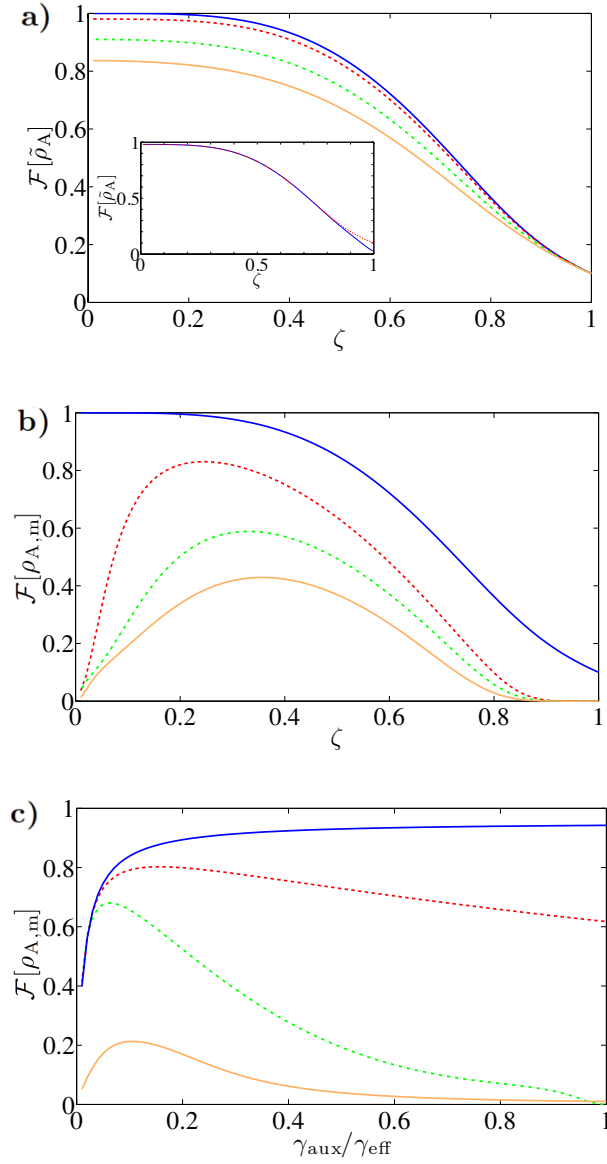


Figure 5.2: (Color online) Fidelity to prepare a)  $\tilde{\rho}_A$  and b)  $\hat{\rho}_{A,m}$  as functions of  $\zeta$  for  $\Gamma_{\text{aux}}/\Gamma_{\text{eff}} = 1$  and different cooperativities. The size of the Hilbert space for the mechanical oscillator is chosen as  $N = 10$ . *Solid blue*:  $C_q = C_m = \infty$ , *Dashed red*:  $C_q = C_m = 100$ , *Dash-dotted green*:  $C_q = C_m = 20$ , *Solid orange*:  $C_q = C_m = 10$ . *Inset*: Comparison of the simulation for  $C_m = C_q = 100$  and different sizes of the Hilbert space. *Solid blue*:  $N = 30$ , *Dashed red*:  $N = 10$ . c) Fidelity to prepare  $\hat{\rho}_{A,m}$  as a function of  $\Gamma_{\text{aux}}/\Gamma_{\text{eff}}$  for  $\zeta = 0.2$ ,  $C_m = C_q = 1000$  and different jump operators  $\hat{J}_1$ . *Solid blue*:  $\hat{J}_1 = \hat{\sigma}^+ - \zeta \hat{b}^\dagger$ , *Dashed red*:  $\hat{J}_1 = \hat{\sigma}^+$ , *Dash-dotted green*:  $\hat{J}_1 = \hat{\sigma}^+ + \zeta \hat{b}^\dagger$ , *Solid orange*:  $\hat{J}_1 = \hat{b}^\dagger$ .

### 5.3.3 Steady state with an engineered environment

In the following we propose a protocol to enhance the fidelity for the preparation of non-Gaussian states. For this purpose, we consider the modified jump operator  $\tilde{J}_0 = \hat{b} - \zeta \hat{\sigma}^-$  for  $\mathcal{L}_0$  (given by Eq. (5.6)) with  $\zeta = (g_q/g)^2$  (we choose  $\zeta \leq 1$ ). It can be realized with the Hamiltonian Eq. (5.1) for  $g \neq g_q$ . The steady state of  $\mathcal{L}_0$  is thus degenerate and composed of  $\hat{\rho}_B$  as defined previously and

$$\tilde{\rho}_A = \frac{1}{1 + \zeta^2} (\zeta |g, 1\rangle + |e, 0\rangle) (\zeta \langle g, 1| + \langle e, 0|). \quad (5.23)$$

In order to lift the degeneracy in a way that leads to an increased population in  $\tilde{\rho}_A$ , we introduce an additional Liouvillian

$$\mathcal{L}_{\text{aux}} = \Gamma_{\text{aux}} \left[ \hat{J}_1 \hat{\rho} \hat{J}_1^\dagger - \frac{1}{2} \{ \hat{J}_1^\dagger \hat{J}_1, \hat{\rho} \}_+ \right], \quad (5.24)$$

with jump operator  $\hat{J}_1 = \hat{\sigma}^+ - \zeta \hat{b}^\dagger$ . This jump operator can be realized by including  $H_{\text{aux}} \neq 0$  in the Hamiltonian of Eq. (5.1) with a blue detuning  $\delta^{\text{aux}} = \omega_t = -\Delta$ . This yields  $\Gamma_{\text{aux}} = 2 (g_q^{\text{aux}})^2 / \kappa_{\text{aux}}$  and  $\zeta = (g^{\text{aux}}/g_q^{\text{aux}})^2 = (g_q/g)^2$ . Together with the noise terms  $\mathcal{L}_m$  and  $\mathcal{L}_q$ , the steady state is given by

$$\tilde{\rho}_{\text{SS}} = \alpha_{\text{aux}} \tilde{\rho}_A + \beta_{\text{aux}} \hat{\rho}_B. \quad (5.25)$$

In the presence of the inherent noise, the fidelity to prepare the system in the entangled non-Gaussian state  $\tilde{\rho}_A$  is strongly enhanced by  $\mathcal{L}_{\text{aux}}$  as shown in Fig. 5.2 a) <sup>3</sup>. For example, for  $C_m = C_q = 100$  and  $\zeta = 0.2$ , the fidelity for the preparation of  $\tilde{\rho}_A$  is close to one,  $\mathcal{F}[\tilde{\rho}_A] = 0.98$ . Even for much smaller cooperativities, *e.g.*, for  $C_m = C_q = 10$ , the fidelity is  $\mathcal{F}[\tilde{\rho}_A] = 0.82$ .

Despite the increment of the fidelity for the preparation of  $\tilde{\rho}_A$ , the amount of entanglement of the steady state depends on  $\zeta$ . For small  $\zeta$ , the state is close to the ground state of the harmonic oscillator and shows only little entanglement. To prevent this, we propose to measure the qubit in the basis

$$|+\rangle_q = \frac{(\zeta |e\rangle + |g\rangle)}{\sqrt{1 + \zeta^2}}, \quad (5.26)$$

<sup>3</sup>Some care has to be taken in the numerical study as the system only exhibits a steady state for  $\zeta < 1$ : in the regime where the bosonic operator  $\hat{b}^\dagger$  dominates, no steady state is reached. Consequently, the Hilbert space for the phononic mode needs to be sufficiently large, as a finite Hilbert space generally might yield a steady state although it does not exist. This is illustrated in the inset of Fig. 5.2 a), where the steady state obtained for a Hilbert space of size  $N = 10$  is compared to  $N = 30$ . It demonstrates that in the regime of interest, namely where the fidelity to prepare  $\tilde{\rho}_A$  is high, they are in good agreement and the numerical study is valid.

$$|-\rangle_{\text{q}} = \frac{(|e\rangle - \zeta|g\rangle)}{\sqrt{1 + \zeta^2}}, \quad (5.27)$$

and postselect to keep only the  $|+\rangle_{\text{q}}$ -result. This prepares the mechanical oscillator in

$$\hat{\rho}_{\text{SS},\text{m}} = \alpha_{\text{m}}\hat{\rho}_{\text{A},\text{m}} + \beta_{\text{m}}\hat{\rho}_{\text{B},\text{m}}, \quad (5.28)$$

with

$$\hat{\rho}_{\text{A},\text{m}} = \frac{(|0\rangle + |1\rangle)(\langle 0| + \langle 1|)}{2} \quad (5.29)$$

and

$$\hat{\rho}_{\text{B},\text{m}} = |0\rangle\langle 0|. \quad (5.30)$$

In Fig. 5.2 b), we show that the maximal fidelity is  $\mathcal{F}[\hat{\rho}_{\text{A},\text{m}}] = \alpha_{\text{m}} = 0.83$  for  $\zeta = 0.25$  and cooperativities  $\mathcal{C}_{\text{m}} = \mathcal{C}_{\text{q}} = 100$ . In comparison, when only the system's inherent noise is included, the maximal fidelity is  $\mathcal{F}[\hat{\rho}_{\text{A}}] = 4/9$  for  $\mathcal{C}_{\text{m}} = \mathcal{C}_{\text{q}} = \infty$ . In full analogy, Fock states can be prepared via a suitable choice of the measurement basis. For instance, by measuring in the  $|g\rangle$  and  $|e\rangle$ -basis and postselecting to keep the  $|g\rangle$ -result, we can prepare the  $|1\rangle$ -state for the mechanical oscillator. For  $\zeta = 0.25$  and cooperativities  $\mathcal{C}_{\text{q}} = \mathcal{C}_{\text{m}} = 100$ , a fidelity of  $\mathcal{F} \approx 0.83$  is achievable.

Furthermore, we investigate the dependence of  $\mathcal{F}[\hat{\rho}_{\text{A},\text{m}}]$  on  $\Gamma_{\text{aux}}/\Gamma_{\text{eff}}$  as shown in Fig. 5.2c). We also analyze different jump operators  $\hat{J}_1$  and demonstrate that the optimal configuration to maximize  $\mathcal{F}[\hat{\rho}_{\text{A},\text{m}}]$  is achieved for  $\hat{J}_1 = \hat{\sigma}^+ - \zeta\hat{b}^\dagger$  and  $\Gamma_{\text{aux}}/\Gamma_{\text{eff}} \approx 1$ . Note that throughout this subsection we rely on numerical simulations since the perturbation theory of Sec. 5.3.1 is only valid in the regime  $\Gamma_{\text{aux}}/\Gamma_{\text{eff}} \ll 1$ .

### 5.3.4 Insights from perturbation theory

In this section we show how the previous results can be understood within perturbation theory. As the optimal case  $\Gamma_{\text{eff}} = \Gamma_{\text{aux}}$  cannot be described within perturbation theory, we focus on the perturbative limit  $\Gamma_{\text{aux}} \ll \Gamma_{\text{eff}}$ . We consider the general jump operator

$$\hat{J}_1 = \hat{\sigma}^+ + \eta\hat{\sigma}^- + \nu\hat{b} - \zeta\hat{b}^\dagger \quad (5.31)$$

that prepares the qubit and the oscillator in the steady state given by Eq. (5.25). Perturbation theory shows that the maximal value for both  $\mathcal{F}[\tilde{\rho}_{\text{A}}]$  and  $\mathcal{F}[\rho_{\text{A},\text{m}}]$  is obtained for  $\nu = \eta = 0$ . We thus choose  $\hat{J}_1 = \hat{\sigma}^+ - \zeta\hat{b}^\dagger$  to compare with the numerical study<sup>4</sup>. Within perturbation theory to first order, the steady state of

<sup>4</sup>Note that in principle the perturbation theory also applies for  $\zeta \leq 0$ . However, care has to be taken as the range of validity of the analytical result depends on  $\zeta$ . This is because it is carried out assuming a finite-sized Hilbert space with maximal occupation number two for the harmonic oscillator. For  $\zeta \leq 0$ , high-occupation number states of the harmonic oscillator are excited more frequently than for  $\zeta \geq 0$ .

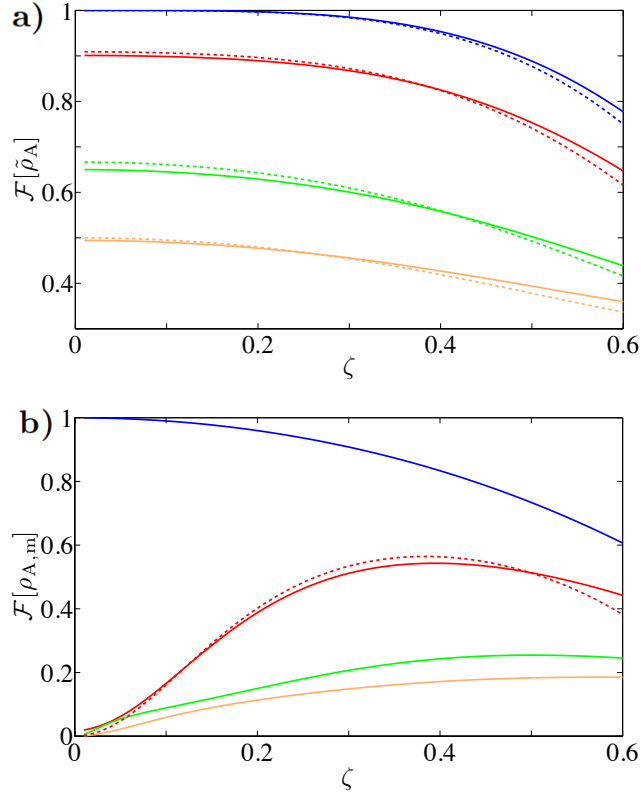


Figure 5.3: (Color online) Fidelity for the preparation of a)  $\tilde{\rho}_A$  and b)  $\hat{\rho}_{A,m}$  as a function of  $\zeta$  in the perturbative regime  $\Gamma_{\text{aux}}/\Gamma_{\text{eff}} = 0.1$ . The different colors show various cooperativities and compare the numerical result (solid line) to the perturbative one (dashed line). *Blue*:  $C_q = C_m = \infty$ , *Red*:  $C_q = C_m = 100$ , *Green*:  $C_q = C_m = 20$ , *Orange*:  $C_q = C_m = 10$ .

$\mathcal{L}_0 + \mathbb{P} (\mathcal{L}_{\text{aux}} + \mathcal{L}^Q + \mathcal{L}^M) \mathbb{P}$  is given by Eq. (5.25) with

$$\begin{aligned} \alpha_{\text{aux}} &= \frac{A (\Gamma_m \zeta^2 + \Gamma_{\text{aux}} (1 - \zeta^2)^2)}{\Gamma_q A + \Gamma_m B + \Gamma_{\text{aux}} C}, \\ \beta_{\text{aux}} &= \frac{A (\Gamma_q + \Gamma_m \zeta^2) + 2\Gamma_{\text{aux}} \zeta^4 (3 - \zeta^2 (2 - \zeta^2))}{\Gamma_q A + \Gamma_m B + \Gamma_{\text{aux}} C}, \end{aligned} \quad (5.32)$$

where  $A = (3 + 4\zeta^2 + \zeta^4)$ ,  $B = 2\zeta^2 (3 + 4\zeta^2 + 2\zeta^4)$ , and  $C = 3 - 2\zeta^2 + 2\zeta^4 - 2\zeta^6 + 3\zeta^8$ . This perturbative result is compared to a numerical simulation in Fig. 5.3 for  $\Gamma_{\text{aux}} \ll \Gamma_{\text{eff}}$ . It is in good agreement with the numerical results, with an increasing deviation for lowered cooperativities.

Also the results for the preparation of  $\hat{\rho}_{\text{SS},m}$  after carrying out the measurement as given by Eq. (5.28) can be understood within perturbation theory.  $\alpha_m$  and  $\beta_m$  are

given by

$$\begin{aligned}\alpha_m &= \frac{2\zeta^2\Gamma_{\text{aux}}(3 - 5\zeta^2 + \zeta^4 + \zeta^6) + 2\zeta^4\Gamma_m(3 + \zeta^2)}{A\Gamma_q + D\Gamma_m + E\Gamma_{\text{aux}}}, \\ \beta_m &= \frac{A\Gamma_q + \Gamma_m\zeta^2(3 + 4\zeta^2 + 3\zeta^4) + 2\Gamma_{\text{aux}}\zeta^4(3 - 2\zeta^2 + \zeta^4)}{A\Gamma_q + D\Gamma_m + E\Gamma_{\text{aux}}},\end{aligned}\quad (5.33)$$

with  $D = \zeta^2(3 + 10\zeta^2 + 5\zeta^4)$  and  $E = \zeta^2(6 - 4\zeta^2 - 2\zeta^4 + 4\zeta^6)$ . A numerical evaluation for different  $\zeta$  as demonstrated in Fig. 5.3 b) shows that the perturbation theory is in accordance with the numerical prediction.

## 5.4 Coherent dynamics

Let us now consider the coherent dynamics corresponding to the regime given by

$$\frac{g_q}{|\delta - \Delta|} \ll 1, \quad \frac{g}{|\delta - \omega_t|} \ll 1. \quad (5.34)$$

Eliminating the cavity mode from Eq. (5.1) (with  $H_{\text{aux}} = 0$ ) gives

$$\hat{H}^{\text{eff}} = \frac{\tilde{\Delta}}{2}\hat{\sigma}_z + \tilde{\omega}_t\hat{b}^\dagger\hat{b} - g(\hat{\sigma}^+\hat{b} + \hat{\sigma}^-\hat{b}^\dagger) + \Omega(\hat{\sigma}^+ + \hat{\sigma}^-), \quad (5.35)$$

where

$$\tilde{\Delta} = \Delta - \frac{2g_q^2}{\delta - \Delta} \quad (5.36)$$

and

$$\tilde{\omega}_t = \omega_t - \frac{2g^2}{\delta - \omega_t} \quad (5.37)$$

are the renormalized frequencies. The cavity-mediated coupling between the qubit and the mechanical oscillator is given by

$$g = \frac{g_q g (2\delta - \omega_t - \Delta)}{(\delta - \Delta)(\delta - \omega_t)}. \quad (5.38)$$

In the good-cooperativity limit, several interesting phenomena can be observed.

First, the Hamiltonian of Eq. (5.35), which is the well-known Jaynes-Cummings Hamiltonian, enables the preparation of arbitrary Fock states following the proposal of Law and Eberly [204]. It relies on switching interaction strengths time-dependently by varying the laser intensities driving the different couplings. This requires  $M$  steps for the preparation of arbitrary superposition states with maximal occupation number  $M$ . Therefore, all dissipation processes have to be slower than the coherent manipulation time, which is fulfilled for

$$\frac{g_q g}{\kappa\Gamma_{q(m)}}, \mathcal{C}_{q(m)} \gg M. \quad (5.39)$$

Second, Eq. (5.35) predicts the occurrence of blockade phenomena, a typical indicator of nonlinear behavior. Due to the presence of the qubit, the photon blockade [205] is observable for  $g_q \gg \kappa, \Gamma_q$ . Additionally, also the phonon blockade can be observed [107, 108]: eliminating the atom to fourth order from Eq. (5.35) (justified for  $g/|\Delta - \omega_t| \ll 1$  and  $|\Delta - \omega_t| > \Gamma_q$ ) yields an effective nonlinear Hamiltonian

$$\hat{H}_{\text{phon}} = \tilde{\omega}_t \hat{b}^\dagger \hat{b} + \frac{g^4}{\Delta - \omega_t^3} (\hat{b}^\dagger \hat{b})^2. \quad (5.40)$$

In addition, the good cooperativity

$$\frac{g_q g}{\kappa \Gamma_{q(m)}}, \mathcal{C}_{q(m)} \gg 1 \quad (5.41)$$

ensures that the splittings effected by the nonlinear interaction are not smeared out by noise processes.

## 5.5 Many-partite system

An intriguing perspective in the field of optomechanics is to couple several nonlinear nanomechanical oscillators to realize a many-partite system. This is required for quantum simulation [105, 206] and might be particularly useful for the preparation of many-partite states for quantum metrology. To achieve this goal, we propose to use a cavity to mediate the interaction between several mechanical oscillators and a single qubit. In order to realize  $N$  nonlinear modes, we suggest to drive the mechanical frequencies stroboscopically. Any physical system with a tunable mechanical frequency, *e.g.*, levitating dielectric spheres, can realize this protocol. In the following, the operators for each mechanical mode are termed  $\hat{b}_i$  ( $i = 1, \dots, N$ ) with corresponding time-dependent frequencies  $\omega_i(t)$  that are switched between a value on resonance  $\omega_{\text{on}}$  and off resonance  $\omega_{\text{off}}$ . The case where the modulation of the couplings is achieved via a sinusoidal drive can be treated in full analogy.

The proposal requires the following conditions:

1. Due to the time-dependence of  $\omega_i(t)$ , also the operators  $\hat{b}_i(\hat{b}_i^\dagger)$  are time-dependent. Requiring  $\hat{b}_i(\hat{b}_i^\dagger)$  to be identical at the time of switching requires it to take place with a periodicity  $\tau = 2\pi n/\omega_{\text{off}}$ .
2. The adiabatic elimination requires  $g/|\delta - \omega_i(t)|, g_q/|\delta - \Delta| \ll 1$  (coherent dynamics) or  $g_{q(m)}/\kappa \ll 1$  (dissipative dynamics).
3. The stroboscopic switching has to be faster than the interaction between the different components of the system, therefore  $g\tau, g_q\tau \ll 1$ .

4. The frequency change has to be the fastest time scale in the system,  $(\omega_{\text{on}} - \omega_{\text{off}})\tau \gg 1$ .
5. The good cooperativity limit  $\mathcal{C}_q, \mathcal{C}_m \gg 1$  is necessary.

In order to verify these conditions, we numerically simulate the stroboscopic driving of two oscillators as illustrated in Fig. 5.4. Initially, the qubit is in an excited state and it is shown that this excitation is coherently shifted to the mechanical oscillators and back to the qubit resulting in Rabi oscillations. We show in the upper panel that the stroboscopic driving is effective if conditions (i)-(v) are fulfilled. The robustness of the setup towards noise is illustrated in the lower panel, where the decay of the oscillations of the stroboscopically-driven system is analyzed for different cooperativities. It shows that the good-cooperativity limit is necessary, as otherwise oscillations decay rapidly. We plot the population of the first oscillator, as all other oscillators coupled to the qubit behave in full analogy. As shown below, the stroboscopic driving enables the individual addressability of each oscillator as opposed to the continuous driving, where only the center-of-mass-mode is coupled.

### 5.5.1 State preparation of the many-partite system

Let us now translate the ideas for state preparation from the single-oscillator to the many-partite case. To start the state-preparation in a well-defined state, each oscillator is cooled to its ground state via stroboscopic driving without coupling to the qubit. It can be shown that the effective coupling strength is  $\propto g/N$ , and the light-scattering-induced dissipation scales  $\propto \Gamma_m/N^2$ , rendering the cooperativity independent of the number of oscillators. Hence, the same conditions as in the single-particle case apply for ground-state cooling<sup>5</sup>. This can be used to prepare all the oscillators in their respective ground state,

$$|\psi\rangle_{\text{ini}} = \otimes_{i=1}^N |0\rangle_i. \quad (5.42)$$

One can now employ dissipative protocols to prepare interesting many-partite non-Gaussian entangled states, *e.g.*, the W-state

$$|\psi\rangle_{\text{W}} = \frac{1}{\sqrt{N}}(|10\dots 0\rangle + \dots + |0\dots 01\rangle). \quad (5.43)$$

This can be achieved as follows. Starting from the ground state given by Eq. (5.42), all oscillators are tuned on resonance. In this case, the interaction between the qubit

---

<sup>5</sup>Note that in systems where other sources of decoherence *e.g.*, heating through a direct thermal contact are dominant, the cooperativity might depend on the number of oscillators. This has to be taken into account accordingly.

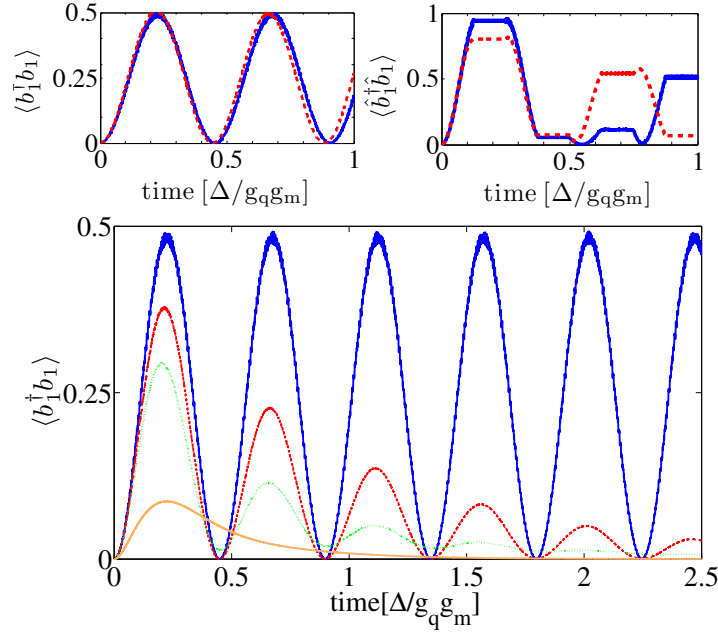


Figure 5.4: (Color online) Dynamics of two stroboscopically-driven mechanical oscillators coupled to an initially excited qubit. *Top*: Comparison between the population of the mechanical mode under the full evolution (solid blue line) and the adiabatically eliminated one (dashed red line), all parameters are given in units of  $g_q g / \delta$  and no dissipation is included. *Left*: Conditions (i)-(v) are fulfilled, *Right*: Condition (i) is not fulfilled. *Bottom*: Evolution under the influence of dissipation over time  $[\delta/gg_q]$  for different cooperativities: *Solid Blue*:  $C_m = C_q = \infty$ , *Dashed red*:  $C_m = C_q = 1000$ , *Dotted green*:  $C_m = C_q = 100$ , *Solid orange*:  $C_m = C_q = 10$ .

and the oscillators can be described in analogy to eqs. (5.6) and (5.24) by the effective Liouvillians  $\mathcal{L}_0^{\text{cm}}[\hat{\rho}] + \mathcal{L}_1^{\text{cm}}[\hat{\rho}]$  with jump operators

$$\hat{J}_0^{\text{cm}} = \hat{b}_{\text{cm}} - \zeta \hat{\sigma}^- \quad (5.44)$$

and

$$\hat{J}_1^{\text{cm}} = \hat{\sigma}^+ - \zeta \hat{b}_{\text{cm}}^\dagger. \quad (5.45)$$

Here

$$\hat{b}_{\text{cm}} = \sum_{i=1}^N \hat{b}_i / \sqrt{N} \quad (5.46)$$

denotes the center-of-mass operator. In full analogy to the single-oscillator case, the system can be dissipatively prepared in a Fock state of the center-of-mass-motion of the mechanical oscillators by performing a measurement of the qubit's state followed by

postselection. This leads to the W-state given by Eq. (5.43), namely  $|\psi\rangle_W = \hat{b}_{\text{cm}}^\dagger |\psi\rangle_{\text{ini}}$ . The fidelity to prepare the system in this dark state is thus given by the fidelity of the protocol for single oscillators and can reach *e.g.*,

$$\mathcal{F}[|\psi\rangle_W \langle\psi|] \approx 0.83 \quad (5.47)$$

for  $\Gamma_{\text{aux}} = \Gamma_{\text{eff}}$  and  $\mathcal{C}_q = \mathcal{C}_m = 100$ .

### 5.5.2 Coherent state preparation of $N$ mechanical oscillators

In the following we develop a method for coherent state preparation of a system consisting of  $N$  mechanical oscillators and a single qubit. Our approach is based on a protocol proposed by Law and Eberly, see [204], that has already been mentioned in Sec. 5.4. Here, we provide its extension to  $N$ -body systems. The goal is to determine the full time evolution  $U(t_{\text{fin}})$  that prepares a system, initially in its ground state  $|\psi\rangle_{\text{ini}}$  (Eq. (5.42)), in a target state  $|\psi\rangle_{\text{target}}$ . The key tool of [204] is to realize that this evolution operator may be obtained by solving the equations of motion of the inverse evolution  $U(-t_{\text{fin}})$  given by

$$|g\rangle \otimes |\psi\rangle_{\text{ini}} = U(-t_{\text{fin}})|g\rangle \otimes |\psi(t_{\text{fin}})\rangle_{\text{target}}. \quad (5.48)$$

That is, it transfers the system from the target state  $|\psi(t_{\text{fin}})\rangle_{\text{target}}$  to its ground state.

In the many-partite case the goal is to evolve the initial state, Eq. (5.42), to the general Fock state

$$|\psi(t_{\text{fin}})\rangle_{\text{target}} = \sum_{n_1=0, \dots, n_N=0}^M c_{n_1 \dots n_N} |n_1, \dots, n_N\rangle, \quad (5.49)$$

with maximal occupation number  $M$  for each of the  $N$  oscillators at time  $t_{\text{fin}}$ . In order to extend the Law-Eberly approach, it is essential to address each of the states separately. This requires a Hamiltonian that is only on resonance with one specific state at a time.

As it has been demonstrated previously, the time-dependent switching of the frequencies of the mechanical oscillators enables single-oscillator addressability. The Hamiltonian of the system is given by the many-partite extension of Eq. (5.35) with  $\hat{H}_{\text{aux}} = 0$ . Being off-resonant, the other oscillators may be adiabatically eliminated during the manipulation of the  $j$ th oscillator, which gives

$$\hat{H}_j^{\text{eff}} = \frac{\Delta}{2} \hat{\sigma}_z + \sum_{i \neq j}^N l_i n_i \hat{\sigma}_z + \omega_j \hat{b}_j^\dagger \hat{b}_j - g_j(t) (\hat{\sigma}^+ \hat{b}_j + \hat{\sigma}^- \hat{b}_j) + \Omega_j(t) (\hat{\sigma}^+ + \hat{\sigma}^-), \quad (5.50)$$

with  $l_i = -2g_i^2/(\Delta - \omega_i)$ . The second term in Eq. (5.50) describes the renormalization of the atomic frequency determined by the occupation number  $n_i$  of all off-resonant

oscillators. It has to be taken into account when turning the  $j$ th oscillator on resonance with the atom. This additional renormalization shift enables a unique addressing of each state of the many-partite system provided that  $\sum_{i \neq j} l_i (n_i - n'_i) = 0$  iff  $n_i = n'_i, \forall i$ .

Hence, the operation that prepares the  $j$ th oscillator in the desired state is given by

$$\hat{U}_j = \hat{U}_j^{(n_1=M, \dots, n_N=M)} \dots \hat{U}_j^{(n_1=1, \dots, n_N=1)}, \quad (5.51)$$

where the dots in the multiplication account for all possible permutations of occupation numbers of the off-resonant oscillators. Each  $\hat{U}_j^{(n_1, \dots, n_N)}$  performs the Law-Eberly protocol on the  $j$ th oscillator under the condition that the other oscillators are in state  $|n_1, \dots, n_N\rangle$ . The mechanism is subsequently applied to all oscillators yielding the full time evolution  $\hat{U}(t_{\text{fin}}) = \hat{U}_N \dots \hat{U}_1$ . In general, the maximal number of necessary steps for the preparation of an arbitrary state Eq. (5.49) is given by

$$\#(\text{steps}) = \sum_{i=0}^{N-1} (M+1)M. \quad (5.52)$$

It increases from  $M$  steps for the preparation of the  $M$ th Fock state in the single-oscillator case to at most  $M^N$  steps in the many-partite case.

As an illustration, let us consider the necessary steps for the preparation of

$$|\psi\rangle_{\text{spec}} = \frac{1}{\sqrt{3}} (|0, 5, 0\rangle + |1, 5, 10\rangle + |1, 1, 1\rangle). \quad (5.53)$$

We consider the inverse evolution  $\hat{U}(-t_{\text{fin}}) = \hat{U}_3^\dagger \hat{U}_2^\dagger \hat{U}_1^\dagger$  preparing Eq. (5.53) in the ground state. Applying

$$\hat{U}_1^\dagger = \hat{U}_1^{\dagger, (n_2=1, n_3=1)} \hat{U}_1^{\dagger, (n_2=5, n_3=10)}, \quad (5.54)$$

as defined in Eq. (5.51), requires 2 steps and prepares the first oscillator in the ground state. The subsequent preparation of the second oscillator is performed by

$$\hat{U}_2^\dagger = \hat{U}_1^{\dagger, (n_1=0, n_3=0)} \hat{U}_1^{\dagger, (n_1=0, n_3=1)} \hat{U}_1^{\dagger, (n_1=0, n_3=10)} \quad (5.55)$$

and requires 11 steps. Finally, we apply  $\hat{U}_3^\dagger = \hat{U}_3^{\dagger, (n_1=0, n_2=0)}$  to the third oscillator, which requires 10 steps. In total, the preparation of Eq. (5.53) can be achieved in 23 steps and the specific operators may be determined in full analogy to the single-particle case [204].



## Chapter 6

# Large spatial quantum superpositions

*We propose a method to prepare and verify spatial quantum superpositions of a nanometer-sized object separated by distances of the order of its size. The protocol consists in coherently expanding the wave function of a ground-state-cooled mechanical resonator, performing a squared position measurement that acts as a double slit, and observing interference after further evolution. Various sources of decoherence are taken into account and the achievable superposition sizes are analyzed for presently available experimental parameters. This method provides unprecedented bounds for objective collapse models of the wave function by merging techniques and insights from cavity quantum optomechanics and matter-wave interferometry. This chapter mainly bases on and uses parts of [61].*

### 6.1 Introduction

Various protocols for the generation of non-Gaussian states have already been analyzed in Chapters 4, 5. We have in particular discussed the creation of nonclassical states via coupling to single photons in Chapter 4, and even considered how dissipation can assist the state preparation in Chapter 5. However, the size of the superpositions prepared in this way is typically only on the order of the ground state  $\Delta\hat{r}$ , which is still subatomic for objects containing billions of atoms. Realizing larger spatial superpositions of nanomechanical objects holds the promise of testing quantum mechanics in a new regime. In principle, superpositions of massive objects at two distinctly separated spatial locations are allowed by quantum mechanics. However, the preparation of superposition states remains challenging for experiments. The reason for this is standard decoherence, describing the quantum-to-classical transition, see [65, 161] for an

introduction. Nevertheless, there exist several conjectures predicting the breakdown of quantum mechanics even in the absence of standard decoherence induced by the environment [121, 207–215]. Testing the prediction of these theories is very challenging due to the above-mentioned standard decoherence [65, 161], which predicts very short lifetimes for large superposition states of massive objects thus easily masking the effects of collapse models. This poses a major challenge to tests of these models, as the predicted effects must be distinguished from standard decoherence. The second major motivation for the preparation of large superposition states lies precisely in their sensitivity towards environmental decoherence. This fragility of the quantum-mechanical superpositions could be used to design sensors of unprecedented sensitivity [59, 93, 94].

In this chapter, we propose a state-preparation protocol that combines the optomechanical approach with the one of matter-wave interferometry. The proposal relies, on the one hand, on techniques from cavity electro/optomechanics to prepare a mechanical resonator in the ground state of its harmonic potential. On the other hand, the protocol mimics matter-wave interferometry by applying an optomechanical double slit that collapses the mechanical oscillator’s state into a superposition of different spatial locations. In order to produce nonlinearities in the system, a method to enlarge the object’s wave function by free evolution is proposed. The size of the prepared superposition may be on the same order as the object’s extension thus providing access to an entirely new parameter regime of quantum mechanics.

### 6.1.1 Reader’s guide

The chapter is organized as follows: in Sec. 6.2, we give a detailed description of the different steps of the state-preparation protocol. In Sec. 6.2.1, we recall the form of the initially-prepared ground state of the nano-mechanical oscillator. This is followed by a description of the wave-function expansion in Sec. 6.2.2, the optomechanical double slit, Sec. 6.2.3, and the formation of the interference pattern, Sec. 6.2.4, after further evolution of the wave function. We proceed to define measures to classify the relevant decoherence in Sec. 6.3, where we define the coherence length of the system in Sec. 6.3.1, describe the reduction of the visibility of the interference pattern in Sec. 6.3.2, reconsider the relevant processes of decoherence in Sec. 6.3.3, and finally give the experimental parameters for the operational regime of the protocol in Sec. 6.3.4. Finally, we apply the protocol to establish new bounds for parameters of collapse models in Sec. 6.4, where we show that it puts new bounds on the CSL model in Sec. 6.4.1, whereas confronting the Penrose-Diósi models remains impossible with this particular setup in Sec. 6.4.2.

## 6.2 The protocol

In this section, we describe the protocol for the creation of large superposition states. It combines techniques from optomechanical resonators with matter-wave interferometry and is described in detail in [62]. As analyzed in the previous Chapters 4, 5, the main difficulty in realizing nonlinearities in optomechanics is the weak single-photon coupling strength [53, 107, 108]. To enhance the optomechanical coupling, the cavity is typically strongly driven rendering all couplings linear (see Sec. 4.2.2 for more details). Different strategies to overcome the linear character of the equations of motion are described in Chapters 4, 5. The linearity results from the position of the dielectric (the same holds for membranes) at the maximal slope of the standing wave in the cavity. Alternatively positioning the nanomechanical object in a minimum of the light field effects a quadratic coupling. It is proportional to the size of the wave packet and thus is typically suppressed by the square of the ground-state size,  $\propto x_0^2$ . In order to enhance the coupling, the proposed protocol exploits the flexibility of the trap by letting the dielectric fall for some time hence coherently expanding its wave function. The transformation of the size of the wave packet from  $x_0$  to  $\sigma$  enhances the quadratic coupling. This gives rise to a nonlinearity that will be used in the state preparation protocol as described below.

### 6.2.1 Step (a): Preparation of the initial state

In a first step, the dielectric sphere is trapped in an optomechanical cavity and cooled to its ground state, as outlined in Chapters 2, 3. As demonstrated in Sec. 3.6, ground-state cooling of levitating dielectric spheres is possible for objects of  $R \lesssim 260$  nm and can be realized with already available experimental resources. If the preparation is perfect, the dielectric's wave function is given by

$$\langle x|0\rangle = \frac{1}{[2\pi x_0^2]^{1/4}} \exp\left[-\frac{x^2}{4x_0^2}\right], \quad (6.1)$$

In a realistic situation, the initial state is given by a thermal state with mean occupation number

$$\bar{n}_{\text{phon}} = (\exp[\beta\hbar\omega] - 1)^{-1}, \quad (6.2)$$

where  $\beta^{-1} = k_{\text{B}}T_{\text{b}}$ , with  $T_{\text{b}}$  being the effective temperature of the dielectrics's center-of-mass movement in one direction. Its density operator can be written as

$$\hat{\rho}(0) = \sum_{n=0}^{\infty} \frac{\bar{n}_{\text{phon}}^n}{(1 + \bar{n}_{\text{phon}})^{n+1}} |n_{\text{phon}}\rangle \langle n_{\text{phon}}| \quad (6.3)$$

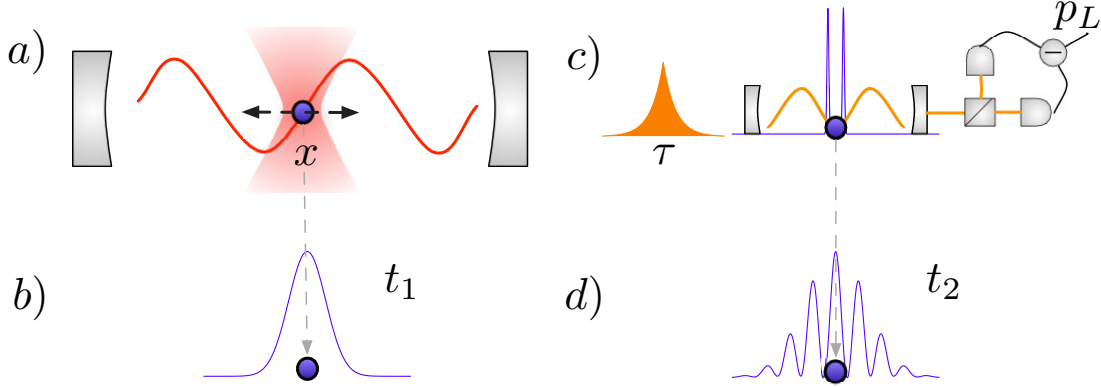


Figure 6.1: Schematic representation of the proposal. (a) The optically trapped object is laser-cooled using a high-finesse optical cavity. (b) The trap is switched off and the wave function expands for some time  $t_1$ . (c) The object enters into a second small cavity where a pulsed (of time  $\tau$ ) interaction is performed using the quadratic optomechanical coupling. The homodyne measurement of the output phase measures  $\hat{x}^2$  and prepares a quantum superposition state conditional on the outcome  $p_L$ . (d) The particle falls for a time  $t_2$  until its center-of-mass position is measured, which after repetition unveils an interference pattern for each  $p_L$ .

in a Fock basis. For sideband cooling, the mean value of the final occupation number depends on cavity properties and dissipation rates and is given by

$$\bar{n}_{\text{phon}} = \left( \frac{\kappa}{4\omega_t} \right)^2 + \frac{1}{4\mathcal{C}}, \quad (6.4)$$

where all parameters have been defined previously, and the linear cooperativity is given by

$$\mathcal{C} = \frac{g^2}{\kappa\Gamma}, \quad (6.5)$$

where  $\Gamma$  contains all sources of noise as listed in Sec. 3.5. Also here, recoil heating due to photon scattering is the dominating decoherence mechanism, see Sec. 3.2. To achieve ground-state cooling it is thus necessary to be in the resolved-sideband limit ( $\omega_t > \kappa$ ) and realize  $\mathcal{C} \geq 1$ . The resulting thermal state thus has the following moments

$$\begin{aligned} \langle \hat{x}^2(0) \rangle &= (2\bar{n}_{\text{phon}} + 1)x_0^2, \\ \langle \hat{p}^2(0) \rangle &= \frac{2\bar{n}_{\text{phon}} + 1}{4x_0^2}, \end{aligned} \quad (6.6)$$

with  $\langle [\hat{x}(0), \hat{p}(0)]_+ \rangle = 0$ .

### 6.2.2 Step (b): Expansion of the wave function

The goal of this step of the protocol is to increase the extension of the object's wave function. This will be useful for the implementation of the optomechanical double slit described in the next section 6.2.3. Thus, this step of the protocol (see Fig. 6.1 b) consists in switching off the trap and letting the wave function evolve freely with the unitary time evolution

$$\hat{U}_0(t) = \exp[-i\frac{\hat{p}^2}{2m}t]. \quad (6.7)$$

Considering the initial state to be the pure ground state, after some time  $t_1$  it is given by

$$\langle x|\hat{U}_0(t_1)|0\rangle = \frac{1}{[2\pi\sigma^2]^{1/4}} \exp\left[-\frac{x^2}{4\sigma^2} + i\phi_{\text{tof}}\frac{x^2}{\sigma^2}\right], \quad (6.8)$$

where  $\sigma^2 = x_0^2(1 + t_1^2\omega_t^2)$  is the size of the expanded wavefunction, and  $\phi_{\text{tof}} = \omega_t t_1/4$  is the global phase accumulated during the free evolution. We do not consider decoherence processes here, but the restrictions they impose on the experimental realization are discussed in Sec. 6.3. Note that, however, during the free expansion of the wave function, the lasers are switched off and the dominating source of decoherence (light scattering) is thus absent.

### Application of the increased size of the wave function

Using the expansion described above, it is possible to increase the size of the wave packet from  $x_0$  to  $\sigma$ . One application of this modified wave function is to enhance the quadratic coupling of the oscillator to the cavity field. Before the wave function expansion, the quadratic part of the Hamiltonian reads

$$\hat{H}_{\text{qu}} = g_{\text{qu}}(\hat{a}_0 + \hat{a}_0^\dagger)\tilde{x}^2, \quad (6.9)$$

where  $\tilde{x} = \hat{x}/x_0$  is the dimensionless position operator of the mechanical resonator, with  $x_0$  being its zero-point motion. The photon-enhanced quadratic optomechanical coupling is given by  $g_{\text{qu}} = k_c x_0 g$ , where  $k_c = 2\pi/\lambda_c$  is the wave number of the cavity mode. In the optomechanical scenario, a Hamiltonian of this form applies when the equilibrium position of the mechanical oscillator is at the antinode of the standing wave, such that  $g_{\text{qu}} \neq 0$  and  $g = 0$ . A fundamental figure of merit of any cavity-mechanical system is the cooperativity as defined previously in Eq. (3.13) for the linear coupling. In comparison, the quadratic cooperativity is given by

$$\mathcal{C}_{\text{qu}} = \frac{g_{\text{qu}}^2}{\kappa\Gamma} = \mathcal{C} \times (k_c x_0)^2, \quad (6.10)$$

with the optomechanical parameters as defined previously. Ground-state cooling requires  $\mathcal{C} \gtrsim 1$ , whereas non-linear effects, such as energy quantization detection [38]

or preparation of non-Gaussian states without using hybrid systems or single photon resources, require  $\mathcal{C}_{\text{qu}} \gtrsim 1$ . The latter is a very demanding condition due to the strong reduction given by  $(k_c x_0)^2 \ll 1$ .

By expanding the wave function to a given size  $\langle \hat{x}^2 \rangle \sim \sigma^2 \gg x_0$  via a free evolution, this regime can be achieved [62], and the enhanced cooperativity is given by

$$\bar{\mathcal{C}}_{\text{qu}} = \frac{g_{\text{qu}}^2}{\kappa\Gamma} = \mathcal{C} \times (k_c \sigma)^2. \quad (6.11)$$

Thus, for sufficiently large  $\sigma$  and  $\mathcal{C}$ , the non-linear regime  $\bar{\mathcal{C}}_{\text{qu}} \gtrsim 1$  can be attained. We remark that this technique is also applicable to other setups where the mechanical frequency can be varied and hence the wave function of the mechanical oscillator is expanded [80, 90].

### 6.2.3 Step (c): The optomechanical double slit

After the expansion of duration  $t_1$ , a second cavity is used to implement an optomechanical double slit (Fig. 6.1 c). The setup is aligned such that the object passes through a small high-finesse optical cavity at an antinode of the cavity mode. Simultaneously, a pulse of length  $\tau \approx 2\pi/\kappa$  is fed into the cavity such that a short interaction is triggered. In this configuration, the optomechanical coupling is  $\propto \hat{x}^2$ . Consequently, the light leaking from the cavity contains information about  $\hat{x}^2$ , which can be extracted by a homodyne measurement. The wave function after the collapse caused by the measurement is given by

$$|\psi\rangle \equiv \frac{\hat{\mathcal{M}}_d \hat{U}_0(t_1) |0\rangle}{\|\hat{\mathcal{M}}_d \hat{U}_0(t_1) |0\rangle\|}. \quad (6.12)$$

Here, the measurement operator  $\hat{\mathcal{M}}_d$  is given by

$$\hat{\mathcal{M}}_d = \exp [i\phi_{\text{ds}}(\hat{x}/\sigma)^2] \left[ \exp \left( -\frac{(\hat{x} - \frac{d}{2})^2}{4\sigma_d^2} \right) + \exp \left( -\frac{(\hat{x} + \frac{d}{2})^2}{4\sigma_d^2} \right) \right]. \quad (6.13)$$

It prepares a quantum superposition of Gaussian wave functions of width  $\sigma_d$  separated by a distance  $d$ , with an added global phase that will be discussed below. The object is in a well-resolved spatial superposition provided that  $d > 2\sigma_d$ . The second limitation is imposed by realizing a non-negligible probability to obtain the result  $d$  when taking the measurement. Therefore, requiring

$$\frac{\left| \langle \frac{d}{2} | \hat{U}_0(t_1) | \frac{d}{2} \rangle \right|^2}{|\langle 0 | \hat{U}_0(t_1) | 0 \rangle|^2} > e^{-1}, \quad (6.14)$$

yields the condition  $\sqrt{8}\sigma > d$ .

Let us now define the dimensionless coupling strength as

$$\chi \equiv \frac{\sigma^2}{2\sigma_d d}. \quad (6.15)$$

Physically, this means that for a fixed measurement outcome  $d$ , the larger the value of  $\chi$ , the more resolved the superposition. Figure 6.2 shows the position probability distribution of the state of Eq. (6.12) with  $d = \sigma/2$  for different measurement strengths  $\chi$ . Note that also a global phase  $\phi_{ds}$  is added during the measurement. Both this phase

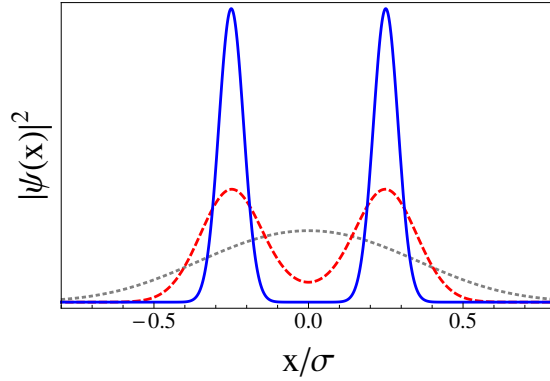


Figure 6.2:  $|\psi(x)|^2 = |\langle x|\psi\rangle|^2$ , see Eq. (6.12), is plotted for  $d = \sigma/2$  and measurement strength  $\chi = 4$  (dotted gray),  $\chi = 10$  (dashed red), and  $\chi = 25$  (solid blue). Note that the superposition is not resolved for the weakest coupling  $\chi = 4$ .

and the one accumulated during the time of flight,  $\phi_{\text{tof}}$  (see Eq. (6.8)) are essential to the implementation. The condition  $|\phi_{ds} + \phi_{\text{tof}}|d^2/(4\sigma^2) \ll 1$  needs to be fulfilled in order to build the interference of the two wave packets centered at  $x = d/2$  and  $x = -d/2$  (see [62] for more details).

### Implementation

The optomechanical Hamiltonian describing this quadratic interaction before displacing the cavity operators is given by

$$\hat{H}_{\text{meas}}(t) = \frac{\hat{p}^2}{2m} + \bar{g}_0 \hat{a}_0^\dagger \hat{a}_0 \tilde{x}^2 + iE(t)(\hat{a}_0 - \hat{a}_0^\dagger). \quad (6.16)$$

The first term describes the kinetic energy of the sphere along the cavity axis (note that there is no harmonic potential since the particle does not need to be trapped during the short interaction time required to measure  $\hat{x}^2$ ). The third term describes the time-dependent driving at frequency  $\omega_L = \omega_c$ , which is used to parametrize the short light pulse. Finally, the second one is the important term describing the optomechanical

coupling when the sphere is placed at the antinode of the cavity mode. We define the dimensionless position operator  $\tilde{x} = \hat{x}/\sigma$ , and the optomechanical coupling rate is given by  $\bar{g}_0 = g_0\sigma^2/x_0^2$ , see Eq. (2.65) for the specific form of  $g_0$  for levitating nanospheres below the optical wavelength. As discussed in [62], note that  $\bar{g}_0$  is enhanced compared to  $g_0$  by a potentially very large factor  $\sigma^2/x_0^2$  depending on the size of the wave packet. The interaction time is assumed to be very small so that methods from pulsed optomechanics can be applied [216]. In contrast to the latter, we do not optimize the pulse shape, but simply assume a time-dependent driving given by

$$E(t) = \sqrt{2\kappa n_{\text{ph}}}\Theta(t), \quad (6.17)$$

where  $\Theta(t)$  is a Heaviside-Theta function of length  $\tau$  and amplitude  $\sim 1/\sqrt{\tau}$  such that  $\int_0^\tau \xi^2(t)dt = 1$ .

### Measurement operator and strength

Let us show here in more detail how the measurement of the phase quadrature of the output light realizes a measurement of  $\hat{x}^2$ . The protocol is based on techniques from pulsed optomechanics [216] consisting in implementing only a very short interaction of duration  $\tau \sim \kappa^{-1}$  such that

$$\frac{\langle \hat{p}^2 \rangle}{2m}\tau = \frac{(2\bar{n}_{\text{phon}} + 1)\omega_t\tau}{4} \ll 1. \quad (6.18)$$

The kinetic term in Eq. (6.16) can thus be neglected yielding

$$\hat{H}_{\text{meas}}(t) \approx \bar{g}_0\hat{a}_0^\dagger\hat{a}_0\tilde{x}^2 + iE(t)(\hat{a}_0 - \hat{a}_0^\dagger). \quad (6.19)$$

We want to establish the connection between the operators in the cavity and the output fields that can be measured and thus apply the input-output formalism [181,182]. The equation of motion for  $\hat{a}_0$  reads

$$\frac{d}{dt}\hat{a}_0(t) = -(i\bar{g}_0\tilde{x}^2 + \kappa)\hat{a}_0(t) + E(t) + \sqrt{2\kappa}\hat{a}_{\text{in}}(t), \quad (6.20)$$

where  $\hat{a}_{\text{in}}$  is the input cavity noise operator. We also assume  $\kappa \gg \bar{g}_0$ , facilitating the adiabatic elimination of the cavity mode by setting  $d/dt \hat{a}_0(t) = 0$ . This leads to

$$\hat{a}_0(t) \approx \left[ E(t) + \sqrt{2\kappa}\hat{a}_{\text{in}}(t) \right] \left[ \frac{1}{\kappa} - \frac{i\bar{g}_0\tilde{x}^2}{\kappa^2} \right]. \quad (6.21)$$

By using the input-output relation

$$\hat{a}_{\text{out}}(t) = \sqrt{2\kappa}\hat{a}_0(t) - \hat{a}_{\text{in}}(t), \quad (6.22)$$

and defining the output phase quadrature

$$\hat{P}_{\text{out}}^L(t) \equiv \frac{i}{\sqrt{2}} \left( \hat{a}_{\text{out}}^\dagger(t) - \hat{a}_{\text{out}}(t) \right), \quad (6.23)$$

one obtains the relation

$$\hat{P}_{\text{out}}^L(t) \approx \hat{P}_{\text{in}}^L(t) + \chi(t)\tilde{x}^2, \quad (6.24)$$

where

$$\chi(t) \equiv \frac{2\bar{g}_0 E(t)}{\kappa\sqrt{\kappa}}, \quad (6.25)$$

and we have neglected the small term  $\sim 2\bar{g}_0\tilde{x}^2\hat{P}_{\text{in}}^L/\kappa$ . Balanced homodyning of the output field measures the time-integrated output quadrature given by [62]

$$\hat{P}_{\text{out}}^L \equiv \frac{1}{\sqrt{\tau}} \int_0^\tau \hat{P}_{\text{out}}^L(t) dt = \hat{P}_{\text{in}}^L + \chi\tilde{x}^2. \quad (6.26)$$

This implies

$$\chi \approx 2\sqrt{2} \frac{\bar{g}\sqrt{n_{\text{ph}}}}{\kappa} \quad (6.27)$$

for the measurement strength. A slight increment can be achieved by optimizing the pulse shape (see [216,217]). For a measurement outcome  $p_L$ , the measurement operator (Eq. (6.12)) describing the collapse of the center-of-mass state of the sphere can also be written as

$$\hat{\mathcal{M}}_d = \exp \left[ i\phi_{\text{ds}}\tilde{x}^2 - (p_L - \chi\tilde{x}^2)^2 \right]. \quad (6.28)$$

This operator prepares a superposition of two wave packets of width

$$\sigma_d \sim \frac{\sigma}{4\sqrt{p_L\chi}} = \frac{\sigma^2}{2d\chi}, \quad (6.29)$$

separated by a distance  $d = 2\sigma\sqrt{p_L/\chi}$ . The global phase accumulated during the interaction with the classical part of the field is given by

$$\begin{aligned} \phi_{\text{ds}} &= - \int_0^\tau \bar{g}_0 \langle \hat{a}_0^\dagger(t)\hat{a}_0(t) \rangle dt \\ &= - \int_0^\tau E^2(t) \left( \frac{1}{\kappa^2} + \frac{\bar{g}_0^2 \langle \tilde{x}^4 \rangle}{\kappa^4} \right) dt \approx - \frac{2\bar{g}_0 n_{\text{ph}}}{\kappa}, \end{aligned} \quad (6.30)$$

where the second term can be neglected in the regime  $\kappa \gg \bar{g}_0$ .

#### 6.2.4 Step (d): The interference pattern

After the preparation of the superposition state by the pulsed interaction, the particle falls freely for another time of flight of duration  $t_2$  as illustrated in Fig. 6.1 c). This time evolution is described by

$$|\psi_f\rangle \equiv \frac{\hat{U}_0(t_2)\hat{\mathcal{M}}_d\hat{U}_0(t_1)|0\rangle}{\|\hat{U}_0(t_2)\hat{\mathcal{M}}_d\hat{U}_0(t_1)|0\rangle\|}. \quad (6.31)$$

The state  $|\psi_f\rangle$  contains interference peaks separated by a distance

$$x_f = \frac{2\pi t_2}{md}, \quad (6.32)$$

under the condition

$$\frac{|\phi_{\text{ds}} + \phi_{\text{tof}}|d^2}{4\sigma^2} \ll 1. \quad (6.33)$$

The peaks are clearly visible when the two wave packets overlap, that is, when

$$d \leq \frac{t_2}{2\sigma_d m}. \quad (6.34)$$

Combining Eq. (6.15) and  $\sigma^2 \approx x_0^2 t_1^2 \omega_t^2$  (valid at  $t_1 \omega_t \gg 1$ ), gives a lower bound for  $t_1$ ,

$$t_1 \lesssim \sqrt{\frac{2t_2 \chi}{\omega_t}}. \quad (6.35)$$

The final step of the protocol consists in performing a position measurement of the center of mass (Fig. 6.1d). This requires a resolution  $\delta x < x_f$ , providing a fourth upper bound for  $d$ ,

$$d < \frac{2\pi t_2}{m\delta x}. \quad (6.36)$$

In contrast to typical time-of-flight experiments in ultracold atoms [75], where many constituents form an interference pattern, in our case, only one sphere is prepared at a time. Naturally, the measurement of the sphere's position does not reveal an interference pattern, but only a single point. In order to obtain the interference pattern and extract useful information from the system, all previous steps have to be repeated for the same parameters providing a different interference pattern for each double slit length  $d$ .

## 6.3 Decoherence

In this section, we review various decoherence mechanisms for the dielectric spheres and describe how they influence the implementation of the protocol to prepare large quantum superpositions. We consider decoherence of position-localization form as discussed in Sec. 3.5. Instead of an exhaustive analysis, in this section, we only review the relevant processes and introduce some additional quantities useful for the description of large superposition states.

### 6.3.1 Coherence length

When preparing large quantum superpositions, it is essential that the measurement protocol prepares a coherent superposition instead of a statistical mixture. This is

the case when the system's coherence length is larger than the separation of the slits described by  $d$ . The coherence length  $\xi(t)$  can be derived from the decay of position correlations described by

$$\mathcal{C}(r, t) = \left\langle \frac{r}{2} |\hat{\rho}(t)| - \frac{r}{2} \right\rangle. \quad (6.37)$$

Let us consider the time evolution of the first moments of  $\hat{r}$  and  $\hat{p}$ , given by

$$\begin{aligned} \langle \hat{r}(t) \rangle &= \langle \hat{r}(0) \rangle + t \frac{\langle \hat{p}(0) \rangle}{m} \\ \langle \hat{p}(t) \rangle &= \langle \hat{p}(0) \rangle \\ \langle \hat{r}^2(t) \rangle &= \langle \hat{r}^2(0) \rangle + \frac{\langle \hat{p}^2(0) \rangle t^2}{2m} + \frac{2\Lambda}{3m^2} t^3 \\ \langle \hat{p}^2(t) \rangle &= \langle \hat{p}^2(0) \rangle + 2\Lambda t \\ \langle [\hat{r}(t), \hat{p}(t)]_+ \rangle &= \frac{2 \langle \hat{p}^2(0) \rangle t}{m} + \frac{2\Lambda t^2}{m}. \end{aligned} \quad (6.38)$$

The parameters are defined in Sec. 3.5 and the dependance on  $t^3$  of  $\langle \hat{x}^2(t) \rangle$  is typical for random forces as described by the position-localization decoherence. The correlation function  $\mathcal{C}(r - r', t)$  can be computed using Eqs. (3.61), (6.38) and can be approximated by

$$\frac{\mathcal{C}(r - r', t)}{\mathcal{C}(0, t)} \approx \begin{cases} \exp\left[-\frac{(r-r')^2}{\xi^2(t)}\right], & (r - r') \ll 2a, \\ \exp\left[-\frac{(r-r')^2}{\xi_s^2(t)} - \gamma t\right], & (r - r') \gg 2a. \end{cases} \quad (6.39)$$

in the long- and short-wavelength limit. The coherence length in the two limits is given by

$$\xi^2(t) = \frac{8 \langle \hat{r}^2(t) \rangle}{4 \langle \hat{r}^2(t) \rangle \langle \hat{p}^2(t) \rangle - \langle [\hat{r}(t), \hat{p}(t)]_+ \rangle^2}, \quad (6.40)$$

and

$$\xi_s^2(t) = \frac{8\sigma^2(t)}{2\bar{n}_{\text{phon}} + 1}. \quad (6.41)$$

Here,  $\sigma^2(t) = x_0^2(1 + t^2\omega_t^2)$  as defined previously.  $\xi_s$  increases monotonically in time and  $\xi(t)$  reaches its maximum

$$\xi_{\text{max}} = \sqrt{2} \left[ \frac{2\omega_t}{3m\Lambda^2(2\bar{n}_{\text{phon}} + 1)} \right]^{1/6} \quad (6.42)$$

at

$$t_{\text{max}} = \left[ \frac{3m(2\bar{n}_{\text{phon}} + 1)}{2\Lambda\omega_t} \right]^{1/3}. \quad (6.43)$$

The achievable coherence length thus depends on the localization parameter,  $\Lambda$ , of the decoherence mechanisms. In order to prepare a coherent superposition, the coherence length has to be larger than the superposition size *i.e.*,  $d < \xi(t_1) \ll \xi_{\text{max}}$ , and  $d < \xi_s(t)$ .

### 6.3.2 Reduction of the visibility

Another effect of the position-localization decoherence is the decay of the visibility of the interference pattern. When neglecting decoherence, the position distribution is given by  $P_0(r, t)$  and has peaks at a distance  $p_f = md/t$ . When decoherence is taken into account, according to Eq. (3.60), the position distribution is given by

$$P(r, t) = \frac{1}{2\pi} \int_{-\infty}^{\infty} dp dr' e^{ipr} \mathcal{B}(p, 0, t) e^{-ipr'} P_0(r', t). \quad (6.44)$$

The visibility of the interference peaks (see [62] for a more detailed description) is thus given by

$$\mathcal{V}(t) = \mathcal{B}\left(\frac{2\pi}{x_f}\right) = \exp[-t\Theta], \quad (6.45)$$

with

$$\Theta = \gamma - \gamma \frac{\sqrt{\pi}a}{d} \operatorname{erf}\left[\frac{d}{2a}\right], \quad (6.46)$$

where  $a$  is the coherence length (see Eq. (3.58)) and  $\gamma$  (Eq. (3.59)) the localization strength. For  $d \ll 2a$ , we can approximate  $\Theta \approx \Lambda d^2/3$ , and  $\Theta \approx \gamma$  in the limit  $d \gg 2a$ . In order to resolve the interference pattern, we require  $\Theta t_2 \ll 1$  implying  $d < \sqrt{3/(\Lambda t_2)}$ , and  $t_2 \ll 1/\gamma$ .

### 6.3.3 Standard decoherence

In this section, we consider the restrictions imposed by the interaction of the nanomechanical oscillator with the environment. The same decoherence processes that have been identified as dominant in Sec. 3.5 are also the most important ones here. Namely, as the lasers are switched off during the time-of-flight (steps (b) and (d)) of the protocol, scattering of air molecules (see Sec. 3.5.2) and blackbody radiation (see Sec. 3.5.3) are dominating. On the other hand, during the measurement protocol photon scattering (see Sec. 2.3.2) is the most important source of decoherence and restricts the choice of parameters in the protocol.

We are interested in preparing nanometer-sized superpositions, therefore, the short-wavelength limit for the scattering of air molecules applies. Here,  $d \gg 2a$ , and decoherence is described by (also see Eq. (3.65))

$$\gamma_{\text{air}} = \frac{16\pi P R^2}{3} \sqrt{\frac{2\pi m}{k_B T}}. \quad (6.47)$$

As illustrated in Fig. 6.3, long coherence times can be achieved, in particular for small spheres, where  $D = 2R$  denotes the diameter of the object.

The second important decoherence mechanism is blackbody radiation. In particular, the emission is dominating due to the increased internal temperature caused by

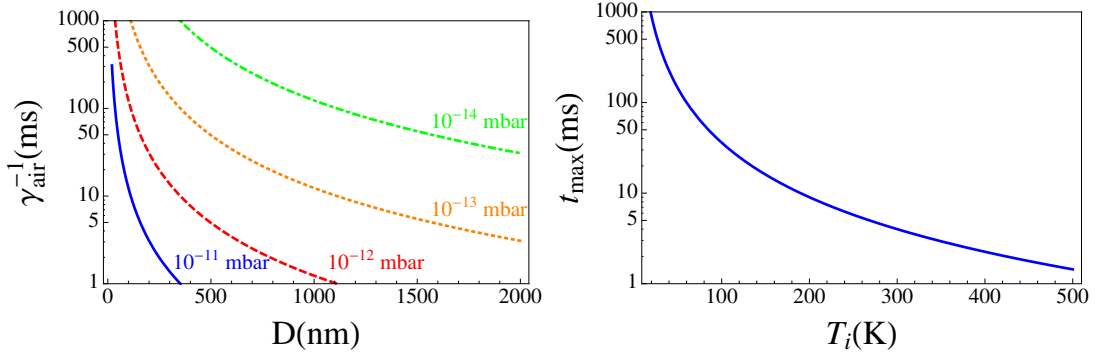


Figure 6.3: *Left panel:* Coherence time  $1/\gamma_{\text{air}}$  as a function of the sphere size. Experimental parameters as defined in the main text and pressures as indicated in the plot. *Right panel:* Coherence time  $t_{\text{max}}$  caused by scattering, emission and absorption of blackbody radiation for different internal temperatures  $T_i$ .

absorption of photons from the laser (see Sec. 3.5.3). In Fig. 6.3, we plot the coherence time  $t_{\text{max}}$  as a function of the temperature of the sphere, where its dependance on the sphere's size is negligible.

Another restriction is imposed by the scattering of photons during the measurement step of the optomechanical double slit (step (c)). Elastic scattering of photons is generally one of the main problems when implementing optomechanics with levitating dielectrics and puts restrictions on the size of the object that can be used, also see Sec. 3.6. When preparing large spatial superpositions, it is also essential to minimize the photon scattering. For this purpose, the sphere only interacts for a short pulse time with the lasers when the optomechanical double slit is applied, in the other steps of expansion, interaction with the lasers is avoided. The decoherence is described by replacing  $x_0$  by  $\sigma$  in Eq. (2.69),

$$\tilde{\Gamma}_{\text{phot}} = \Gamma_{\text{phot}} \frac{\sigma^2}{x_0^2} = \frac{\epsilon_c^2 k_0^6 V^2 \sigma^2}{6\pi} \frac{n_{\text{ph}} c}{2V_c}. \quad (6.48)$$

In order to prevent this form of decoherence on the time scale of the protocol,

$$\int_0^\tau \tilde{\Gamma}_{\text{phot}} dt \ll 1, \quad (6.49)$$

has to be fulfilled. This can be achieved for a sufficiently small  $\sigma$  yielding a condition for the expansion time,

$$t_1 \ll \frac{4g_0}{\omega_t \Gamma_{\text{phot}}}. \quad (6.50)$$

A second restriction arises from the adiabatic elimination, which is justified for  $\kappa \ll \bar{g}_0$

implying [62]

$$t_1 \ll \frac{\kappa}{g_0 \omega_t^2}. \quad (6.51)$$

Inserting these two conditions into Eq. (6.27) for the measurement strength gives

$$\chi \ll \min \left\{ \left( \frac{\kappa}{g_0} \right)^{1/4}, \frac{8g_0^2}{\sqrt{\kappa \Gamma_{\text{phot}}^3}} \right\} = \chi_{\text{max}}. \quad (6.52)$$

The second parameter that needs to be considered is the phase accumulated during the time of flight,  $\phi_{\text{tof}} = t_1 \omega_t / 4$ , which has to be compensated by the one picked up during the measurement protocol, such that  $\phi_{\text{tof}} + \phi_{\text{ds}} \approx 0$ . Following Eq. (6.30) gives

$$\phi_{\text{ds}} = \frac{\omega_t t_1 \kappa x_0^2}{8g_0 \sigma^2} \approx \frac{\kappa}{8g_0 t_1 \omega_t}, \quad (6.53)$$

with  $\sigma^2 \approx x_0^2 t_1^2 \omega_t^2$  for  $t_1 \omega_t \gg 1$ . In combination with Eq. (6.27), this gives

$$\chi \approx (t_1 \omega_t)^{3/2} \sqrt{\frac{g_0}{\kappa}}. \quad (6.54)$$

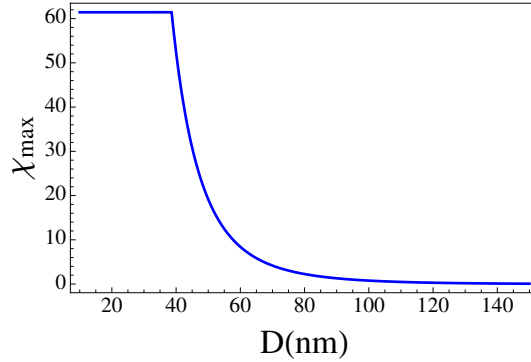


Figure 6.4: Maximally achievable measurement strength  $\chi_{\text{max}}$  for different sphere sizes. All parameters are as given in the main text.

### 6.3.4 Operational regime

Let us now describe the operational regime for the protocol's implementation in an optomechanical setup. The set of experimental parameters is as follows:

- **Dielectric object:** We assume spheres of fused silica with density  $\rho = 2201 \text{ kg/m}^3$ , a dielectric constant  $\text{Re}[\epsilon_r] = 2.1$  and  $\text{Im}[\epsilon_r] \sim 2.5 \times 10^{-10}$ . For the blackbody radiation of the sphere, we choose  $\epsilon_{\text{bb}} = 2.1 + 0.57i$ . We assume the external

temperature at  $T_e = 4.5\text{K}$  and the internal temperature of the sphere due to absorption of laser photons is given by  $T_i \approx 270\text{K}$  (see Sec. 3.5.3). The trapping frequency is given by  $\omega_t = 2\pi \cdot 100\text{kHz}$ .

- **Cavity:** For the cooling, we assume a typical optomechanical cavity as described in Sec. 3.6. For the implementation of the optomechanical double slit, we propose to use a fiber-based cavity of finesse  $\mathcal{F} \approx 1.3 \cdot 10^5$  and cavity length of  $L = 2 \mu\text{m}$  [218, 219]. These cavities are impinged by a laser of  $\lambda_c = 1064\text{nm}$ , have a waist  $W_c = 1.5\mu\text{m}$ , and the measurement strength  $\chi_{\text{max}}$  depends on the size of the sphere, see Fig. 6.4. The pressure is chosen as  $P = 10^{-13}\text{mbar}$ .

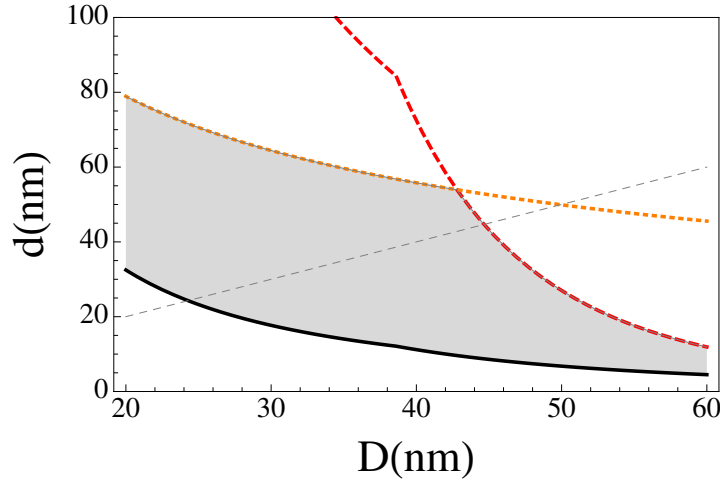


Figure 6.5: Operational regime of the optomechanical protocol. The maximal achievable superposition size  $d$  is plotted for a given diameter of the sphere  $D$ . The experimental parameters are chosen as given in the main text and the expansion times are assumed to be  $t_1 = \min \left\{ \sqrt{\kappa/g_0}/\omega_t, 4g_0/\Gamma_0 \right\}$  and  $t_2 = 10^{-2}/\gamma_{\text{air}}$ . The grey area denotes the superposition sizes that can be realized within the optomechanical setup. *Solid black:* condition  $d > \sigma/\sqrt{\chi}$ , *Dashed red:* condition on the coherence length,  $d < \xi(t_1)$ , *Dotted orange:*  $d < \sqrt{3}/(\Lambda_{\text{tot}}t_2)$  ( $\Lambda_{\text{tot}}$  denotes the total localization rate), *Thin grey:*  $d = D$ . All other conditions mentioned in the section are less restrictive setting up only higher boundaries and are thus not displayed in the plot.

As shown in Fig. 6.5, it is possible to prepare spatial superpositions larger than the size of the dielectric. The lower bound on the superposition size is given by  $d > \sigma/\sqrt{\chi}$ , which is imposed by the necessity to resolve the superposition peaks *i.e.*,  $d > \sigma_d$ . The first upper bound on the achievable superposition size is given by  $d < \xi(t)$ : the superposition size cannot be larger than the coherence length, see Sec. 6.3.1. The

second upper bound is imposed by the decoherence during the second time of flight,  $d < \sqrt{3/(\Lambda t_2)}$ . It is thus, for instance, possible to prepare a sphere of a  $D = 40\text{nm}$  in a superposition of the size of its own extension with  $d = 40\text{nm}$ .

## 6.4 Applications: testing collapse models

One of the most discussed questions in quantum mechanics remains the quantum-to-classical transition. It is generally believed that the standard theory of decoherence [20, 22, 23] provides a description of this phenomenon. Nevertheless, there exists a large number of collapse theories. They predict a collapse of the wave function beyond a certain size of the object and the superposition, independent of the interaction with the environment [208, 210–213, 220–222]. In this section, we will review the principles underlying these models and discuss the predictions that are made. We do not give an overview of the large class of collapse models, but merely discuss the ones most present in the literature *i.e.*, the CSL model and the Penrose-Diósi model. We investigate the parameter regime required to confront the predictions made by the collapse models and distinguish them from standard decoherence. Note that it is much more challenging to confirm these models than to falsify them as any standard source of decoherence, responsible for the disappearance of the interference pattern, needs to be excluded. All exotic decoherence models considered here predict decoherence of the position-localization form, described by Eq. (3.52),

$$\langle \mathbf{r} | \dot{\rho}_S(t) | \mathbf{r}' \rangle = i \langle \mathbf{r} | [\hat{\rho}_S(t), \hat{H}_S] | \mathbf{r}' \rangle - \Gamma \Delta \mathbf{r} \langle \mathbf{r} | \hat{\rho}_S(t) | \mathbf{r}' \rangle. \quad (6.55)$$

This enables one to directly compare the decoherence through the collapse models to the one caused by the interaction with the environment and to identify the regime where the first dominates. The form and strength of the decoherence rate  $\Gamma$  depends on the model that is employed and will be given in the following. We only provide a brief summary of the results here, for more details see [62] and the original papers.

### 6.4.1 The CSL model

One of the most famous models is the continuous spontaneous localization (CSL) model [210, 213, 222], introduced by Ghirardi, Rimini, Weber (GRW) [208]. The idea of the model is to add a stochastic nonlinear term to the Schrödinger equation. It predicts a localization of the wave function with a strength directly proportional to the mass. Its two phenomenological parameters are constrained by the fact that on the one hand, the model should predict a collapse of the wave function for large objects, and on the other hand reproduce the quantum-mechanical results for small objects. These two

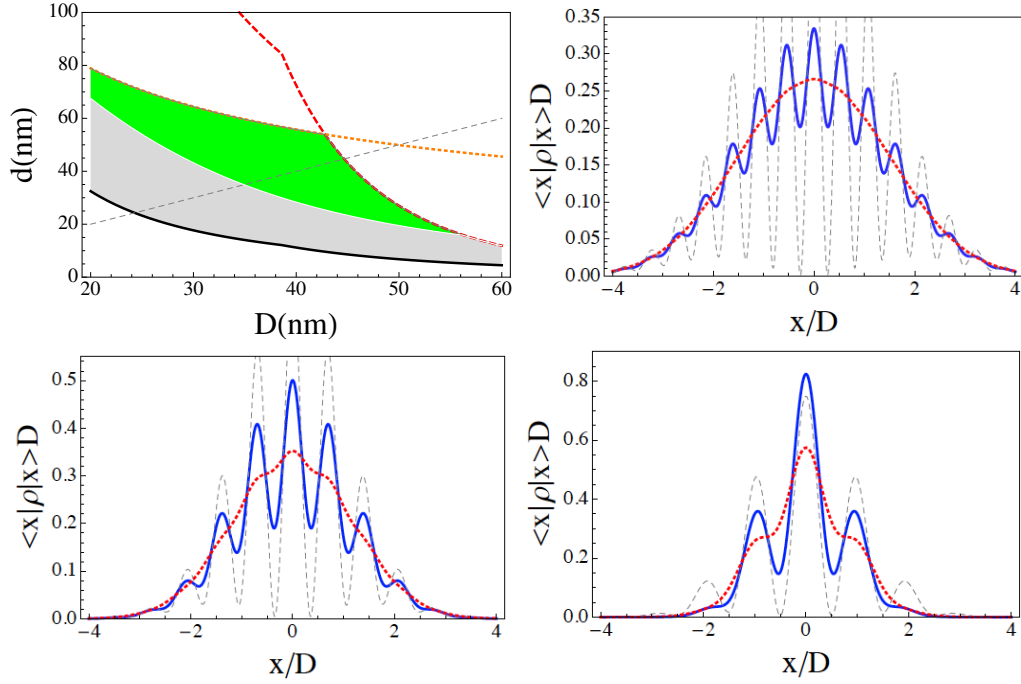


Figure 6.6: *Upper left panel:* Plot of the superposition size  $d$  depending on the diameter  $D$  of the sphere for the parameters given in Fig. 6.5. The green area indicates the regime, where the CSL model with an increased collapse rate  $\tilde{\gamma}_{\text{CSL}}^0 = 10^4 \gamma_{\text{CSL}}^0$  can be tested. *Upper right panel:* Simulation of the interference pattern for  $D = 40\text{nm}$  and superposition size  $d = D$ . *Dashed Grey line:* Interference pattern neglecting decoherence, *Solid blue:* Interference taking into account standard decoherence, *Dashed red:* Decoherence caused by the CSL model. *Lower left panel:* Interference pattern for  $d = 1.3D$ , all parameters and color lines as defined previously, *Lower right panel:* Interference pattern for  $d = 0.7D$ , all parameters and color lines as defined previously.

parameters make the model testable, their value is bounded by experimental data and some philosophical reasoning, see [223] for a recent review. The two free parameters are the localization distance,  $a_{\text{CSL}}$ , and the single-nucleon collapse rate,  $\gamma_{\text{CSL}}^0$ . The decay rate in the single-nucleon case is thus given by

$$\Gamma_{\text{CSL}}(\Delta\mathbf{r}) = \gamma_{\text{CSL}}^0 \left( 1 - \exp \left[ -\frac{\Delta\mathbf{r}^2}{4a_{\text{CSL}}^2} \right] \right). \quad (6.56)$$

The standard values originally proposed in [208] are  $a_{\text{CSL}} = 100\text{ nm}$  and  $\gamma_{\text{CSL}}^0 = 10^{-16}\text{ Hz}$ . However,  $\gamma_{\text{CSL}}^0$  has recently been reestimated by Adler to be 8-10 orders of magnitude larger than originally predicted [215, 222]. A short derivation [62] gives

$\Gamma_{\text{CSL}} = d^2 \Lambda_{\text{CSL}}$  with

$$\Lambda_{\text{CSL}} = \frac{m^2}{m_0^2} \frac{\gamma_{\text{CSL}}^0}{4a_{\text{CSL}}^2} f\left(\frac{R}{a_{\text{CSL}}}\right). \quad (6.57)$$

Here,  $m_0$  denotes the mass of a single nucleon and  $f(x)$  is given by

$$f(x) = \frac{6}{x^4} \left[ 1 - \frac{2}{x^2} + \left( 1 + \frac{2}{x^2} \right) e^{-x^2} \right]. \quad (6.58)$$

This leads to a collapse rate

$$\gamma_{\text{CSL}} = \frac{m^2}{m_0^2} \gamma_{\text{CSL}}^0 f\left(\frac{R}{a_{\text{CSL}}}\right) \quad (6.59)$$

growing quadratically with the number of nucleons per sphere for  $R < a_{\text{CSL}}$ .

Employing the set of parameters described in Sec. 6.3.4, it is possible to tighten the bounds on the CSL model. Namely, it is possible to test the prediction by Adler with  $\tilde{\gamma}_{\text{CSL}}^0 = 10^4 \gamma_{\text{CSL}}^0$ . This is illustrated in Fig. 6.5, where we show that the decoherence imposed by the CSL model dominates standard decoherence in the green region of the diagram. The interference pattern obtained after the time-of-flight-measurement thus shows some additional blurring in the presence of the decoherence through the CSL model. The outcome of this protocol is consequently sufficient to falsify the CSL model, for a corroboration of the theory, it would be necessary to distinguish the induced effect from environmental decoherence.

### 6.4.2 Gravitationally-induced decoherence

The influence of gravity on quantum superpositions and its action as a mechanism for the collapse of the wave function have been discussed extensively in the literature. The most famous analyses are the independent works of Diósi [207, 214, 224–226] and Penrose [212, 227]. The model can be casted into the von-Neumann-Newton equation, which has the form of Eq. (6.55) with the decoherence rate given by

$$\Gamma_{\text{NN}} = \frac{1}{2} (U_g(\mathbf{r}, \mathbf{r}) - U_g(\mathbf{r}', \mathbf{r}')) + U_g(\mathbf{r}, \mathbf{r}'). \quad (6.60)$$

Here,

$$U_g(\mathbf{r}, \mathbf{r}') = -G \int \frac{\rho(\mathbf{x}|\mathbf{r})\rho(\mathbf{x}'|\mathbf{r}')}{|\mathbf{x} - \mathbf{x}'|} d\mathbf{x}d\mathbf{x}', \quad (6.61)$$

denotes the Newtonian interaction between two spheres centered at  $\mathbf{r}, \mathbf{r}'$  with mass densities  $\rho(\mathbf{x}|\mathbf{r})$  at position  $\mathbf{x}$  of a sphere with cm position  $\mathbf{r}$  and  $G$  is the gravitational constant. For a rigid homogeneous sphere, the mass density is uniform and given by

$$\bar{\rho} = \frac{3m}{4\pi R^3}. \quad (6.62)$$

This gives

$$\Gamma_{\text{NN}} = \begin{cases} Gm^2/(2R^3)\Delta r^2, & \Delta r \ll R, \\ 6Gm^2/(5R), & \Delta r \gg R. \end{cases} \quad (6.63)$$

The localization parameter can thus be written as

$$\Lambda_{\text{NN}} = \frac{gm^2}{2R^3} \quad (6.64)$$

and the saturation distance as  $2a_{\text{NN}} = R$ .

The decoherence of this model is much weaker than the ones predicted by the CSL and cannot be tested with the proposed protocol. Note however that the decoherence rate can be strongly enhanced by considering a different mass density at the microscopic level [60, 214]. In particular, in this case the mass density of the sphere is not assumed to be smeared out homogeneously over the entire volume of the sphere, but only on a much smaller length scale,  $r_0 \ll R$ . The localization parameter is thus enhanced to

$$\tilde{\Lambda}_{\text{NN}} = \left(\frac{R}{r_0}\right)^3 \Lambda_{\text{NN}}. \quad (6.65)$$

This assumption is taken in the famous proposal by Marshall [60], where the authors propose to test the Penrose model with a superposition of a micromirror. However, this choice of the mass density leads to divergencies in the von-Neumann-Newton equation describing the dynamics. To avoid this problem, we assume the mass density to be spread out over the volume of the entire sphere in this thesis. Unfortunately, this makes it impossible to test this model with the proposed protocol as standard decoherence will mask the effect of the Penrose-Diósi model. See [62] for a more detailed discussion.



## Chapter 7

# Conclusion and Outlook

During the past years, levitating dielectrics have been established as a novel optomechanical setup and have seen vast interest from both the theoretical and the experimental side [64, 77–80, 88, 97–101, 118]. They are predicted to allow for ground-state cooling even at room temperature due to the absence of clamping losses avoided through the levitation of the mechanical oscillator. Remarkable experimental progress has been made on the implementation of cooling both via feedback- and cavity-cooling techniques [97–99, 101]. In this thesis we study these systems from two different perspectives, represented by the main parts **Theory** and **Protocols**.

The first part of the thesis focusses on providing a consistent **Theory** for the quantum-mechanical description of the setup. We derive a general master equation for the interaction between arbitrary dielectrics and light in Chap. 2. Our approach takes into account the quantum-mechanical motion of the dielectric, the quantum nature of light, and scattering processes to all orders in perturbation theory. It is applicable to dielectrics of arbitrary size and does not rely on the point-particle approximation. Within this framework, we determine coupling strengths and decoherence rates, enabling us to predict final phonon numbers achievable with laser cooling in Chap. 3. We show that ground-state cooling is possible for small spheres,  $R \lesssim 260$  nm, but remains impractical for larger ones, at least with cavity-cooling methods. The limitation is set by recoil heating via elastic photon scattering.

Several directions of research might potentially offer a solution to this problem: the first one relies on choosing shapes for the dielectric and the mode function that are well-fitted to each other. This could be achieved by employing the framework derived in Chap. 2 and minimizing both the cavity decay rate  $\kappa$  and the decoherence rate  $\Gamma$  with respect to the mode profile and the shape of the dielectric. Another solution might be to introduce additional degrees of freedom to the system. For example, coupling to vibrational or whispering gallery modes, inserting an additional qubit into the dielectric

(*e.g.*, in the form of an NV-center), or even charging the sphere, would increase the flexibility and the possibilities for cooling and state manipulation. Coupling to the vibrational or whispering gallery modes [79] implements a multi-mode optomechanical setup with modes varying in life time, coupling strength, and frequency. Some of them might be used as auxiliary modes, enabling more efficient cooling schemes similar to Raman cooling of atoms [228]. In particular the high-frequency vibrational modes of small nanoparticles open up an entirely new parameter regime. Although it has been shown in Sec. 3.4 that couplings between vibrational modes and the light field are weak for spherical objects, differently-shaped dielectrics could be used to enable stronger interactions. Similar in spirit is the approach of introducing an additional degree of freedom, such as an NV-center to the levitating object [229]. However, the effect of a single qubit on a mechanical oscillator is typically weak, due to the difference in mass, and methods to increase this coupling are required. One is confronted with a similar problem when introducing charges: the charge-to-mass scaling with the size of the object is unfavorable as the mass increases proportional to the volume ( $\propto R^3$ ), while charges accumulate on the surface of the object, and thus scale  $\propto R^2$ . Consequently, the charge-to-mass ratio is always small compared to *e.g.*, ions and reaching efficient coupling strengths is challenging. Another path to ground-state cooling of larger spheres is to entirely avoid the use of lasers and to exploit magnetic fields instead. This has been proposed in [230], where it is shown that a superconducting microsphere trapped by magnetic fields may be cooled to its ground state and even prepared in quantum superpositions. This opens a new size regime inhibited for optically levitated dielectrics due to strong photon scattering.

The second part of this thesis focuses on **Protocols** for the preparation of non-Gaussian states in optomechanical systems. The protocols proposed in Chap. 4 and Chap. 5 rely on coupling the macroscopic system (the optomechanical oscillator) to a small quantum system in a non-Gaussian state (*e.g.*, a single photon, or a two-level atom). We propose methods to imprint the non-Gaussian state of the small system onto the macroscopic oscillator. Chap. 4 promotes three protocols for the coupling of single photons to the mechanical system applicable in different cavity regimes. Chap. 5 proposes to couple the mechanical oscillator to a two-level system *e.g.*, by adding an additional atom to the optomechanical cavity. We explore dissipative methods and show that steady-state preparation of the nanomechanical oscillator in a non-Gaussian state is possible with fidelity close to one. However, the states prepared this way exhibit only a subatomic superposition size  $\Delta\hat{r} = \sqrt{\hbar/2M\omega_t} \sim 100\text{nm}/\sqrt{N_{\text{atom}}}$ . The novel perspectives offered by levitating dielectrics are exploited in Chap. 6, where we propose an optomechanical version of a double slit experiment to prepare levitating dielectrics in superpositions on the order of their own size. We show that this setup

---

may be used to put more restrictive bounds on collapse theories [208], but that theories on gravitationally-induced decoherence remained challenging [212]. To confront these conjectures, larger superpositions with more massive objects are required. As mentioned previously, the limitations on the size of the object are imposed by recoil heating, strongly increasing with the object's size (see Chap. 2). Due to absorption of photons, the internal temperature of the sphere is above the temperature of its environment and emitted blackbody radiation puts a fundamental limit on the achievable superposition size (see Chap. 6). Both of these sources of decoherence can be circumvented using magnetically-levitated spheres [230], where photon scattering is negligible due to the absence of lasers. These systems hence might lead to more macroscopic superpositions and pave the way to tests of models predicting gravitationally-induced decoherence [212]. Moreover, some ideas contained in the proposal of Chap. 6 might also be relevant for other applications. The optomechanical double-slit protocol exhibits some similarity to matter-wave interferometry [14], and further approaches between the two systems *e.g.*, preparation of the initial state of the interfering object with optomechanical methods, are an interesting perspective [102]. Besides, the main concept behind the increment of the quadratic interaction in this proposal is the expansion of the wave function's ground state size which could be useful in other application *e.g.*, in quantum tunneling.

As mentioned in the introduction (Sec. 1.1), we see the three major applications of optomechanical systems, namely

- quantum transducers
- tests of the foundations of quantum mechanics
- quantum metrology.

There have been several proposals of using nanomechanical resonators as quantum transducers (see, eg, [54, 186]), a potential advantage of levitating spheres in this context is their controllability even at room temperature, making them akin to other room-temperature devices, such as NV-centers. Regarding tests of the foundations of quantum mechanics, Chap. 6 describes some first steps into this direction, and we believe that levitated spheres are the ideal testbed for foundational questions as they allow for unprecedented superposition sizes. But most importantly, there is much potential to be explored in the area of metrology. Various applications have been promoted in this direction [59, 94], but particularly the possibility to prepare large quantum superpositions promises a further increment in sensitivity. In this context, extensions to many-partite systems, where several dielectrics are trapped in the cavity (as outlined in Chap. 5), may bring improvements.

From a broader perspective, the novel optomechanical system of levitated spheres provides a toolbox for the manipulation of dielectrics in a new parameter regime. Methods that have been developed for the manipulation of single atoms in optical cavities over the years [29] are now applied to nanodielectrics. This leads to unprecedented isolation and control over these objects several orders of magnitude larger than a single atom. Hence, levitating dielectrics offer a platform to study systems ranging from microorganisms [77] to novel nanomaterials [231], offering a diversity of new perspectives. The contribution of this thesis to this quickly-growing line of research is to aim at providing a theoretical background and suggesting several protocols for the preparation of nonclassical states. Nevertheless, the most exciting development in this research program is expected from the experimental implementation of the setup. Similar to the field of cold atoms [75], experiments and theory are closely connected in optomechanics, with vivid interchange and stimulation of ideas. The experimental implementation of levitating dielectrics [97, 100, 101] is thus expected to come in hand with a plethora of new, exciting questions and further challenges for theoretical studies.

# Chapter 8

## List of parameters

We give a list of the parameters and operators used throughout this thesis in the order of their appearance. Some merely auxiliary variables are not included in the list. Note that we set  $\hbar = 1$  throughout this thesis.

<b>Symbol</b>	<b>Definition</b>	<b>Defined in</b>
$V$	Volume of the dielectric	Sec. 2.2.1
$M$	Mass of the dielectric	Sec. 2.2.1
$\rho$	density distribution of the dielectric	Sec. 2.2.1
$\epsilon_r$	relative dielectric constant	Sec. 2.2.1
$\epsilon_0$	vacuum permittivity	Sec. 2.2.1
$\mu = \mu_0$	permeability	Sec. 2.2.1
$\hat{r}$	center-of-mass (cm) mode	Sec. 2.2.1
$\hat{H}_{\text{tot}}$	total Hamiltonian	Sec. 2.2.2
$\hat{H}_{\text{M}}$	motional Hamiltonian for the dielectric	Sec. 2.2.2
$\hat{H}_{\text{L}}$	Hamiltonian for the electromagnetic field	Sec. 2.2.2
$\hat{H}_{\text{LM}}$	interaction between the light and matter	Sec. 2.2.2
$\hat{H}_{\text{S}}$	system Hamiltonian	Sec. 2.2.2
$\hat{H}_{\text{B}}$	bath Hamiltonian	Sec. 2.2.2
$\hat{H}_{\text{BS}}$	interaction between system and bath	Sec. 2.2.2
$\hat{p}$	momentum of the dielectric	Sec. 2.2.2
$\omega_n$	frequency of the dielectric's eigenmodes	Sec. 2.2.2
$c_{\text{sound}}$	sound velocity	Sec. 2.2.2
$R$	extension of the dielectric, radius for a sphere	Sec. 2.2.2
$\hat{E}_{\text{tot}}$	total electric field	Sec. 2.2.2
$\hat{B}_{\text{tot}}$	total magnetic field	Sec. 2.2.2
$\hat{E}_{\text{B}}$	homogeneous field (bath modes)	Sec. 2.2.2

$\hat{E}_S$	inhomogeneous field (system modes)	Sec. 2.2.2
$\mathbf{k}$	wave vector of the bath modes	Sec. 2.2.2
$\omega_{\mathbf{k}}$	frequency of the bath modes	Sec. 2.2.2
$\omega_0$	frequency of the system mode	Sec. 2.2.2
$V_0$	volume of the system mode	Sec. 2.2.2
$f(\mathbf{x})$	profile of the system mode	Sec. 2.2.2
$\hat{a}_{\mathbf{k}}(\hat{a}_{\mathbf{k}}^\dagger)$	annihilation (creation) operator of the bath	Sec. 2.2.2
$\hat{a}_0(\hat{a}_0^\dagger)$	annihilation (creation) operator of the system	Sec. 2.2.2
$\hat{P}_{\text{tot}}$	polarization of the dielectric	Sec. 2.2.2
$\alpha_p$	polarizability	Sec. 2.2.2
$\epsilon_c$	modified dielectric constant	Sec. 2.2.2
$\alpha = \langle a_0 \rangle$	displacement of the inhomogeneous mode	Sec. 2.2.2
$\xi$	phase of the displacement	Sec. 2.2.2
$\mathcal{E}_S$	classical part of the light field	Sec. 2.2.2
$\hat{W}(\hat{r})$	interaction between the bath modes	Sec. 2.2.2
$\hat{H}_0$	noninteracting part of the Hamiltonian	Sec. 2.2.2
$\hat{E}_B^{(+)}$	annihilation (creation) part of the EM field	Sec. 2.3.1
$\hat{E}_{\text{in}}$	incoming field	Sec. 2.3.1
$\mathcal{V}_{\mathbf{k},\mathbf{k}'}(\hat{r})$	matrix element of the scattering interaction	Sec. 2.3.1
$\mathcal{T}_{\mathbf{k},\mathbf{k}'}(\hat{r})$	transition matrix	Sec. 2.3.1
$\hat{V}(\hat{r})$	operator corresponding to $\mathcal{V}_{\mathbf{k},\mathbf{k}'}(\hat{r})$	Sec. 2.3.1
$\hat{T}(\hat{r})$	operator corresponding to $\mathcal{T}_{\mathbf{k},\mathbf{k}'}(\hat{r})$	Sec. 2.3.1
$\hat{\rho}_{\text{tot}}$	density operator for the total system	Sec. 2.3.2
$\hat{\rho}_B$	density operator for the bath	Sec. 2.3.2
$\hat{\rho}_S$	density operator for the system	Sec. 2.3.2
$\lambda_c$	wavelength of the inhomogeneous mode	Sec. 2.3.2
$\mathcal{F}(t, \hat{r})$	interaction between the bath and the system	Sec. 2.3.2
$ \Omega\rangle$	vacuum state	Sec. 2.3.2
$n_{\text{phot}} =  \alpha ^2$	cavity occupation number	Sec. 2.3.3
$\Delta\hat{r}$	variance of the cm operator	Sec. 2.3.3
$\eta$	Lamb-Dicke parameter	Sec. 2.3.3
$\hat{b}(\hat{b}^\dagger)$	annihilation (creation) of a cm excitation	Sec. 2.3.3
$x_0$	ground-state size	Sec. 2.3.3
$\omega_t$	trapping frequency of the dielectric	Sec. 2.3.3
$\omega_t^0$	trapping frequency in Born approx.	Sec. 2.3.3
$\Delta^M$	renormalization of the trapping frequency	Sec. 2.3.3
$\hat{H}_{\text{rn}}^{\text{shift}}$	renormalization contribution $\propto \hat{r}$	Sec. 2.3.3
$\mathcal{L}^M[\hat{\rho}_S]$	Liouvillian for the mechanical motion	Sec. 2.3.3

---

$\Gamma_{\text{phot}}$	photon decoherence rate for the cm mode	Sec. 2.3.3
$g^0$	optomechanical coupling in Born approx.	Sec. 2.3.3
$g$	renormalized optomechanical coupling	Sec. 2.3.3
$g_{\text{rn}}$	renormalization to the optomechanical coupling	Sec. 2.3.3
$\mathcal{L}^{\text{L}}[\hat{\rho}_{\text{S}}]$	Liouvillian describing the cavity decay	Sec. 2.3.3
$\kappa$	cavity decay rate	Sec. 2.3.3
$\tilde{\omega}_0$	renormalized cavity resonance frequency	Sec. 2.3.3
$\Delta^{\text{L}}$	renormalization to the cavity resonance frequency	Sec. 2.3.3
$\hat{H}_{\text{rn}}$	total renormalization of the Hamiltonian	Sec. 2.3.3
$\omega_{\text{L}}$	laser frequency	Sec. 2.3.3
$\delta$	detuning of $\omega_{\text{L}}$ from $\tilde{\omega}_0$	Sec. 2.3.3
$\hat{H}_{\text{rn}}^0$	total renormalization in Born approx.	Sec. 2.4.1
$\omega_{\text{t}}$	trapping frequency in Born approx.	Sec. 2.4.1
$g^0$	optomechanical coupling in Born approx.	Sec. 2.4.1
$g_{\text{rn}}^0$	lowest renormalization to optomech. coupl.	Sec. 2.4.1
$\Delta^{\text{M},0}$	lowest renormalization of the trapping	Sec. 2.4.1
$\kappa^0$	cavity decay rate in Born approx.	Sec. 2.4.1
$\Gamma^0$	photon decoherence in Born approx.	Sec. 2.4.1
$E(\mathbf{x}, t)$	EM field in the classical formulation	Sec. 2.A
$E_{\text{in}}(\mathbf{x}, t)$	incoming EM field in the classical formulation	Sec. 2.A
$\mathcal{G}(\mathbf{x}', \mathbf{x})$	propagator	Sec. 2.A
$\mathbf{F}_{\text{tot}}$	total force on the dielectric	Sec. 2.A
$\mathbf{P}_{\text{mech}}$	mechanical momentum	Sec. 2.A
$\mathbf{P}_{\text{field}}$	field momentum	Sec. 2.A
$\rho_e$	charge density	Sec. 2.A
$\mathbf{J}$	current	Sec. 2.A
$\mathbf{T}$	Maxwell's stress tensor	Sec. 2.A
$c_{\mathbf{k}}(t)$	coefficient of the wave function	Sec. 2.B
$h(\mathbf{x}, \hat{r}, t)$	Fourier transformation of the coefficient	Sec. 2.B
$c_0(t)$	coefficient of the inhomogeneous mode	Sec. 2.B
$a_n, b_n, c_n, d_n$	expansion coefficients of the Mie solution	Sec. 2.C
$\sigma_{\text{scatt}}$	scattering cross section of the Mie solution	Sec. 2.C
$\hat{E}_{\text{cav}}(\mathbf{x}, t)$	Cavity field	Sec. 3.2
$\mathcal{E}_{\text{cav}}(\mathbf{x}, t)$	Classical part of the cavity field	Sec. 3.2
$\mathcal{E}_{\text{tw}}(\mathbf{x}, t)$	Classical part of the tweezers	Sec. 3.2
$E_0$	field strength of the tweezer	Sec. 3.2
$P_{\text{t}}$	laser power of the tweezer	Sec. 3.2
$W_{\text{t}}$	beam waist of the tweezer	Sec. 3.2

$f_{\text{cav}}$	beam profile of the cavity field	Sec. 3.2
$L$	cavity length	Sec. 3.2
$W_0$	waist of the cavity	Sec. 3.2
$f(\mathbf{k}, \mathbf{k}')$	classical scattering amplitude	Sec. 3.2
$\kappa_0$	intrinsic cavity decay	Sec. 3.2
$\Gamma_{\text{cav}}$	photon decoherence rate for the cavity	Sec. 3.2
$\Gamma$	total decoherence rate including all relevant sources	Sec. 3.2
$\mathcal{C}$	cooperativity	Sec. 3.2
$\bar{n}_{\text{phon}}$	steady-state phonon number	Sec. 3.3
$\bar{n}_{\text{adiab}}$	the same in adiabatic approximation	Sec. 3.3
$\bar{n}_{\text{sb}}$	the same for sideband cooling	Sec. 3.3
$\hat{R}(\phi_1, \phi_2, \phi_3)$	Euler rotation matrix and Euler angles	Sec. 3.4.1
$\mathbf{u}(\mathbf{x})$	Deformation field of the dielectric	Sec. 3.4.1
$V_{\text{E}}(\mathbf{x})$	elasticity potential	Sec. 3.4.1
$\epsilon_{ij}(\mathbf{x})$	elasticity tensor	Sec. 3.4.1
$\sigma_{ij}(\mathbf{x})$	stress tensor	Sec. 3.4.1
$\lambda_{\text{E}}, \mu_{\text{E}}$	Lamé constants	Sec. 3.4.1
$Y$	Young's modulus	Sec. 3.4.1
$\sigma_{\text{E}}$	Poisson ratio	Sec. 3.4.1
$I_i$	dielectric's moment of inertia	Sec. 3.4.1
$v_i(\mathbf{x})$	momentum density	Sec. 3.4.1
$H_0^{\text{el}}$	elasticity Hamiltonian	Sec. 3.4.1
$c_{\parallel}$	velocity of compression waves in the dielectric	Sec. 3.4.1
$\hat{Q}_n$	position operator of a vibrational phonon	Sec. 3.4.1
$\hat{P}_n$	momentum operator of a vibrational phonon	Sec. 3.4.1
$\hat{V}_{\text{ext}}(\mathbf{x})$	additional external potential	Sec. 3.4.1
$\hat{c}_n(\hat{c}_n^\dagger)$	annihilation (creation) operator of a vibrational phonon	Sec. 3.4.2
$q_{0,n}$	ground state size of the vibrational excitations	Sec. 3.4.2
$\xi_{nm}$	coupling between the internal modes	Sec. 3.4.2
$\gamma_n$	coupling between the cm and the vibrational modes	Sec. 3.4.2
$\gamma$	localization strength	Sec. 3.5.1
$a$	localization distance	Sec. 3.5.1
$\Lambda$	localization parameter	Sec. 3.5.1
$\rho(q)$	number density of incoming particles	Sec. 3.5.2
$v(q)$	velocity distribution of incoming particles	Sec. 3.5.2
$\lambda_{\text{th}}$	thermal wavelength of scattered particles	Sec. 3.5.2
$\mathcal{B}(p, r - r', t)$	Influence of decoherence on total dynamics	Sec. 3.5.2
$\mathcal{L}_{\text{air}}$	Liouvillian for scattering of air molecules	Sec. 3.5.2

---

$\Gamma_{\text{air}}$	decoherence rate for scattering of air molecules	Sec. 3.5.2
$m$	mass of scattered air molecules	Sec. 3.5.2
$P$	pressure	Sec. 3.5.2
$k_{\text{B}}$	Boltzmann constant	Sec. 3.5.2
$\gamma_{\text{air}}$	localization strenght for air molecules	Sec. 3.5.2
$P_{\text{e(a)}}^{\text{bb}}$	power emitted (absorbed) by blackbody radiation	Sec. 3.5.3
$T_{S(E)}$	Temperature of the system (the environment)	Sec. 3.5.3
$\epsilon_{\text{bb}}$	blackbody permittivity	Sec. 3.5.3
$P_{\text{abs}}$	power absorption from the lasers	Sec. 3.5.3
$I$	laser intensity	Sec. 3.5.3
$\sigma_{\text{SB}}$	Stefan-Boltzmann constant	Sec. 3.5.3
$\Lambda_{\text{bb}}$	localization rate for blackbody radiation	Sec. 3.5.3
$S_{\text{cav}}$	fluctuation spectrum of the spring constant	Sec. 3.5.4
$R_{n \rightarrow n+1}$	transition rate	Sec. 3.5.4
$\Gamma_{\text{shot}}$	decoherence rate due to shot noise	Sec. 3.5.4
$S_{\text{vib}}$	fluctuation spectrum of the trap frequency	Sec. 3.5.5
$\Gamma_{\text{trap}}$	decoherence rate due to trap fluctuations	Sec. 3.5.5
$\epsilon_{\Theta}$	dependance of the dielectric constant on rotations	Sec. 3.5.6
$\Gamma_{\text{anis}}$	decoherence rate due to sphere anisotropy	Sec. 3.5.6
$\omega_{\text{r}}$	rotational frequency of the dielectric	Sec. 3.5.6
$\mathcal{F}$	cavity finesse	Sec. 3.6
$P_{\text{c}}$	laser power	Sec. 3.6
$n_{\text{min}}$	minimal phonon number	Sec. 3.6
$L[f]$	Laplace transformation of a function	Sec. 3.6
$\hat{H}_{\text{out}}$	energy of the output modes	Sec. 4.2
$\hat{H}_{\text{cav-out}}$	coupling between the cavity and the output modes	Sec. 4.2
$\hat{a}_{\text{out(in)}}$	output (input) mode of the cavity	Sec. 4.2
$\hat{U}_{\text{r}}(t)$	transformation operator to the rotating frame	Sec. 4.2
$\gamma(\omega)$	coupling between the cavity and the output modes	Sec. 4.2
$\hat{D}_{a0}$	displacement operator for the cavity	Sec. 4.2
$\beta$	displacement of the mechanical mode	Sec. 4.2
$\alpha_{\omega}$	displacement of the output mode	Sec. 4.2
$\hat{D}_{\text{b}}$	displacement operator for the mechanical mode	Sec. 4.2
$\hat{D}_{\text{out}}$	displacement operator for the output	Sec. 4.2
$\hat{\mathcal{D}}$	total displacement operator	Sec. 4.2
$\hat{H}_{\text{tot}}^{\text{r}}$	total red-detuned Hamiltonian	Sec. 4.2
$\hat{H}_{\text{tot}}^{\text{b}}$	total blue-detuned Hamiltonian	Sec. 4.2
$\Omega_{\text{L}}$	driving strength of the cavity	Sec. 4.2

$ n_b n_{a0} \Omega\rangle$	state with $n_b$ photons, $n_{a0}$ photons, vacuum in the output	Sec. 4.2
$t_h$	pulse length for the one-photon reflected protocol	Sec. 4.3
$\phi_{\text{in}}(\omega)$	shape of the photon pulse	Sec. 4.3
$x_{\text{in}}$	spatial position to send the pulse	Sec. 4.3
$c_b, c_{a0}, c(\omega)$	coefficients for the mechanical, cavity and output mode	Sec. 4.3
$\hat{A}_{\text{out}}$	annihilation (creation) operator of the output	Sec. 4.3
$\lambda(t)$	variation of the center of the trap	Sec. 4.3
$\hat{X}_{\text{out}}$	quadrature of the output mode	Sec. 4.3
$\alpha_x$	displacement of the output mode in position basis	Sec. 4.3
$p_+, q_+$	amplifying parameters	Sec. 4.3
RMS)	two-mode-squeezed state	Sec. 4.5
$\hat{S}(r_{\text{sq}} e^{i\phi})$	squeezing operator	Sec. 4.5
$r_{\text{sq}}$	squeezing parameter	Sec. 4.5
$\mathcal{F}_{\text{tel}}$	teleportation fidelity	Sec. 4.5
$\mathcal{K}$	teleportation map	Sec. 4.5
$ \psi\rangle_e$	light state to be teleported	Sec. 4.5
$\hat{\mathcal{X}}(\theta)$	quadrature phase operator	Sec. 4.6
$\delta z$	resolution for the time-of-flight measurement	Sec. 4.6
$\hat{H}_{\text{L-out}}$	Hamiltonian of the cavity mode and the output modes	Sec. 4.A
$\hat{a}_1(\hat{a}_1^\dagger)$	cavity mode	Sec. 5.2
$\hat{a}_2(\hat{a}_2^\dagger)$	auxiliary cavity mode	Sec. 5.2
$\hat{\sigma}^-(\hat{\sigma}^+)$	annihilation (creation) operator of the qubit	Sec. 5.2
$\hat{H}_{\text{mq}}$	Interaction between the mechanical resonator and the qubit	Sec. 5.2
$\Delta$	laser detuning from the atomic frequency	Sec. 5.2
$g_q$	coupling between the cavity and the qubit	Sec. 5.2
$\Omega$	driving of the qubit	Sec. 5.2
$\delta_{\text{aux}}$	laser detuning from the auxiliary cavity mode	Sec. 5.2
$g_q^{\text{aux}}$	coupling between the auxiliary mode and the qubit	Sec. 5.2
$g^{\text{aux}}$	coupling between the auxiliary mode and the resonator	Sec. 5.2
$\Gamma_m$	decoherence rate of the mechanical oscillator	Sec. 5.2
$\Gamma_q$	decoherence rate of the qubit	Sec. 5.2
$\mathcal{L}^{\text{Q}}[\hat{\rho}]$	Liouvillian for the qubit's decoherence	Sec. 5.2
$\mathcal{C}_q$	cooperativity of the qubit	Sec. 5.2
$\mathcal{C}_m$	cooperativity of the mechanical resonator	Sec. 5.2
$\mathcal{L}_0[\hat{\rho}]$	Liouvillian for the lowest-order adiabatic elimination	Sec. 5.3
$\hat{J}_0$	dominant jump operator	Sec. 5.3
$\Gamma_{\text{eff}}$	effective decay rate	Sec. 5.3
$\hat{\rho}_{\text{SS}}$	steady state	Sec. 5.3

$\hat{\rho}_A(\hat{\rho}_B)$	degenerate steady states	Sec. 5.3
$\mathcal{L}_{\text{pert}}$	perturbative Liouvillian	Sec. 5.3
$\mathcal{L}_{\text{eff}}$	effective Liouvillian	Sec. 5.3
$\mathcal{L}_0^\diamond$	Liouvillian acting on left states	Sec. 5.3
$\chi_i$	left eigenvector of $\mathcal{L}_0^\diamond$	Sec. 5.3
$\alpha_n, \beta_n$	coefficients for the dark state	Sec. 5.3
$\mathcal{F}$	fidelity for the state preparation	Sec. 5.3
$\zeta$	relation between qubit and mechanical oscillator	Sec. 5.3.3
$\hat{J}_1$	auxiliary jump operator	Sec. 5.3.3
$\mathcal{L}_{\text{aux}}$	auxiliary Liouvillian	Sec. 5.3.3
$\Gamma_{\text{aux}}$	auxiliary dissipation	Sec. 5.3.3
$\tilde{\rho}_A$	steady state for engineered-noise preparation	Sec. 5.3.3
$\alpha_{\text{aux}}, \beta_{\text{aux}}$	steady state coeff. for eng.-noise prep.	Sec. 5.3.3
$\hat{\rho}_{A,m}, \hat{\rho}_{B,m}$	steady state of the mech. oscillator	Sec. 5.3.3
$\alpha_{\text{aux}}, \beta_{\text{aux}}$	steady state coeff. of the mech. oscillator	Sec. 5.3.3
$\hat{H}_{\text{phon}}$	effective Hamiltonian after tracing the qubit	Sec. 5.4
$\hat{b}_i$	$i$ th oscillator in the many-mode system	Sec. 5.5
$\omega_i(t)$	time-dependent oscillator frequencies	Sec. 5.5
$\omega_{\text{on}}(\omega_{\text{off}})$	frequency of the oscillators on (off) resonance	Sec. 5.5
$\tau$	switching time of the stroboscopic drive	Sec. 5.5
$\hat{b}_{\text{cm}}$	annihilation operator of the many-sphere mode	Sec. 5.5
$\hat{J}_{0(1)}^{\text{cm}}$	dissipation operator of the many-sphere mode	Sec. 5.5
$\mathcal{L}_0^{\text{cm}}[\hat{\rho}], \mathcal{L}_1^{\text{cm}}[\hat{\rho}]$	effective Liouvillian for the many-sphere mode	Sec. 5.5
$\hat{H}_j^{\text{eff}}$	effective Hamiltonian for the many-sphere system	Sec. 5.5
$\omega_i, g_i$	frequency and coupling in the many-sphere system	Sec. 5.5
$T_b$	effective temperature of the cm mode	Sec. 6.2.1
$\hat{H}_{\text{qu}}$	Hamiltonian with quadratic coupling	Sec. 6.2.1
$g_{\text{qu}}$	quadratic coupling strength	Sec. 6.2.1
$\mathcal{C}_{\text{qu}}, (\bar{\mathcal{C}}_{\text{qu}})$	(enhanced) quadratic cooperativity	Sec. 6.2.1
$k_c$	cavity wave number	Sec. 6.2.1
$\tilde{x}$	renormalized position operator	Sec. 6.2.1
$\hat{U}_0(t)$	operator for the free time evolution	Sec. 6.2.2
$\phi_{\text{tof}}$	phase accumulated during the time of flight	Sec. 6.2.2
$t_1, (t_2)$	duration of the first (second) time of flight	Sec. 6.2.2
$\hat{\mathcal{M}}_d$	measurement operator	Sec. 6.2.3
$d$	superposition distance of the prepared state	Sec. 6.2.3
$\sigma_d$	width of the prepared peaks	Sec. 6.2.3
$\phi_{\text{ds}}$	phase accumulated during the double-slit preparation	Sec. 6.2.3

---

$\chi$	coupling strength of the optomechanical double slit	Sec. 6.2.3
$\hat{H}_{\text{meas}}$	quadratic Hamiltonian before displacement	Sec. 6.2.3
$E(t)$	time-dependent driving of the cavity	Sec. 6.2.3
$\bar{g}_0$	wave-packet-enhanced optomechanical coupling	Sec. 6.2.3
$\hat{P}_{\text{out}}^{\text{L}}(t), (\hat{P}_{\text{in}}^{\text{L}}(t))$	output (input) phase quadrature	Sec. 6.2.3
$p_{\text{L}}$	measurement outcome of the double slit	Sec. 6.2.3
$x_f$	separation of the interference peaks	Sec. 6.2.4
$\mathcal{C}(r, t)$	decay of position correlations	Sec. 6.3.1
$\xi(t)$	coherence length	Sec. 6.3.1
$\mathcal{V}(t)$	visibility of the interference peaks	Sec. 6.3.2
$D$	diameter of the sphere	Sec. 6.3.3
$\Lambda_{\text{CSL}}$	localization rate of the CSL model	Sec. 6.4.1
$\gamma_{\text{CSL}}$	collapse rate of the CSL model	Sec. 6.4.1
$a_{\text{CSL}}$	localization distance of the CSL model	Sec. 6.4.1
$\Lambda_{\text{NN}}$	localization rate of the gravitationally-induced model	Sec. 6.4.1
$a_{\text{NN}}$	localization distance of the CSL model	Sec. 6.4.1

# Bibliography

- [1] N. Bohr. I. On the constitution of atoms and molecules, *The London, Edinburgh, and Dublin Philosophical Magazine and Journal of Science* **26**, 1 (1913).
- [2] E. Schrödinger: *Abhandlungen zur Wellenmechanik*, JA Barth Leipzig, 1928.
- [3] W. Heisenberg. Über quantentheoretische Kinematik und Mechanik, *Mathematische Annalen* **95**, 683 (1926).
- [4] P.A.M. Dirac. The principles of quantum mechanics, *The International Series of Monographs on Physics, Oxford: Clarendon Press* **1** (1947).
- [5] A.L. Schawlow and C.H. Townes. Infrared and optical masers, *Physical Review* **112**, 1940 (1958).
- [6] T.H. Maiman. Stimulated optical radiation in ruby, *Nature Physics* **187**, 1493 (1960).
- [7] R.P. Feynman. Simulating physics with computers, *International Journal of Theoretical Physics* **21**, 467 (1982).
- [8] P.W. Shor. Polynomial-time algorithms for prime factorization and discrete logarithms on a quantum computer, *SIAM journal on computing* **26**, 1484 (1997).
- [9] P. Schindler, M. Müller, D. Nigg, J. Barreiro, E. Martinez, M. Hennrich, T. Monz, S. Diehl, P. Zoller and R. Blatt. Quantum simulation of dynamical maps with trapped ions, *Nature Physics* **9**, 361 (2013).
- [10] X.S. Ma, T. Herbst, T. Scheidl, D. Wang, S. Kropatschek, W. Naylor, B. Wittmann, A. Mech, J. Kofler, E. Anisimova, V. Makarov, T. Jennewein, R. Ursin and A. Zeilinger. Quantum teleportation over 143 kilometres using active feed-forward, *Nature* **20**, 269 (2012).
- [11] C.H. Bennett, G. Brassard et al. . Quantum cryptography: Public key distribution and coin tossing, *Proceedings of IEEE International Conference on Computers, Systems and Signal Processing* **175** (1984).

- 
- [12] V. Giovannetti, S. Lloyd and L. Maccone. Advances in quantum metrology, *Nature Photonics* **5**, 222 (2011).
- [13] E. Schrödinger. Die gegenwärtige Situation in der Quantenmechanik, *Naturwissenschaften* **23**, 807 (1935).
- [14] K. Hornberger, S. Gerlich, P. Haslinger, S. Nimmrichter and M. Arndt. *Colloquium* : Quantum interference of clusters and molecules, *Review of Modern Physics* **84**, 157 (2012).
- [15] C. Davisson and L.H. Germer. The Scattering of Electrons by a Single Crystal of Nickel, *Nature* **119**, 558 (1927).
- [16] H.v.J. Halban and P. Preiswerk. Preuve expérimentale de la diffraction des neutrons., *Comptes Rendus de l'Académie des Sciences* **203**, 73 (1936).
- [17] I. Estermann and O. Stern. Beugung von Molekularstrahlen, *Zeitschrift für Physik* **61**, 95 (1930).
- [18] L. Hackermüller, K. Hornberger, B. Brezger, A. Zeilinger and M. Arndt. Decoherence of matter waves by thermal emission of radiation, *Nature* **427**, 711 (2004).
- [19] S. Gerlich, S. Eibenberger, M. Tomandl, S. Nimmrichter, K. Hornberger, P.J. Fagan, J. Tüxen, M. Mayor and M. Arndt. Quantum interference of large organic molecules, *Nature Communications* **2**, 263 (2011).
- [20] A. Caldeira and A. Leggett. Influence of damping on quantum interference: An exactly soluble model, *Physical Review A* **31**, 1059 (1985).
- [21] A.J. Leggett, S. Chakravarty, A.T. Dorsey, M.P.A. Fisher, A. Garg and W. Zwerger. Dynamics of the dissipative two-state system, *Reviews of Modern Physics* **59**, 1 (1987).
- [22] E. Joos and H.D. Zeh. The emergence of classical properties through interaction with the environment, *Zeitschrift für Physik B* **59**, 223 (1985).
- [23] W.H. Zurek. Decoherence and the Transition from Quantum to Classical, *Physics Today* **44**, 36 (1991).
- [24] V.B. Braginsky, Y.I. Vorontsov and K.S. Thorne. Quantum nondemolition measurements, *Science* **209**, 547 (1980).

- 
- [25] C.M. Caves, K.S. Thorne, R.W. Drever, V.D. Sandberg and M. Zimmermann. On the measurement of a weak classical force coupled to a quantum-mechanical oscillator. I. Issues of principle, *Reviews of Modern Physics* **52**, 341 (1980).
- [26] G. Cella and A. Giazotto. Invited review article: interferometric gravity wave detectors, *Review of Scientific Instruments* **82**, 101101 (2011).
- [27] V.B. Braginsky, V. Borisovich and F.Y. Khalili: *Quantum measurement*, Cambridge University Press, 1995.
- [28] S.K. Lamoreaux. Casimir forces: Still surprising after 60 years, *Physics Today* **60**, 40 (2007).
- [29] H. Walther, B.T.H. Varcoe, B.G. Englert and T. Becker. Cavity quantum electrodynamics, *Reports on Progress in Physics* **69**, 1325 (2006).
- [30] T. Kippenberg and K. Vahala. Cavity Optomechanics: Back-Action at the Mesoscale, *Science* **321**, 1172 (2008).
- [31] F. Marquardt and S. Girvin. Optomechanics, *Physics* **2**, 40 (2009).
- [32] M. Aspelmeyer, P. Meystre and K. Schwab. Quantum optomechanics, *Physics Today* **65**, 29 (2012).
- [33] M. Aspelmeyer, T.J. Kippenberg and F. Marquardt. Cavity Optomechanics, *arXiv:1303.0733* (2013).
- [34] K.W. Murch, K.L. Moore, S. Gupta and D.M. Stamper-Kurn. Observation of quantum-measurement backaction with an ultracold atomic gas, *Nature Physics* **4**, 561 (2008).
- [35] F. Brennecke, S. Ritter, T. Donner and T. Esslinger. Cavity optomechanics with a Bose-Einstein condensate, *Science* **322**, 235 (2008).
- [36] M.H. Schleier-Smith, I.D. Leroux, H. Zhang, M.A. Van Camp and V. Vuletić. Optomechanical Cavity Cooling of an Atomic Ensemble, *Physical Review Letters* **107**, 143005 (2011).
- [37] S. Groeblacher, J.B. Hertzberg, M.R. Vanner, S. Gigan, K.C. Schwab and M. Aspelmeyer. Demonstration of an ultracold micro-optomechanical oscillator in a cryogenic cavity, *Nature Physics* **5**, 485 (2009).
- [38] J.D. Thompson, B.M. Zwickl, A.M. Jayich, F. Marquardt, S.M. Girvin and J.G.E. Harris. Strong dispersive coupling of a high-finesse cavity to a micromechanical membrane, *Nature* **452**, 72 (2008).

- [39] A. Schliesser, P. Del’Haye, N. Nooshi, K.J. Vahala and T.J. Kippenberg. Radiation Pressure Cooling of a Micromechanical Oscillator Using Dynamical Backaction, *Physical Review Letters* **97**, 243905 (2006).
- [40] J. Chan, T.P.M. Alegre, A.H. Safavi-Naeini, J.T. Hill, A. Krause, S. Groblacher, M. Aspelmeyer and O. Painter. Laser cooling of a nanomechanical oscillator into its quantum ground state, *Nature* **478**, 89 (2011).
- [41] J.D. Teufel, D. Li, M.S. Allman, K. Cicak, A.J. Sirois, J.D. Whittaker and R.W. Simmonds. Circuit cavity electromechanics in the strong-coupling regime, *Nature* **471**, 204 (2011).
- [42] F. Hocke, X. Zhou, A. Schliesser, T.J. Kippenberg, H. Huebl and R. Gross. Electromechanically induced absorption in a circuit nano-electromechanical system, *New Journal of Physics* **14**, 123037 (2012).
- [43] A.D. O’Connell, M. Hofheinz, M. Ansmann, R.C. Bialczak, M. Lenander, E. Lucero, M. Neeley, D. Sank, H. Wang, M. Weides, J. Wenner, J.M. Martinis and A.N. Cleland. Quantum ground state and single-phonon control of a mechanical resonator, *Nature* **464**, 697 (2010).
- [44] S. Mancini, D. Vitali and P. Tombesi. Optomechanical Cooling of a Macroscopic Oscillator by Homodyne Feedback, *Physical Review Letters* **80**, 688 (1998).
- [45] I. Wilson-Rae, N. Nooshi, W. Zwerger and T.J. Kippenberg. Theory of Ground State Cooling of a Mechanical Oscillator Using Dynamical Backaction, *Physical Review Letters* **99**, 093901 (2007).
- [46] I. Wilson-Rae, N. Nooshi, J. Dobrindt, W. Zwerger and T.J. Kippenberg. Cavity-Assisted Back Action Cooling of Mechanical Resonators, *New Journal of Physics* **10**, 095007 (2008).
- [47] F. Marquardt, J.P. Chen, A.A. Clerk and S.M. Girvin. Quantum Theory of Cavity-Assisted Sideband Cooling of Mechanical Motion, *Physical Review Letters* **99**, 093902 (2007).
- [48] C. Genes, D. Vitali, P. Tombesi, S. Gigan and M. Aspelmeyer. Ground-state cooling of a micromechanical oscillator: Comparing cold damping and cavity-assisted cooling schemes, *Physical Review A* **77**, 033804 (2008).
- [49] J.I. Cirac, R. Blatt, P. Zoller and W.D. Phillips. Laser cooling of trapped ions in a standing wave, *Physical Review A* **46**, 2668 (1992).

- 
- [50] J. Teufel, T. Donner, D. Li, J. Harlow, M. Allman, K. Cicak, A. Sirois, J. Whittaker, K. Lehnert and R. Simmonds. Sideband cooling of micromechanical motion to the quantum ground state, *Nature* **475**, 359 (2011).
- [51] E. Verhagen, S. Deleglise, S. Weis, A. Schliesser and T. Kippenberg. Quantum-coherent coupling of a mechanical oscillator to an optical cavity mode, *Nature* **482**, 63 (2012).
- [52] X. Zhou, F. Hocke, A. Schliesser, A. Marx, H. Huebl, R. Gross and T.J. Kippenberg. Slowing, advancing and switching of microwave signals using circuit nanoelectromechanics, *Nature Physics* **9**, 179 (2013).
- [53] K. Stannigel, P. Komar, S.J.M. Habraken, S.D. Bennett, M.D. Lukin, P. Zoller and P. Rabl. Optomechanical Quantum Information Processing with Photons and Phonons, *Physical Review Letters* **109**, 013603 (2012).
- [54] P. Rabl, S.J. Kolkowitz, F.H.L. Koppens, J.G.E. Harris, P. Zoller and M.D. Lukin. A quantum spin transducer based on nanoelectromechanical resonator arrays, *Nature Physics* **6**, 602 (2010).
- [55] K. Hammerer, M. Aspelmeyer, E.S. Polzik and P. Zoller. Establishing Einstein-Poldosky-Rosen Channels between Nanomechanics and Atomic Ensembles, *Physical Review Letters* **102**, 020501 (2009).
- [56] A.N. Cleland and M.L. Roukes. A nanometre-scale mechanical electrometer, *Nature* **392**, 160 (1998).
- [57] Y.T. Yang, C. Callegari, X.L. Feng, K.L. Ekinici and M.L. Roukes. Zeptogram-scale nanomechanical mass sensing, *Nano Letters* **6**, 583 (2006).
- [58] H.Y. Chiu, P. Hung, H.W.C. Postma and M. Bockrath. H.-Y. Chiu, P. Hung, H. W. Ch. Postma, and M. Bockrath., *Nano Letters* **8**, 43424346 (2008).
- [59] A.A. Geraci, S.B. Papp and J. Kitching. Sensitive Force-Detection with Optically-Levitated Microspheres in Vacuum, *Optics in the Life Sciences* page OTMB3 (2011).
- [60] W. Marshall, C. Simon, R. Penrose and D. Bouwmeester. Towards Quantum Superpositions of a Mirror, *Physical Review Letters* **91**, 130401 (2003).
- [61] O. Romero-Isart, A.C. Pflanzer, F. Blaser, R. Kaltenbaek, N. Kiesel, M. Aspelmeyer and J.I. Cirac. Large Quantum Superpositions and Interference of Massive Nanometer-Sized Objects, *Physical Review Letters* **107**, 020405 (2011).

- [62] O. Romero-Isart. Quantum superposition of massive objects and collapse models, *Physical Review A* **84**, 052121 (2011).
- [63] I. Pikovski, M.R. Vanner, M. Aspelmeyer, M. Kim and Č. Brukner. Probing Planck-scale physics with quantum optics, *Nature Physics* **8**, 393 (2012).
- [64] O. Romero-Isart, A.C. Pflanzer, M.L. Juan, R. Quidant, N. Kiesel, M. Aspelmeyer and J.I. Cirac. Optically levitating dielectrics in the Quantum Regime: Theory and Protocols, *Physical Review A* **83**, 013803 (2011).
- [65] M. Schlosshauer: *Decoherence and the Quantum-to-Classical Transition*, Springer, Heidelberg, 2008.
- [66] V. Adiga, B. Ilic, R. Barton, I. Wilson-Rae, H. Craighead and J. Parpia. Approaching intrinsic performance in ultra-thin silicon nitride drum resonators, *Journal of Applied Physics* **112**, 064323 (2012).
- [67] V. Adiga, B. Ilic, R. Barton, I. Wilson-Rae, H. Craighead and J. Parpia. Modal dependence of dissipation in silicon nitride drum resonators, *Applied Physics Letters* **99**, 253103 (2011).
- [68] A. Eichler, J. Moser, J. Chaste, M. Zdrojek, I. Wilson-Rae and A. Bachtold. Nonlinear damping in mechanical resonators made from carbon nanotubes and graphene, *Nature Nanotechnology* **6**, 339 (2011).
- [69] G.D. Cole, I. Wilson-Rae, K. Werbach, M.R. Vanner and M. Aspelmeyer. Phonon-tunnelling dissipation in mechanical resonators, *Nature communications* **2**, 231 (2011).
- [70] I. Wilson-Rae. Intrinsic dissipation in nanomechanical resonators due to phonon tunneling, *Physics Rev. B* **77**, 245418 (2008).
- [71] I. Wilson-Rae, R.A. Barton, S.S. Verbridge, D.R. Southworth, B. Ilic, H.G. Craighead and J.M. Parpia. High- $Q$  Nanomechanics via Destructive Interference of Elastic Waves, *Physical Review Letters* **106**, 047205 (2011).
- [72] A. Ashkin. Acceleration and Trapping of Particles by Radiation Pressure, *Physical Review Letters* **24**, 156 (1970).
- [73] A. Ashkin: *Optical trapping and manipulation of neutral particles using lasers*, World Scientific, Singapore, 2006.
- [74] A.D. Cronin, J. Schmiedmayer and D.E. Pritchard. Optics and interferometry with atoms and molecules, *Review of Modern Physics* **81**, 1051 (2009).

- 
- [75] I. Bloch, J. Dalibard and W. Zwerger. Many-body physics with ultracold gases, *Review of Modern Physics* **80**, 885 (2008).
- [76] P. Zoller, T. Beth, D. Binosi, R. Blatt, H. Briegel, D. Bruss, T. Calarco, J.I. Cirac, D. Deutsch, J. Eisert, A. Ekert, C. Fabre, N. Gisin, P. Grangiere, M. Grassl, S. Haroche, A. Imamoglu, A. Karlson, J. Kempe, L. Kouwenhoven, S. Kröll, G. Leuchs, M. Lewenstein, D. Loss, N. Lütkenhaus, S. Massar, J.E. Mooij, M.B. Plenio, E. Polzik, S. Popescu, G. Rempe, A. Sergienko, D. Suter, J. Twamley, G. Wendin, R. Werner, A. Winter, J. Wrachtrup and A. Zeilinger. Quantum information processing and communication, *European Physical Journal D* **36**, 203 (2005).
- [77] O. Romero-Isart, M.L. Juan, R. Quidant and J.I. Cirac. Towards Quantum Superposition of Living Organisms, *New Journal of Physics* **12**, 033015 (2010).
- [78] D.E. Chang, C.A. Regal, S.B. Papp, D.J. Wilson, O. Painter, H.J. Kimble and P. Zoller. Optomechanics with levitated nanospheres, *Proceedings of the National Academy of Sciences U.S.A.* **107**, 1005 (2010).
- [79] P.F. Barker. Doppler Cooling a Microsphere, *Physical Review Letters* **105**, 073002 (2010).
- [80] S. Singh, G. Phelps, D. Goldbaum, E. Wright and P. Meystre. All-optical optomechanics: an optical spring mirror, *Physical Review Letters* **105**, 213602 (2010).
- [81] M. Gangl and H. Ritsch. Collective dynamical cooling of neutral particles in a high- $Q$  optical cavity, *Physical Review A* **61**, 011402 (1999).
- [82] V. Vuletić and S. Chu. Laser Cooling of Atoms, Ions, or Molecules by Coherent Scattering, *Physical Review Letters* **84**, 3787 (2000).
- [83] V. Vuletić, H.W. Chan and A.T. Black. Three-dimensional cavity Doppler cooling and cavity sideband cooling by coherent scattering, *Physical Review A* **64**, 033405 (2001).
- [84] R. Miller, T.E. Northup, K.M. Birnbaum, A. Boca, A.D. Boozer and H.J. Kimble. Trapped atoms in cavity QED: coupling quantized light and matter, *Journal of Physics B* **38**, 551 (2005).
- [85] A. Ashkin and J.M. Dziedzic. Optical levitation by radiation pressure, *Applied Physics Letters* **19**, 283 (1971).
- [86] A. Ashkin and J.M. Dziedzic. Stability of optical levitation by radiation pressure, *Applied Physics Letters* **24**, 586 (1974).

- [87] A. Ashkin and J.M. Dziedzic. Optical levitation in high vacuum, *Applied Physics Letters* **28**, 333 (1976).
- [88] A.C. Pflanzner, O. Romero-Isart and J.I. Cirac. Master-equation approach to optomechanics with arbitrary dielectrics, *Physical Review A* **86**, 013802 (2012).
- [89] W. Lechner, S.J.M. Habraken, N. Kiesel, M. Aspelmeyer and P. Zoller. Cavity Optomechanics of Levitated Nanodumbbells: Nonequilibrium Phases and Self-Assembly, *Physical Review Letters* **110**, 143604 (2013).
- [90] D.E. Chang, K.K. Ni, O. Painter and H.J. Kimble. Ultrahigh-Q mechanical oscillators through optical trapping, *New Journal of Physics* **14**, 045002 (2012).
- [91] K.K. Ni, R. Norte, D.J. Wilson, J.D. Hood, D.E. Chang, O. Painter and H.J. Kimble. Enhancement of Mechanical  $Q$  Factors by Optical Trapping, *Physical Review Letters* **108**, 214302 (2012).
- [92] Z.Q. Yin, T. Li and M. Feng. Three-dimensional cooling and detection of a nanosphere with a single cavity, *Physical Review A* **83**, 013816 (2011).
- [93] A.A. Geraci, S.B. Papp and J. Kitching. Short-Range Force Detection Using Optically Cooled Levitated Microspheres, *Physical Review Letters* **105**, 101101 (2010).
- [94] A. Arvanitaki and A.A. Geraci. Detecting High-Frequency Gravitational Waves with Optically Levitated Sensors, *Physical Review Letters* **110**, 071105 (2013).
- [95] R. Kaltenbaek, G. Hechenblaikner, N. Kiesel, U. Johann and M. Aspelmeyer. MAQRO-Testing the foundations of quantum physics in space, *Bulletin of the American Physical Society* **58** (2013).
- [96] T. Li, S. Kheifets, D. Medellin and M.G. Raizen. Measurement of the Instantaneous Velocity of a Brownian Particle, *Science* **328**, 1673 (2010).
- [97] T. Li, S. Kheifets and M.G. Raizen. Millikelvin cooling of an optically trapped microsphere in vacuum, *Nature Physics* **7**, 527 (2011).
- [98] T. Monteiro, J. Millen, G. Pender, F. Marquardt, D. Chang and P. Barker. Dynamics of levitated nanospheres: towards the strong coupling regime, *New Journal of Physics* **15**, 015001 (2013).
- [99] J. Gieseler, B. Deutsch, R. Quidant and L. Novotny. Subkelvin parametric feedback cooling of a laser-trapped nanoparticle, *Physical Review Letters* **109**, 103603 (2012).

- 
- [100] J. Gieseler, L. Novotny and R. Quidant. Thermal nonlinearities in a nanomechanical oscillator, *arXiv:1307.4684* (2013).
- [101] N. Kiesel, F. Blaser, U. Delic, D. Grass, R. Kaltenbaek and M. Aspelmeyer. Cavity cooling of an optically levitated nanoparticle, *arXiv:1304.6679* (2013).
- [102] P. Asenbaum, S. Kuhn, S. Nimmrichter, U. Sezer and M. Arndt. Cavity cooling of free silicon nanoparticles in high-vacuum, *arXiv:1306.4617* (2013).
- [103] S.L. Braunstein and P. van Loock. Quantum information with continuous variables, *Review of Modern Physics* **77**, 513 (2005).
- [104] S. Rips and M.J. Hartmann. Quantum Information Processing with Nanomechanical Qubits, *Physical Review Letters* **110**, 120503 (2013).
- [105] M. Ludwig and F. Marquardt. Quantum many-body dynamics in optomechanical arrays, *arXiv:1208.0327* (2012).
- [106] Y. Chen. Macroscopic Quantum Mechanics: Theory and Experimental Concepts of Optomechanics, *arXiv:1302.1924* (2013).
- [107] A. Nunnenkamp, K. Børkje and S.M. Girvin. Single-Photon Optomechanics, *Physical Review Letters* **107**, 063602 (2011).
- [108] P. Rabl. Photon Blockade Effect in Optomechanical Systems, *Physical Review Letters* **107**, 063601 (2011).
- [109] P. Werner and W. Zwerger. Macroscopic quantum effects in nanomechanical systems, *Europhysics Letters* **65**, 158 (2004).
- [110] S. Rips, M. Kiffner, I. Wilson-Rae and M.J. Hartmann. Steady-state negative Wigner functions of nonlinear nanomechanical oscillators, *New Journal of Physics* **14**, 023042 (2012).
- [111] S. Rips, I. Wilson-Rae and M. Hartmann. Nonlinear nanomechanical resonators for quantum optoelectromechanics, *arXiv:1206.0147* (2012).
- [112] S. Bose, K. Jacobs and P. Knight. Preparation of nonclassical states in cavities with a moving mirror, *Physical Review A* **56**, 4175 (1997).
- [113] S. Mancini, V. Manko and P. Tombesi. Ponderomotive control of quantum macroscopic coherence, *Physical Review A* **55**, 3042 (1997).
- [114] S. Bose, K. Jacobs and P. Knight. Scheme to probe the decoherence of a macroscopic object, *Physical Review A* **59**, 3204 (1999).

- [115] A. Armour, M. Blencowe and K. Schwab. Entanglement and decoherence of a micromechanical resonator via coupling to a Cooper-pair box, *Physical Review Letters* **88**, 148301 (2002).
- [116] I. Wilson-Rae, C. Galland, W. Zwerger and A. Imamolu. Exciton-assisted optomechanics with suspended carbon nanotubes, *New Journal of Physics* **14**, 115003 (2012).
- [117] T. Ramos, V. Sudhir, K. Stannigel, P. Zoller and T.J. Kippenberg. Nonlinear Quantum Optomechanics via Individual Intrinsic Two-Level Defects, *Physical Review Letters* **110**, 193602 (2013).
- [118] A.C. Pflanzer, O. Romero-Isart and J.I. Cirac. Optomechanics assisted with a qubit: From dissipative state preparation to many-body physics, *arXiv:1305.6840* (2013).
- [119] K. Hammerer, M. Wallquist, C. Genes, M. Ludwig, F. Marquardt, P. Treutlein, P. Zoller, J. Ye and H.J. Kimble. Strong Coupling of a Mechanical Oscillator and a Single Atom, *Physical Review Letters* **103**, 063005 (2009).
- [120] S. Camerer, M. Korppi, A. Jöckel, D. Hunger, T.W. Hänsch and P. Treutlein. Realization of an Optomechanical Interface Between Ultracold Atoms and a Membrane, *Physical Review Letters* **107**, 223001 (2011).
- [121] A.J. Leggett. Testing the limits of quantum mechanics: motivation, state of play, prospects, *Journal of Physics: Condensed Matter* **14**, R415 (2002).
- [122] W. Dür, C. Simon and J.I. Cirac. Effective size of certain macroscopic quantum superpositions, *Physical Review Letters* **89**, 210402 (2002).
- [123] J.I. Korsbakken, K.B. Whaley, J. Dubois and J.I. Cirac. Measurement-based measure of the size of macroscopic quantum superpositions, *Physical Review A* **75**, 042106 (2007).
- [124] F. Marquardt, B. Abel and J. von Delft. Measuring the size of a quantum superposition of many-body states, *Physical Review A* **78**, 012109 (2008).
- [125] F. Fröwis and W. Dür. Measures of macroscopicity for quantum spin systems, *New Journal of Physics* **14**, 093039 (2012).
- [126] S. Nimmrichter and K. Hornberger. Macroscopicity of Mechanical Quantum Superposition States, *Physical Review Letters* **110**, 160403 (2013).

- 
- [127] G.C. Ghirardi, A. Rimini and T. Weber. Disentanglement of quantum wave functions: Answer to Comment on Unified dynamics for microscopic and macroscopic systems , *Physical Review D* **36**, 3287 (1987).
- [128] I. Favero and K. Karrai. Optomechanics of deformable optical cavities, *Nature Photonics* **3**, 201 (2009).
- [129] C. Genes, A. Mari, D. Vitali and P. Tombesi. Quantum effects in optomechanical systems, *Advances in Atomic, molecular and optical Physics* **57**, 33 (2009).
- [130] D. Kleckner and D. Bouwmeester. Sub-kelvin optical cooling of a micromechanical resonator, *Nature* **444**, 75 (2006).
- [131] S. Gigan, H.R. Bohm, M. Paternostro, F. Blaser, G. Langer, J.B. Hertzberg, K.C. Schwab, D. Bauerle, M. Aspelmeyer and A. Zeilinger. Self-cooling of a micromirror by radiation pressure, *Nature* **444**, 67 (2006).
- [132] A.M. Jayich, J.C. Sankey, B.M. Zwickl, C. Yang, J.D. Thompson, S.M. Girvin, A.A. Clerk, F. Marquardt and J.G.E. Harris. Dispersive optomechanics: a membrane inside a cavity, *New Journal of Physics* **10**, 095008 (2008).
- [133] P.F. Barker and M.N. Shneider. Cavity cooling of an optically trapped nanoparticle, *Physical Review A* **81**, 023826 (2010).
- [134] D. Leibfried, R. Blatt, C. Monroe and D. Wineland. Quantum dynamics of single trapped ions, *Review of Modern Physics* **75**, 281 (2003).
- [135] J.M. Raimond, M. Brune and S. Haroche. Manipulating quantum entanglement with atoms and photons in a cavity, *Review of Modern Physics* **73**, 565 (2001).
- [136] F.J. García de Abajo. Colloquium: Light scattering by particle and hole arrays, *Review of Modern Physics* **79**, 1267 (2007).
- [137] E.M. Purcell and C.R. Pennyparker. Scattering and absorption of light by non-spherical dielectric grains, *Astrophysical Journal* **186**, 705 (1973).
- [138] S. Ström. On the integral equations for electromagnetic scattering, *American Journal of Physics* **43**, 1060 (1975).
- [139] J.A. Stratton: *Electromagnetic Theory*, McGraw-Hill, New York, 1941.
- [140] H. van de Hulst: *Light Scattering by Small Particles*, John Wiley, New York, 1957.

- 
- [141] C.F. Bohren and D.R. Huffman: *Absorption and Scattering of Light by Small Particles*, Wiley, New York, 1983.
- [142] J.D. Jackson: *Classical Electrodynamics*, Wiley, New York, 1998.
- [143] M.L. Goldberger and K.M. Watson: *Collision Theory*, Wiley, New York, 1994.
- [144] J.J. Sakurai: *Modern Quantum Mechanics*, Addison-Wesley, Reading, 1964.
- [145] L. Diósi. Quantum Master equation of a particle in a Gas Environment, *Europhysics Letters* **30**, 63 (1995).
- [146] K. Hornberger and J.E. Sipe. Collisional decoherence reexamined, *Physical Review A* **68**, 012105 (2003).
- [147] S.L. Adler. Normalization of Collisional Decoherence: Squaring the Delta Function and an Independent Cross Check, *Journal of Physics A* **39**, 14067 (2006).
- [148] K. Hornberger. Master Equation for a Quantum Particle in a Gas, *Physical Review Letters* **97**, 060601 (2006).
- [149] K. Hornberger. Monitoring Approach to Open Quantum Dynamics using Scattering Theory, *Europhysics Letters* **77**, 50007 (2007).
- [150] J.I. Cirac, R. Blatt, A.S. Parkins and P. Zoller. Spectrum of resonance fluorescence from a single trapped ion, *Physical Review A* **48**, 2169 (1993).
- [151] C. Yeh. Perturbation approach to the diffraction of electromagnetic waves by arbitrarily shaped dielectric obstacles, *Physical Review* **135**, A1193 (1964).
- [152] V.A. Erma. Exact solution for the scattering of electromagnetic waves from conductors of arbitrary shape:II. General case, *Physical Review* **176**, 1544 (1968).
- [153] A. Ashkin. Forces of a single-beam gradient laser trap on a dielectric sphere in the ray optics regime, *Biophysical Journal* **61**, 569 (1992).
- [154] A. Galindo and P. Pascual: *Quantum Mechanics II*, Springer, Heidelberg, 2012.
- [155] H.P. Breuer and F. Pertruccione: *The Theory of Open Quantum Systems*, Oxford University Press, Oxford, 2002.
- [156] G. Gouesbet. Generalized Lorenz-Mie theories, the third decade: A perspective, *Journal of Quantitative Spectroscopy and Radiative Transfer* **110**, 1223 (2009).

- 
- [157] C. Genes, D. Vitali and P. Tombesi. Simultaneous cooling and entanglement of mechanical modes of a micromirror in an optical cavity, *New Journal of Physics* **10**, 095009 (2008).
- [158] L. Landau and E. Lifschitz: *Theory of Elasticity, 2nd Edition, Vol.7 of Course of Theoretical Physics*, Pergamon Press, Oxford, 1970.
- [159] H. Goldstein, C. Poole and J. Safko: *Classical Mechanics, 3rd Edition*, Addison Wesley, San Francisco, 2002.
- [160] G.B. Arfken, H.J. Weber and F.E. Harris: *Mathematical Methods for Physicists: A Comprehensive Guide*, Elsevier, Amsterdam, 2007.
- [161] E. Joos, H. Zeh, C. Kiefer, D. Giulini, J. Kupsch and I.O. Stamatescu: *Decoherence and the Appearance of a Classical World in Quantum Theory*, Springer, New York, 2003.
- [162] M.R. Gallis and G.N. Fleming. Environmental and spontaneous localization, *Physical Review A* **42**, 38 (1990).
- [163] L. Lanz, B. Vacchini and O. Melsheimer. Quantum theory: the role of microsystems and macrosystems, *Journal of Physics A* **40**, 3123 (2007).
- [164] K. Hansen and E.E.B. Campbell. Thermal radiation from small particles, *Physical Review E* **58**, 5477 (1998).
- [165] M. Gehm, K. O'Hara, T. Savard and J. Thomas. Dynamics of noise-induced heating in atom traps, *Physical Review A* **58**, 3914 (1998).
- [166] L.P. Pitaevskii and S. Stringari: *Bose-Einstein Condensation*, Clarendon press, 2003.
- [167] C. Enss and S. Hunklinger: *Low-Temperature Physics*, Springer, Heidelberg, 2005.
- [168] V. Narayana and R.O. Pohl. Tunneling States of Defects in Solids, *Review of Modern Physics* **42**, 201 (1970).
- [169] R.O. Pohl, X. Liu and E. Thompson. Low-temperature thermal conductivity and acoustic attenuation in amorphous solids, *Review of Modern Physics* **74**, 991 (2002).
- [170] C. Seoánez, F. Guinea and A.H. Castro Neto. Surface dissipation in nanoelectromechanical systems: Unified description with the standard tunneling model and effects of metallic electrodes, *Physical Review B* **77**, 125107 (2008).

- [171] L.G. Remus, M.P. Blencowe and Y. Tanaka. Damping and decoherence of a nanomechanical resonator due to a few two-level systems, *Physical Review B* **80**, 174103 (2009).
- [172] R. Rivière, S. Deléglise, S. Weis, E. Gavartin, O. Arcizet, A. Schliesser and T.J. Kippenberg. Optomechanical sideband cooling of a micromechanical oscillator close to the quantum ground state, *Physical Review A* **83**, 063835 (2011).
- [173] B.F. Schutz. Networks of gravitational wave detectors and three figures of merit, *Classical and Quantum Gravity* **28**, 125023 (2011).
- [174] C. Cohen-Tannoudji, J. Dupont-Roc and G. Grynberg: *Photons and Atoms-Introduction to Quantum Electrodynamics*, Wiley-VCH, New York, 1997.
- [175] D. Kleckner, I. Pikovski, E. Jeffrey, L. Ament, E. Eliel, J. van den Brink and D. Bouwmeester. Creating and verifying a quantum superposition in a micro-optomechanical system, *New Journal of Physics* **10**, 095020 (2008).
- [176] J.M. Dobrindt, I. Wilson-Rae and T.J. Kippenberg. Parametric Normal-Mode Splitting in Cavity Optomechanics, *Physical Review Letters* **101**, 263602 (2008).
- [177] U. Akram, N. Kiesel, M. Aspelmeyer and G.J. Milburn. Single-photon optomechanics in the strong coupling regime, *New Journal of Physics* **12**, 083030 (2010).
- [178] F. Khalili, S. Danilishin, H. Miao, H. Müller-Ebhardt, H. Yang and Y. Chen. Preparing a Mechanical Oscillator in Non-Gaussian Quantum States, *Physical Review Letters* **105**, 070403 (2010).
- [179] S. Lloyd and S.L. Braunstein. Quantum Computation over Continuous Variables, *Physical Review Letters* **82**, 1784 (1999).
- [180] E. Knill, R. Laflamme and G.J. Milburn. A scheme for efficient quantum computation with linear optics, *Nature* **409**, 46 (2001).
- [181] C.W. Gardiner and P. Zoller: *Quantum Noise*, Springer, Berlin, 2004.
- [182] D.F. Walls and G.G.J. Milburn: *Quantum optics*, Springer, Heidelberg, 2007.
- [183] A.I. Lvovsky, H. Hansen, T. Aichele, O. Benson, J. Mlynek and S. Schiller. Quantum State Reconstruction of the Single-Photon Fock State, *Physical Review Letters* **87**, 050402 (2001).

- 
- [184] L. Duan and H.J. Kimble. Scalable Photonic Quantum Computation through Cavity-Assisted Interactions, *Physical Review Letters* **92**, 127902 (2004).
- [185] J.I. Cirac, P. Zoller, H.J. Kimble and H. Mabuchi. Quantum State Transfer and Entanglement Distribution among Distant Nodes in a Quantum Network, *Physical Review Letters* **78**, 3221 (1997).
- [186] K. Stannigel, P. Rabl, A.S. Sørensen, P. Zoller and M.D. Lukin. Optomechanical Transducers for Long-Distance Quantum Communication, *Physical Review Letters* **105**, 220501 (2010).
- [187] C.H. Bennett, G. Brassard, C. Crépeau, R. Jozsa, A. Peres and W.K. Wootters. Teleporting an unknown quantum state via dual classical and Einstein-Podolsky-Rosen channels, *Physical Review Letters* **70**, 1895 (1993).
- [188] S.L. Braunstein and H.J. Kimble. Teleportation of Continuous Quantum Variables, *Physical Review Letters* **80**, 869 (1998).
- [189] H. Schwager, J.I. Cirac and G. Giedke. Interfacing nuclear spins in quantum dots to a cavity or traveling-wave fields, *New Journal of Physics* **12**, 043026 (2010).
- [190] J. Fiurášek. Improving the fidelity of continuous-variable teleportation via local operations, *Physical Review A* **66**, 012304 (2002).
- [191] A.A. Clerk, F. Marquardt and K. Jacobs. Back-action evasion and squeezing of a mechanical resonator using a cavity detector, *New Journal of Physics* **10**, 095010 (2008).
- [192] K. Vahala, M. Herrmann, S. Knünz, V. Batteiger, G. Saathoff, T.W. Hänsch and T. Udem. A phonon laser, *Nature Physics* **5**, 682 (2009).
- [193] J.C. Sankey, C. Yang, B.M. Zwickl, A.M. Jayich and J.G.E. Harris. Strong and tunable nonlinear optomechanical coupling in a low-loss system, *Nature Physics* **6**, 707 (2010).
- [194] J.F. Poyatos, J.I. Cirac and P. Zoller. Quantum Reservoir Engineering with Laser Cooled Trapped Ions, *Physical Review Letters* **77**, 4728 (1996).
- [195] S. Mancini, D. Vitali, G. V. and P. Tombesi. Stationary entanglement between macroscopic mechanical oscillators, *European Physical Journal D* **22**, 417 (2003).
- [196] P. Rabl, A. Shnirman and P. Zoller. Generation of squeezed states of nanomechanical resonators by reservoir engineering, *Physical Review B* **70**, 205304 (2004).

- [197] D. Vitali, S. Mancini and P. Tombesi. Stationary entanglement between two movable mirrors in a classically driven Fabry-Perot cavity, *Journal of Physics A* **40**, 8055 (2007).
- [198] M.J. Hartmann and M.B. Plenio. Steady State Entanglement in the Mechanical Vibrations of Two Dielectric Membranes, *Physical Review Letters* **101**, 200503 (2008).
- [199] M. Ludwig, K. Hammerer and F. Marquardt. Entanglement of mechanical oscillators coupled to a nonequilibrium environment, *Physical Review A* **82**, 012333 (2010).
- [200] C.A. Muschik, E.S. Polzik and J.I. Cirac. Dissipatively driven entanglement of two macroscopic atomic ensembles, *Physical Review A* **83**, 052312 (2011).
- [201] Y.D. Wang and A.A. Clerk. Reservoir-Engineered Entanglement in Optomechanical Systems, *Physical Review Letters* **110**, 253601 (2013).
- [202] H. Tan, L.F. Buchmann, H. Seok and G. Li. Achieving steady-state entanglement of remote micromechanical oscillators by cascaded cavity coupling, *Physical Review A* **87**, 022318 (2013).
- [203] K. Stannigel, P. Rabl and P. Zoller. Driven-dissipative preparation of entangled states in cascaded quantum-optical networks, *New Journal of Physics* **14**, 063014 (2012).
- [204] C.K. Law and J.H. Eberly. Arbitrary Control of a Quantum Electromagnetic Field, *Physical Review Letters* **76**, 1055 (1996).
- [205] K.M. Birnbaum, A. Boca, R. Miller, A.D. Boozer, T.E. Northup and H.J. Kimble. Photon blockade in an optical cavity with one trapped atom, *Nature* **87**, 7047 (2005).
- [206] A. Tomadin, S. Diehl, M. Lukin, P. Rabl and P. Zoller. Reservoir engineering and dynamical phase transitions in optomechanical arrays, *Physical Review A* **86**, 033821 (2012).
- [207] L. Diósi. Gravitation and quantum-mechanical localization of macro-objects, *Physics Letters A* **105**, 199 (1984).
- [208] G.C. Ghirardi, A. Rimini and T. Weber. Unified dynamics for microscopic and macroscopic systems, *Physical Review D* **34**, 470 (1986).

- 
- [209] A. Frenkel. Spontaneous localizations of the wave function and classical behavior, *Foundations of Physics* **20**, 159 (1990).
- [210] G.C. Ghirardi, P. Pearle and A. Rimini. Markov processes in Hilbert space and continuous spontaneous localization of systems of identical particles, *Physical Review A* **42**, 78 (1990).
- [211] J. Ellis, N.E. Mavromatos and D.V. Nanopoulos. String theory modifies quantum mechanics, *Physics Letters B* **293**, 37 (1992).
- [212] R. Penrose. On gravity's role in quantum state reduction, *General Relativity and Gravitation* **28**, 581 (1996).
- [213] A. Bassi and G.C. Ghirardi. Dynamical reduction models, *Physics Reports* **379**, 257 (2003).
- [214] L. Diósi. Notes on certain Newton gravity mechanisms of wavefunction localization and decoherence, *Journal of Physics A* **40**, 2989 (2007).
- [215] S.L. Adler and A. Bassi. Physics. Is quantum theory exact?, *Science* **325**, 275 (2009).
- [216] M.R. Vanner, I. Pikovski, G.D. Cole, M. Kim, Č. Brukner, K. Hammerer, G.J. Milburn and M. Aspelmeyer. Pulsed quantum optomechanics, *Proceedings of the National Academy of Sciences* **108**, 16182 (2011).
- [217] M.R. Vanner. Selective Linear or Quadratic Optomechanical Coupling via Measurement, *Physical Review X* **1**, 021011 (2011).
- [218] T. Steinmetz, Y. Colombe, D. Hunger, T. Hansch, A. Balocchi, R. Warburton and J. Reichel. Stable fiber-based Fabry-Pérot cavity, *Applied Physics Letters* **89**, 111110 (2006).
- [219] D. Hunger, T. Steinmetz, Y. Colombe, C. Deutsch, T.W. Hänsch and J. Reichel. A fiber Fabry-Pérot cavity with high finesse, *New Journal of Physics* **12**, 065038 (2010).
- [220] L. Diósi. Quantum Master Equation of a Particle in a Gas Environment, *Europhysics Letters* **30**, 63 (1995).
- [221] B. Vacchini. On the precise connection between the GRW master equation and master equations for the description of decoherence, *Journal of Physics A* **40**, 2463 (2007).

- [222] P. Pearle. Combining stochastic dynamical state-vector reduction with spontaneous localization, *Physical Review A* **39**, 2277 (1989).
- [223] W. Feldmann and R. Tumulka. Parameter diagrams of the GRW and CSL theories of wavefunction collapse, *Journal of Physics A* **45**, 065304 (2012).
- [224] L. Diósi. A universal master equation for the gravitational violation of quantum mechanics, *Physics Letters A* **20**, 377 (1987).
- [225] L. Diósi. Models for universal reduction of macroscopic quantum fluctuations, *Physical Review A* **40**, 1165 (1989).
- [226] L. Diósi. Intrinsic time-uncertainties and decoherence: comparison of 4 models, *Brazilian Journal of Physics* **35**, 260 (2005).
- [227] I.M. Moroz, R. Penrose and P. Tod. Spherically-symmetric solutions of the Schrödinger-Newton equations, *Classical and Quantum Gravity* **15**, 2733 (1998).
- [228] I. Marzoli, J.I. Cirac, R. Blatt and P. Zoller. Laser cooling of trapped three-level ions: Designing two-level systems for sideband cooling, *Physical Review A* **49**, 2771 (1994).
- [229] M. Scala, M. Kim, G. Morley, P. Barker and S. Bose. Matter Wave Interferometry of a Levitated Thermal Nano-Oscillator Induced and Probed by a Spin, *arXiv:1306.6579* (2013).
- [230] O. Romero-Isart, L. Clemente, C. Navau, A. Sanchez and J.I. Cirac. Quantum Magnetomechanics with Levitating Superconducting Microspheres, *Physical Review Letters* **109**, 147205 (2012).
- [231] F.A. Zwanenburg, A.S. Dzurak, A. Morello, M.Y. Simmons, L.C.L. Hollenberg, G. Klimeck, S. Rogge, S.N. Coppersmith and M.A. Eriksson. Silicon quantum electronics, *Review of Modern Physics* **85**, 961 (2013).

# Acknowledgements

First and foremost I would like to thank my supervisor Ignacio Cirac. It was a great experience to work with him and I feel deeply indebted for all the guidance, support, patience, and extraordinary ideas I have received during these years. Learning from Ignacio and discussing physics with him has strongly influenced my thinking and inspired me in many ways. His creativity, knowledge and kindness made him the best advisor and teacher I could have wished for. I will always be grateful to him.

This work would not have been possible without Oriol Romero-Isart, my co-advisor to whom I am greatly indebted. I would like to thank him for his never-ceasing passion for our joint work, all the long discussions about physics, his genuine ideas, proof-reading my thesis on this year's hottest weekend, and his patience with my stubbornness. Working and interacting with him had a great influence on my approach to research– and I truly enjoyed it.

It is a pleasure to thank Wilhelm Zwerger and Rudolf Gross, who kindly agreed to be part of the commission of my Ph.D. examination.

I would also like to thank our experimental collaborators Markus Aspelmeyer, Nikolai Kiesel, Romain Quidant, and Matthieu Juan. During several research visits, they taught me much about cavities, real-world nanospheres, optical tweezers, and all the experimental details theorists never think about.

I am also indebted to John Preskill and Jeff Kimble for giving me the opportunity to visit IQIM at Caltech for several months – the stimulating atmosphere and discussions there were an important inspiration for this work.

Another thanks goes to all my coworkers at MPQ. They created such a good, interactive, and cooperative atmosphere and made MPQ a great place to work for me. I want to specially point out my (former) office mates Leonardo Mazza and Birger Horstmann for the singing, the deep discussions and for cheering me up when I was losing motivation. Heike Schwager and Fernando Pastawski became some of my closest friends during these years, and I would like to thank them for all the fun and support. Also, work at this institute would not have been such a unique experience without the ingenious contributions of Martin Schütz, Michael Lubasch, and Eric Kessler. I would further like to thank Geza Giedke, Mari-Carmen Bañuls, Stefan Kühn, Johannes Kofler, Gemma de las Cuevas, Matteo Rizzi, Carlos Navarrete, and Eliska Greplova for many interesting discussions about physics, geography, future, and many other things. Andrea Kluth and Veronika Lechner for invaluable support with any administrative difficulties.

Most importantly, I would like to thank my family, especially my parents for their

unconditional love and support. My grandmother for her cheerful approach to life and being such an inspiring example. Knowing that I could always rely on them made a difference, and goes far beyond the acknowledgements of this thesis.

Finally, I would like to thank Philipp for making me so happy in our life together.

Funding from the Max-Planck society and the Elite Network of Bavaria within the program QCCC is gratefully acknowledged.